

APPENDIX K

Hydrodynamic Modeling Report and supplement

Prepared by Scott A. Jenkins Consulting,

February 2010

Figure 10 consists of two contour plots showing salinity distribution. The top plot is a cross-shore section with Depth (m) on the y-axis (0.0 to -20.0) and Cross Shore Distance (m) on the x-axis (0 to 3000). It shows a high-salinity plume (red/orange) originating from the outfall tower (4.8 m above seafloor) and spreading along the seabed. The bottom plot is a longshore section with Depth (m) on the y-axis (0.0 to -20.0) and Longshore Distance (m) on the x-axis (0 to 4500). It shows the same plume spreading along the seabed, with a net downcoast transport indicated by an arrow labeled 'U'. Both plots include a color scale for Salinity (ppt) ranging from 33 to 55.

Submitted to:
Poseidon Resources
17011 Beach Boulevard, Suite 900
Huntington Beach, CA 92647

C-1

TABLE OF CONTENTS

Executive Summary	2
1) Introduction	38
A) Physical Setting	39
B) Climate Variation and Fresh Water Supplies	45
2) Model Description and Capabilities	51
3) Model Initialization	64
A) Storm Water Flow Rates	69
B) Ocean Water Levels & Tidal Oscillations	74
C) Bathymetry	79
D) Wave Climate	81
E) Current Forcing	98
F) Wind Mixing	107
G) Ocean Salinity	108
H) Ocean Temperature	110
I) HBGS Operating Temperature	111
J) Plant Flow Rates & Concentrated Sea Water Discharge Salinity	112
K) Event Scenarios Derived from Historical Data 1980-2000	119
L) Calibration	126
4) Event Analysis of Dilution & Dispersion of Concentrated Sea Water	128
A) Description of Low flow-Case Conditions	129
B) Findings for Low flow Month	131
C) Description of Average-Case Conditions	144
D) Findings for Average Month	145

E) Summary of Dilution & Dispersion Results	155
F) Drift Rates & Exposure Time	158
5) Long-Term Analysis of Dilution of Concentrated Sea Water	163
A) Saline Anomalies at the Outfall	167
B) Saline Anomalies 50 meters from the Outfall	172
C) Saline Anomalies 100 meters from the Outfall	175
D) Saline Anomalies 150 meters from the Outfall	178
E) Saline Anomalies 300 meters from the Outfall	182
F) Saline Anomalies 500 meters from the Outfall	185
G) Saline Anomalies 1000 meters from the Outfall	188
H) Saline Anomalies 2000 meters from the Outfall	190
I) Summary of Long-Term Dilution Analysis	192
6) In-Plant Waste Stream From AES Huntington Beach	219
A) Model Initialization	220
B) Results	221
7) Storm Water From Santa Ana River & Talbert Channel	230
A) Model Initialization	231
B) Results	231
8) Tidal Discharge From Talbert Marsh	245
A) Model Initialization	246
B) Results	248
9) Wastefield From OCSD Deep Outfall	258
A) Model Initialization	259
B) Results	263

10)	Conclusions	271
11)	Bibliography	285

APPENDICES

- A: NPDES MONITORING DATA FOR AES HUNTINGTON
BEACH FOR 1998-1999
- B: TIDE_FEM GOVERNING EQUATIONS AND CODE
- C: TID_DAYS CODE
- D: OCEANRDS CODE
- E: SEDXPORT CODE
- F: MULTINODE CODE
- G: REFRACTION/DIFFRACTION PLOTS OF HISTORIC WAVES
- H: CALIBRATION DATA

Hydrodynamic Modeling of Source Water Make-Up and Concentrated Seawater Dilution for the Ocean Desalination Project at the AES Huntington Beach Generating Station

by Scott A. Jenkins, Ph. D. and Joseph Wasyl

Executive Summary

California experiences multi-decadal climate variability in rainfall leading to alternating periods of dry and wet climate, each lasting 20-30 years. A dry period extended from about 1945-1977, followed by an episodically wet period from 1978-1998, that included the occurrence of six strong El Niño events. Because of the previous durations of these climate cycles, we are likely at an end of a wet cycle and due to return to a period of dry climate similar to what prevailed in California from 1945-1977. Such a transition in climate would put increasing pressures on already limited supplies of fresh water, making the development of alternative sources in California a necessity.

Poseidon Resources plans to construct and operate a reverse osmosis (RO) desalination plant in the southeastern portion of the City of Huntington Beach adjacent to the AES Huntington Beach Generating Station (HBGS). Up to 50 million gallons per day (mgd) of treated water from this plant will be blended with other supplies to provide supplemental water to water utilities located in southern California. The source of water for the desalination plant will be seawater drawn from the ocean about 1,840 ft (561 m) offshore. The source water will be pre-treated and filtered through reverse osmosis membranes to produce high quality drinking water. The plant's product drinking water will be blended with other sources and distributed to consumers. The concentrated seawater produced by the reverse osmosis process will be mixed with the cooling water and then conveyed

through the existing outfall structure located about 1,500 ft (460 m) offshore. The physical effect of desalinating seawater by reverse osmosis is in principle no different to the ocean environment than the effects of evaporation; except that it would take 2000 desalination plants of the size being proposed by Poseidon Resources at Huntington Beach to match the evaporative losses occurring naturally in the waters of the Southern California Bight.

Hydrodynamic modeling of water mass dilution and dispersion was performed in a nearshore domain surrounding the HBGS which extends seaward to the edge of the continental shelf and alongshore from Seal Beach to Crystal Cove State Beach. (The model used in this study is *SEDXPORT*, developed at Scripps Institution of Oceanography for the US Navy's Coastal Water Clarity Program. It has been thoroughly peer reviewed, and has been extensively calibrated and validated in numerous applications throughout the Southern California Bight). The model studied the ocean response to the proposed 50 mgd desalination plant using two separate modeling approaches: 1) event analyses of theoretical extreme cases, and 2) continuous long term simulations using the historical sequence ocean and plant operating variables. The latter approach was applied to two distinct historical periods: one resulting in 7,523 modeled solutions between 1980 and mid 2000 that characterized the period before HBGS was re-powered; the other involving 578 modeled solutions that characterized the post re-powering period using data collected between 1 January 2002 and 30 July 2003.

The event analysis involved some potential situations for operating the desalination plant when the generating plant is operating at very low generating levels. We refer to these as "*low flow cases*" and they produce the highest in-the-pipe concentrations of sea salts from the desalination process. The most extreme of

these low flow cases occurs when the generating plant is in *standby* mode, producing no power and providing no heating of the discharge water. The term “standby mode” broadly refers to a condition when the generating station is spinning an arbitrary collection of pumps with unheated discharge. But, not all possible combinations of pumps during “standby mode” are adequate for the desalination plant to produce product water at a rate of 50 mgd. Throughout this study, we will consider only those cases of standby mode when at least two circulation pumps are on-line (producing 126.7 mgd), because a minimum flow of 100 mgd is required to produce 50 mgd of product water. (No other pump combinations are available within the hydraulic architecture of the generating station that will provide flow rates between 100 mgd and 126.7 mgd).

The low flow cases are evaluated in combination with extreme conditions in the ocean environment involving tranquil, dry weather, La Niña type summer climate. By superimposing two conditions that seldom occur together (low plant flow cases and a calm ocean) the maximum potential impact of the desalination plant on the local ocean environment can be assessed because the dose level of sea salts is highest when the dilution of those salts by mixing and ventilation is lowest. The event analysis also evaluated an “*average case*” based on seasonal mean ocean conditions and average plant flow rates to determine the most likely degree of dilution of desalination plant discharge in nearshore waters.

Numerical modeling of the dilution and dispersion of concentrated seawater discharge from the proposed desalination plant has found that salinities of the receiving water become elevated above mean seawater salinities near the bottom in the immediate neighborhood of the outfall, and only then, when a number of extreme environmental and plant operating conditions occur simultaneously.

Between 1980 and mid 2003, the low flow case resulting from only one generating unit being on line occurred 37 % of the time while the unheated standby mode accounted for less than 1 % of the occurrences. On the other hand, the occurrence of the benign environmental extremes is about 1 week every 3 to 7 years, primarily in summer during strong La Niña conditions. The joint probability for the simultaneous occurrence of these operating and environmental extremes is between 0.27% and 0.64% for the low-flow cases involving active power generation, and between 0.04 % and 0.1% for the standby mode, depending on the length of ENSO (El Niño Southern Oscillation) cycles. In the model simulation of low flow case, these conditions were extended over 30 days, so that the recurrence interval for the low-flow results of this study are actually about 1 month every 13 to 31 years. The extreme operational conditions of the generating plant (low power generation and cooling water consumption) are mutually exclusive with these extreme environmental conditions. Because of this, dilution and dispersion of the concentrated seawater by-product were repeated using more nominal plant operating conditions and average climate conditions. Based on historical data representative of these conditions, the study made the following findings regarding dilution and dispersion of concentrated seawater by-product.

Dilution and Dispersion Before Completion of HBGS Re-Powering:

The dilution and dispersion results for the vent analyses are summarized in Table ES-1. Maximum event impacts during the low flow conditions produce an initial vertical jet of high salinity water that breaches the surface and subsequently sinks to the seafloor, spreading outward from the base of the outfall tower. The highest salinities in the core of the discharge jet are 55.0 ppt at mid-depth (Figure

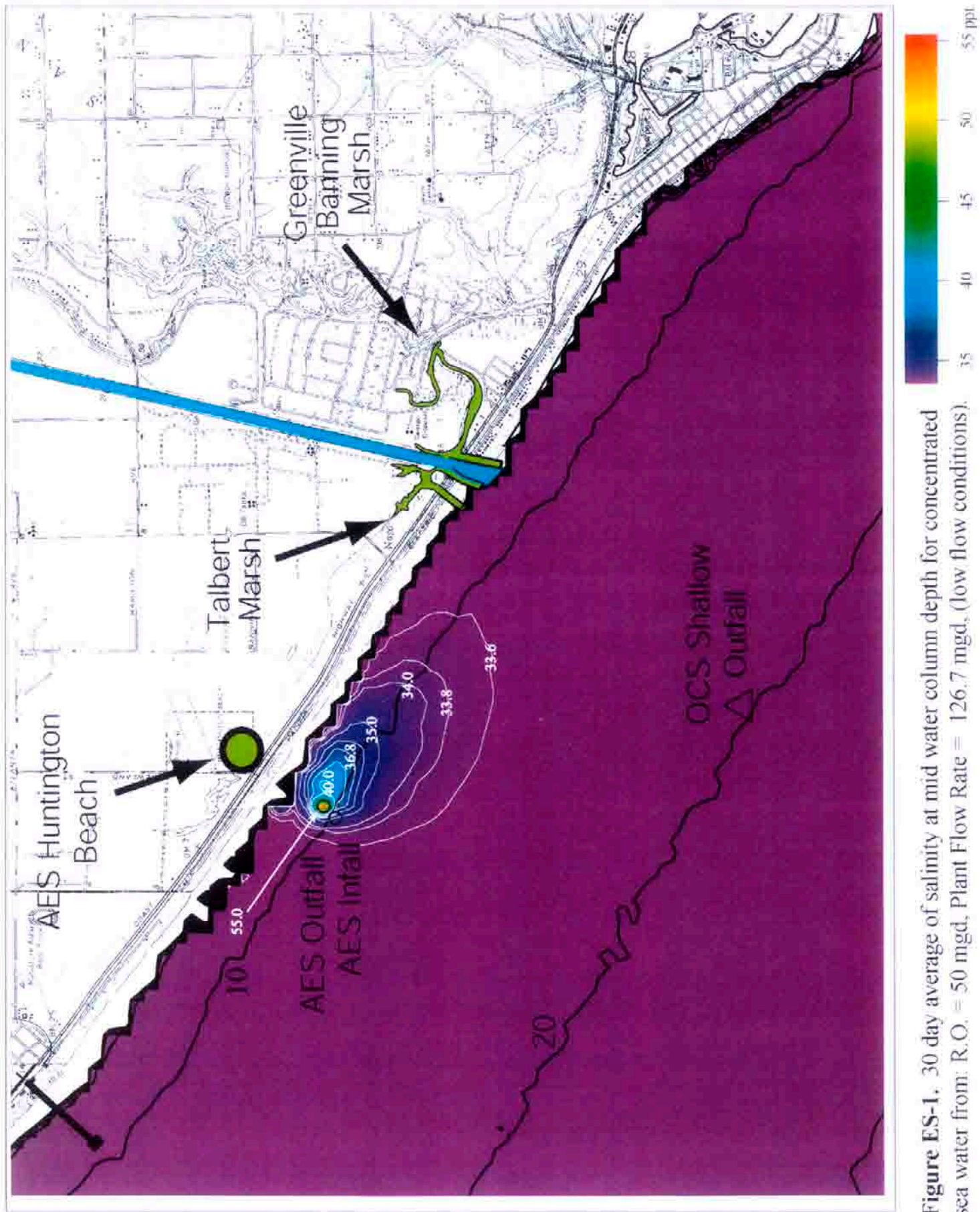


Figure ES-1. 30 day average of salinity at mid water column depth for concentrated sea water from: R.O. = 50 mgd, Plant Flow Rate = 126.7 mgd, (low flow conditions).

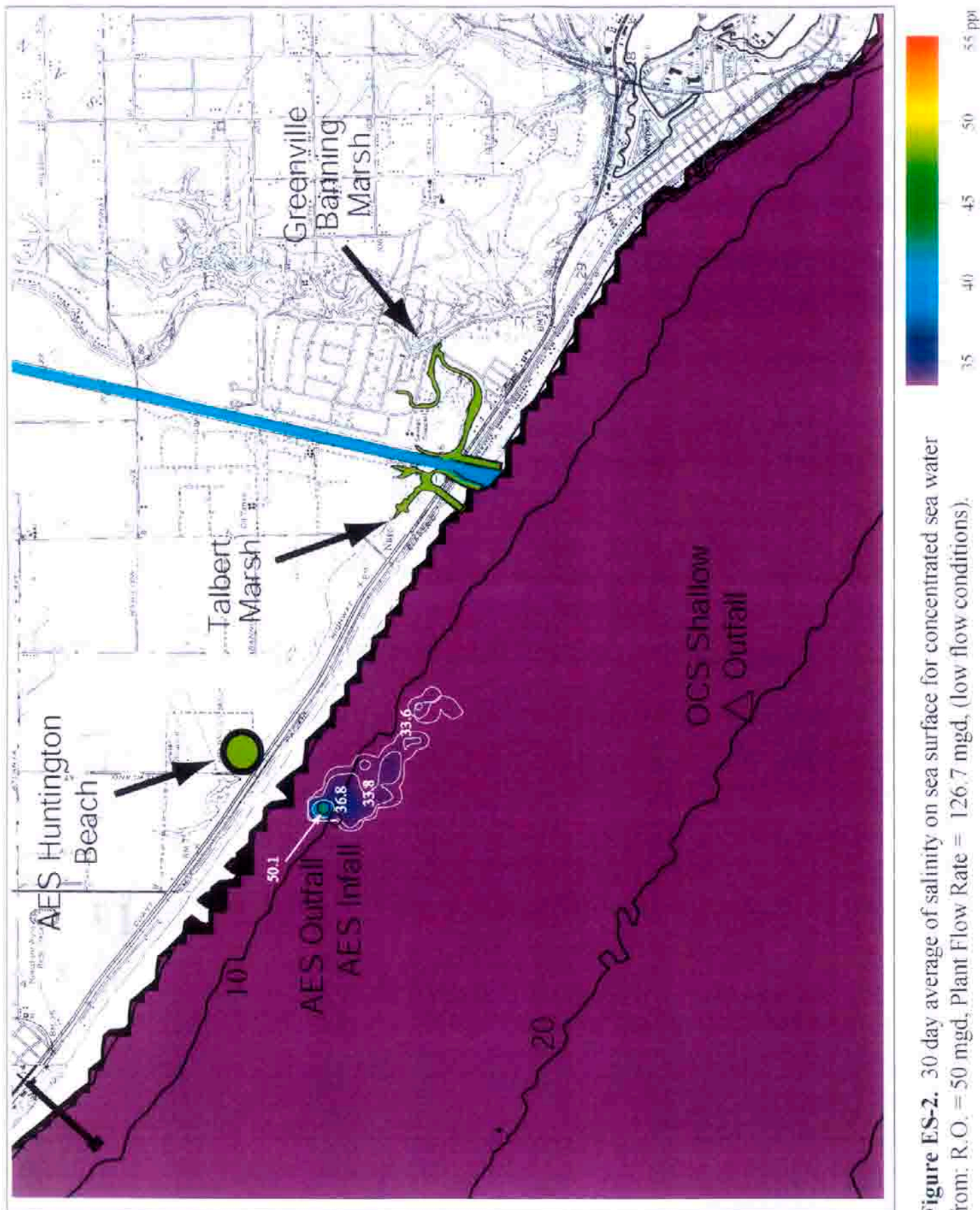


Figure ES-2. 30 day average of salinity on sea surface for concentrated sea water from: R.O. = 50 mgd, Plant Flow Rate = 126.7 mgd, (low flow conditions).

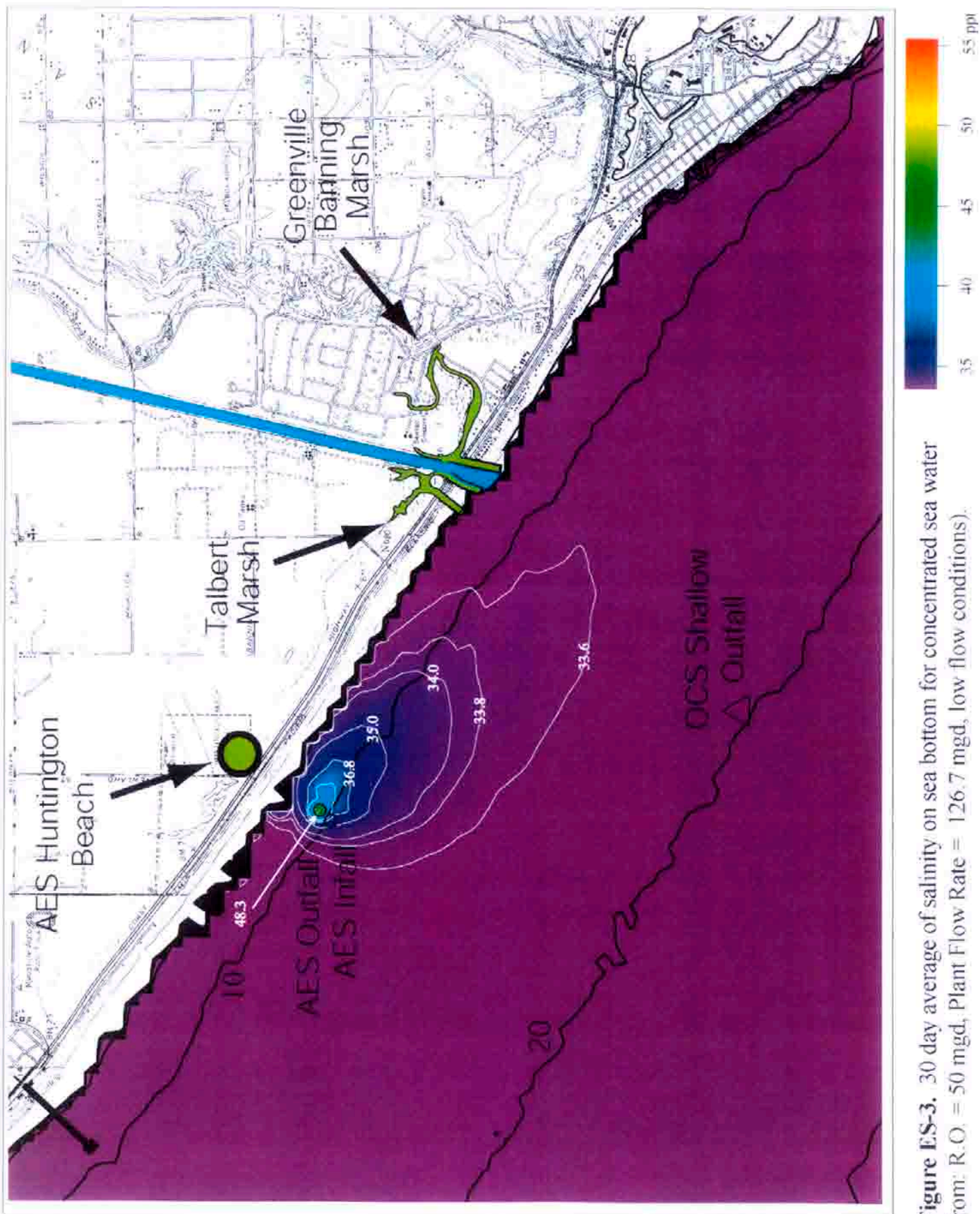


Figure ES-3. 30 day average of salinity on sea bottom for concentrated sea water from: R.O. = 50 mgd, Plant Flow Rate = 126.7 mgd, low flow conditions).

ES-1), falling to 50.1 ppt on the sea surface directly above the outfall tower (Figure ES-2). The highest salinities on the seafloor are 48.3 ppt at the base of the outfall tower, rapidly decreasing with increasing distance from the tower (Figure ES-3). At most, 15.6 acres of benthic area are impacted by an increase in salinity that exceeds 36.9 ppt, that is 10% above the average ambient level of 33.5 ppt. Bottom salinities exceed ambient levels by more than 1% over an area of 263 acres. These elevated salinities effect only sandy, soft bottom habitat with no low relief exposed rocky substrate, and no surf grass or eel grass beds. The maximum area of pelagic habitat subjected to elevated salinity exceeding 10% of ambient is 18.3 acres while 151 acres of pelagic habitat experience an increase in salinity exceeding ambient by more than 1%. Minimum dilution of the concentrated seawater by-product at the shoreline is 32 to 1, (Figure ES-4) consistent with dye measurements from the recent study commissioned by the California Energy Commission (KOMEX, 2003). Two percent of the concentrated seawater by-product may be re-circulated in a sustained low flow case.

Dispersion and dilution contours of sea salts for the theoretical extreme of the standby mode are very similar to those shown in Figures ES-1 through ES-4. The absence of power plant heat produces a heavier combined discharge that is more slowly assimilated by the receiving waters. As a result, Table ES-1 indicates that the impacted benthic area around the outfall is marginally increased during standby mode to 18.2 acres, while the impacted pelagic area increases to 20.1 acres.

Table ES-1: Summary of Event Analysis of Dispersion and Dilution

Model Conditions	Composite Low-flow Month	Composite Average Month	Composite Standby Month
Recurrence Probability	0.27% - 0.64%	50.0%	0.04% - 0.1%
Maximum Seabed Salinity	48.3 ppt	37.6 ppt	50.4 ppt
Maximum Mid-Water Column Salinity	55.0 ppt	41.7 ppt	55.2 ppt
Maximum Surface Salinity	50.1 ppt	38.3 ppt	53.1 ppt
Maximum Benthic Area of 10% Saline Anomaly	15.6 acres	6.8 acres	18.2 acres
Maximum Pelagic Area of 10% Saline Anomaly	18.3 acres	8.3 acres	20.1 acres
Maximum Benthic Area of 1% Saline Anomaly	263 acres	172 acres	284 acres
Maximum Pelagic Area of 1% Saline Anomaly	151 acres	130 acres	163 acres
Dilution of Concentrated Seawater at Plant Infall ^a	100 to 1	500 to 1	90 to 1
Minimum Saline Dilution 305 m from Discharge Structure ^a	10 to 1	20 to 1	8 to 1
Minimum Saline Dilution at Shoreline ^a	32 to 1	190 to 1	30 to 1

^a Dilution of Raw Concentrate from RO Process

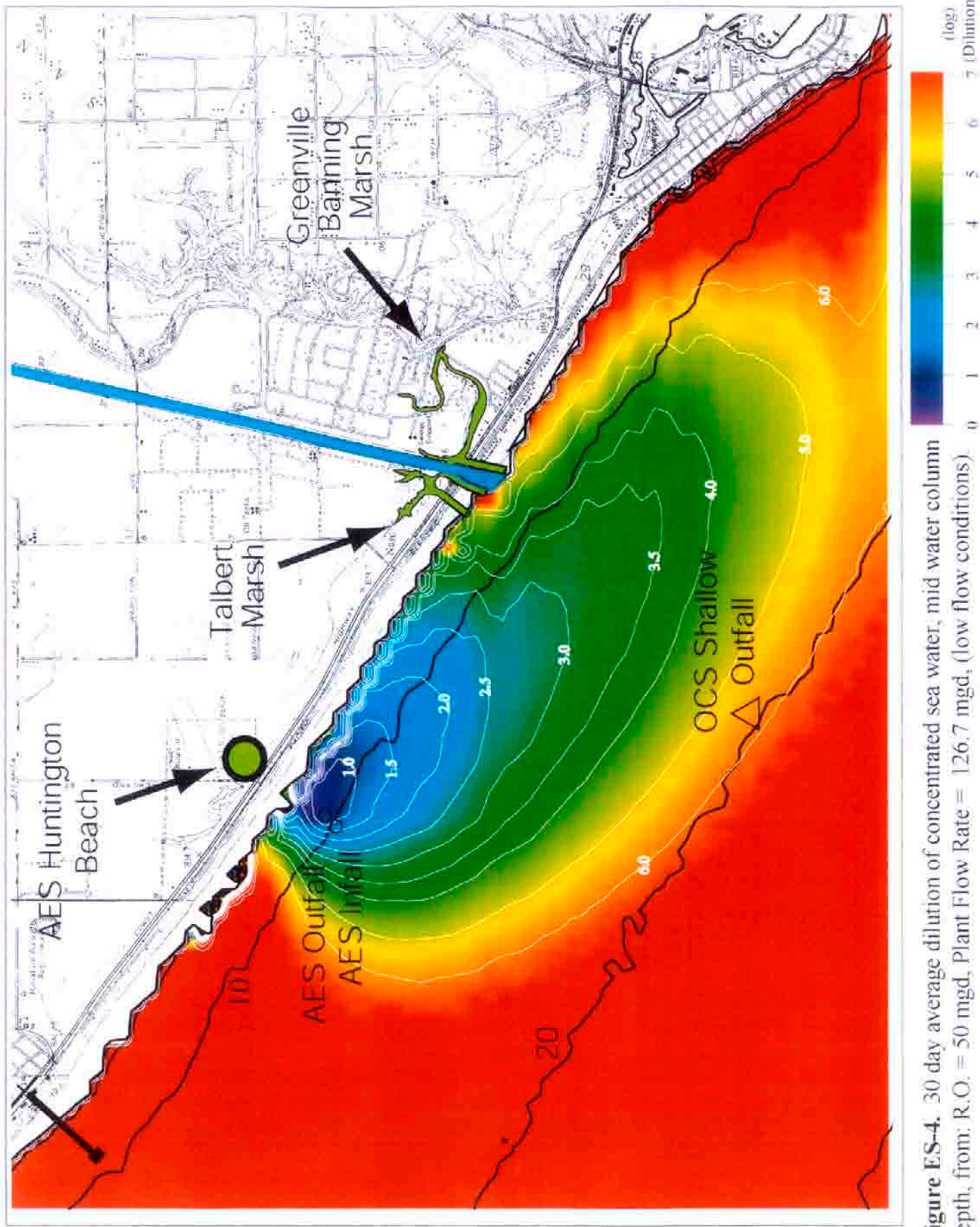


Figure ES-4. 30 day average dilution of concentrated sea water, mid water column depth, from: R.O. = 50 mgd, Plant Flow Rate = 126.7 mgd, (low flow conditions)

For average case events, the salinity in the water column directly above the discharge tower reaches 41.7 parts per thousand, (Figure ES-5), dropping to 38.3 ppt on the sea surface above the outfall tower (Figure ES-6). Maximum salinity on the sea bed is 37.6 ppt at the base of the outfall structure (Figure ES-7). The maximum area of benthic habitat subjected to a 10% increase in salinity is only 6.8 acres, while the area of pelagic habitat experiencing a similar increase is 8.3 acres. The benthic footprint of the 1% saline anomaly is 172 acres and the pelagic footprint is 130 acres. Except for the initial core of the discharge jet salinities under average conditions are everywhere within the range of natural variability. The percentage of re-circulated concentrated seawater by-product under average conditions is only 0.7%. Minimum dilution of the raw concentrate at the shoreline is 190 to 1 (Figure ES-8).

In vertical cross sections through the outfall in the cross-shore and longshore directions, the numerical hydrodynamic model finds that the saline plume emitted from the combined flows of the generating plant cooling water and the concentrated seawater of the desalination plant consists of a higher saline core between the surface and the bottom surrounded by a broad-scale salt wedge feature with weakly elevated salinities. (Salt wedge is a feature common to estuaries and coastal waters near river mouths. It refers to a vertical distribution of salinity in which heavier, higher salinity water forms a wedge-shaped water mass under lighter, lower salinity water). The core is formed in the immediate vicinity of the outfall by a jet of combined effluent discharged vertically upward from the top of the outfall tower. The core typically extends 40-50 meters away from the outfall with salinities of about 50 parts per thousand (ppt) for low flow-case conditions and 38 ppt for average case conditions. Maximum core salinity reaches

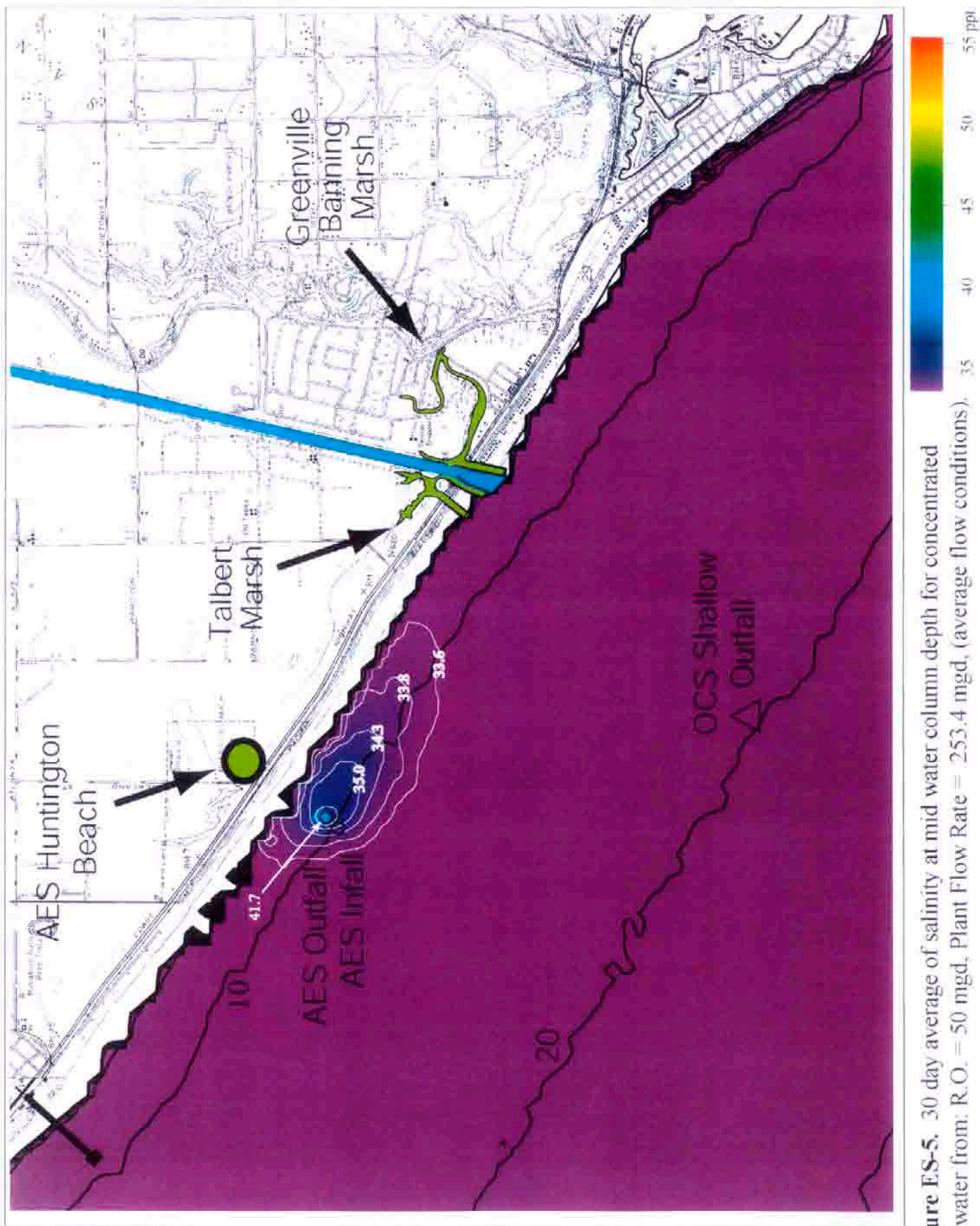


Figure ES-5. 30 day average of salinity at mid water column depth for concentrated sea water from: R.O. = 50 mgd, Plant Flow Rate = 253.4 mgd, (average flow conditions).

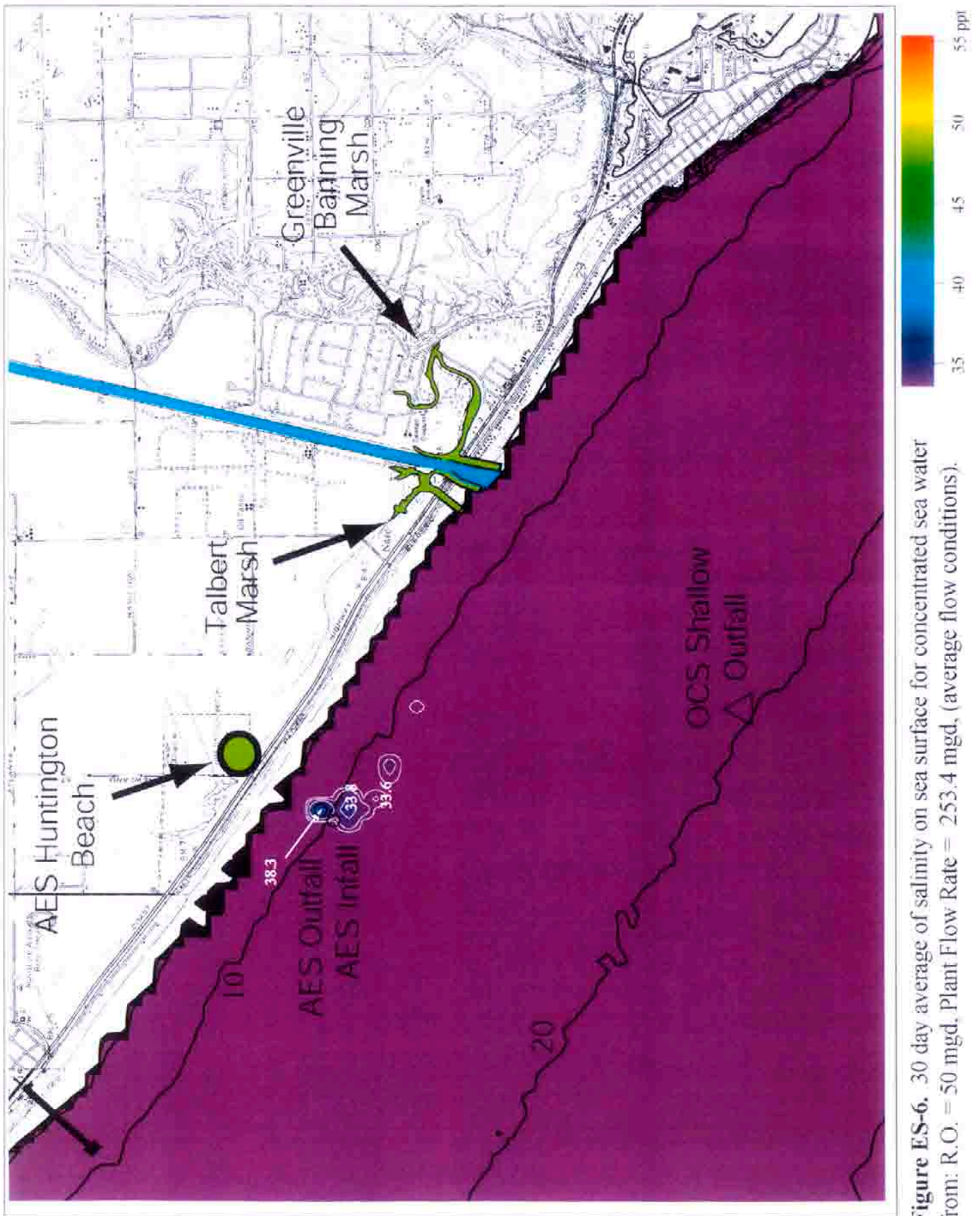


Figure ES-6. 30 day average of salinity on sea surface for concentrated sea water from: R.O. = 50 mgd, Plant Flow Rate = 253.4 mgd, (average flow conditions).

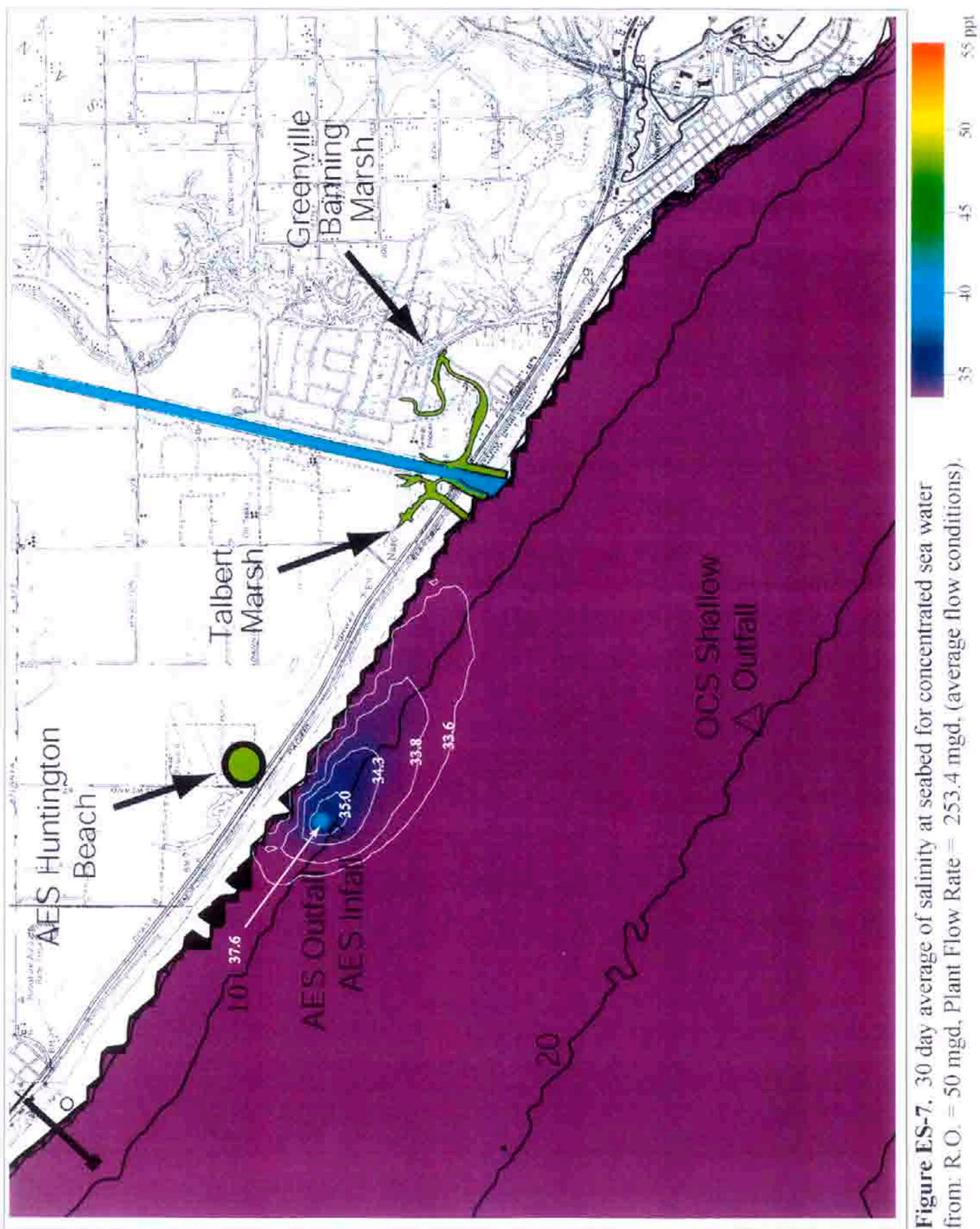


Figure ES-7. 30 day average of salinity at seabed for concentrated sea water from: R.O. = 50 mgd, Plant Flow Rate = 253.4 mgd, (average flow conditions).

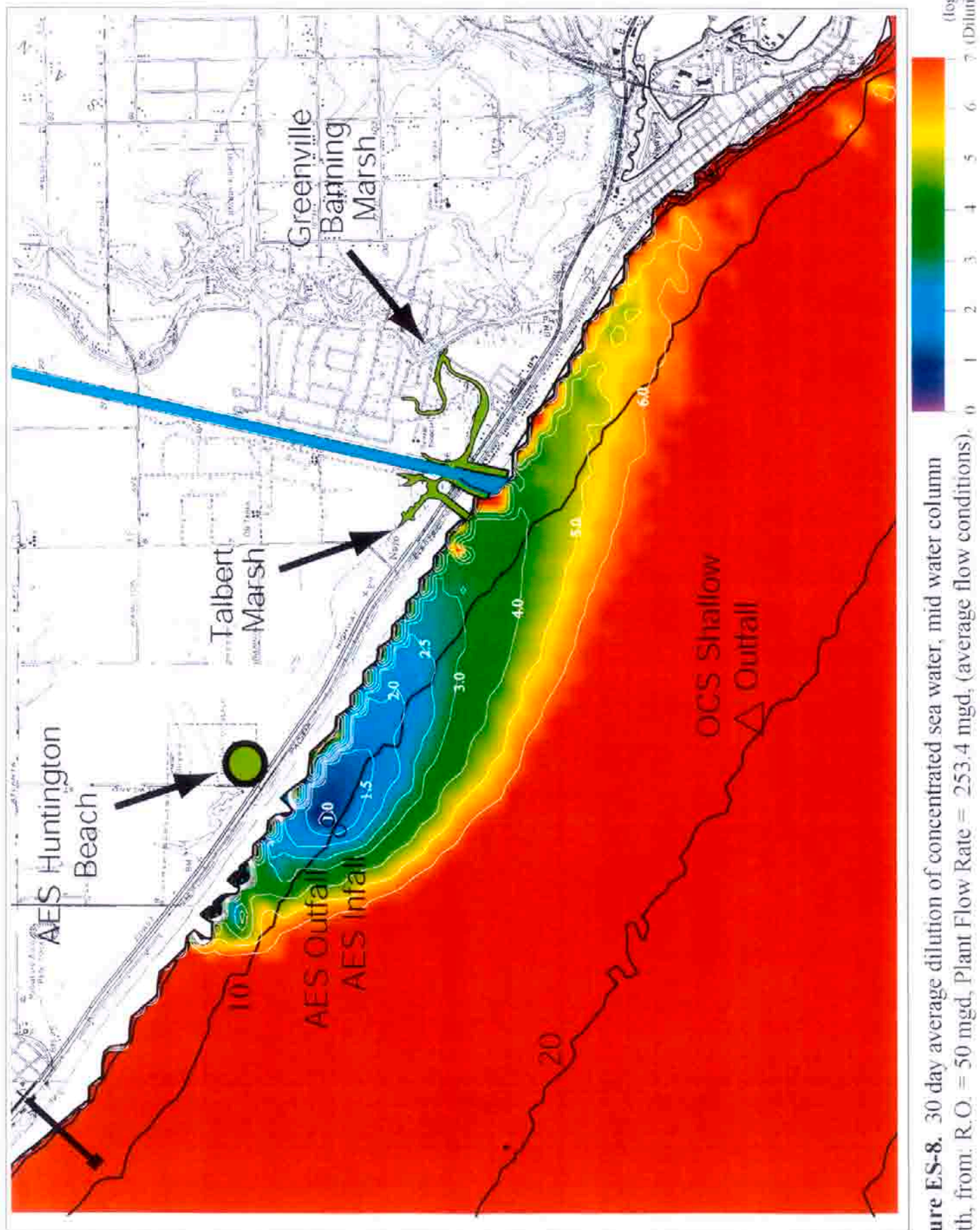


Figure ES-8. 30 day average dilution of concentrated sea water, mid water column depth, from: R.O. = 50 mgd, Plant Flow Rate = 253.4 mgd, (average flow conditions).

55.0 ppt in the discharge jet immediately above the outfall tower for low flow case and 41.7 ppt for average case. Because of density differences the higher salinity water surrounding the core of the plume behaves like a distinct layer comparable to a “salt wedge” in an ocean/estuarine mixing environment. In the salt wedge, salinities vary from a couple to only a fraction of a ppt over ambient mean ocean salinities. Salt wedge salinities for both low flow and average case are within the envelope of natural variability. The salt wedge extends offshore for about 800 meters seaward of the outfall for low flow case and about 600 meters for average case. The total along shore dispersion of the detectable limits of the salt wedge is 2,150 meters for low flow case and 3,000 meters for average case, both with a downdrift bias toward the southeast.

The predominant net current around the outfall is alongshore directed toward the southeast. Organisms drifting with this current will pass through the saline plume and be exposed to elevated salinities for varying periods of time depending on whether they pass through the narrow, high salinity core or the broad-scale salt wedge with its weakly elevated salinities. In a low flow case scenario drifting organisms would be subjected to maximum salinities of the core (53-55 ppt) for at most 7 minutes, but may linger in the salt wedge at 0.1 ppt above ambient ocean salinities for as long as 10 hours (Figure ES-9). Exposure times at salinities 10 % above ambient levels would be 2.7 hours for the low flow case and 30 minutes under average conditions. Exposure to maximum core salinities under average conditions (40- 41.7 ppt) would be no more than 10 minutes while exposure to the weakly elevated salt wedge salinities would be no more than 7 hours.

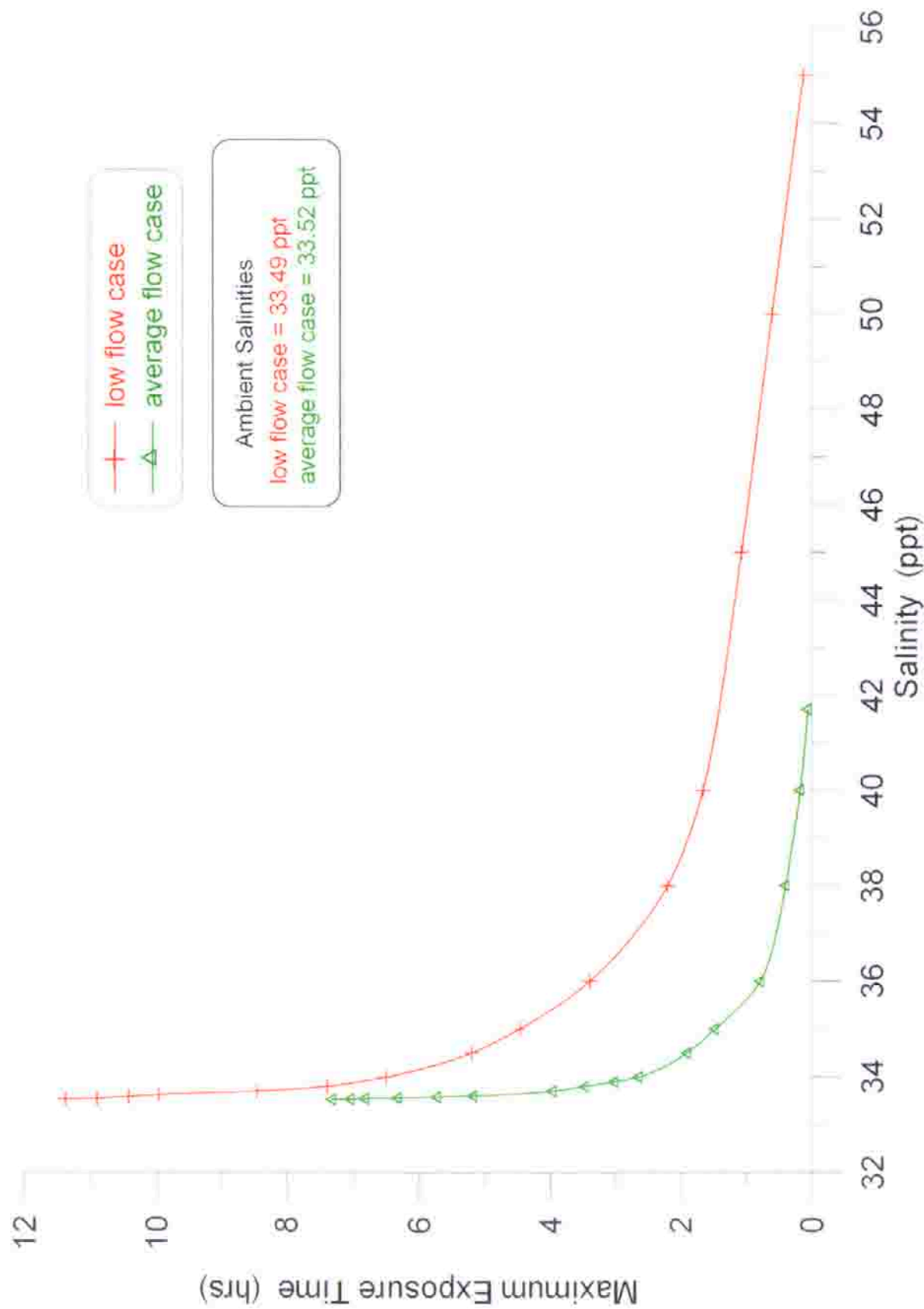


Figure ES-9. Maximum exposure time of a drifting organism passing through the discharge plume of concentrated seawater from the AES Huntington Beach outfall for low flow case conditions (red, plant flow rate = 126.7 mgd) and average case conditions (green, plant flow rate = 253.4 mgd).

In the long-term analysis, the hydrodynamic model solves for 7,523 daily outcomes from the uninterrupted monitoring data of ocean conditions and plant operating conditions that have occurred between 1980 and mid 2000. The objective of this portion of the analysis is to resolve all the intermediate cases that are possible between the low flow and average case event scenarios. In addition, the long term analysis examines the changes to the dispersion of the saline plume resulting from cold water discharges from HBGS occurring during standby mode when the *Delta-T* (ΔT) of the discharge stream is zero. (ΔT is the temperature difference between ocean water and plant discharge).

The modeled long-term outcomes were the result of 20.5 year long continuous time series of daily records for seven controlling operational and environmental inputs. These seven variables may be organized into *boundary conditions* and *forcing functions*. The boundary conditions control the source strength (concentrated sea salts) and background conditions and include: ocean salinity, generating plant flow rates, ocean temperature, and ocean water levels. The period of record from 1980 until July 2000 was the longest period for which an unbroken record of all seven variables could be obtained and wave data was the limiting data base. However, the latter portion of this period was probably atypical from the present operational stand point because the generating station was under going re-fit and equipment modernization. Although there were instances of the plant operating with three and four generating units in the first seven years of the 1980- July 2000 period of record the preponderance of the record shows that the plant seldom supplied other than 2 different flow rates (127.6 or 253.4 mgd) most of the time. This historic 2 mode operational pattern introduced a *bimodal* statistical pattern into the model results (Figure ES-10).

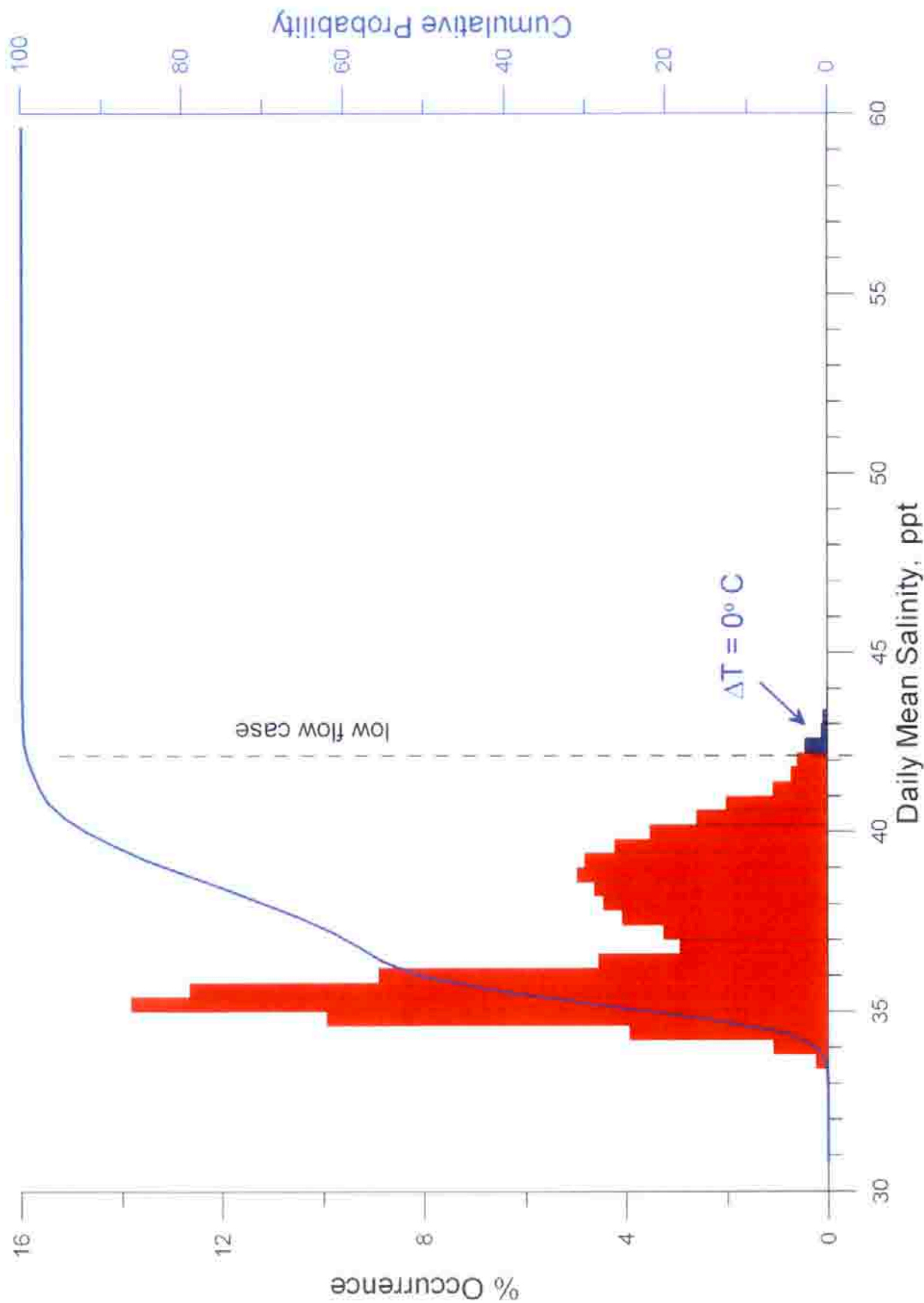


Figure ES-10. Histogram of daily maximum salinity at mid-depth and 150 meters from the AES outfall for desalination production rate of 50 mgd. Percent occurrence based on historic observations of ocean mixing and water mass mass properties, and AES daily plant flow rates, 1980-2000.

Over the 20.5 year simulation period, the combined end-of-pipe salinity was found to vary from a minimum of 37 ppt with all 4 generating units on line, to a maximum of 56.4 ppt for cold water discharges during standby mode ($\Delta T = 0^\circ\text{C}$). The two predominantly recurring peaks in the probability density function for end-of-pipe salinity are centered at 41.6 ppt and 55.2 ppt, consistent with the average and low flow case values, respectively. The results are summarized in Table ES-2. The high salinity peak (low-flow rate peak) was attributed to the operation of only one generating unit, while the lower salinity peak (mid-flow rate peak) resulted from operation of two generating units. The salinities of the low-flow rate peak start out at 55 ppt in the water column above the outfall and fall off to 39 ppt at 150 meters away (the approximate outer limit of the 10 % salinity anomaly), accounting for between 42% and 48% of the modeled outcomes (Figure ES-10). On the sea floor, the low-flow rate operational condition (one generating unit) produces salinities that typically range from 47.5 ppt at the foot of the outfall to 37.0 ppt at 150 meters from the outfall (Figure ES-11) having the same recurrence rates as found in the water column. During times when two generating units (or more) were operated (mid-flow rate peak), salinities varied in the water column from 41.6 ppt at the outfall to 35.2 ppt at 150 meters away with a recurrence rate of 52 % to 58%. On the sea floor, 2 generating unit operation (mid-flow rates) causes salinity to range from 38.6 ppt at the foot of the outfall to 34.8 ppt at 150 meters away with the same recurrence rate as for the water column.

Beyond 150 meters from the outfall, the probability density distribution for the discharge plume salinities no longer exhibits bi-modal character. Because the salinity contrast with the ambient water is greater for the low-flow rate peak, it becomes smeared by higher mixing rates promoted along stronger concentration

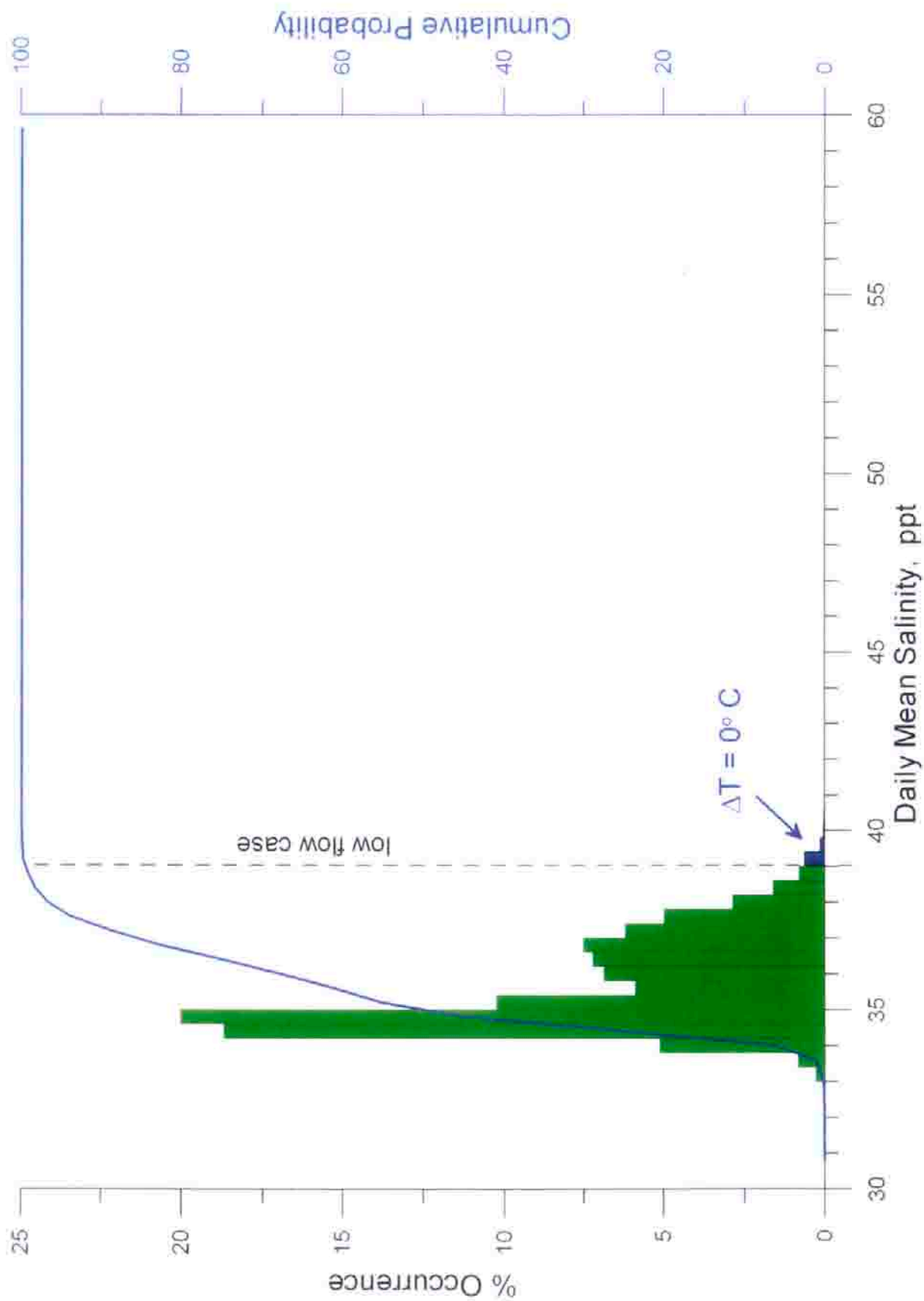


Figure ES-11. Histogram of daily maximum salinity at the bottom and 150 meters from the AES outfall for desalination production rate of 50 mgd. Percent occurrence based on historic observations of ocean mixing and water mass mass properties, and AES daily plant flow rates, 1980-2000.

Table ES-2. Generalized Salinity Plume from 7,523 outcomes, 1980- July 2000

Distance from Outfall (m)	One Generating Unit ^a		Two Generating Units	
	Characteristic Salinity (ppt)	Recurrence Rate (%)	Characteristic Salinity (ppt)	Recurrence Rate (%)
0 Mid-depth	55.2	48%	41.6	52%
0 Bottom	47.5	48%	38.6	52%
50 Mid-depth	45.4	48%	37.4	52%
50 Bottom	40.0	48%	36.0	52%
100 Mid-depth	43.0	47%	36.6	53%
100 Bottom	37.8	43%	35.0	57%
150 Mid-depth	39.0	42%	35.2	58%
150 Bottom	37.0	42%	34.8	58%
300 Mid-depth	36.2	40%	34.6	60%
300 Bottom	36.0	40%	34.6	60%
500 Mid-depth	35.0	25%	34.0	75%
500 Bottom	35.2	30%	34.4	70%
1000 Mid-depth	34.0	18%	33.6	82%
1000 Bottom	34.2	18%	33.6	82%
2000 Mid-depth	33.5	100%	33.5	100%
2000 Bottom	33.5	100%	33.5	100%

^a includes cold water discharges, $T = 0^{\circ}\text{C}$

^b red indicates values associated with bimodal probability density distributions

^c green indicates values associated with uni-modal probability density distributions

gradients and it merges with the mid-flow rate peak in the distribution to form an asymmetric uni-modal distribution. The characteristics of this distribution are a mid-flow rate peak at lower salinities with a low-flow rate shoulder extending into higher salinity ranges. Salinities in the mid-flow rate peak of this distribution range from 34.6 ppt at 300 meters from the outfall and decay down to ambient ocean salinity at 2,000 meters from the outfall with a recurrence rate of 60% to 82% before reaching ambient ocean salinity levels. Salinities are only a fraction of a ppt greater on the bottom than in the water column over this range. For the low-flow rate shoulder of the probability density distribution, salinities vary from 36.2 ppt at a distance of 300 meters from the outfall, decaying to ambient salinity 2,000 meters away, with recurrence rate of 40 % down to 18% before reaching ambient ocean salinity levels.

The bi-modal statistical bias imprinted on the model results by the historical plant flow rates throughout the re-fitting period appears to exhibit itself only in the nearfield of the outfall. The recurrence pattern of two distinct outcomes of approximately equal likelihood, one of high salinity and the other of more moderate salinity, is only apparent in the inner and outer core of the discharge plume, extending out to about 150 meters from the out fall (Figures ES-10 & ES-11). This is an area of about 17.5 acres. In the salt wedge portion of the plume from 500 meters out and beyond, operational patterns do not appear to alter the results by more than about 1 ppt, with salinities occurring between 34 ppt and 35 ppt or less regardless of historic operational tendencies. In the intermediate zone between 150 and 500 meters from the outfall, operational patterns cause salinity variations between 36 ppt or about 34.5 ppt. Such variations mean the difference between exceeding the upper limit of the natural ocean salinity range for this location, or not.

Among the 7,523 model solutions derived from the historic database prior to re-powering the generating station (1980-2000), there were no outcomes producing salinities in the receiving water that exceeded those of the low flow event scenario, so long as electrical power was being generated ($\Delta T > 0$ °C). However, a relatively rare subset of these 7,523 solutions involved standby mode occurrences when the plant was spinning at least 2 circulation pumps but not generating electricity ($\Delta T = 0$ °C). These standby mode outcomes produced salinities in the receiving waters that exceeded the low flow event scenario by no more than 1 ppt, but accounted for less than 1% of all possible outcomes (Figures ES-10 & ES-11) involving adequate flow to produce 50 mgd of desalinated product water. Therefore, the low flow event scenario as characterized in ES-1 through ES-4 and in Table ES-1 is a reasonable representation of a long-term worst case when the generating station is producing power.

Dilution and Dispersion After Completion of HBGS Re-Powering:

After completion of the re-powering of the AES Huntington Beach Generating Station in late 2001, higher generation levels and plant flow rates have been maintained that exceed those observed for the late 1980's and throughout the 90's. To determine the implications of this shift in operational patterns on the probable dispersion and dilution of sea salts from the desalination plant, the long-term analysis methodology was repeated for the post re-powering period, 2 January 2002 - 30 July 2003. The dilution results for the post re-powering period are summarized in Table ES-3 with salinity probability density functions shown in Figures ES-12 and ES-13 at 150 meters away from the outfall. Comparing Figures ES-12 and ES-13 with Figure ES-10 with ES-11 we find that the low flow rate

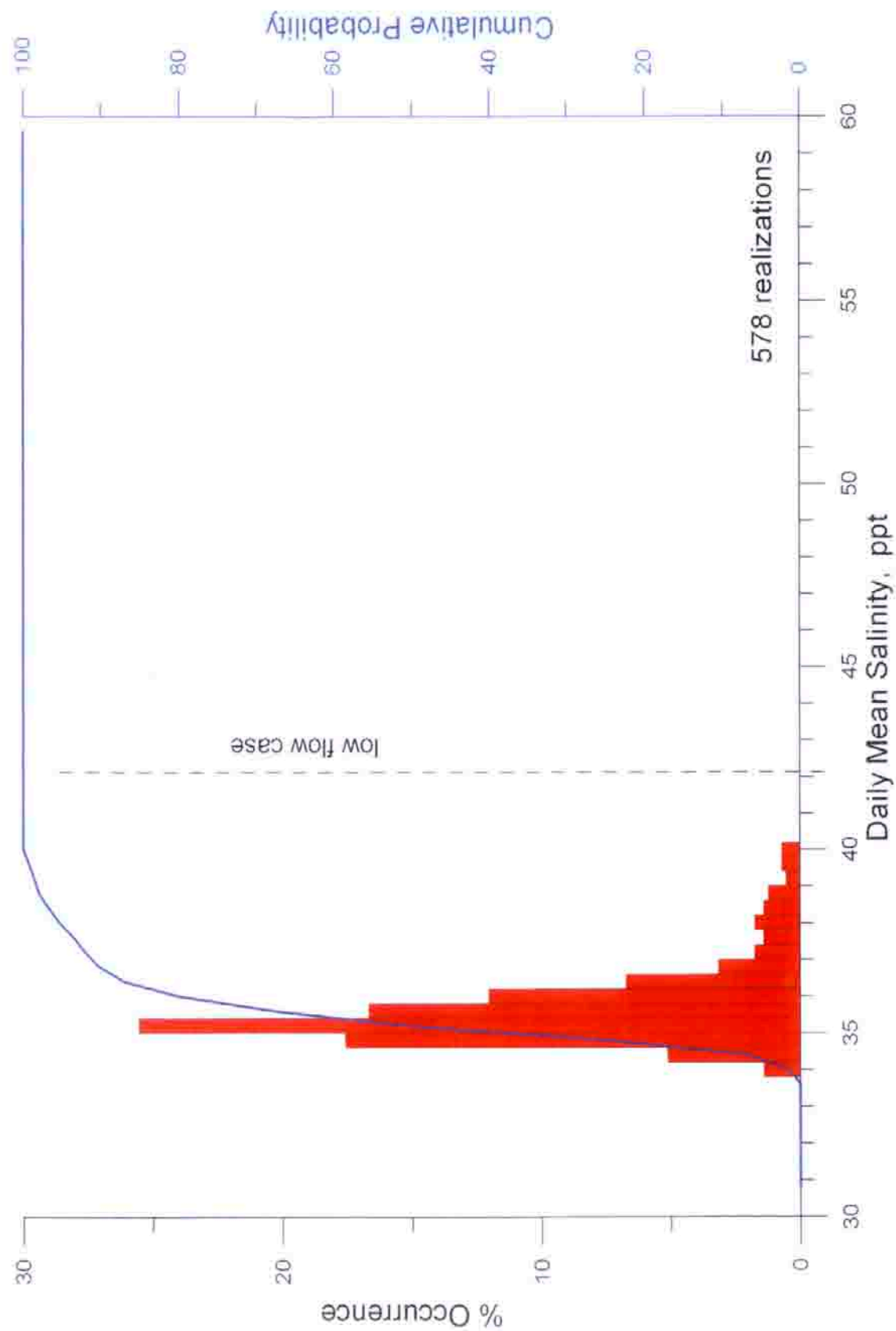


Figure ES-12. Histogram of daily maximum salinity at mid-depth and 150 meters from the AES outfall for desalination production rate of 50 mgd. Percent occurrence based on historic observations of ocean mixing and water mass properties, and AES daily plant flow rates for the post re-powering period, 1 Jan 2002 - 30 July 2003.

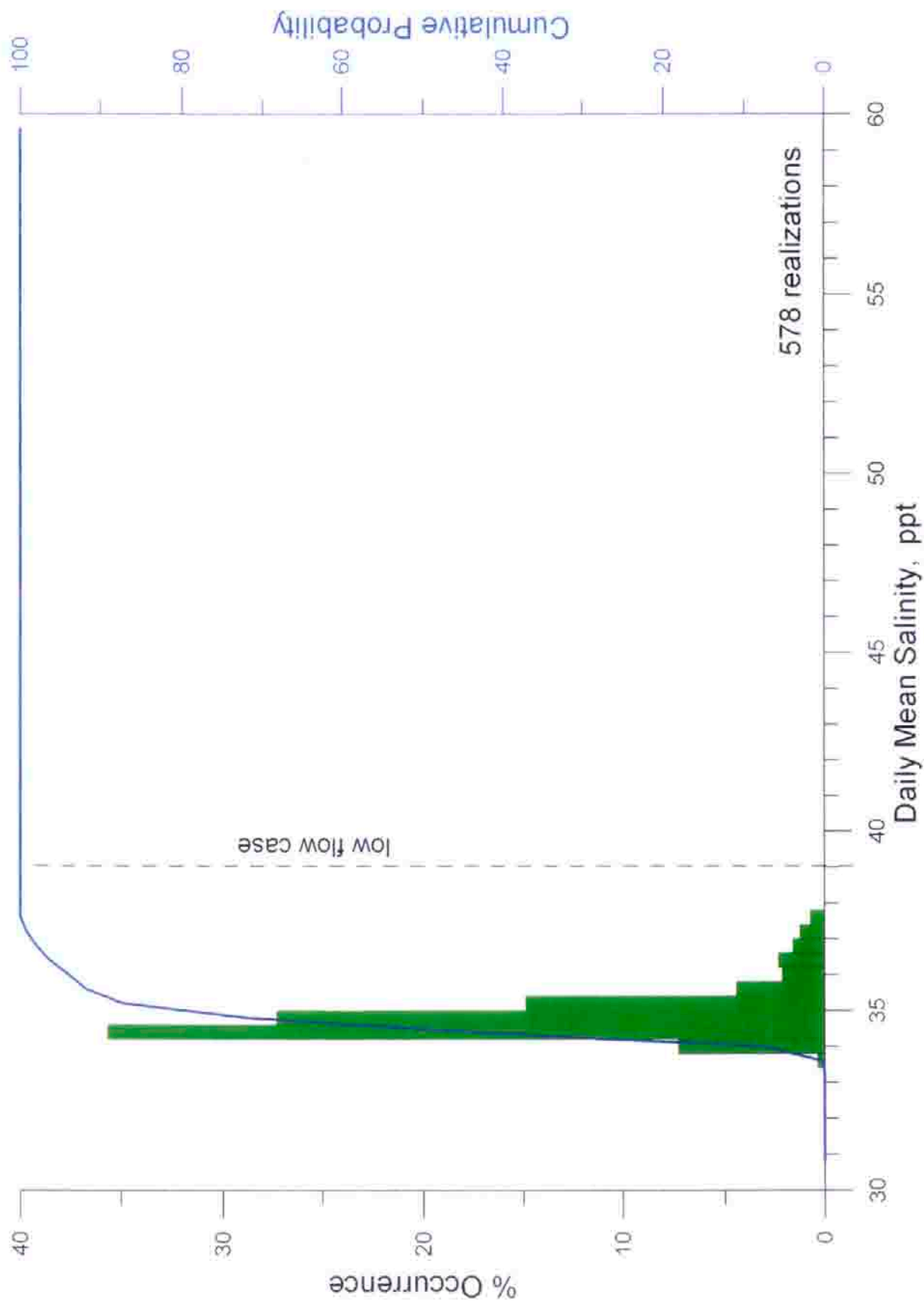


Figure ES-13. Histogram of daily maximum salinity at the bottom and 150 meters from the AES outfall for desalination production rate of 50 mgd. Percent occurrence based on historic observations of ocean mixing and water mass mass properties, and AES daily plant flow rates for the post re-powering period, 1 Jan 2002 - 30 July 2003.

Table ES-3. Generalized Salinity Plume from 578 outcomes, January 02- July 03

Distance from Outfall (m)	Low Flow Rate Condition ^a		Nominal Flow Rate Condition	
	Characteristic Salinity (ppt)	Recurrence Rate (%)	Characteristic Salinity (ppt)	Recurrence Rate (%)
0 Mid-depth	55.2	9%	43.0	91%
0 Bottom	47.5	9%	39.0	91%
50 Mid-depth	45.4	9%	38.0	91%
50 Bottom	40.0	9%	35.0	91%
100 Mid-depth	42.8	8%	37.4	92%
100 Bottom	37.8	6%	35.6	94%
150 Mid-depth	38.0	6%	35.4	94%
150 Bottom	37.2	6%	35.2	94%
300 Mid-depth	36.0	3%	34.6	97%
300 Bottom	36.0	3%	34.6	97%
500 Mid-depth	35.0	1%	34.0	99%
500 Bottom	35.2	1%	34.2	99%
1000 Mid-depth	33.6	100%	33.6	100%
1000 Bottom	33.8	100%	33.8	100%
2000 Mid-depth	33.5	100%	33.5	100%
2000 Bottom	33.5	100%	33.5	100%

^a includes all operating conditions pumping 126.7 mgd or less

^b red indicates values associated with bimodal probability density distributions

^c green indicates values associated with uni-modal probability density distributions

peak at is greatly reduced and represents only about 6% of the 578 daily outcomes during the post re-powering period. After re-powering, the histogram distribution at 150 meters from the outfall is predominantly unimodal and centered on 35 ppt with 92% of the outcomes giving salinities elevated less than the 10 % above ambient. Beyond 150 meters away from the outfall, no outcomes from the 7 controlling variables during the post re-powering period give rise to salinities exceeding 40 ppt. Furthermore, no outcomes at any distance from the outfall during post re-powering conditions produce salinities in the receiving waters as high as the low flow event scenario in ES-1 through ES-4 and Table ES-1. If the flow rate history of the generating station during the post re-powering period (January 2002- July 2003) is representative of the foreseeable future, then salinities in the receiving waters due to the low flow event scenario are unlikely to ever be exceeded.

Source Water Quality at HBGS Intakes

In the remaining sections of this report (Sections 6-9) a hydrodynamic modeling study was conducted to determine if storm water and waste water are possible constituents of the source water at the intake to desalination plant. The storm water analysis considered flood discharges of the Santa Ana River and Talbert Channel watersheds and was also extended to include computations of recirculation of generating plant effluent between the offshore outfall and in-fall. Analysis of source water make-up further considered the dispersion of the wastefield from the 120" diameter deep ocean outfall located offshore of the Santa Ana River and operated by Orange County Sanitation District (OCSD).

The source water quality modeling was performed for a nearshore domain surrounding the AES Huntington Beach plant which extends alongshore from Seal Beach to Crystal Cove State Beach. The model was initialized for three sets of

extreme environmental conditions to evaluate low flow case effects: 1) a wet weather El Niño winter condition to determine the quantity of ocean water and storm water from the Santa Ana River and the Talbert Channel reaching the AES intakes; and, 2) a summer El Niño condition when net transport by waves and currents flows northward to determine if the OCSD wastefield and Talbert Marsh tidal discharges can reach the AES intakes. The El Niño modeling scenarios provide a reasonable prediction of the maximum quantity of storm water runoff and OCSD wastefield reaching the AES intakes. The conclusions of the source water quality analysis are as follows:

Based on representative and historical data, the investigation provided a reasonable estimate of the likely mix of seawater and storm water at the AES Huntington Beach Generating Plant intakes during a period with extremely high storm runoff from both the Santa Ana River and Talbert Channel:

Over the 24-hour extreme runoff period, source water drawn at the infall is comprised of 0.0003% storm water from the Santa Ana River and Talbert Channel (Figure ES-14). Dilution of Santa Ana River and Talbert Channel storm water is 316 thousand to 1 at the depth of the infall velocity cap.

Over the seven-day extreme runoff period spanning the peak flood runoff event, source water drawn at the infall is comprised of only 0.0001% storm water from the Santa Ana River and Talbert Channel. Santa Ana River and Talbert Channel storm water is diluted to 1 million to 1 at the depth of the infall velocity cap.

For the duration of the 30-day extreme runoff period, the average make-up of the source water reaching the intakes would contain no detectable amount of

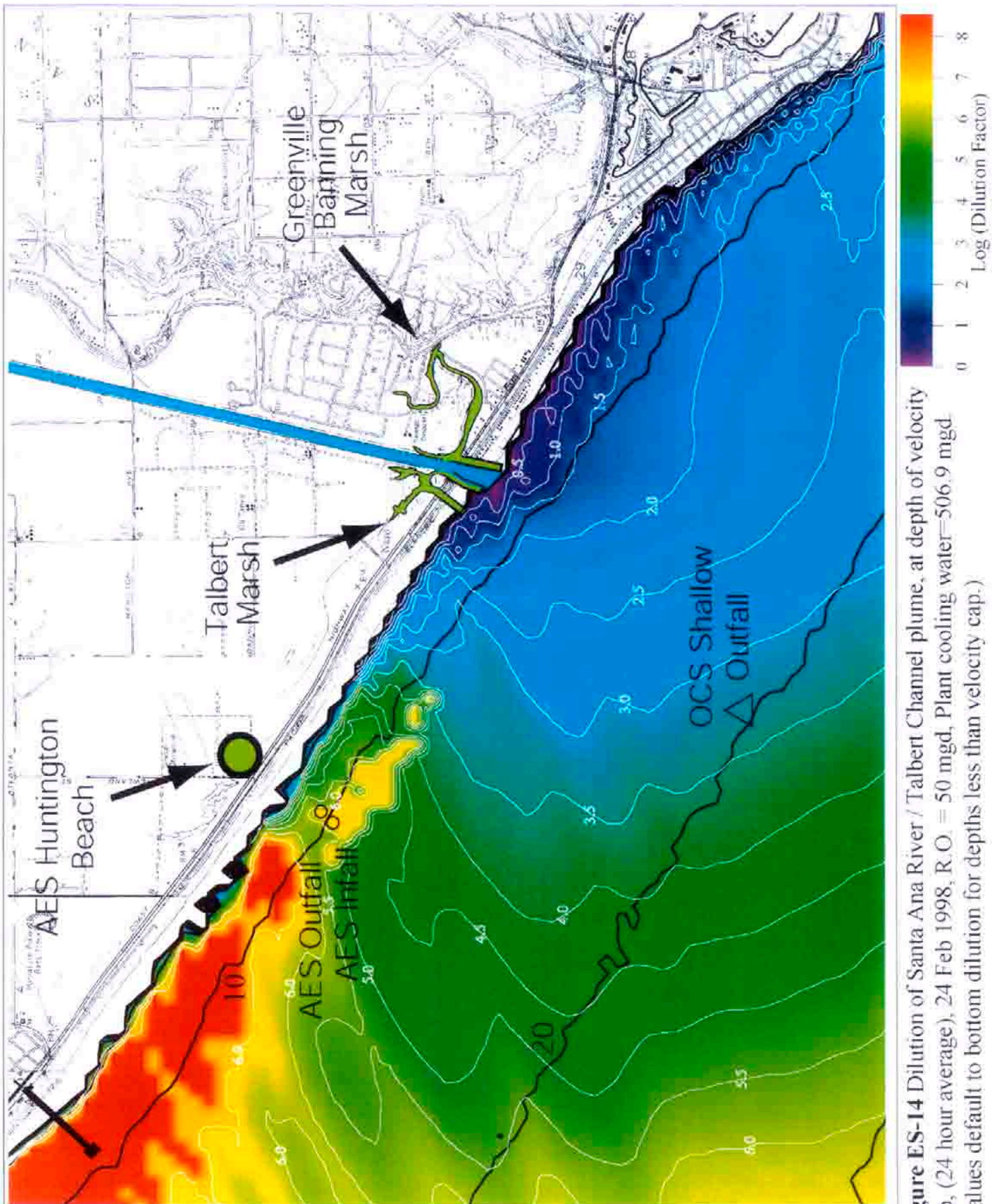


Figure ES-14 Dilution of Santa Ana River / Talbert Channel plume, at depth of velocity cap, (24 hour average), 24 Feb 1998, R.O. = 50 mgd, Plant cooling water=506.9 mgd. (Values default to bottom dilution for depths less than velocity cap.)

storm water (Figure ES-15). Dilution of Santa Ana River and Talbert Channel storm water at the infall velocity cap is 10 million to 1.

For sustained high runoff and low flow operational conditions over a 7-day period of extreme wet weather, only a negligible amount of generating station storm water is re-circulated from the outfall to the infall. At most, 0.3% of the combined plant discharge is recirculated of which no more than 2.1% can be plant storm water based on NPDES permit restrictions. Hence plant storm water is at most 0.007% of the source water in a low flow case scenario (Figure ES-16). For maximum power plant generating levels, only 0.0004% of the source water can be expected to be recirculated plant storm water and about 0.003% for normal power generating levels. At all generation levels, the addition of the concentrated seawater by-product to the discharge of the AES power generating plant eliminates the positive buoyancy of the thermal plume and thereby reduces the size and temperature anomaly of the thermal footprint in the offshore waters. On average, the addition of concentrated sea water by-product to the thermal effluent of the generating station will reduce the size of the thermal plume by about 46%.

For low flow case summer El Niño conditions during flood tide (when typical coastal transport is most likely to reverse and flow northward), the wastefield of the OCSD deep outfall was found to disperse no closer than the 15 meter depth contour off Huntington Beach, about 2 km offshore (Figure ES-17). Dilution of the wastefield at the intake to AES Huntington Beach was calculated at 1 part per thirty million, indicating that even without the OCSD Disinfection Resolution of 2002, no total coliforms from the wastefield would be detectable in the source water. Similar calculations on the dispersion of tidal flux from the Talbert Marsh during spring tides found dilution of marsh waters to be 1 part per

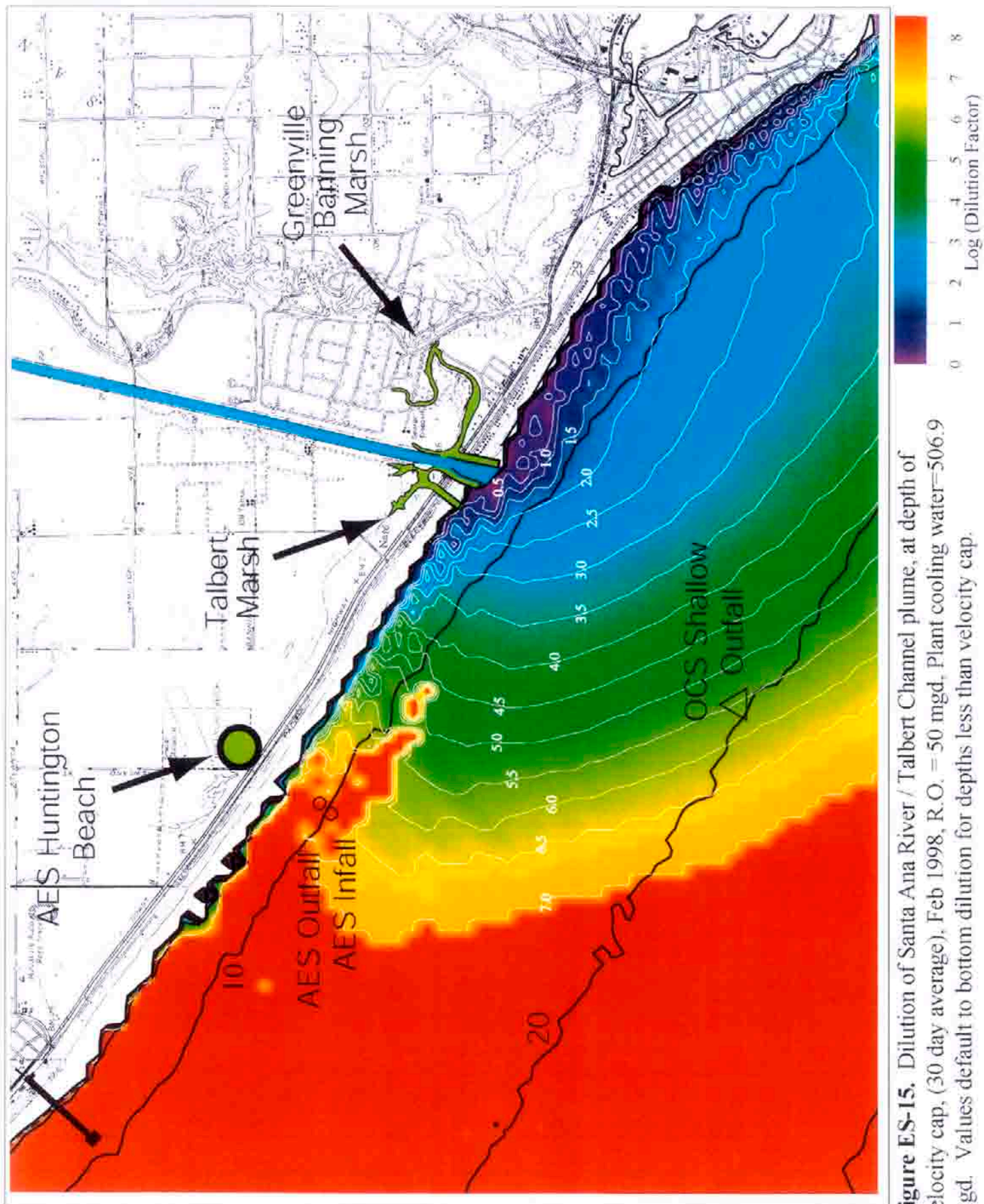


Figure ES-15. Dilution of Santa Ana River / Talbert Channel plume, at depth of velocity cap, (30 day average), Feb 1998, R.O. = 50 mgd, Plant cooling water=506.9 mgd. Values default to bottom dilution for depths less than velocity cap.

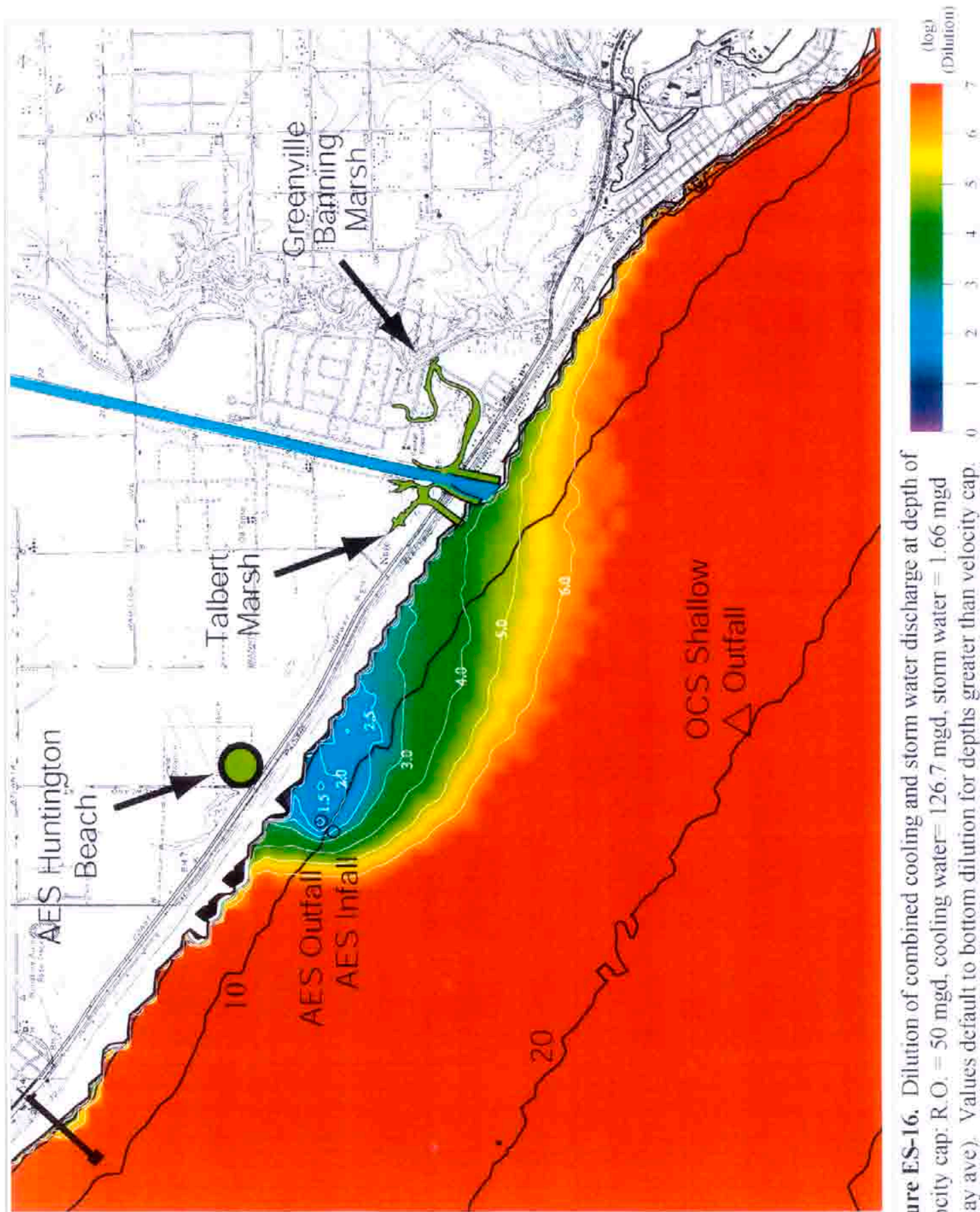


Figure ES-16. Dilution of combined cooling and storm water discharge at depth of velocity cap: R.O. = 50 mgd, cooling water= 126.7 mgd, storm water = 1.66 mgd (7 day ave). Values default to bottom dilution for depths greater than velocity cap.

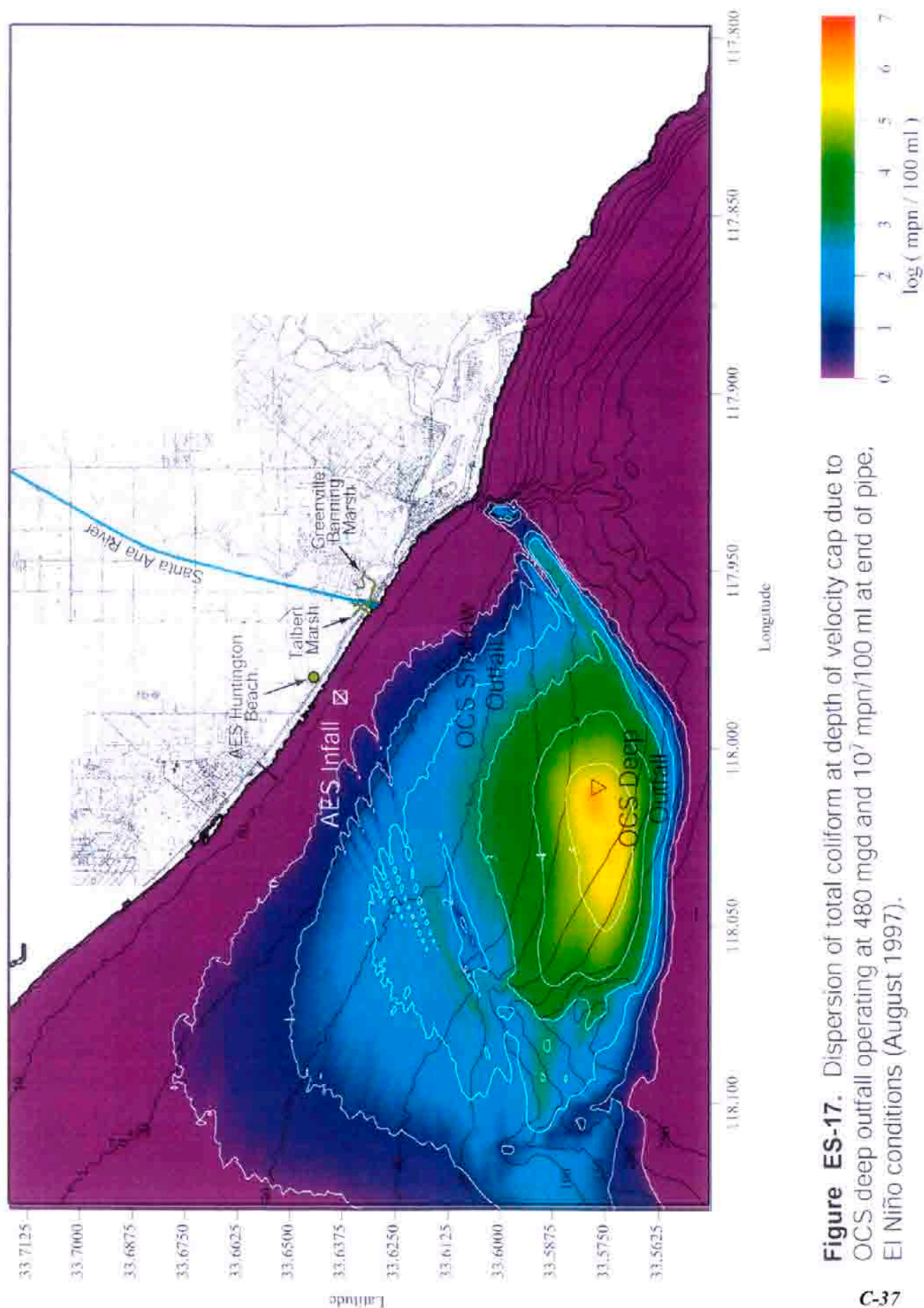


Figure ES-17. Dispersion of total coliform at depth of velocity cap due to OCS deep outfall operating at 480 mgd and 10^7 mpn/100 ml at end of pipe, El Niño conditions (August 1997).

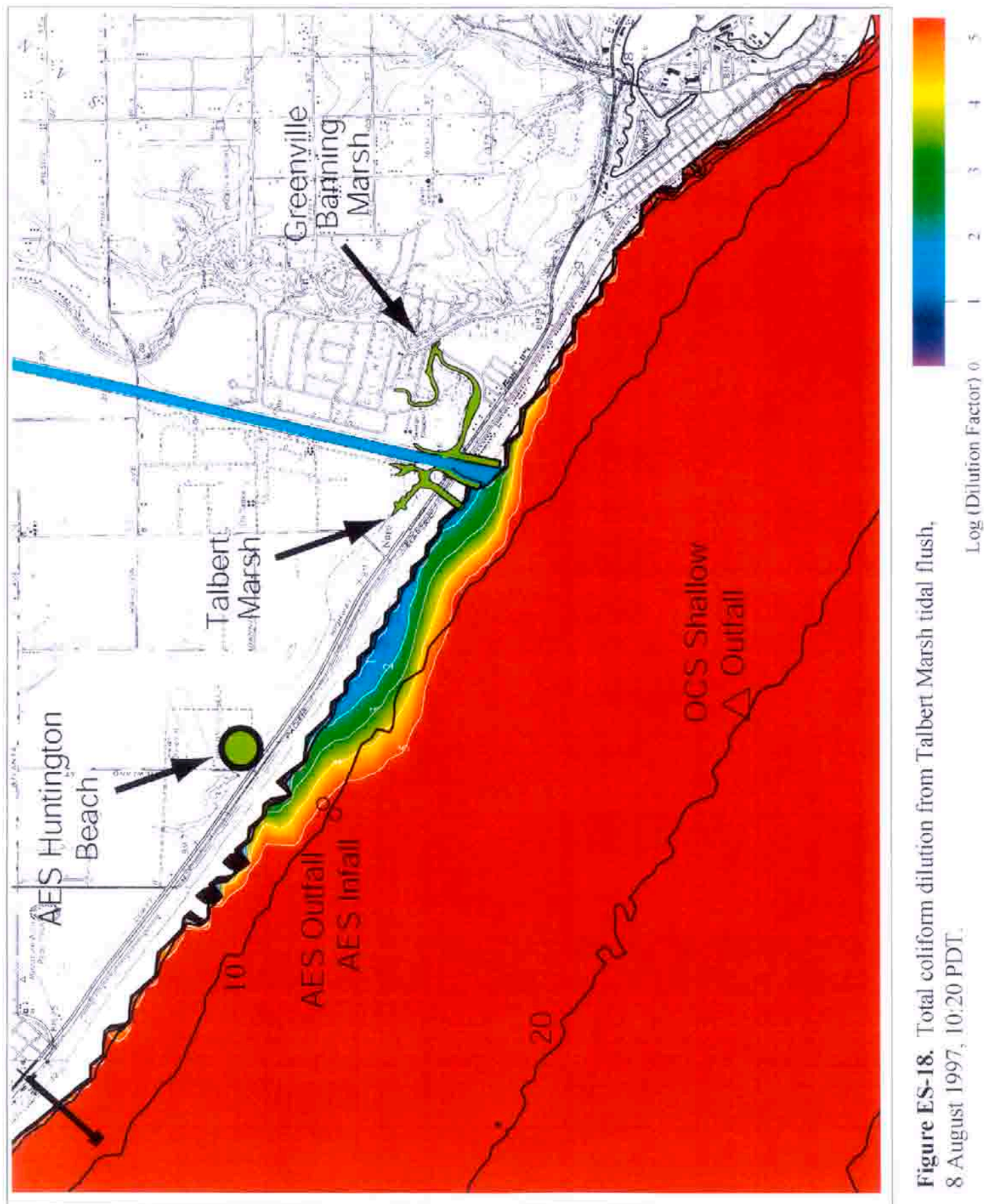


Figure ES-18. Total coliform dilution from Talbert Marsh tidal flush, 8 August 1997, 10:20 PDT.

one hundred thousand at the intake, indicating that marsh coliforms would be non-detectable in source water (Figure ES-18).

SECTION 1: INTRODUCTION

1) Introduction

A) Physical Setting

This study investigates basic water quality issues related to the proposed Huntington Beach Desalination Project to be sited in the southeastern portion of the City of Huntington Beach adjacent to the AES Huntington Beach Generating Station (HBGS). The proposed desalination project would be connected to the existing cooling water circulation system of the generating station. Physical specifications for the cooling water infall and outfall are listed in the NPDES permit #CA 0001163 (CRWQCB, 1993). The NPDES permit does not give a latitude and longitude for the infall location. Consequently, Poseidon Resources contracted an offshore surveying company (Tenera Environmental) to locate the infall using sidescan sonar and Trimble Geoexplorer differential GPS to obtain a precise fix on the infall location. Based on these survey techniques, the cooling water infall was determined to be located at latitude 33° 38' 18.8" N, longitude 117° 59' 01" W, (see Tenera, 2004), approximately 1,840 ft (561 m) offshore from the mean high tide line (Figure 1.1). Water is drawn through a velocity cap atop a rectangular infall tower (Figure 1.2) located 15.8 feet (4.8 meters) above the ocean floor where the total water depth 34.1 feet (10.4 meters) below mean sea level (MSL), based on National Ocean Survey digital bathymetry. The maximum mean water velocity at the inlet to the conduit is 2.0 feet per second (fps) (0.6 m/sec). Intake water velocity at the mean lower-low tide elevation above the velocity cap is nil.

The cooling water discharges from a seafloor structure identical in dimension to the infall tower except for the absence of a velocity cap (Figure 1.2). Instead, the discharge tower is capped with a debris screen having a 12" x 18"

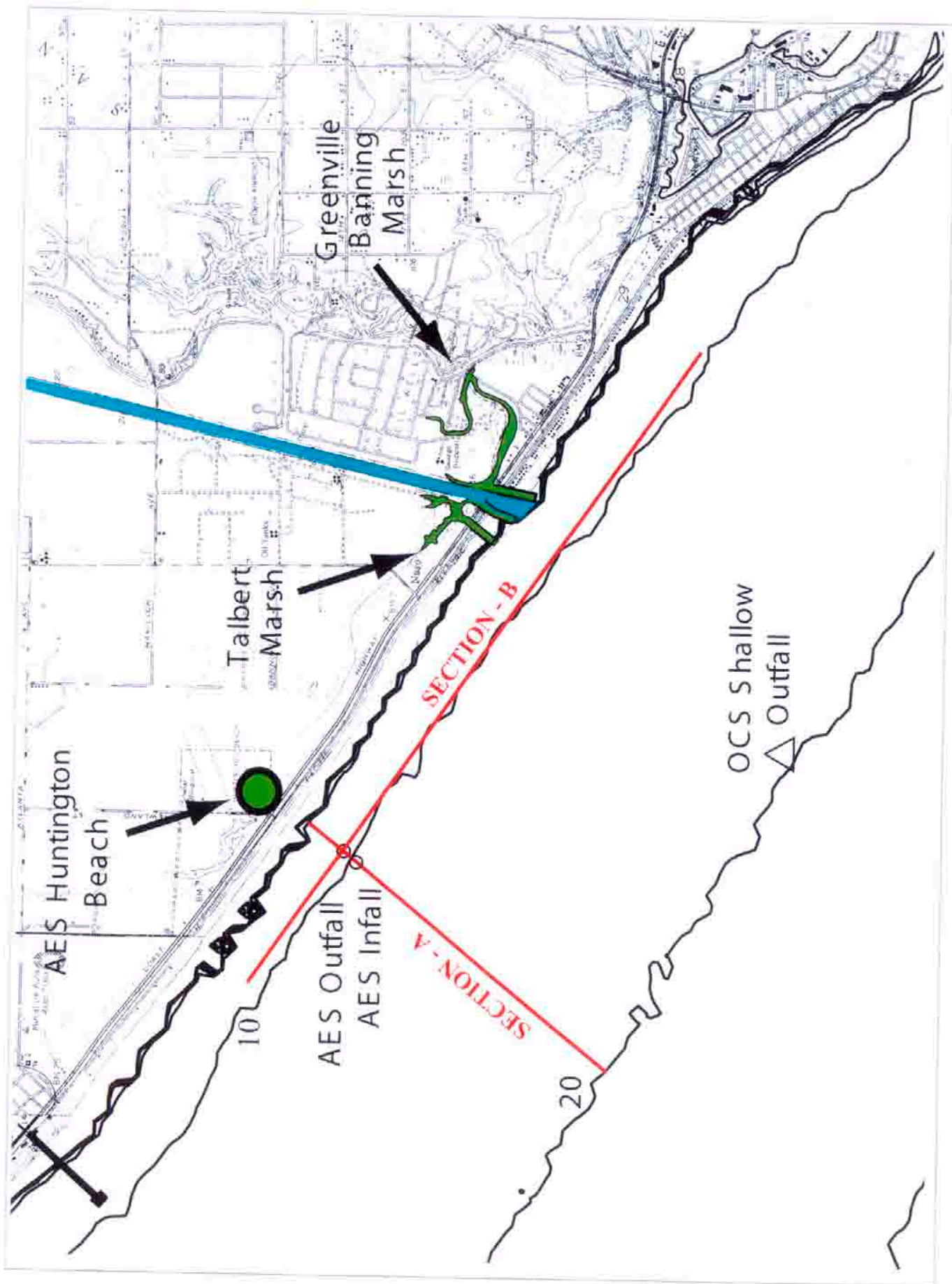


Figure 1.1. Location map for salinity profiles of source water and dilution modeling.

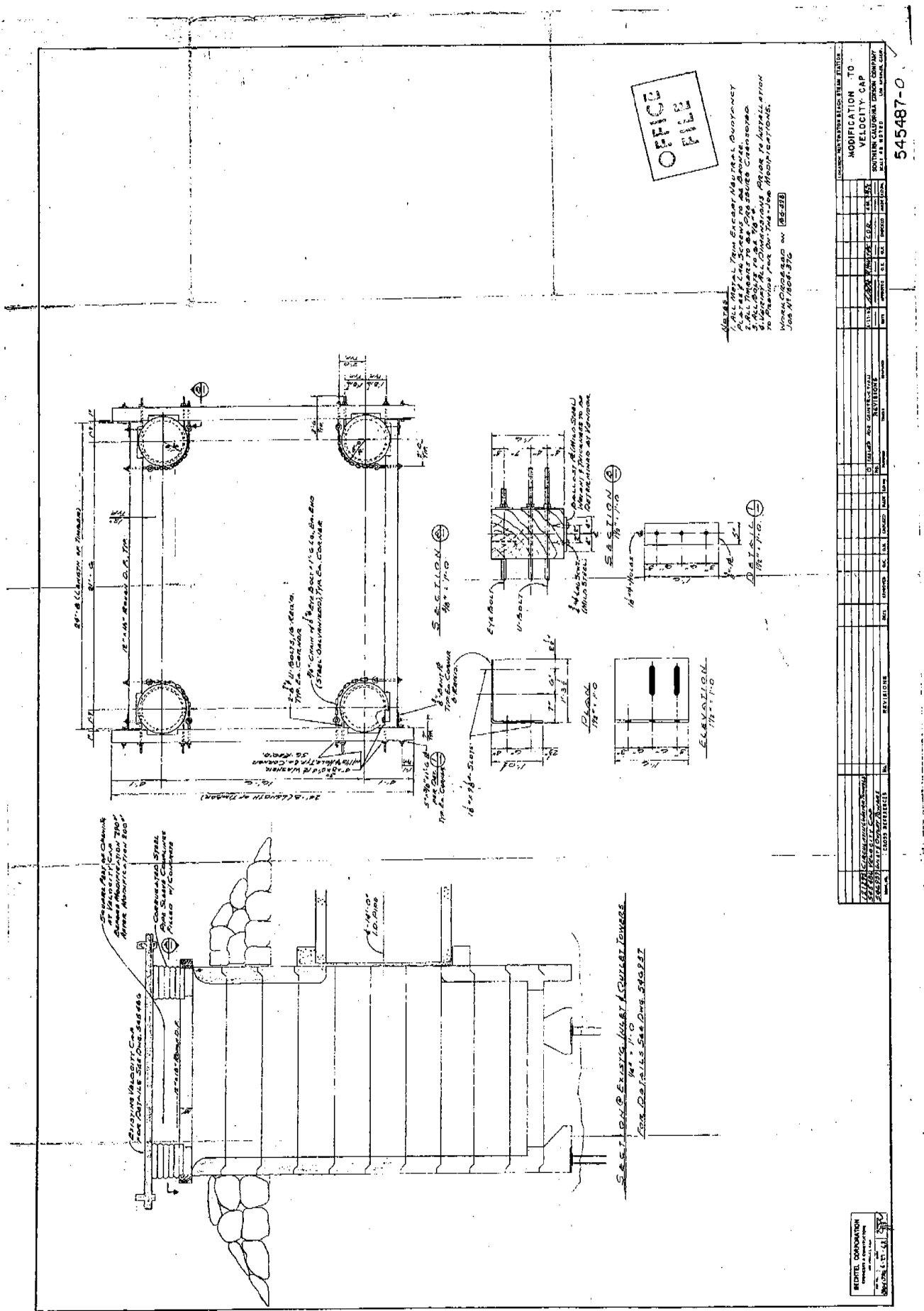


Figure 1.2 Mechanical drawing of infall and outfall tower, AES Huntington Beach Power Plant. Note, velocity cap on outfall tower replaced with 12" x 18" mesh screen constructed of 1" x 3" flatbar.

mesh constructed from 1" x 3" flat bar. The discharge tower is located at latitude 1.1 33° 38' 19" N, longitude 117° 58' 57" W, (Figure 1.1). The outfall terminates approximately 1,500 feet (457 meters) offshore where the seabed is 27.9 feet (8.5 meters) below mean sea level, based on National Ocean Survey digital bathymetry. The certified maximum plant flow rate is 516 million gallons per day (mgd). Discharges to the outfall consist almost entirely of condenser cooling water (with a maximum rated flow rate after re-powering of 507 mgd). A small amount of in-plant waste streams are discharged into the condenser cooling water. The maximum daily discharge of in-plant waste streams (including plant storm water) certified under the NPDES permit is 1.66 mgd, or 0.3% of the certified maximum discharge. Except during storm events, the daily discharge of in-plant waste streams is typically 0.1 mgd. The NPDES monitoring data on plant discharges for 1998, 1999 and 2000 are contained in Appendix A and show that the maximum daily discharge of in-plant waste streams was 0.73 mgd, occurring during February 1998. These in-plant waste streams contain oil and grease residues limited and monitored under the terms of the NPDES permit, plus suspended solids from the storm water runoff of the generating station's impervious surfaces.

Because the plant in-fall is only 340 ft (103.5 m) seaward of the plant outfall, an operational concern of the desalination proposal is the potential for re-circulation of the in-plant waste stream through the plant in-fall. A mitigating physical feature for this re-circulation concern is the configuration of the existing in-fall structure (Figure 1.2) which draws in water from approximately the middle of the water column where slightly more than 10 meters of local water depth is available for dilution (Figure 1.1). The addition of concentrated seawater by-product to the waste stream will render it denser than ambient seawater, causing it

to sink below the depth of the velocity cap on the infall tower (Figure 1.2). These physical processes pertaining to re-circulation of the combined discharge of the generating station and desalination plant are studied in Sections 4 and 6 by means of numerical hydrodynamic modeling techniques.

Approximately 9,000 ft (2.7 km) from the infall to AES Huntington Beach is the mouth of the Santa Ana River and adjacent Talbert Channel (Figure 1.1). The Santa Ana River has a drainage area of about 4,400 km², much of which is comprised of impervious urban surfaces that produce daily mean discharges of storm water as high as 8,000 cubic ft per second (cfs). The Santa Ana River also drains the adjacent Greenville Banning Marsh through a diversion channel (Figure 1.3). The Talbert Channel located about 400 m upcoast of the Santa Ana River mouth drains the Talbert Marsh into which the Huntington Beach Channel discharges storm water from the City of Huntington Beach through a system of storm drains and pumping stations. Therefore the proximity of these combined sources of storm water to the AES infall present a potential water quality concern for the source water which a desalination plant would ingest. These concerns are evaluated in Sections 7 and 8 of this study as well as Archibald (2002, 2004).

The technical approach used to evaluate the scenarios for these re-circulation and dilution issues involved the use of hydrodynamic transport models driven by historic wave, current and river flow rate data for known events. The production of concentrated seawater by-product by the proposed desalination plant was overlaid on these events to determine the potential range of variability in dilution and re-circulation outcomes.

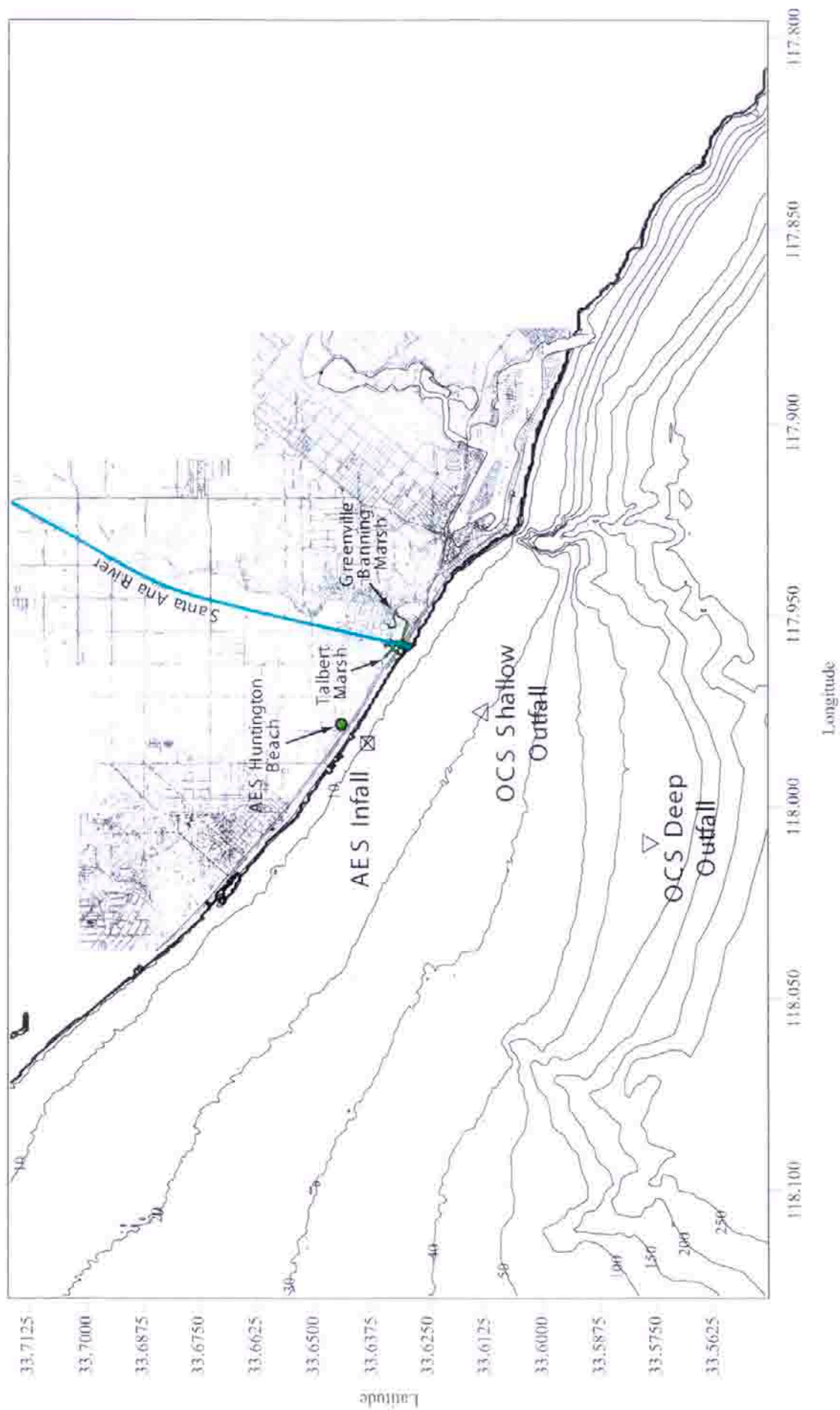


Figure 1.3. Location map for source-water modeling analysis due to fluxes from farfield sources.

B) Climate Variations and Fresh Water Supplies

The California coast is subject to climate cycles of about 20-30 years duration known as the Pacific/ North American pattern (for atmospheric pressure) or the Pacific Decadal Oscillation (for sea surface temperature). A dry period extended from about 1945-1977, followed by an episodically wet period from 1978-1998 that included the occurrence of 6 strong El Niño events (Inman and Jenkins 1997; and Goddard and Graham 1997). Based on the historic duration of these cycles, 1998 was likely the end of the wet cycle of climate in California with a return to the dry climate that prevailed from 1945-1977 (White and Cayan 1998).

To illustrate the historical evidence for these dry and wet climate cycles in Southern California, we evaluate the rain gage records for Santa Ana, Laguna Beach and San Diego (panel-a of Figures 1.4-1.6). The records were analyzed for climate trends using the Hurst (1951, 1957) procedure that was first used for determining decadal climate effects on the storage capacity of reservoirs (Inman and Jenkins, 1999). Climate trends become apparent when the data are expressed in terms of cumulative residuals Q_n taken as the continued cumulative sum of departures of annual values of a time series Q_i from their long term mean value Q_a such that $Q_n = \sum_0^n (Q_i - Q_a)$ where n is the sequential value of the time series.

The records for the total period of rainfall and their cumulative residual graphs are shown in Figures 1.4-1.6. All records show decadal scale climate changes (panel-b of Figures 1.4-1.6). Dry periods are shown by segments of the cumulative residuals having negative (downward) slopes while the wet periods have positive (upward) slopes. A dry period is found in all three records from 1945-1997, (negative slopes) while a wet period (positive slope) is shown from

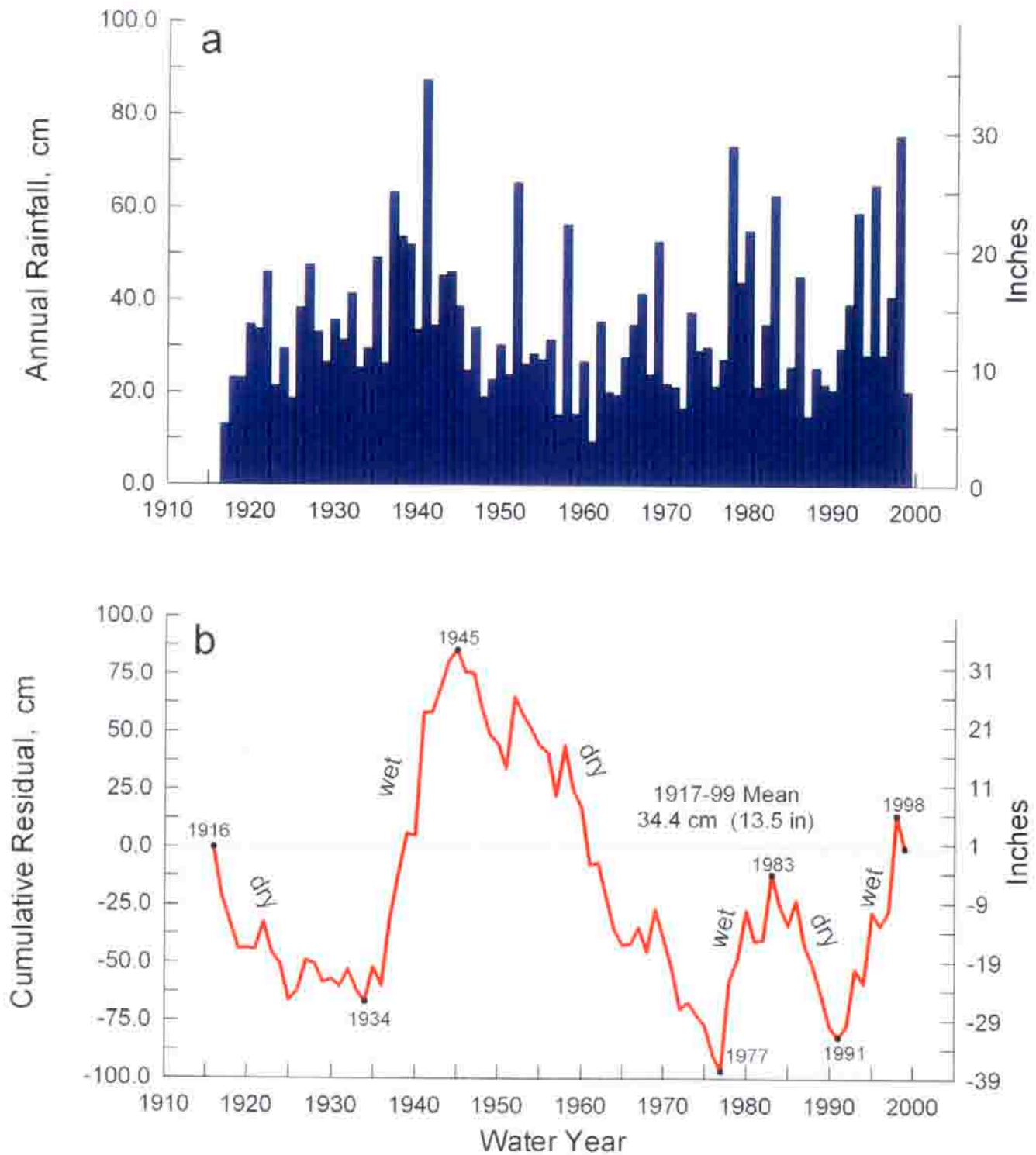


Figure 1.4. a) Total record of annual rainfall, Santa Ana, CA (National Weather Service) and b) Cumulative residual of the annual rainfall for the the period 1917-1999.

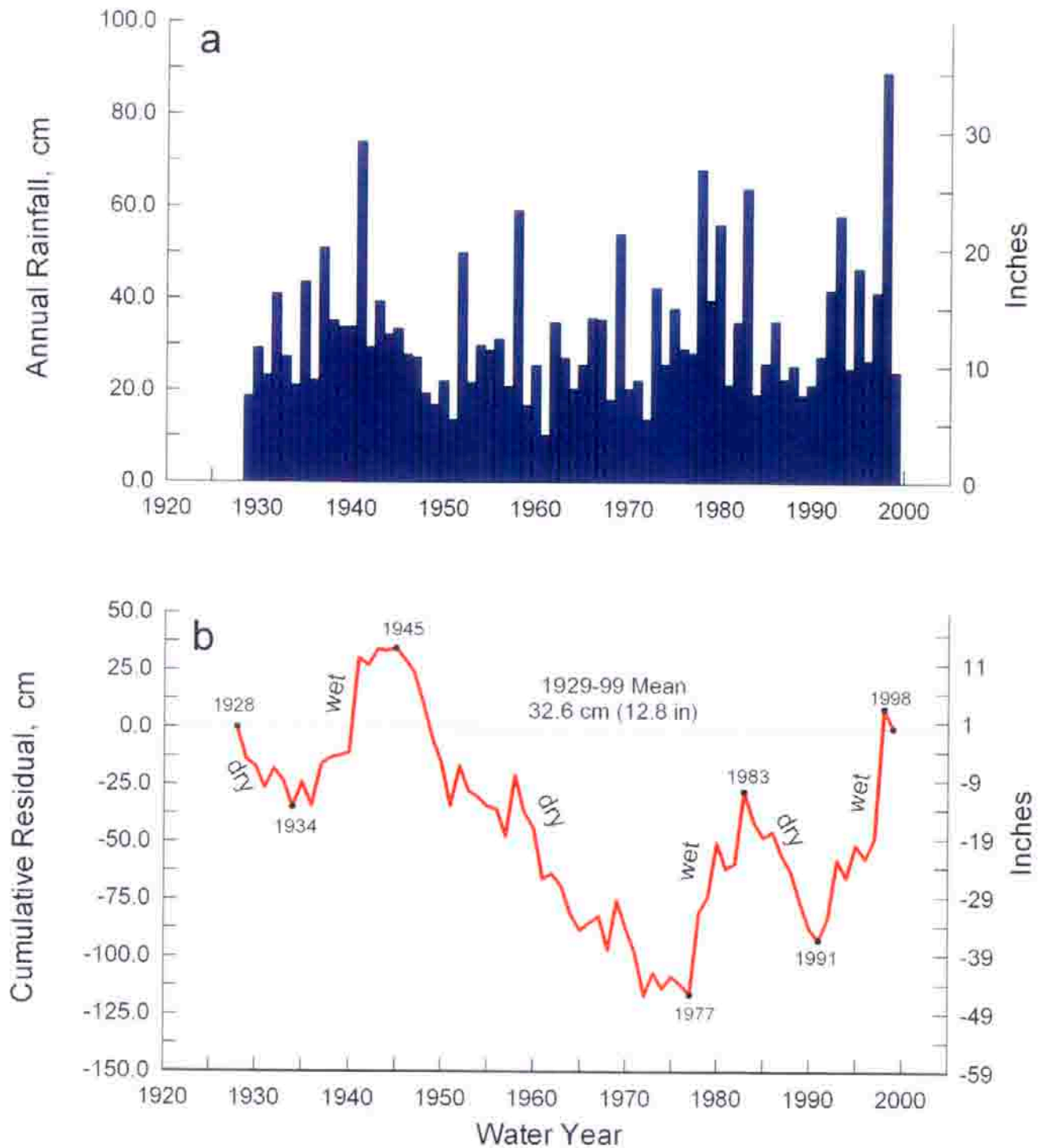


Figure 1.5. a) Total record of annual rainfall, Laguna Beach, CA (National Weather Service) and b) Cumulative residual of the annual rainfall for the the period 1929-1999.

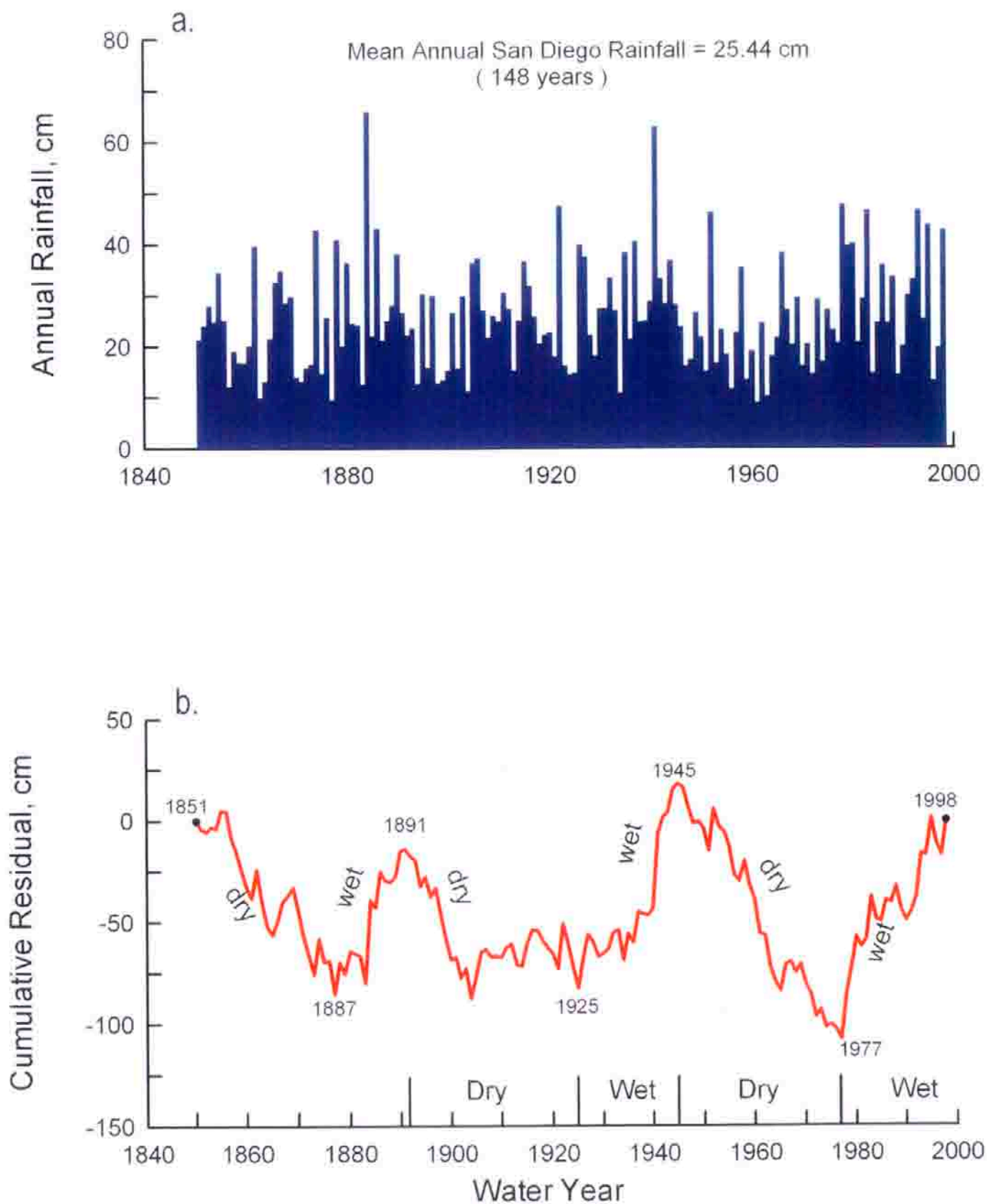


Figure 1.6 Annual rainfall histogram (a) and cumulative residual (b) for the city of San Diego, California.

1978-1998. The wet period of the climate cycle is more irregular caused by 6 strong El Niño events (water years 1978, 80, 83, 93, 95, and 98) and one 4 year period (1987-1990) of low rainfall.

The analysis shows that the average annual rainfall increased by about 38% from the dry to the wet portions of the cycle. Furthermore, both the minimum and maximum ranges in rainfall are higher in the wet period, while the averages of the 6 major rainfall events in 21 year periods before and after the climate change (1977/78) are about 8 to 9 inches greater during the wet period. Therefore, the expected transition back into the dry period for the next 20-30 years is likely to cause severe reductions in terminal storage levels of Southern California reservoirs. The development of alternative fresh water sources such as the proposed desalination project at AES Huntington Beach is likely to prove extremely timely while addressing a significant societal need.

The physical effect of desalinating seawater by reverse osmosis is in principle no different than the effects of evaporation. CalCOFI ocean surveys of the Southern California Bight have measured evaporative losses at 93.4 cm/yr (Roemmich, 1989; Bograd, et. al., 2001). The surface area of coastal waters inside the continental margin of the Southern California Bight is 160,000 km². Factoring evaporation rate over surface area, it is concluded that the coastal ocean of the Southern California Bight loses 1.49×10^{11} m³ of pure water constituent to evaporation each year. In contrast, a desalination plant producing product water at a rate of 50 mgd will extract 6.9×10^7 m³ of pure water constituent from the coastal ocean in one year's time, (but even then, only if it were operated continuously without any down time for maintenance). Consequently, it would take 2,163 desalination plants the size of the Huntington Beach project to match the

evaporative losses from the ocean that occur naturally in the Southern California Bight each year.

SECTION 2: MODEL DESCRIPTION AND CAPABILITIES

2) Model Description and Capabilities

This two-part study addresses the concerns of desalination plant source discharge dilution and source water issues by utilizing a coupled set of numerical tidal and wave transport models to evaluate dilution and dispersion when the proposed desalination plant is functioning at its maximum production capacity of 50 mgd. The numerical model used to simulate tidal currents in the nearshore and shelf region of Newport/Huntington Beach is the finite element model **TIDE_FEM**. Wave-driven currents are computed from the shoaling wave field by a separate model, **OCEANRDS**. The dispersion and transport of concentrated seawater and storm water discharge by the wave and tidal currents is calculated by the finite element model known as **SEDXPORT**. The “wiring-diagram” showing the architecture for how these models were coupled together is shown in Figure 2.1.

The finite element research model, **TIDE_FEM**, (Jenkins and Wasyl, 1990; Inman and Jenkins, 1996) was employed to evaluate the tidal currents in a nearshore region extending between Seal Beach and Crystal Cove State Beach (Figure 1.3). **TIDE_FEM** was built from some well-studied and proven computational methods and numerical architecture that have done well in predicting shallow water tidal propagation in Massachusetts Bay (Connor and Wang, 1974) and along the coast of Rhode Island, (Wang, 1975), and have been reviewed in basic text books (Weiyan, 1992) and symposia on the subject, e.g., Gallagher (1981). The governing equations and a copy of the core portion of the **TIDE_FEM** FORTRAN code are found in Appendix B. **TIDE_FEM** employs a variant of the vertically integrated equations for shallow water tidal propagation after Connor and Wang (1975). These are based upon the Boussinesq

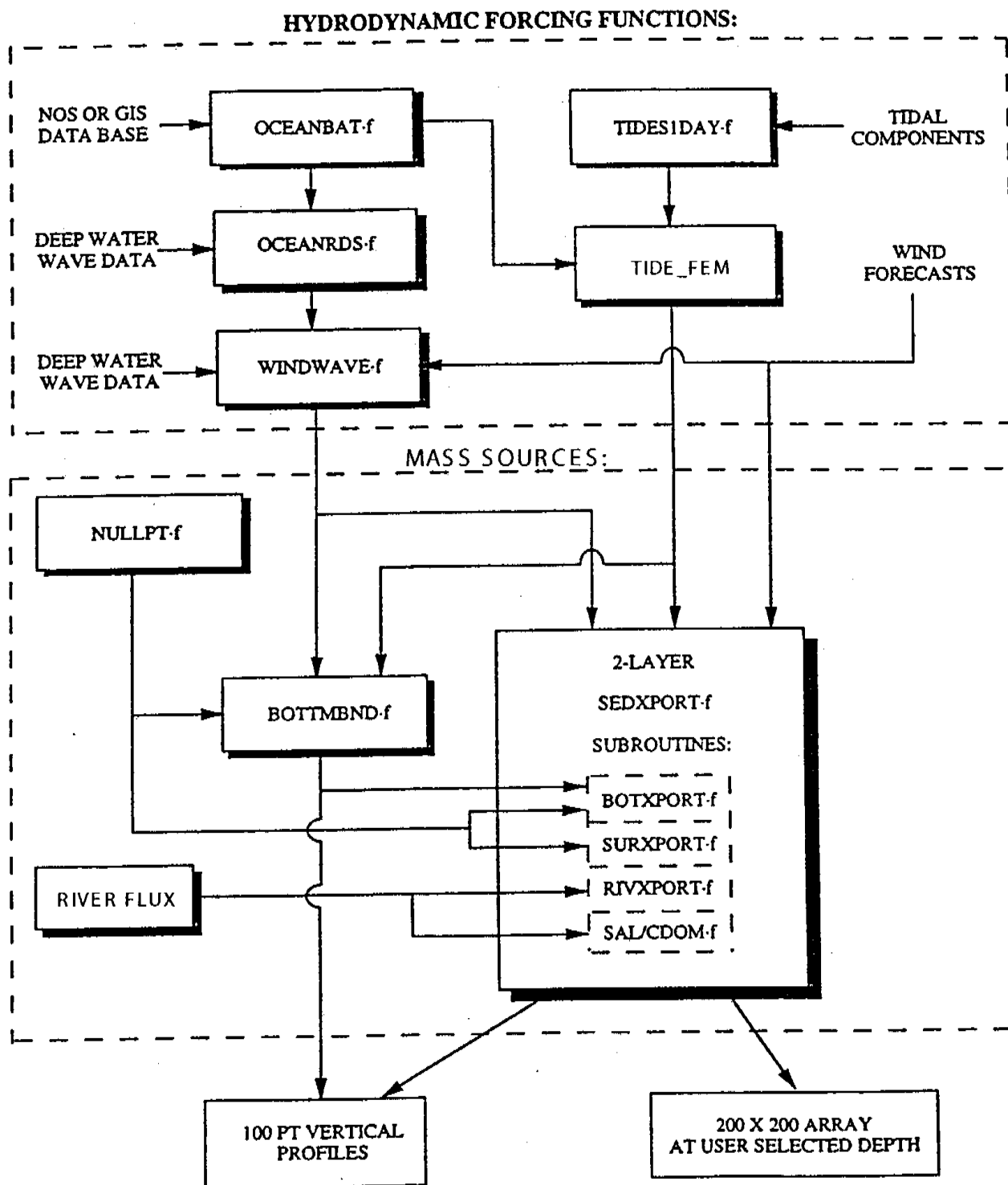


Figure 2.1. SEDXPORT architecture and computational sequence.

approximations with Chezy friction and Manning's roughness. The finite element discretization is based upon the commonly used **Galerkin weighted residual method** to specify integral functionals that are minimized in each finite element domain using a variational scheme, see Gallagher (1981). Time integration is based upon the simple **trapezoidal rule** (Gallagher, 1981). The computational architecture of **TIDE_FEM** is adapted from Wang (1975), whereby a transformation from a **global** coordinate system to a **natural** coordinate system based on the unit triangle is used to reduce the weighted residuals to a set of order-one ordinary differential equations with constant coefficients. These coefficients (**influence coefficients**) are posed in terms of a **shape function** derived from the natural coordinates of each nodal point in the computational grid. The resulting systems of equations are assembled and coded as banded matrices and subsequently solved by **Cholesky's method**, see Oden and Oliveira (1973) and Boas (1966). The hydrodynamic forcing used by **TIDE_FEM** is based upon inputs of the tidal constituents derived from Fourier decomposition of tide gage records. Tidal constituents are input into the module **TID_DAYS**, which resides in the hydrodynamic forcing function cluster (see Appendix C for a listing of **TID_DAYS** code). **TID_DAYS** computes the distribution of sea surface elevation variations at Huntington Beach and adjacent nearshore after compensating for phase shifts associated with travel time between the Los Angeles tide gage station (NOAA #941-0660) and Huntington Beach. Forcing for **TIDE_FEM** is applied by the distribution in sea surface elevation across the deep water boundary of the computational domain in Figure 1.3. Here the tidal currents reduce to the deep water solutions to Laplace's tidal equations (Lamb, 1932). The x-component (longitudinal) of the deep water tidal current is given by:

$$u_{x,\infty} = \frac{ig}{a} \left[\frac{2\Omega s \cot\theta (\xi - \bar{\xi}) + \omega \left(\frac{d\xi}{d\theta} - \frac{d\bar{\xi}}{d\theta} \right)}{\omega^2 - (2\Omega \cos\theta)^2} \right] \quad (1)$$

while the y-component (latitudinal) is:

$$u_{y,\infty} = \frac{g}{a} \left[\frac{s\omega \csc\theta (\xi - \bar{\xi}) \Omega \cos\theta \left(\frac{d\xi}{d\theta} - \frac{d\bar{\xi}}{d\theta} \right)}{\omega^2 - (2\Omega \cos\theta)^2} \right] \quad (2)$$

where θ is the co-latitude; $\bar{\xi}$ is the equilibrium tide; g is the acceleration of gravity; Ω is the angular speed of rotation of the earth, a is the mean radius of the earth; s is an integer; ω is the radian frequency of the potential tide as determined from the tidal constituents.

Wave driven currents were calculated from wave measurements by the CDIP arrays at Huntington Beach, San Clemente, Oceanside, CA, see CDIP (2004). These measurements were back refracted out to deep water to correct for island sheltering effects between the monitoring sites and AES Huntington Beach. The waves were then forward refracted onshore to give the variation in wave heights, wave lengths and directions throughout the nearshore around AES Huntington Beach. The numerical refraction-diffraction code used for both the back refraction from the San Clemente array out to deep water, and the forward refraction to the AES Huntington Beach site is **OCEANRDS** and may be found in Appendix D. This code calculates the simultaneous refraction and diffraction patterns of the swell and wind wave components propagating over bathymetry replicated by the

OCEANBAT-f code, (Figure 2.1). **OCEANBAT-f** generates the associated depth fields for the computational grid networks of both **TID_FEM** and **OCEANRDS** using packed bathymetry data files derived from the National Ocean Survey (NOS) depth soundings. The structured depth files written by **OCEANBAT-f** are then throughput to the module **OCEANRDS-f**, which performs a refraction-diffraction analysis from deep water wave statistics. **OCEANRDS-f** computes local wave heights, wave numbers, and directions for the swell component of a two-component, rectangular spectrum. These values are then throughput to **WINDWAVE-f**, which completes the refraction-diffraction analysis of the two-component spectrum including wind wave effects up to Nyquist frequencies.

The wave data computed throughout the domain of Figure 1.3 are throughput to a wave current algorithm in **SEDXPORT** which calculates the wave-driven longshore currents, $v(r)$. These currents were linearly superimposed on the tidal current. The wave-driven longshore velocity, $v(r)$, is determined from the longshore current theories of Longuet-Higgins (1970), according to:

$$\begin{aligned}
 \bar{v}(r) &= v_o \left(\frac{10}{49} \frac{r}{X_b} - \frac{5}{7} \ln \frac{r}{X_b} \right) \text{ if } 0 \leq r \leq X_b \\
 &= v_o \frac{10}{49} \left(\frac{r}{X_b} \right)^{5/2} \text{ if } r > X_b \\
 v_o &= \frac{5\pi}{8} \frac{0.41}{C_D} (gh_b)^{1/2} \beta \sin \alpha_b
 \end{aligned} \tag{3}$$

where r is the shoreline-normal coordinate, X_b is the width of the surf zone, taken as $X_b = 5/4 H_b \tan\beta$, H_b is the breaker height from the refraction solution, $\tan\beta$ is the beach slope, α_b is the breaker angle, h_b is the breaker depth, taken as $h_b = 5/4 H_b$. C_D is the drag coefficient, and g is the acceleration of gravity. Inspection of (3) reveals that the longshore transport is strongest in the neighborhood of the breakpoint, $r = X_b$, where the longshore currents approach a maximum value of $v(r) = v_o$.

Once the tidal and wave driven currents are resolved by **TIDE_FEM** and **OCEANRDS** and **WINDWAVE**, the dilution and dispersion of flood water runoff and concentrated seawater discharge in those flows is computed by the stratified transport model **SEDXPORT** (Figure 2.1). The **SEDXPORT** code is a time stepped finite element model which solves the advection-diffusion equations over a fully configurable 3-dimensional grid. The vertical dimension is treated as a two-layer ocean, with a surface mixed layer and a bottom layer separated by a pycnocline interface. The code accepts any arbitrary density and velocity contrast between the mixed layer and bottom layer that satisfies the Richardson number stability criteria and composite Froude number condition of hydraulic state.

In both Section 6 of this study, the flood water runoff is represented as sources in the surface mixed layer while the concentrated seawater is represented by a point source either in the bottom layer or the mixed layer depending on the pycnocline cline depth of the particular model scenario. The AES infall is similarly treated as a sink. The source initializations for the Santa Ana River, Talbert Channel, OCSD outfall, AES outfall and infall are handled by a companion code called **MULTINODE** that couples the computational nodes of **TIDE_FEM** and **OCEANRDS** with **SEDXPORT**. The codes do not time split advection and

diffusion calculations, and will compute additional advective field effects arising from spatial gradients in eddy diffusivity, i.e., the so-called “gradient eddy diffusivity velocities” after Armi (1979). Eddy mass diffusivities are calculated from momentum diffusivities by means of a series of Peclet number corrections based upon TSS and TDS mass and upon the mixing source. Peclet number corrections for the surface and bottom boundary layers are derived from the work of Stommel (1949) with modifications after Nielsen (1979), Jensen and Carlson (1976), and Jenkins and Wasyl (1990). Peclet number correction for the wind-induced mixed layer diffusivities are calculated from algorithms developed by Martin and Meiburg (1994), while Peclet number corrections to the interfacial shear at the pycnocline are derived from Lazara and Lasheras (1992a;1992b). The momentum diffusivities to which these Peclet number corrections are applied are due to Thorade (1914), Schmidt (1917), Durst (1924), and Newman (1952) for the wind-induced mixed layer turbulence and to Stommel (1949) and List, et al. (1990) for the current-induced turbulence. The primitive equations for the **SEDXPORT** code may be found in Appendix E and in Appendix F for **MULTINODE**.

In it's most recent version, **SEDXPORT** has been integrated into the Navy's Coastal Water Clarity Model and the Littoral Remote Sensing Simulator (LRSS) (see Hammond, et al., 1995). The **SEDXPORT** code has been validated in mid-to-inner shelf waters (see Hammond, et al., 1995; Schoonmaker, et al., 1994). Validation of the **SEDXPORT** code was shown by three independent methods: 1) direct measurement of suspended particle transport and particle size distributions by means of a laser particle sizers; 2) measurements of water column optical properties; and, 3) comparison of computed stratified plume dispersion patterns with LANDSAT imagery. An example of the resolution of plumes by the **SEDXPORT**

model is shown in Figure 2.2 for the Santa Margarita River. In this figure the isocontours of suspended sediment concentrations computed by **SEDXPORT** (red lines) are overlaid on the LANDSAT image. The colored patchwork on the land delineate the primary and secondary drainage basins of streams discharging into the nearshore following the storm of 23 January 1993.

SEDXPORT has been built in a modular computational architecture (Figure 2.1). The modules are divided into two major clusters: 1) those which prescribe hydrodynamic forcing functions; and, 2) those which prescribe the mass sources acted upon by the hydrodynamic forcing to produce dispersion and transport. The cluster of modules for hydrodynamic forcing ultimately prescribes the velocities and diffusivities induced by wind, waves, and tidal flow for each depth increment at each node in the grid network.

The lower set of modules in Figure 2.1 compute the mixing and transport induced by the forcing functions acting on mass sources, including flood water runoff from the Santa Ana River and Talbert Channel and the concentrated seawater discharged from the RO process. The subroutine **BOTXPORT-f** in **SEDXPORT-f** solves for the mixing and advection of the negatively buoyant concentrated seawater in response to the wave and tidal flow using an rms vorticity-based time splitting scheme. The subroutine **RIVXPORT-f**, performs a similar computation on the positively buoyant flood water runoff from the Santa Ana River and Talbert Channel. Both **BOTXPORT** and **RIVXPORT** solve the eddy gradient form of the advection diffusion equation for the water column density field where u is the vector velocity from a linear combination of the wave

Comparison

Suspended Particulate--LANDSAT RGB Image

Modeled Concentration Contours (Log10)

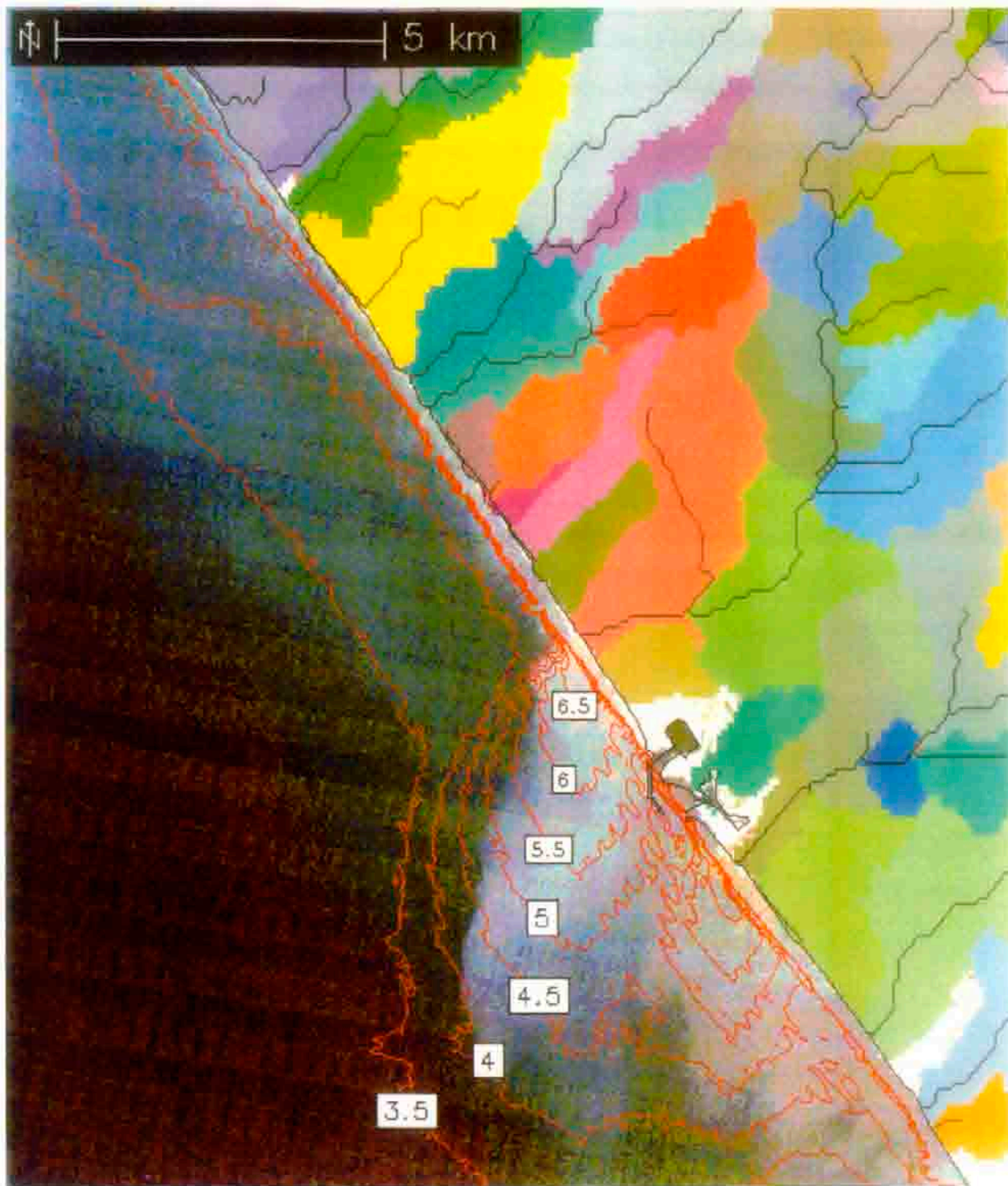


Figure 2.2. Comparisons of the SEDXPORT plume model with a LANDSAT image of the Santa Margarita River discharge on January 23, 1993. Modeled sediment concentration contours are expressed in base-10 log scale of particle number per ml. The color patchwork on the land denotes drainage basins of local streams.

$$\frac{\partial \rho}{\partial t} = (\mathbf{u} - \nabla \epsilon) \cdot \nabla \rho - \epsilon \nabla^2 \rho \quad (4)$$

and tidal currents, ϵ is the mass diffusivity and ρ is the water mass density. The water mass density is a function of temperature, T , and salinity, S , according to the equation of state expressed in terms of the specific volume, $\alpha = 1/\rho$, or:

$$\frac{d\alpha}{\alpha} = \frac{1}{\alpha} \frac{\partial \alpha}{\partial T} dT + \frac{1}{\alpha} \frac{\partial \alpha}{\partial S} dS \quad (5)$$

The factor $\partial \alpha / \partial T$, which multiplies the differential temperature changes, is known as the coefficient of thermal expansion and is typically 2×10^{-4} per $^{\circ}\text{C}$ for seawater; the factor $\partial \alpha / \partial S$ multiplying the differential salinity changes, is the coefficient of saline contraction and is typically 8×10^{-4} per part per thousand (ppt) where 1.0 ppt = 1.0 g/L of total dissolved solids (TDS). For a standard seawater, the specific volume has a value $\alpha = 0.97264$. If the percent change in specific volume by equation (5) is less than zero, then the new water mass is heavier than standard seawater, and lighter if the percent change is greater than zero. Solutions to the density field calculated from equation (1) by **SEDXPORT** are used to calculate the field salinity, $S_{(x, y, z)}$, from equation (5) for an assumed T for the ambient ocean and river water and ΔT for plant thermal effluent. The salinity field in turn can be used to solve for the spacial varying dilution factor, $D_{(x, y, z)}$ according to:

* Fresh Water Runoff Dilution:

$$D_{(x,y,z)} = \frac{S_o}{S_o - S_{(x,y,z)}} \quad (6)$$

** Concentrated Seawater Dilution:

$$D_{(x,y,z)} = \frac{S_b - S_o}{S_{(x,y,z)} - S_o} \quad (7)$$

where S_o is the ambient seawater salinity in ppt, S_b is the end-of-the-pipe salinity of concentrated seawater and $S_{(x,y,z)}$ is the local salinity from the model solution in ppt. In equation (6) the total dissolved solids of the fresh water runoff is assumed to be 0.0 ppt. Model solutions will find a significant variation in the salinity with water depth, z . Therefore we introduced a depth averaged dilution factor, \bar{D} :

$$\bar{D}_{(x,y,z)} = \frac{1}{H_{(x,y)}} \int_0^H D_{(x,y,z)} dz \quad (8)$$

where $H = H_{(x,y)} = h + \eta$ is the local water depth, h is the local water depth below mean sea level and η is the tidal amplitude.

The diffusivity, ϵ , in equation (4) controls the strength of mixing and dilution of the concentrated seawater and flood water constituents, and varies with position

in the water column relative to the pycnocline interface. Vertical mixing includes two mixing mechanisms at depths above and below the pycnocline: 1) fossil turbulence from the bottom boundary layer, and 2) wind mixing in the surface mixed layer. The pycnocline depth is treated as a zone of hindered mixing and varies in response to the wind speed and duration. Below the pycnocline, only turbulence from the bottom wave/current boundary layer contributes to the local diffusivity. Nearshore, breaking wave activity also contributes to mixing. The surf zone is treated as a line source of turbulent kinetic energy by the subroutine **SURXPORT-f**. This subroutine calculates seaward mixing from fossil surf zone turbulence, and seaward advection from rip currents embedded in the line source. Both the eddy diffusivity of the line source and the strength and position of the embedded rip currents are computed from the shoaling wave parameters evaluated at the breakpoint, as throughput of **OCEANRDS-f**.

SECTION 3: MODEL INITIALIZATION

3) Model Initialization

Altogether there are seven primary variables that enter into a solution for the simultaneous dispersion and dilution of the waste heat from the generating station and concentrated seawater from the desalination plant. These seven variables may be organized into *boundary conditions* and *forcing functions*. The boundary condition variables control the source strength (concentrated sea salts) and background conditions. Some of these change daily (primary boundary conditions) while others vary slowly in time (stationary boundary conditions). The primary boundary conditions are:

- *Power Plant Flow Rates
- *Ocean Salinity
- *Ocean Temperature
- *Ocean Water Levels (tides and sea level anomalies)

Storm water flows (such as from the Santa Ana River and Talbert Marsh) also vary daily, but their effect on the receiving water is captured by the daily ocean salinity data. However for the purpose of providing input to the Sanitary Survey (Archibald, 2002, 2004) we will consider their source loading during extreme events (see Sections 7 & 8). Similarly, the generating station “Delta-T” (the amount that the generating station raises the cooling water above the ambient ocean temperature) is added to the daily variation in ambient ocean temperature. The stationary boundary conditions are the local bathymetry, that typically has seasonal variation inshore of closure depth (about 15 m depth). The forcing function variables affect the strength of ocean mixing and ventilation and include:

- * waves
- * currents
- *winds.

In the following sub-sections, overlapping 20.5 year long records for each of the seven controlling variables are reconstructed. These long-term records contain 7,523 consecutive days of daily mean values between 1980 and 2000.

Long-term monitoring of ocean properties in the coastal waters surrounding AES Huntington Beach has been on going for about 30 years as required for compliance with NPDES permits for two separate ocean outfalls, namely, the thermal outfall of AES Huntington Beach and the treated sewage outfall offshore of the Santa Ana River operated by Orange County Sanitation Department (OCSD). These data were accessed from the NPDES monitoring reports that are periodically released (MBC 1980- 2002 for the AES Huntington Beach outfall and OCSD,1993, 2000 for the OCSD outfall). In attempting to reconstruct 20-year long, continuous, unbroken records of all seven controlling variables for the dilution and dispersion modeling problem, certain gaps were found in some of the data bases. These gaps were filled by using monitoring data measured at the Scripps Pier in La Jolla, about 67.7 miles to the southeast of AES Huntington Beach . The Scripps Pier site has many physical features in common with the nearshore area around AES Huntington Beach. Both sites have a submarine canyon nearby. Consequently internal waves are an active mechanism at both sites in causing daily (diurnal) variations in salinity, temperature, and other ocean properties. The longer period variations at seasonal and multiple year time scales are the same at both sites due to their proximity. Consequently the Scripps Pier Shore Station data (SIO, 2001) and the Coastal Data Information Program monitoring at Scripps Pier (CDIP, 2004) are

used as surrogates to fill gaps in the long term records of physical ocean properties at AES Huntington Beach. These properties will be shown to exhibit considerable natural variability over the period of record from 1980 to mid 2000 due to daily and seasonal changes, but most especially due to climate changes of global scale.

The seasonal variations in the exposure of the hemispheres to the sun produce inter-annual changes in the duration of daylight and the angle of the sun's irradiance. These effects modulate solar heating, resulting in the inter-annual variation of the earth's atmospheric pressure field which in turn introduces seasonal climatic effects. Inter-annual variations are enhanced by the higher convective effects of land and the greater concentration of land mass relative to water in the temperate latitudes of the northern hemisphere.

Upon occasion the typical seasonal weather cycles are abruptly and severely modified on a global scale. These intense global modifications are signaled by anomalies in the pressure fields between the tropical eastern Pacific and Malaysia known as the *El Niño/Southern Oscillation* (ENSO) (e.g., Diaz & Markgraf, eds., 1992). The intensity of the oscillation is often measured in terms of the *Southern Oscillation Index* (SOI), defined as the monthly mean sea level pressure anomaly in mb normalized by the standard deviation of the monthly means for the period 1951-1980 at Tahiti, minus that at Darwin, Australia. A negative SOI (lower pressure at Tahiti, higher pressure at Darwin) is known as an *El Niño* or warm ENSO event, because of the arrival of unusually warm surface water off the coast of Peru at the time of Christmas; hence, the term *El Niño*. Warm water also occurs along the coast of California and both regions experience unusually heavy rainfall. A positive SOI is known as *La Niña* and it signals the occurrence of colder than

normal surface water in the eastern Pacific, but stronger southwest monsoons in the Indian Ocean with heavy rainfall in India and in the Ethiopian plateau.

ENSO events occur about every 3 to 7 years with dominant spectral peaks at about 3 and 6 plus years. However these ENSO events may induce climate changes that occur on decadal time scales of one quarter to one half century. These changes are often discussed in terms of two atmospheric patterns (PNA, NAO) and a sea surface temperature pattern (PDO). Both PNA and PDO are long period (i.e., inter-decadal) analogs of the seasonal (inter-annual) variations of global pressure and temperature, while NAO is an intensification and relaxation of the January phase of the inter-annual variation. They are aliased by the inter-annual changes because they have the same structure and appear as extreme cases of the inter-annual patterns. This aliasing has delayed the general understanding and acceptance of these concepts.

The Pacific/North American (PNA) pattern is associated with an atmospheric dipole in pressure anomaly over the Pacific Ocean/North America region whose polarity reversals lead to wet and dry climate along the Pacific coast of North America (Wallace & Gutzler, 1981). High pressure anomaly over the North Pacific Ocean and low pressure anomaly over the North American Continent result in dry (La Niña) climate along the coast of central and southern California; while the opposite polarity in these longitudinal (zonal) dipole patterns leads to wet (El Niño) climate. Inman & Jenkins (1999) show that the coastal rivers of central and southern California have streamflow and sediment fluxes during the wet phase of PNA (1969-1995) that exceed those during the preceding dry phase (1944-1968) by factors of 3 and 5 respectively.

The Pacific (inter) Decadal Oscillation (PDO) is a sea surface temperature pattern associated with the La Niña/El Niño phases of ENSO cycles, with the leading pattern of PDO situated in the tropical Pacific Ocean (Goddard & Graham, 1997; Mantua et al., 1997). The El Niño phase of the PDO cycle is characterized by a weakening of the trade winds that results in an eastward movement (slosh) of the warm pool of equatorial water normally contained in the western Pacific by the trades during La Niña conditions. The stronger trade wind systems during the La Niña phase of PDO are part of a general spin-up of the atmospheric circulation which causes the North and South Pacific Gyres to rotate faster. Both effects (wind and current) induce upwelling that maintains cold water masses along the west coast of the Americas, which sustains the typically cool dry coastal climate of these regions during the La Niña dominated periods of the PDO and PNA.

A) Storm Water Flow Rates

The historic occurrences of major flood events on the Santa Ana River will dictate the ensemble of environmental forcing parameters used to initialize the model for evaluation of source water issues related to potential ingestion of storm water by the AES Huntington Beach infall. We seek the largest historic floods for which wave and tidal data are simultaneously available.

To determine the likely maximum contribution of storm flow from the Santa Ana River and the Talbert Channel at the intake to the desalination plant, a composite monthly flow rate record was constructed using historic peak flow events of both the Santa Ana River and the Talbert Channel. The USGS has published annual mean flow volumes since 1940 and daily event based runoff volumes for the Santa Ana River during water years 1997-98 and 1998-99 (USGS,

2000). The Santa Ana River stream gage station (USGS #11078000) has an upstream drainage area of 4,400 square kilometers. The annual mean flow volumes at gage #11078000 for 1940-99 are listed in Table 1.

Because the oceanographic conditions which control the dispersion of the Santa Ana River storm water vary daily, it is necessary to select an event year from Table 1 for which daily flow rate data is available. The largest event year for which such daily flow rate data is available was water year 1998, which is the fourth largest event year in the period of record. Within that year, the highest flow month was February which accounted for 330 million of the 407 million cubic meters of flow volume occurring in water year 1998. The peak flow event occurred 24 February 1998.

Corresponding daily flow rate data for the Talbert Channel was not available for February 1998. Therefore a surrogate drainage basin was adopted for which flow rate data was simultaneously available at other times for both the surrogate and the Talbert Channel. These simultaneous flow rate data sets were used to construct a streamflow rating function, which establishes an analytic relation between the flow rate of the surrogate and the flow rate of the Talbert Channel. The rating function has the following form

$$Q_T = a_0 + a_1 Q_s + a_2 Q_s^2 \quad (9)$$

where Q_T is the flow rate of the Talbert Channel, Q_s is the flow rate of the surrogate and a_0 , a_1 and a_2 are parameters determined by regression analysis of the simultaneous data sets. The San Diego Cr. was selected as the surrogate for this

Table 1. Annual Mean Flow Volume for the Santa Ana River, USGS #11078000.

Water Year ^b	Streamflow 10 ⁶ m ³ /yr.	Water Year ^b	Streamflow 10 ⁶ m ³ /yr.	Water Year ^b	Streamflow 10 ⁶ m ³ /yr.
1940	3.84	1965	1.25	1990	16.6
1941	104	1966	25.8	1991	52.7
1942	.714	1967	42.2	1992	55.3
1943	79.8	1968	9.02	1993	547
1944	20.2	1969	480	1994	4.64
1945	7.50	1970	2.86	1995	346
1946	3.48	1971	5.09	1996	7.71
1947	2.50	1972	5.63	1997	39.8
1948	.0893	1973	16.7	1998	407
1949	.000	1974	12.1	1999	5.22
1950	.804	1975	7.68		
1951	.0893	1976	3.57		
1952	20.5	1977	3.30		
1953	.625	1978	272		
1954	1.70	1979	33.5		
1955	.268	1980	498		
1956	4.64	1981	18.6		
1957	.179	1982	22.1		
1958	23.8	1983	344		
1959	.447	1984	49.1		
1960	.804	1985	48.6		
1961	.000	1986	79.4		
1962	5.00	1987	14.6		
1963	1.52	1988	25.5		
1964	1.16	1989	23.4		

analysis for the following reasons:

- 1) Daily flow rate data available for February 1998.
- 2) Geographic proximity.
- 3) Similar basin hydrology, land use and demographics.
- 4) Both basins discharge into coastal marshes.

The resulting streamflow rating function giving Talbert Channel flow from San Diego Cr. flow is shown in Figure 3.1. The measured flow rate data appear as crosses in this figure and the best fit line from the regression analysis gives $a_0 = 0.0461156$, $a_1 = 0.0166263$ and $a_2 = -0.0000194$. The r-squared for this regression is 0.78 to 0.79, which is typical precision for this type of approximation, (Inman and Jenkins, 2000).

Since the mouths of the Santa Ana River and the Talbert Channel are essentially co-located by a system of jetties (Figure 1.3) a composite flow rate history was generated (Figure 3.2) for use in the model problem to predict the source water make-up at the AES intakes. Inspection of Figure 3.2 indicates that the maximum daily flow rate was 8,890 cfs for the combined Santa Ana River and Talbert Channel flow (24 February 1998). The seven day average of the combined flow rate around the peak flow event was 5,798 cfs and the thirty day average flow rate for the composite extreme event month was 2,732 cfs. The in-plant waste stream of storm water from the AES Huntington Beach facilities during this same period had a peak daily discharge of 0.72689 mgd, a seven day peak period average of 0.4741 mgd and a 30-day average of 0.186552 mgd, (see Appendix A).

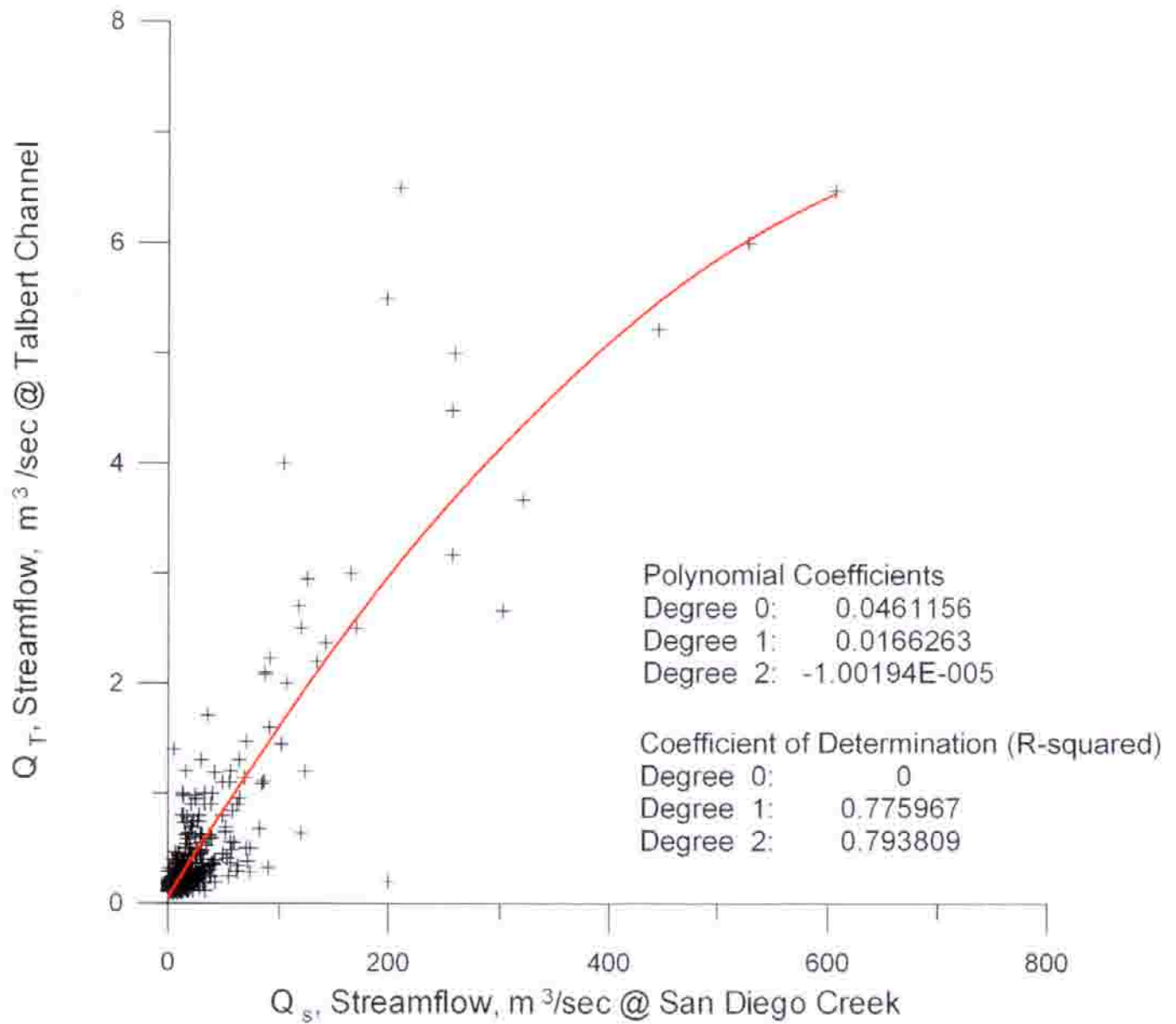


Figure 3.1. Talbert Channel streamflow rating function based on San Diego Creek surrogate.

B) Ocean Water Levels & Tidal Oscillations

The local water depth around outfall of the AES Huntington Beach generating station is nominally 27.9 feet relative to mean sea level. Spring tidal ranges can reach as high as 8.9 feet or 32 % of the local mean water depth. Hence tides can significantly vary the local water volume around the outfall that is available for dilution. The nearest ocean tide gage station that measures ocean water levels near AES Huntington Beach is located at Newport Harbor. However this tide gage was not functional throughout the entire 1980-2000 period of record used for the modeling. Consequently the ocean water level input was de-faulted to the next closest tide gage station at Los Angeles (NOAA #941-0660). This tide gage was last leveled using the 1960-78 tidal epoch, but tide tables based on the 1960-78 tidal epoch frequently mis-represent high and low tide elevations. This is due to several factors including: 1) the long-term upward creep in eustatic sea level during the last part of the modern sea level high stand 2) seasonal warming and cooling of the ocean and 3) climate effects. Flick & Cayan (1984) have shown that seasonal warming and cooling accounts for an interannual variation in mean sea level of about 0.5 ft. El Niño or ENSO events can result in sea level anomalies of 1.0 ft. or more due to the thermal expansion effects of the coastal warm water anomalies of El Niño and by the inverse barometer effects on sea level associated with the ENSO induced North Pacific low pressure anomaly. Therefore, we base our analysis on direct water level measurements rather than on tide table estimates.

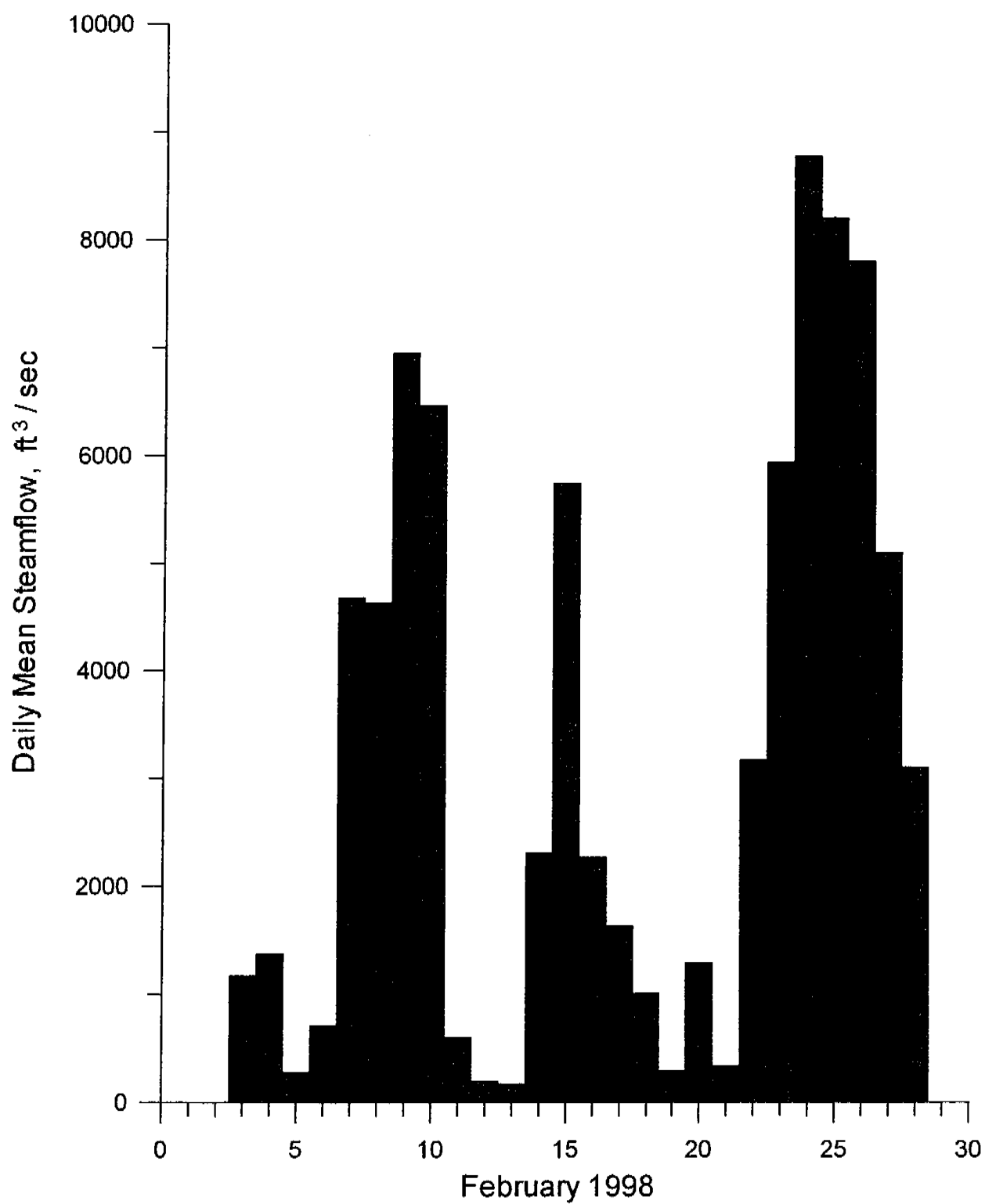


Figure 3.2. Combined daily mean flow rate of the Santa Ana River and Talbert Channel.

Water levels measured by the Los Angeles Tide Gage (NOAA #941-0660) have been archived by NOAA (2000) for the preceding 20.5 year period, 1980 through mid 2000. Time series of the daily high and low ocean water levels were reconstructed from these archival measurements for each year in this period of record. Here, tide measurements are recorded in one hour intervals. This sampling interval is too coarse to use these records directly as forcing functions for the tidal hydraulics computations. If the tidal flow becomes critical in any shallow water region of the model, by achieving the phase speed of a shallow water tidal wave, $c = \sqrt{gh}$, then the 2-dimensional Courant-Friedricks-Lewy (CFL) criterion (Gallagher, et al. 1981) is used as a generalized constraint to ensure stability of the finite element calculations. Some nodes must be closely spaced with $\Delta x = 30$ m in order to resolve the geometry around the infall and outfall towers (Figure 1.2). The CFL criterion requires a minimum time step length:

$$\Delta t \leq \frac{\Delta x}{2c} \quad (10)$$

For a spring tide condition, maximum water depths could vary from 3 m to 7 m at certain sections of the infall and outfall towers. Therefore, the tidal forcing function must be resolved into time step intervals of less than 2.7 sec. if the tidal currents approached critical speeds in the channel at the Santa Ana River mouth or less than 3.2 sec. if critical flow was approached over the top of the infall and outfall towers.

The tides were reconstructed at 2 sec time intervals from the Los Angeles tidal measurements using the amplitudes and phases of 21 non-zero tidal constituents derived from the long-term records of the tide gage. This tidal reconstruction was performed by the program, **TID_DAYS**, which is found in Appendix C. **TID_DAYS** uses a version of LONG'S CODE from U. S. Dept. of Commerce SP #98_1988. Figure 3.3 shows a comparison between the reconstructed tides at Los Angeles (solid line) versus the hourly measurements (triangles) for the tidal month of February 1998 used in the model problem for source water and dilution issues in Section 4. The tidal constituents for Los Angeles that were input to **TID_DAYS** are based upon the NOAA datums derived from the 1960-78 tidal epoch. This was the last time that NOAA had updated datum elevations for the Los Angeles gage and corresponds to the predominant dry La Niña dominated period. Because of sea level anomalies due to El Niño warming of the coastal ocean, and inverse barometer effects due to storm passage, the reconstructed tides were assigned a positive sea level anomaly to minimize the variance between the measured water elevations in February 1998 and the reconstructed tides at 2 second intervals. That anomaly varied from +0.2 ft to +0.9 ft. during February 1998.

To initialize the model problem to study the transport of OCSD wastefield water masses during El Niño summer conditions in Section 9, the **TID_DAYS** code in Appendix C was configured for 2 sec. time steps to reconstruct the tidal elevation during a period of reversal in the coastal transport. The wave record was searched for two to five day blocks having sustained reversals in the net littoral drift. The month of August 1997 was found to have the desired low flow case current reversals for investigating whether the OCSD waste field might reach the

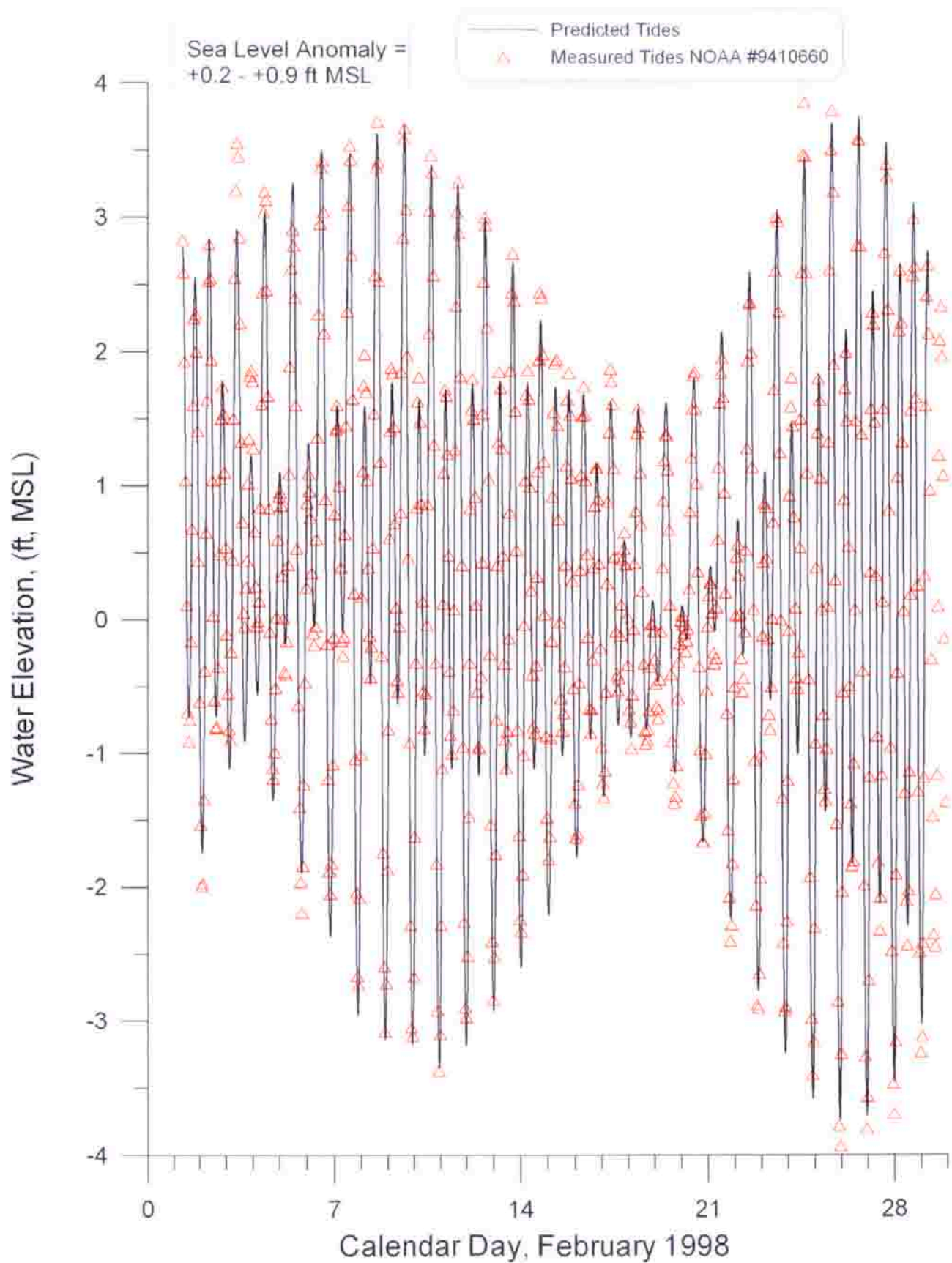


Figure 3.3. Predicted tides vs measured water levels at Los Angeles, CA, NOAA Tide gage #941-0660, February 1998.

AES intakes. The reconstructed water level elevation for August 1997 are shown in Figure 3.4. Similar reconstructions were done for the month of May during the La Niña year of 1999 to provide Syzygian tides with minimal tidal ranges for the low flow case dilution analysis in Section 4. The maximum ocean water level was +5.35 ft. NGVD during the 1997 El Niño, 1.31 ft. higher than the astronomic tides of the tide tables. The minimum ocean water level was -4.66 ft. NGVD, occurring during the 1988 winter. The 20.5 year record of daily high and low water levels is plotted in Panel-d of Figure 3.23 found at the end of this section, summarizing the complete set of boundary conditions.

C) Bathymetry

Bathymetry provides a controlling influence on all of the coastal processes that affect dispersion and dilution. The bathymetry consists of two parts: 1) a stationary component in the offshore where depths are roughly invariant over time, and 2) a non-stationary component in the nearshore where depth variations do occur over time. The stationary bathymetry generally prevails at depths that exceed *closure depth* which is the depth at which net on/offshore transport vanishes. Closure depth is typically -12 m to -15 m MSL in the San Pedro Littoral Cell, [Inman et al. 1993]. The stationary bathymetry was derived from the National Ocean Survey (NOS) digital database. Gridding is by latitude and longitude with a 3 x 3 arc second grid cell resolution yielding a computational domain of 30.9 km x 18.5 km. Grid cell dimensions along the x-axis (longitude) are 77.2 meters and 92.6 meters along the y-axis (latitude).

For the non-stationary bathymetry data inshore of closure depth (less than -15 m MSL) nearshore and beach surveys were conducted by the US Army Corps

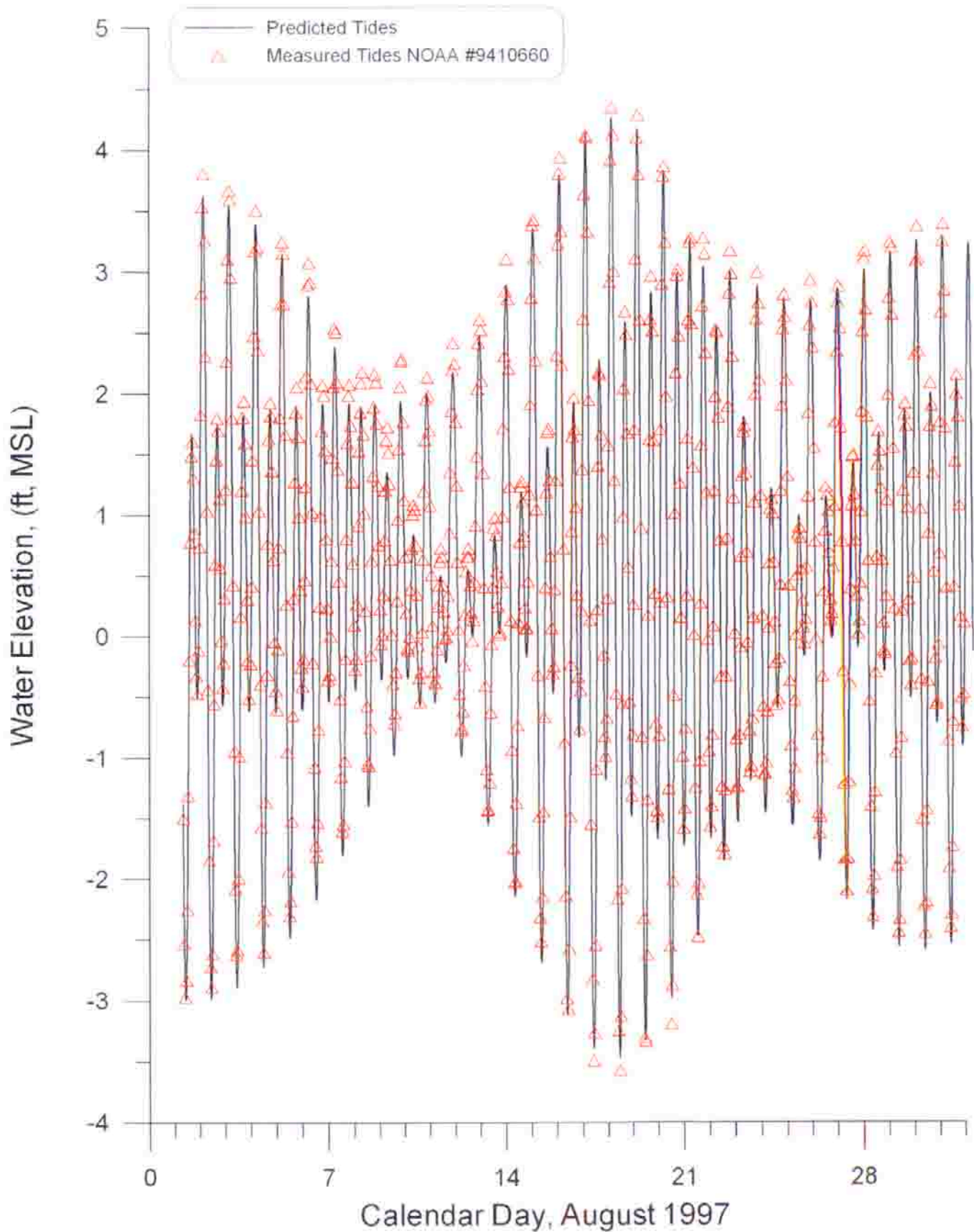


Figure 3.4. Predicted tides vs measured water levels at Los Angeles, CA, NOAA Tide gage #941-0660, August 1997.

of Engineers in 1985, 1990, 1996 and have been compiled in Everts, 1997. These nearshore and beach survey data were used to update the NOS database for contemporary nearshore and shoreline changes that have occurred following the most recent NOS surveys. Maps of the bathymetry in the near and farfield of the AES outfall are found in Figures 1.1 and 1.3 respectively.

To perform both the required wave shoaling and transport computations in the farfield of the infall and outfall, a relatively coarse-scale resolution of the bottom bathymetry is required which gives at least two grid points per wavelength of the highest frequency wave to be shoaled. The farfield grid to compute the effects of distant sources of storm water and pollution reaching the infall (Figure 1.3). A nearfield grid is nested inside the farfield grid and is used to calculate recirculated flow between the outfall and infall (Figure 1.1).

D) Wave Climate

Waves are the principle driving mechanism of mixing and current ventilation in the very nearshore region off Huntington Beach. This wave dominated region consists primarily of the surfzone but extends seaward into the wave shoaling zone a few surf zone widths beyond the point of wave breaking. Waves are also the most difficult of the 7 controlling variables to get long unbroken records. The availability of wave data in the lower Southern California Bight is what limited the period of record for this long term model analysis to 1980 - July 2000. Waves have been routinely monitored at several locations in the lower Southern California Bight since 1980 by the Coastal Data Information Program, (CDIP, 2004).

In the eastern North Pacific Ocean (where storms and swells effecting California are spawned) the La Niña condition leads to surface pressure

distributions and upper level wind systems that cause frontal cyclones from the Gulf of Alaska to follow storm tracks into the Pacific northwest (Figure 3.5a). During El Niño, surface pressures over the eastern North Pacific decline while jet stream flow develops extreme southward meanders, steering ocean storms into the Southern California Bight (Figure 3.5b).

Along the southern California coast a period of mild-stable weather occurred during the 30 years between the mid-1940's and mid-1970's when La Niña dominated storm systems like Figure 3.5a, (Inman and Jenkins, 1997) prevailed. Winters were moderate with low rainfall, and winds were predominantly from the west-northwest. The principal wave energy was from Aleutian lows having storm tracks which usually did not reach southern California (Figure 3.5a). Summers were mild and dry with the largest summer swells coming from very distant southern hemisphere storms.

The wave climate in southern California changed, beginning with the El Niño years of 1978-79 and extending at least until the present. The prevailing northwesterly winter waves were replaced by high energy waves approaching from the west or southwest (Figure 3.5b), and the previous southern hemisphere swell waves of summer have been replaced by shorter period tropical storm waves during late summer months from the more immediate waters off Central America (Inman, et al., 1996).

Data of instrumented buoys and light vessels in the North Pacific show that wave heights have increased significantly and continuously during the past 25 years. The measurements of six buoys between latitude 34°N and 56°N in the

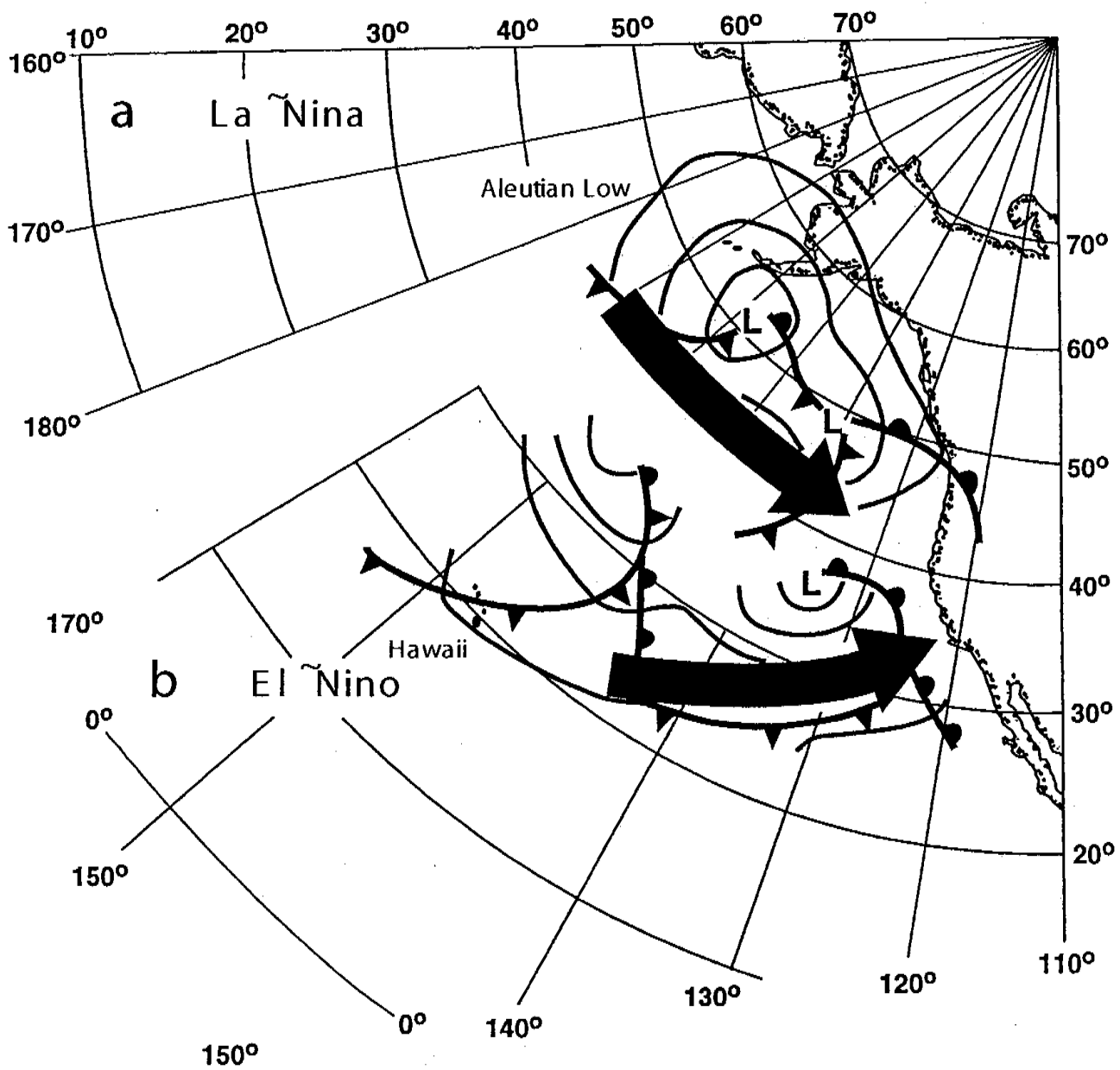


Figure 3.5. Typical storm track for a) La Nina and b) El Nino winter seasons.

eastern North Pacific cover the 25 year time interval from 1975-1999 (Allen and Komar, 2000). Over this period, the average annual (root-mean square) wave height increased progressively from about 1.6 m. to 1.9 m, generating a landward wave energy flux that ranged for these average waves from about 93×10^6 kW to 131×10^6 kW over the same period (Inman and Jenkins, 2000). This is highly significant because the transport rates and direction in the nearshore are directly proportional to the wave energy flux. To account for this recent trend, the model results of this study are based on the contemporary wave climate record of 1980-99.

El Niño storms generate two distinct swell patterns. These storms typically have an intense low pressure cyclone with an associated cold front, Figure 3.6. The storms that brought the extreme floods in February 1998 were El Niño storms. They are distinctive from the frontal cyclones occurring during La Niñas in that the cyclone portion of the storm tracks to much lower latitudes, (Figure 3.5b), and the associated cold front is very long, extending well into subtropical latitudes and entraining sub-tropical moisture. Consequently the pre-frontal winds which blow along the leading edge of the cold front have a very long fetch, while the warm subtropical moisture intensifies these winds through cyclogenesis. The intense, long fetch of the pre-frontal side of an El Niño storms gives rise to very high energy swells from the south-southwest. On the cold post frontal side of an El Niño storm, the winds blow from the west-northwest, but decrease rapidly with distance away from the cyclone (labeled L in Figure 3.6). Consequently the post frontal winds have a much shorter effective fetch and the post frontal north-northwesterly swells are less intense than the pre-frontal south-southwesterly swells. On the other hand the propagation of these storms is retarded when they

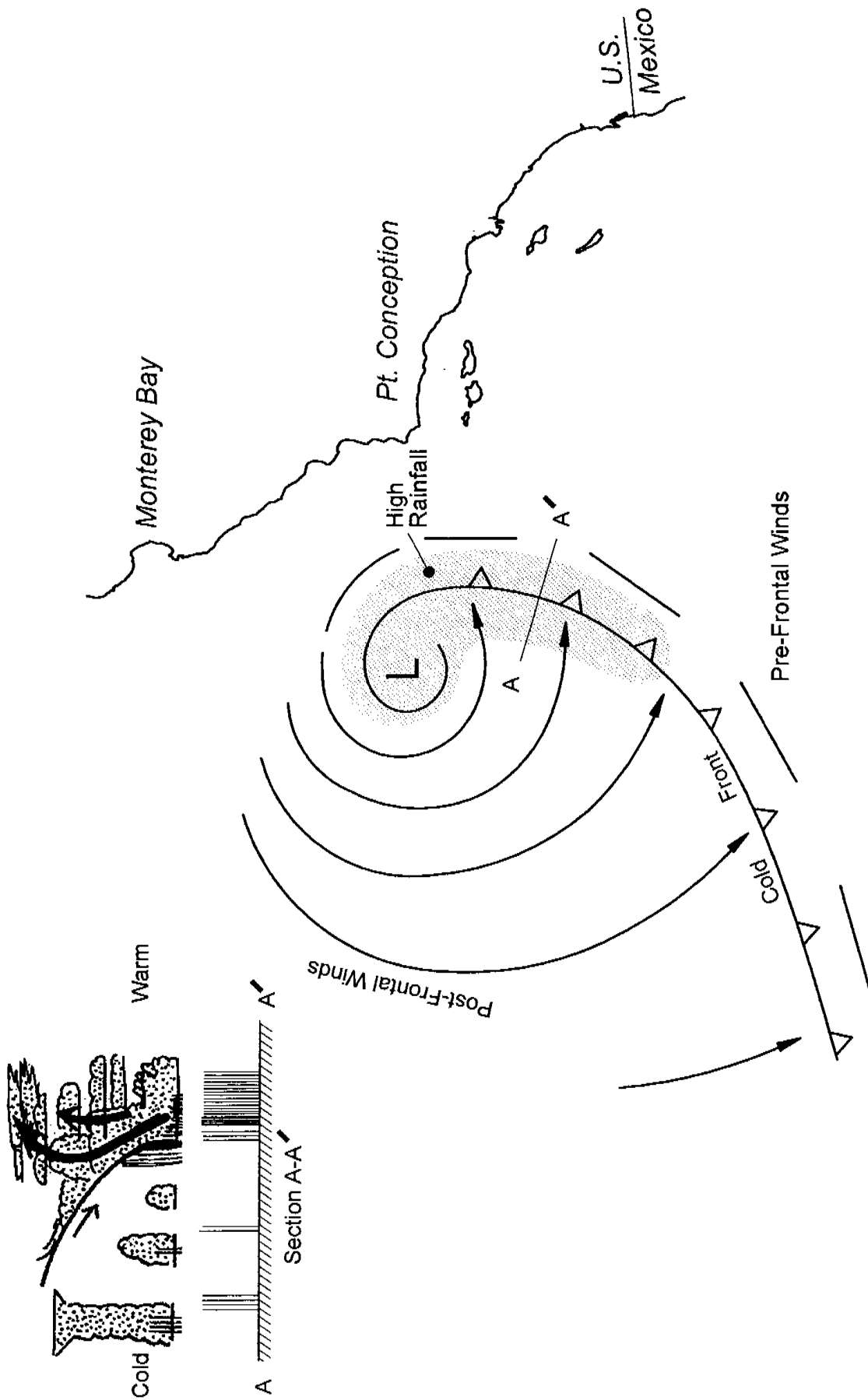


Figure 3.6. Anatomy of El Niño storms.

encounter the orography of the Southern California Bight, and thus the post-frontal swells are often more persistent and longer lived. In total, the El Niño storms have two distinct swell patterns that are directionally bipolar with regard to littoral drift along the lower reaches of the Bight. These directional characteristics tend to diminish the typical southward directed littoral drift, and instead act to drive the littoral drift back and forth along the coast with a small net direction.

In considering the predominant wave directions for high energy swells reaching the Huntington Beach area, the sheltering effects of the Channel Island System must be taken into account. Figure 3.7 shows that only certain gaps or “*wave windows*” between the islands and intervening land masses will allow the high energy, long period swells of distant storms to reach Huntington Beach. There are two distinct wave windows: 1) a *south window* providing wave exposure to swells approaching from between 160° and 200° true; 2) a *west window* open to swells from 255° to 279°. All remaining directions between these wave windows are open only to locally generated wind waves that are not likely to effect mixing and dilution below the thermocline.

For calibration and simulations of dispersion and dilution at AES Huntington Beach continuous unbroken wave records are required and must provide wave height, period and direction. Waves have been routinely monitored at several locations in the lower Southern California Bight since 1980 by the Coastal Data Information Program, (CDIP, 2004). The nearest CDIP directional wave monitoring sites are:

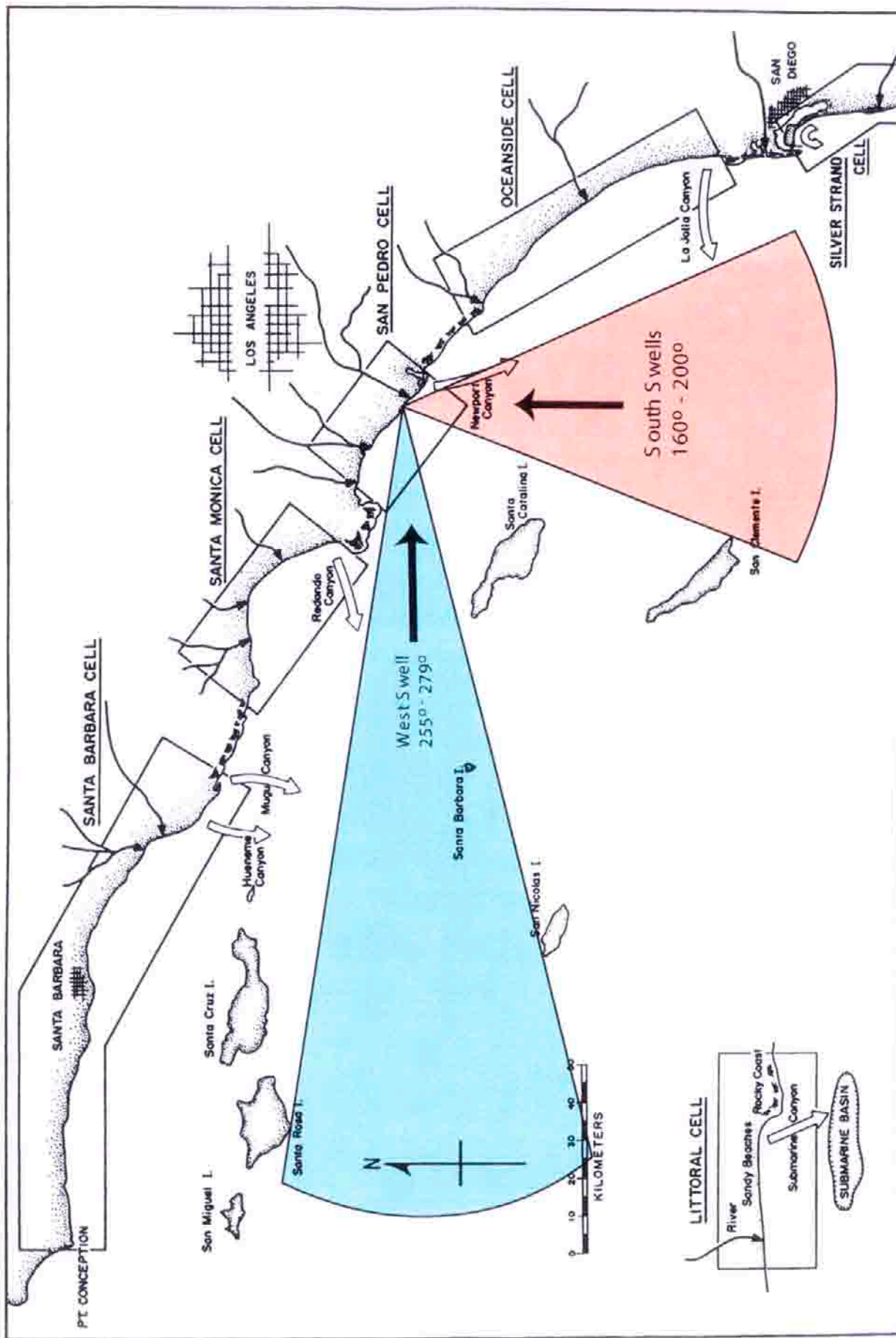


Figure 3.7. Island Sheltering Effects at AES Huntington Beach, CA Power Plant.

a) Huntington Beach Array

- Station ID: 07201
- Location:
 - 33 37.9'North, 117 58.7'West
 - Approximately 1 mile west of lifeguard headquarters at Huntington Beach, CA
- Water Depth (m): 10
- Instrument Description:
 - Underwater Directional Array
- Measured Parameters:
 - Wave Energy
 - Wave Period
 - Wave Direction

b) San Clemente

- Station ID: 05201
- Location:
 - 33 25.2'North, 117 37.8'West
 - 1000 ft NW of San Clemente Pier
- Water Depth (m): 10
- Instrument Description:
 - Underwater Directional Array
- Measured Parameters:
 - Wave Energy
 - Wave Period
 - Wave Direction

c) Oceanside Array

- Station ID: 00401
- Location:
 - 33 11.4'North, 117 23.4'West
 - 500 feet SW of pier
- Water Depth (m): 10
- Instrument Description:
 - Underwater Directional Array
- Measured Parameters:
 - Wave Energy
 - Wave Period
 - Wave Direction

In addition to these CDIP sites waves have been monitored at Torrey Pines Beach from 1972 until 1984 by the SAS Stations deployed by Scripps Institution of Oceanography, (SIO), Pawka (1982). These data sets possessed gaps at various times due to system failure and a variety of start ups and shut downs due to program funding and maintenance. The undivided data sets were pieced together into a continuous record from 1980-2000 and entered into a structured preliminary data file. The data in the preliminary file represent partially shoaled wave data specific to the local bathymetry around each monitoring site. To correct these data to the nearshore of Huntington Beach, they are entered into a refraction/diffraction numerical code, back-refracted out into deep water to correct for local refraction and island sheltering, and subsequently forward refracted into the immediate neighborhood of Huntington Beach. Hence, wave data off each monitoring site was used to hindcast the waves at Huntington Beach.

The backward and forward refractions of CDIP and SIO data to correct it to Huntington Beach was done using the numerical refraction-diffraction computer code, **OCEANRDS**. The primitive equations for this code are lengthy, so a listing of the FORTRAN codes of **OCEANRDS** appear in Appendix D. These codes calculate the simultaneous refraction and diffraction patterns propagating over a Cartesian depth grid. A large outer grid was used in the back refraction calculations to correct for island sheltering effects, while a high resolution inner grid was used for the forward refraction over the complex bathymetry around Huntington Beach and the OCSD deep outfall. **OCEANRDS** uses the parabolic equation method (PEM), Radder (1979), applied to the mild-slope equation, Berkhoff (1972). To account for very wide-angle refraction and diffraction relative to the principle wave direction, **OCEANRDS** also incorporates the high order PEM Pade approximate

corrections modified from those developed by Kirby (1986a-c). Unlike the recently developed REF/DIF model due to Dalrymple, et al. (1984), the Pade approximates in “OCEANRDS” are written in tesseral harmonics, per Jenkins and Inman (1985); in some instances improving resolution of diffraction patterns associated with steep, highly variable bathymetry such as found near the Newport Submarine Canyon. These refinements allow calculation of the evolution and propagation of directional modes from a single incident wave direction; which is a distinct advantage over the more conventional directionally integrated ray methods which are prone to caustics (crossing wave rays) and other singularities in the solution domain where bathymetry varies rapidly over several wavelengths.

An example of a reconstruction of the wave field throughout the Bight is shown in Figure 3.8 using the back refraction calculation of the CDIP data from the San Clemente array. Wave heights are contoured in meters according to the color bar scale and represent 6 hour averages, not an instantaneous snapshot of the sea surface elevation. Note how the sheltering effects of Catalina and San Clemente Islands have induced longshore variations in wave height throughout the Southern California Bight. Figure 3.9 shows the deep water significant wave heights, periods and directions resulting from the series of back-refraction calculations for the complete CDIP and SIO data set at $\Delta t = 6$ hour intervals over the 1980-2000 period of record. The data in Figure 3.9 are the values used as the deep water boundary conditions on the farfield grid (Figure 1.3) for the forward refraction computations into the Huntington Beach region. The deep water wave angles are plotted with respect to the direction (relative to true north) from which

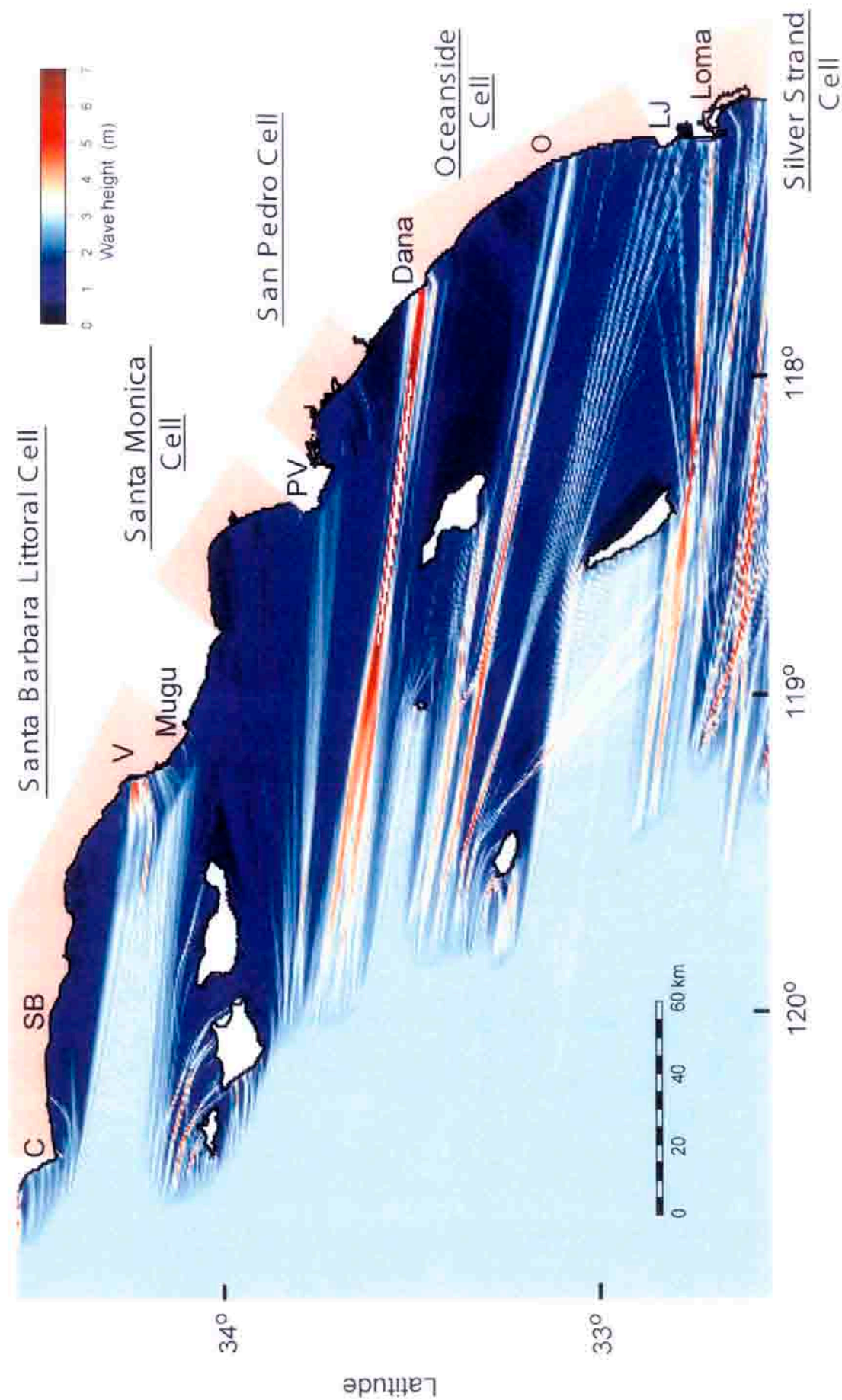


Figure 3.8. Back refraction of San Clemente CDIP data, for 13 January 1993 storm with 3 m high 15 sec waves approaching the Southern California Bight from 285°, an example of a moderate El Niño storm.

the waves are propagating at the deep water boundary of the farfield grid (Figure 1.3). Inspection of Figure 3.9 reveals that a number of large swells lined up with the wave windows open to Huntington Beach during the El Niño's of 1980-83, 1986-88, 1992-95, and 1997-98. The largest of these swell events was the 18 January 1988 storm, producing 4.5 m deep water swells off Huntington Beach (see event #6 in Figure 3.9).

Figure 3.10 gives an example of the forward refraction calculation over the farfield grid of the Huntington Beach region for the largest swells occurring during the peak flow month of February 1998. These swells occurring 5 February 1998 not concurrent with the peak flow event in the Santa Ana River which occurred later in the month on 24 February 1998. The 5 February 1998 swells were pre-frontal southwesterly for-runners of the El Niño storm that struck the Huntington Beach region with a series of powerful squalls between 7 and 10 February 1998. This was the second largest flood event of February 1998. The highest rainfall producing storm of the month was accompanied by southwesterly swells that were almost as large as the 5 February 1998 fore-runners. These swells arrived concurrent with the peak rainfall event of 24 February 1998 El Niño storm and produced the regional refraction pattern shown in Figure 3.11. Comparing the refraction patterns of both storms in Figures 3.10 and 3.11, we find a region of intensified wave heights at the AES infall. This is referred to as a *bright spot* in the refraction pattern and represents an area where wave energy has been focused, (in this case by the refraction caused by a small canyon in the shelf directly offshore of AES Huntington Beach). The increased wave heights in the bright spot at the infall increase the mixing and turbulence generated by the seabed

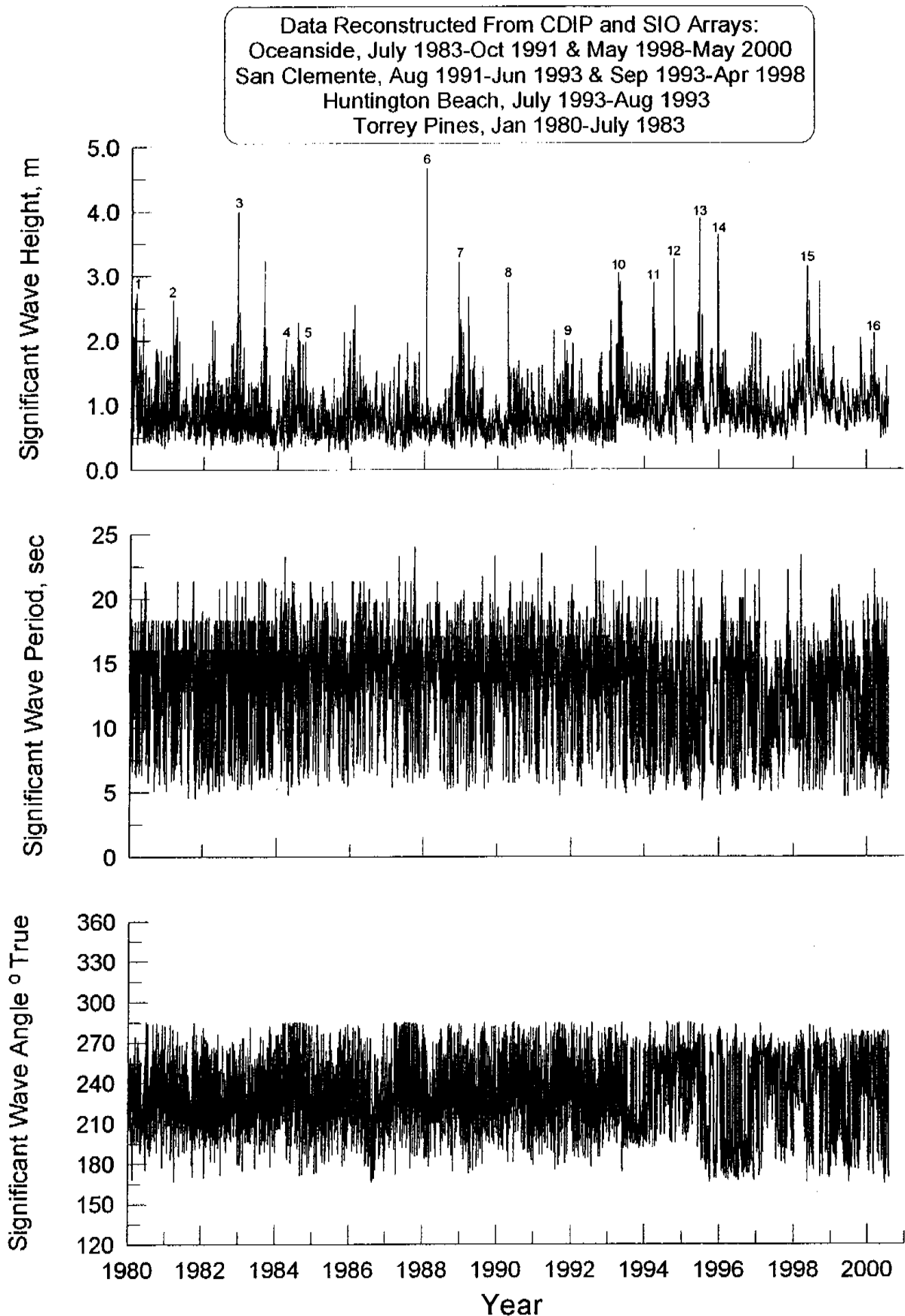


Figure 3.9. Deep water wave data for disperion and dilution analysis at AES Huntington Beach, CA.

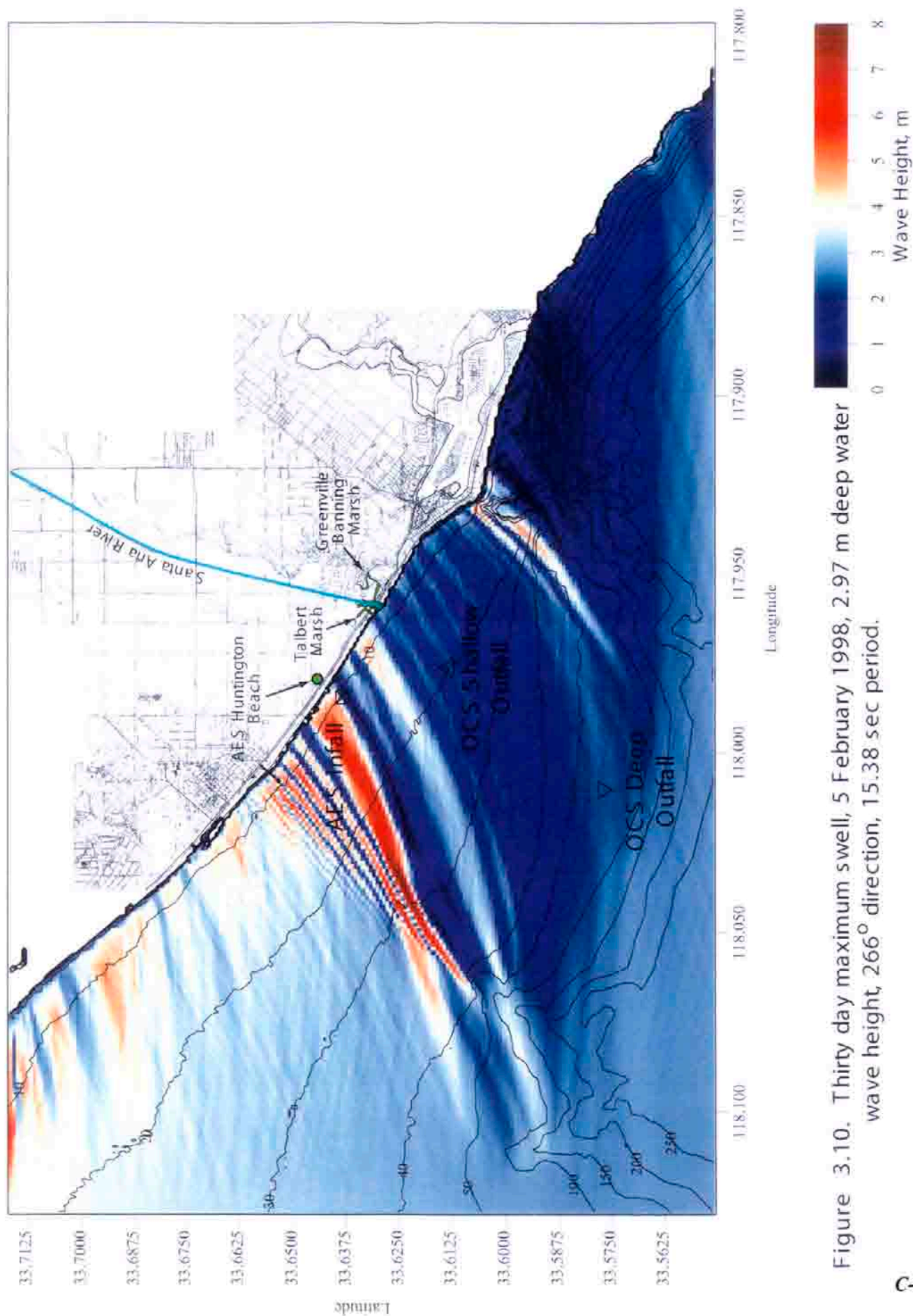


Figure 3.10. Thirty day maximum swell, 5 February 1998, 2.97 m deep water wave height, 266° direction, 15.38 sec period.

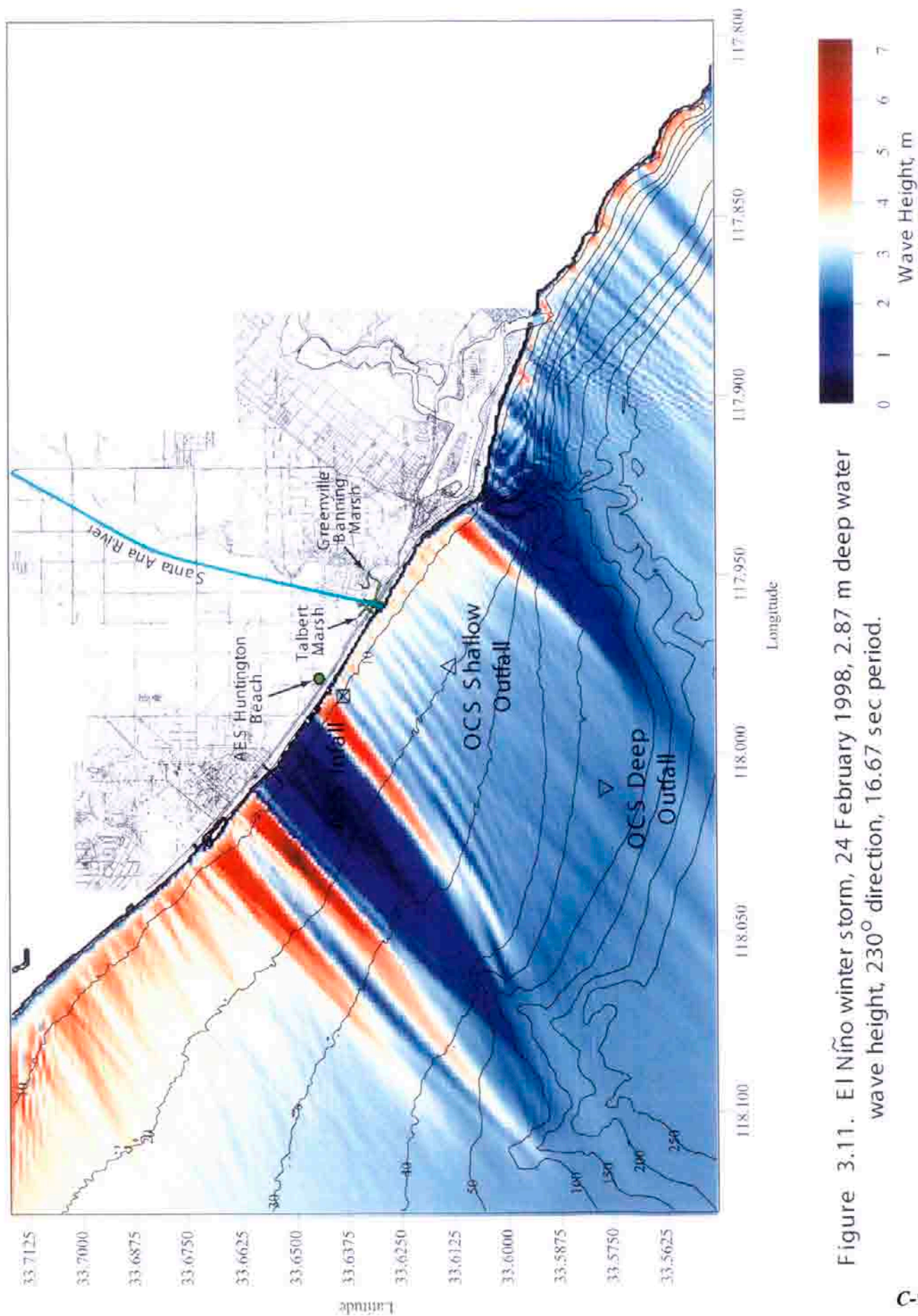


Figure 3.11. El Niño winter storm, 24 February 1998, 2.87 m deep water wave height, 230° direction, 16.67 sec period.

boundary layer and by oscillatory wakes of the infall tower structure. This increases the likelihood of the heavier than seawater by-products of the RO process being mixed upward into the water column from the discharge and subsequently recirculated through the infall. Therefore these El Niño winter storm waves serve to provide low flow case scenarios for evaluating re-circulation effects on source water make-up (Sections 7-9).

To evaluate maximum likelihood scenarios for the northward transport of bacteria from Talbert Marsh or the wastefield from the OCSD deep outfall toward the AES infall, we consider summer time El Niño wave conditions like those that occurred 7 August 1997, Figure 3.12. The extreme southerly direction of these waves (from 190°) produce northward flowing wave induced mass transport in shallow water. Inspection of Figure 3.12 shows a fairly uniform shoaling of incident waves between the Santa Ana River and the AES infall. We also find that the bright spot of intensified wave mixing has moved north of the AES infall. This shift in the bright spot does not diminish the low flow case pessimism because the OCSD wastefield is buoyant and does not require intense local mixing to raise it in the water column to the elevation of the infall velocity cap.

Refraction patterns for other storms evaluated from the period of record for effects on source water and dilution are contained in Appendix G. In addition to these, Appendix G contains the refraction of the 30 day average minimum wave and the average annual wave. The 20.5 year record of daily mean wave height is plotted in Panel-b of Figure 3.24 found at the end of this section, summarizing the complete set forcing functions.

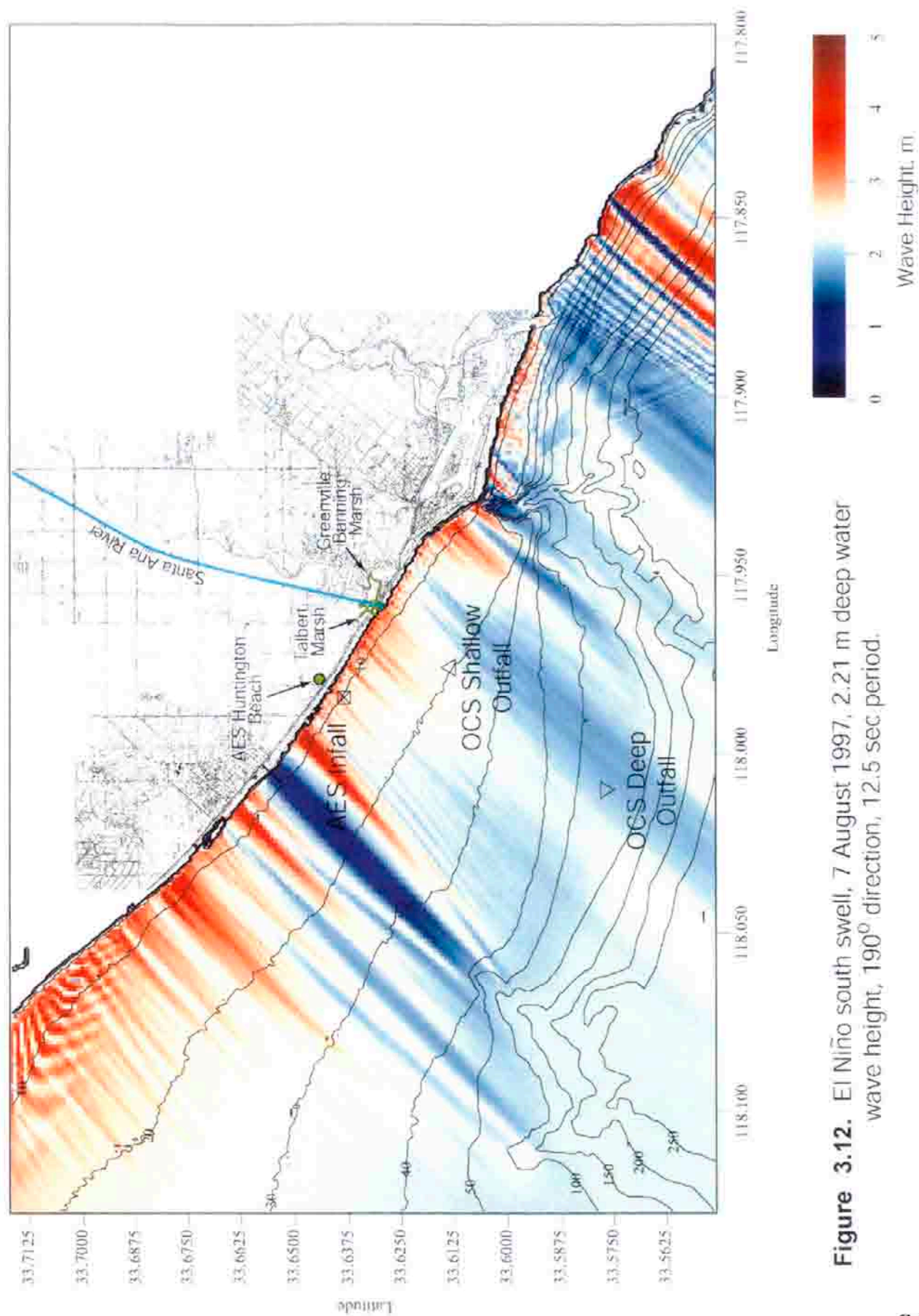


Figure 3.12. El Niño south swell, 7 August 1997, 2.21 m deep water wave height, 190° direction, 12.5 sec period.

E) Current Forcing

While waves dominate the initial dilution and dispersion of heat and concentrated seawater discharge in the inshore domain, the tidal currents control dilution and dispersion in the offshore domain, particularly in the immediate neighborhood of the AES outfall. Tidal currents were calculated using the tidal constituents from the tide gage station at Los Angeles (NOAA #941-0660). Current forcing is predominantly tidal in the offshore domain of the Huntington Beach coastal region in Figure 1.3, and is a combination of tidal and wave-induced currents in the nearshore domain.

Tidal currents are mixed semi-diurnal with both progressive and standing components in the mid to inner shelf. Tidal currents flow parallel to the shore in a northwestward direction on flood tide (Figure 3.13) and southeastward on an ebb tide (Figure 3.14). The tidal current speed diminishes towards shore due to friction in the shallow coastal boundary layer, and the phase of the tidal motion varies in the cross-shore direction such that during tidal reversals from ebb to flood, the phase of the inshore motion is lagging the offshore motion (Figure 3.15). The maximum currents in the offshore domain are typically 40 to 70 cm/sec. Along the Huntington/Newport Beach coast the tidal currents are ebb dominated such that over one tidal day (24 hr 50 min) the net current flows downcoast to the southeast as shown in Figure 3.16 for the peak runoff event day of 24 February 1998. Each progressive vector plot in Figures 3.13 to 3.16 is composed of self-scaling vectors in units of cm/sec proportional to the vector length in the lower left hand corner, which represents the largest current vector found anywhere on the plot.

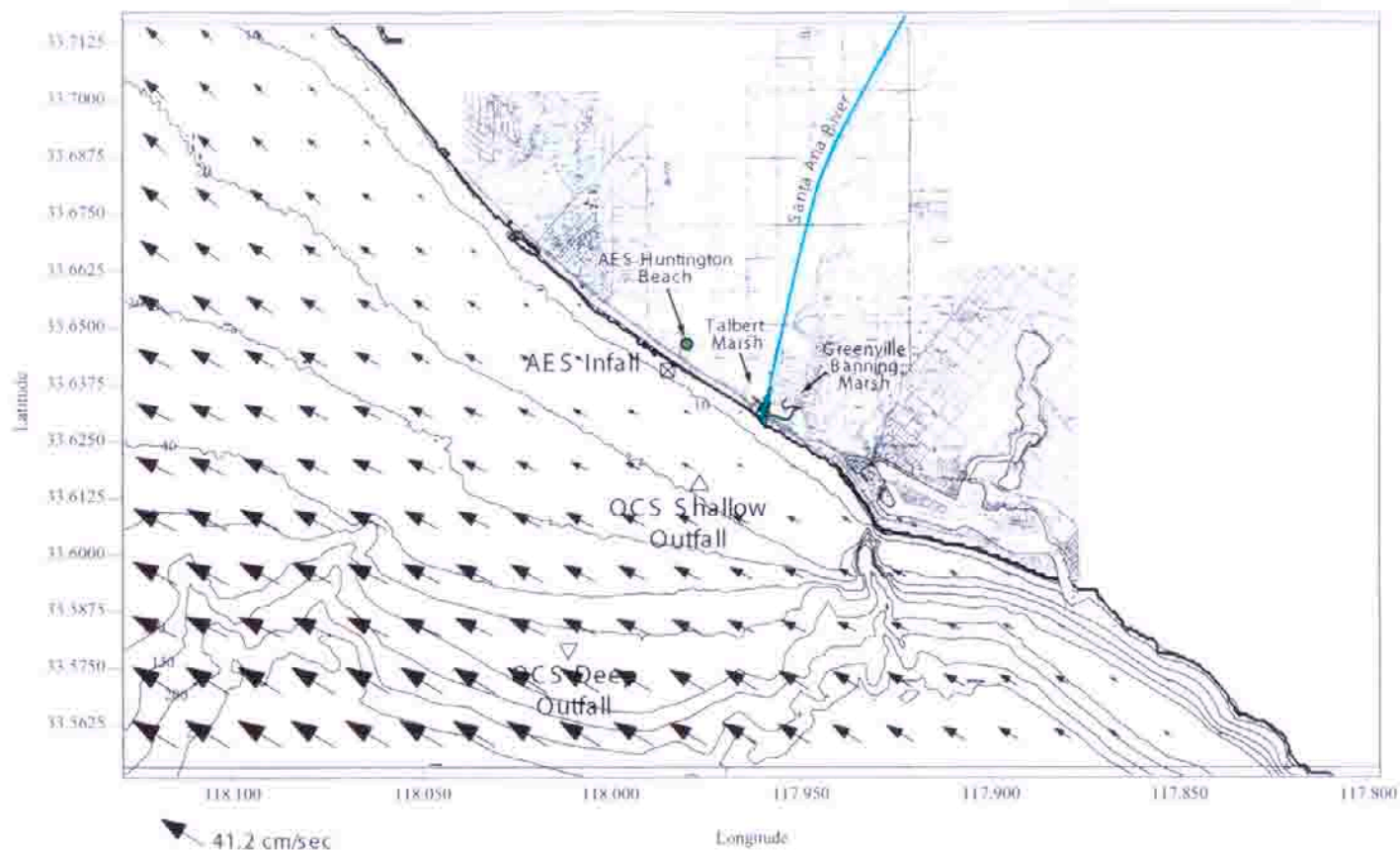


Figure 3.13. Tidal current simulation for Newport - Huntington Beach, flood tide, 24 February 1998, 04:09 PST. Current vector magnitude relative to largest vector arrow shown (41.2 cm/sec).

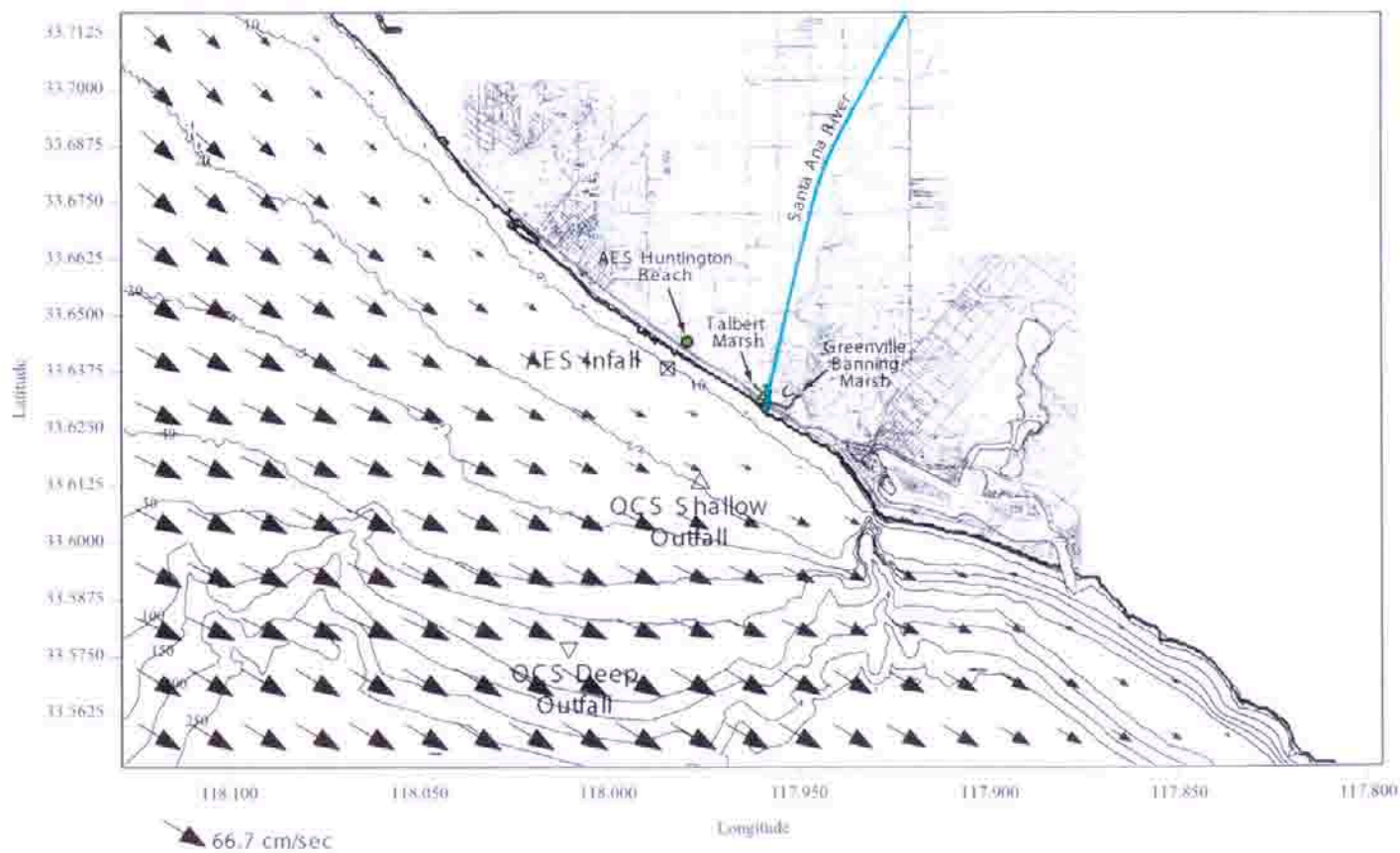


Figure 3.14. Tidal current simulation for Newport - Huntington Beach, ebb tide, 24 February 1998, 10:54 PST. Current vector magnitude relative to largest vector arrow shown (66.7 cm/sec).

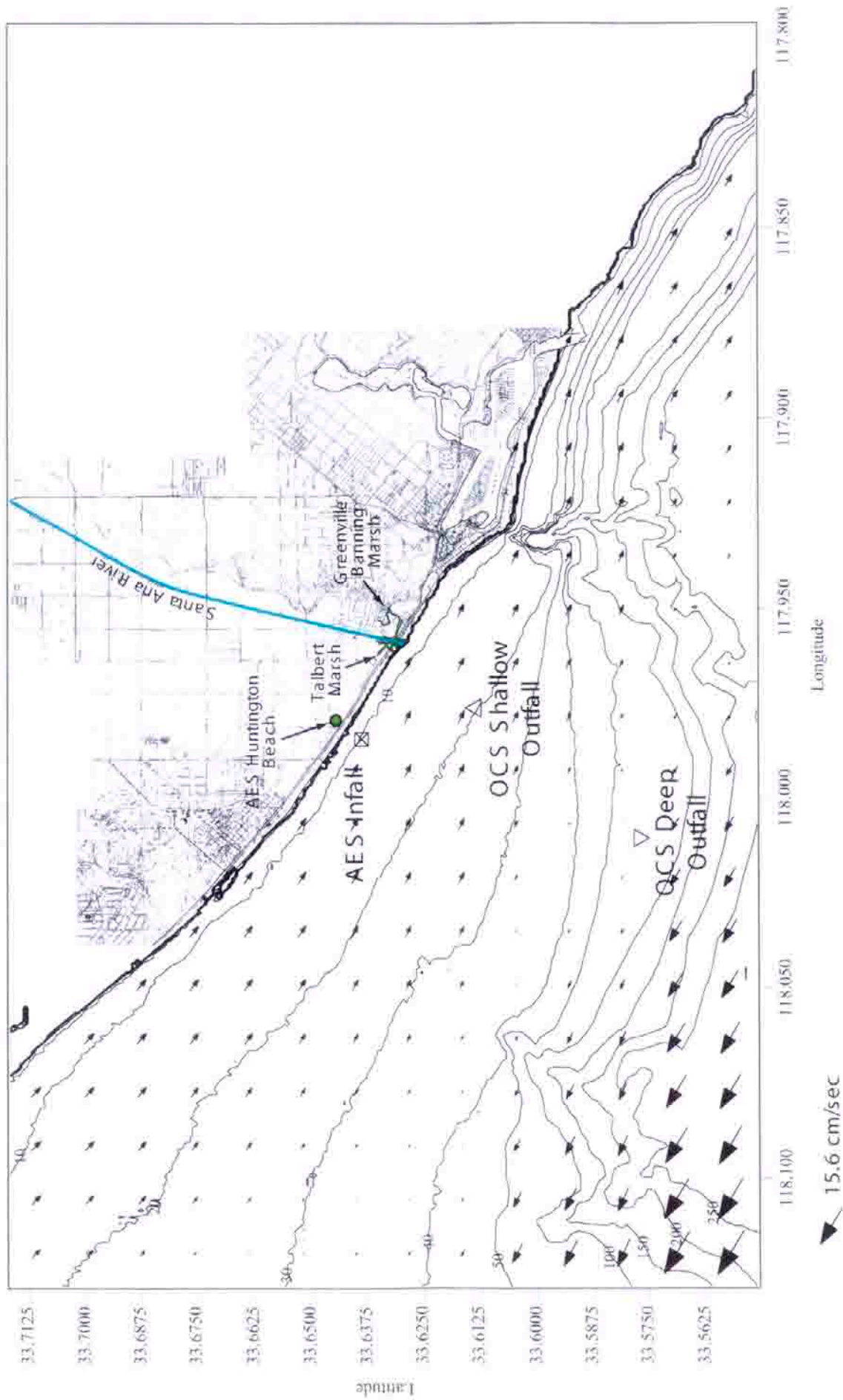


Figure 3.15. Tidal current simulation for Newport - Huntington Beach, ebb to flood tide transition, 24 February 1998, 14:10 PST. Current vector magnitude relative to largest vector arrow shown (15.6 cm/sec).

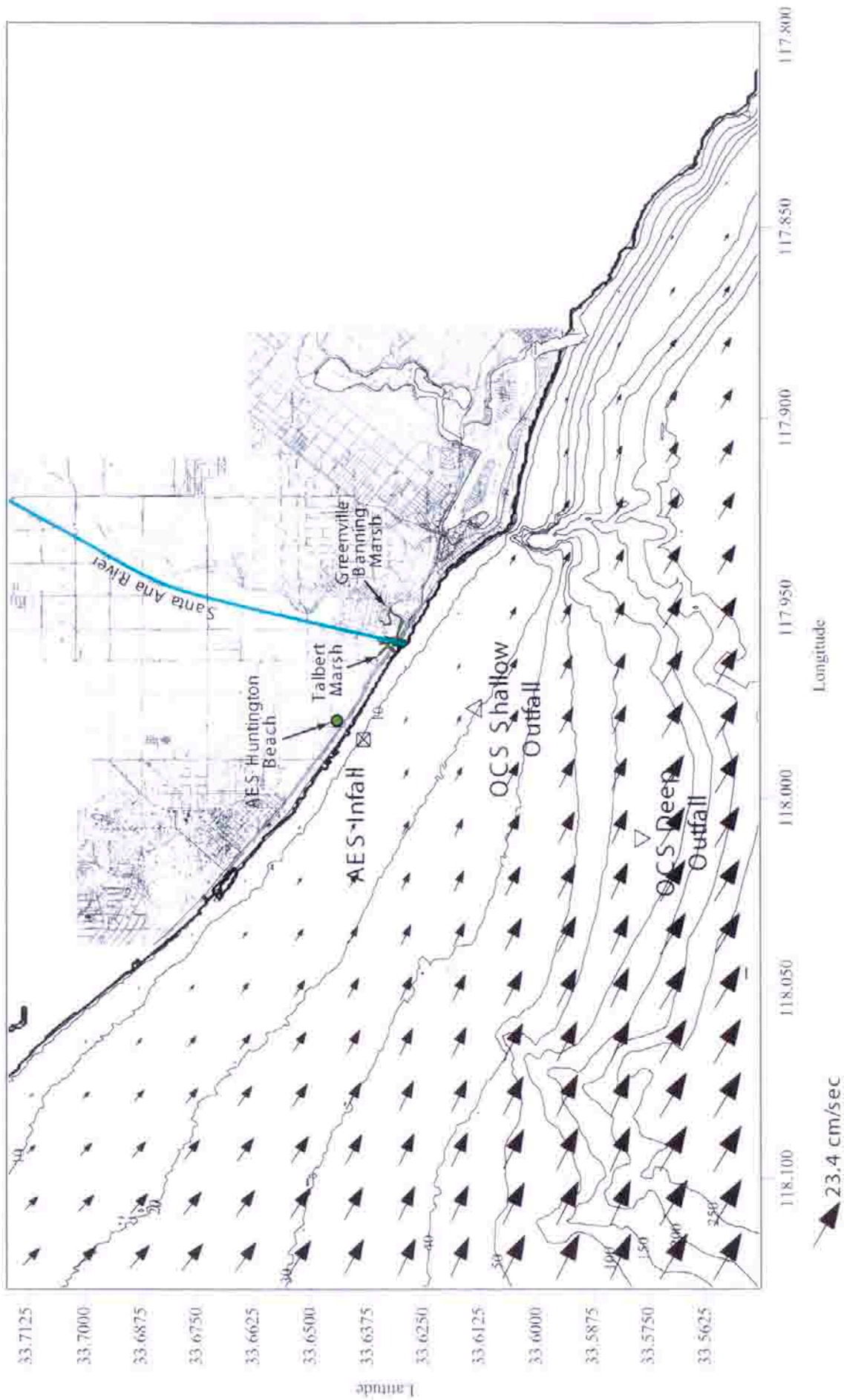


Figure 3.16. Tidal current simulation for Newport - Huntington Beach, tidal day, 24 February 1998. Current vector magnitude relative to largest vector arrow shown (23.4 cm/sec).

Wave induced currents predominate nearshore where wave shoaling effects are maximum. Wave induced currents increase with increasing wave height and remain significant over a nearshore domain extending 4 to 5 surf zone widths seaward of the shoreline. They flow longshore generally in the direction of longshore energy flux and away from areas of high waves (bright spots) and towards areas of low waves (shadows). These longshore currents increase with increasing wave height and obliquity. Figure 3.17 gives an example of the wave induced longshore currents for the El Niño storm of 24 February 1998. Note how these currents are confined to the very nearshore and how they are directionally controlled by the local refraction in Figure 3.11.

Figure 3.18 gives the progressive vector plot for the 7 day average of the combined tidal and wave-induced current field during the peak flow period of the Santa Ana River (Figure 3.2). We note that the net transport over a 7-day period is downcoast to the southeast due to the ebb dominance of the tidal currents. Inshore the net transport is very small because the wave and tidal currents tend to cancel out one another over a 7-day period. However over shorter periods of time for the summer El Niño conditions in August 1997 sustained large south swells cause a reversal in the net transport in the inshore domain (Figure 3.19). These inshore current structures will be overlaid on the spring flood tide condition on 17 August 1997 with sustained northerly transport throughout the middle and inner shelf domain (Figure 3.20). Together these 2 current fields (Figure 3.19 & Figure 20) produce a composite low flow case model scenario for evaluating the potential for dispersion of the OCSD wastefield into the neighborhood of the AES in-fall. The 20.5 year record of daily maximum tidal currents is plotted in Panel-b of Figure

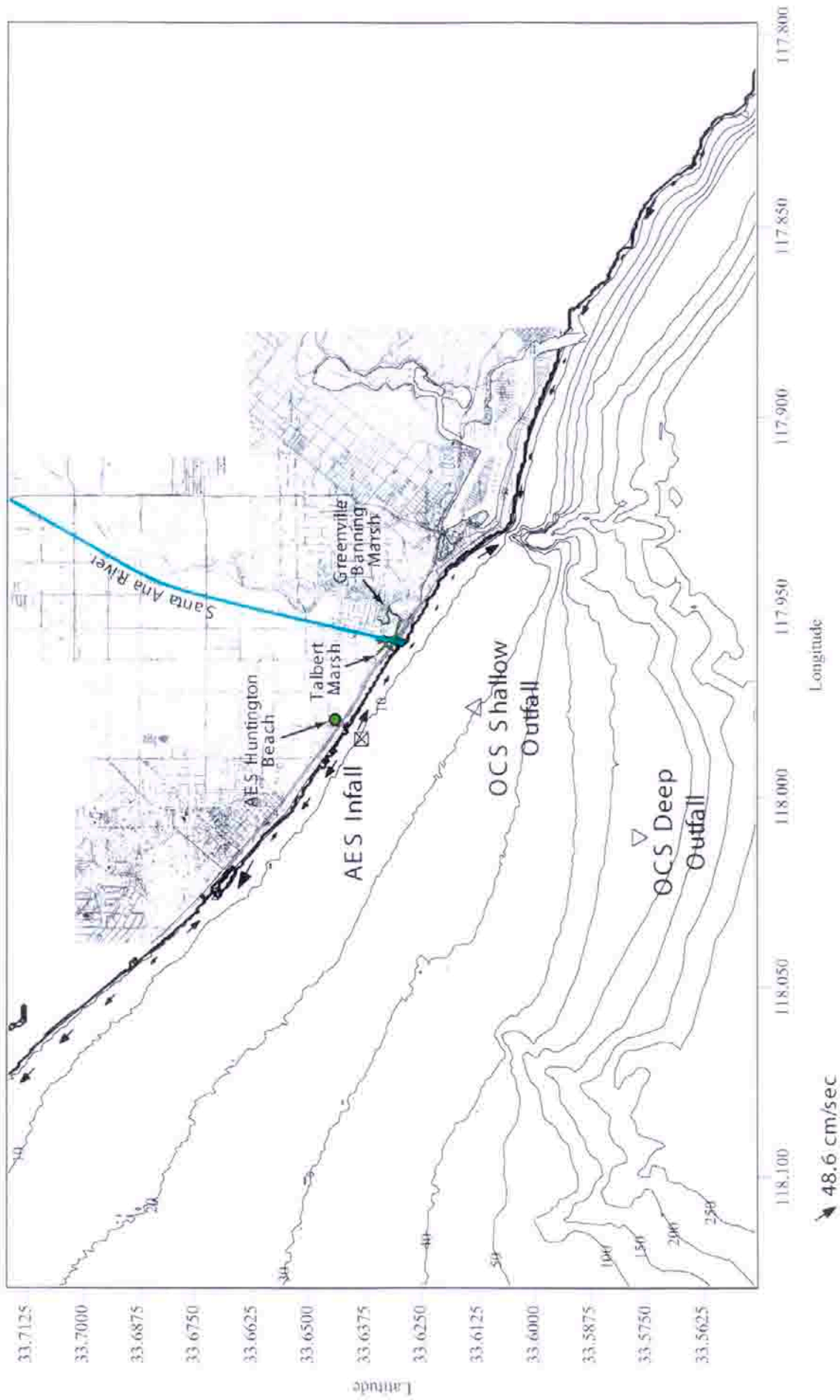


Figure 3.17. Wave current simulation for Newport - Huntington Beach, 24 hour average, 24 February 1998, 23:38 P.S.T. Current vector magnitude relative to largest vector arrow shown (48.6 cm/sec).

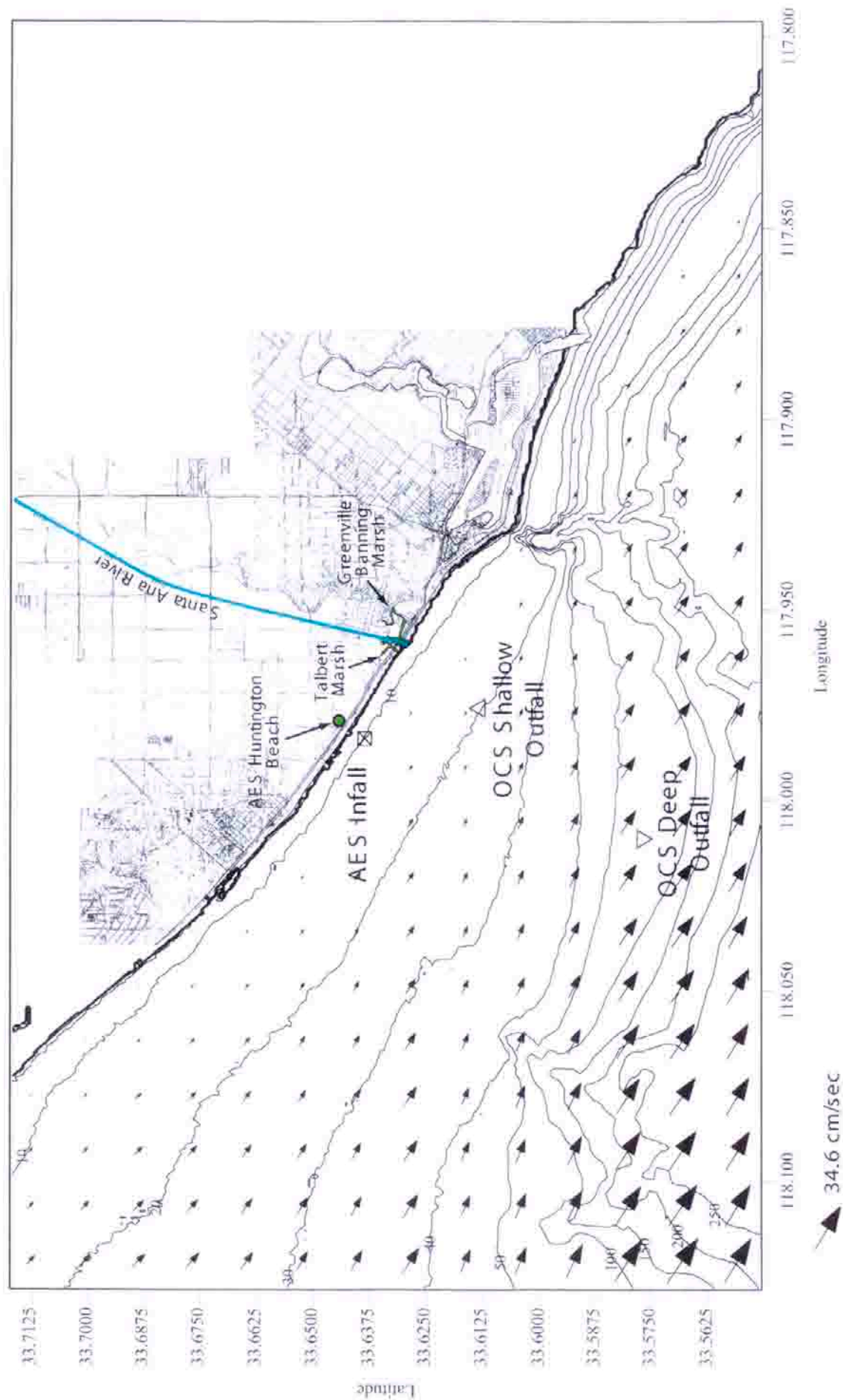


Figure 3.18. Mean current simulation (7 day average) for Newport - Huntington Beach, 22-28 February 1998, Current vector magnitude relative to largest vector arrow shown (34.6 cm/sec).

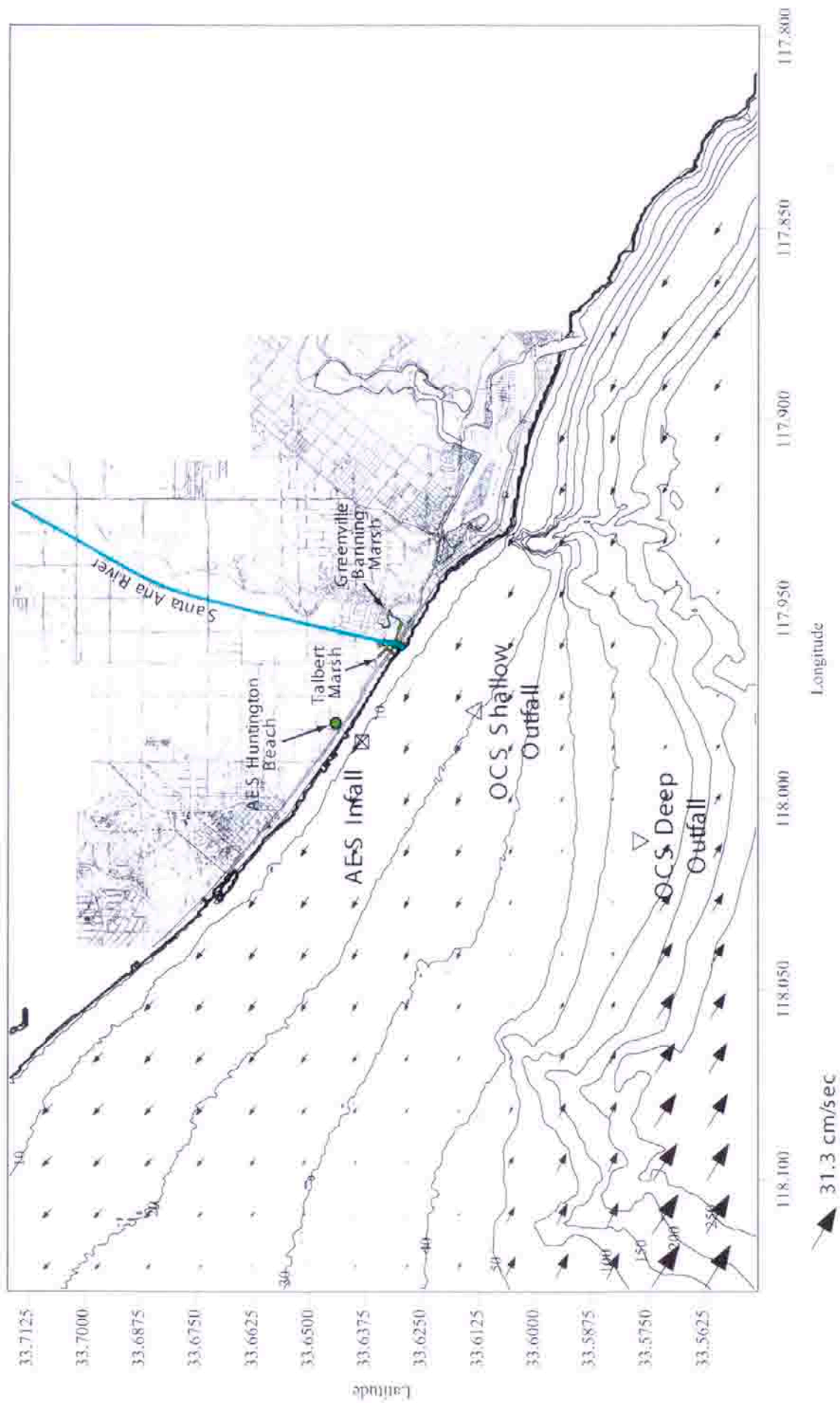


Figure 3.19. Mean current simulation (3 day average, El Niño) for Newport - Huntington Beach, 7-10 August 1997, Current vector magnitude relative to largest vector arrow shown (31.3 cm/sec).

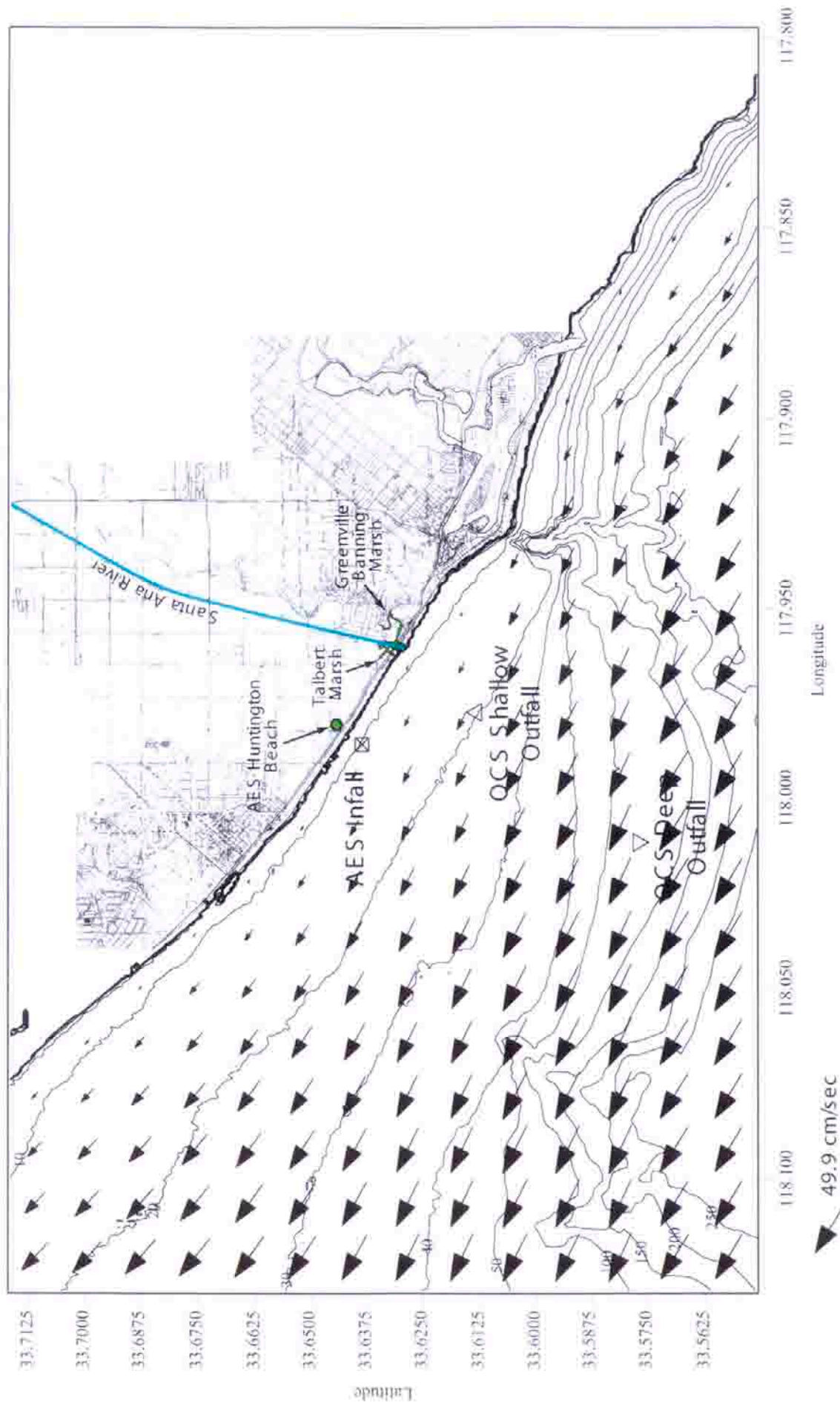


Figure 3.20. Current simulation for Newport - Huntington Beach, flood tide, 17 August 1997, 00:21 PST, Current vector magnitude relative to largest vector arrow shown (49.9 cm/sec).

3.24 found at the end of this section, summarizing the complete set forcing functions.

F) Wind Mixing

Winds provide considerable mixing in the surface layer off Huntington Beach Daily that typically extends down to depths of 10-20 m. Winds also provide wind drift which although weak can bridge the gap between the off shore tidally dominated regime and the inshore wave-dominated regime. The collection of historical wind data are compiled in US Surface Airways Data available from the National Climate Data Center document library (NCDC , 2004). The closest NCDC Surface Airways monitoring location relative to Huntington Beach is Long Beach Daugherty Field. Here, human observations of surface winds were collected and archived by NCDC beginning 1 January 1964 until 31 August 1996, after which wind observations were taken by means of the Automated Surface Observing System (ASOS). Combining these 2 data bases, a continuous surface wind record was assembled for the period 1980-2000 as shown in Panel-c of Figure 3.24, along with the other forcing functions summarized at the end of this section. Because the lower Southern California Bight is a “wind drought” region due to orographic blocking by the Penninsular Range, the 20.5 year mean wind speed is only 5.6 knots. However, El Niño storms and North Pacific cold fronts episodically increase wind speeds to a maximum 24 hour mean of 19.6 knots, as occurred during the 1997 El Niño storms. The minimum daily mean wind speed is 0 knots. The long term record in Figure 3.24 shows a well defined inter annual (seasonal) modulation of daily mean winds, with a 3-7 year intensification associated with El Niño.

G) Ocean Salinity

Ocean salinity variation exerts a modulating effect on the concentration of sea salts discharged from the desalination plant. The proposed desalination plant will divert approximately 100 mgd of heated HBGS condenser seawater through a reverse osmosis system (RO) before in-plant waste streams are added to the cooling water discharge. The RO system will produce 50 mgd of product from the 100 mgd of cooling water diverted from the condenser cooling stream. The RO system will discharge 50 mgd of concentrated seawater by-product at twice ambient ocean salinity, which is subsequently diluted in the remaining cooling water discharge stream. Therefore, the concentration of sea salts in the discharge varies directly with ocean salinity at the intake to the generating station.

Figure 3.21a shows the variation in daily mean salinity in the coastal waters off Huntington Beach derived from 20.5 years of NPDES monitoring data of the AES and OCSD outfall for the period from 1980 until mid-2000. Gaps in these daily records were filled salinity monitoring data from the Scripps Pier Shore Station located 109 km (67.8 miles) to the south east of the AES outfall, (SIO, 2001). Inspection of Figure 3.21a indicates that the ocean salinity varies naturally by 10% between summer maximums and winter minimums, with a long term average value of 33.52 parts per thousand (ppt). Maximum salinity was 34.34 ppt during the 1998 summer El Nino when southerly winds transported high salinity water from southern Baja up into the Southern California Bight. Minimum salinity was about 31.02 ppt during the 1993 winter floods. The variation between maximum and minimum salinity is about 3.32 ppt, which is about 10% of the average value of 33.5 ppt. An ocean salinity histogram is given in Figure 3.21b that indicates the ocean salinity exceeded the 33.5 ppt average value during 2,488

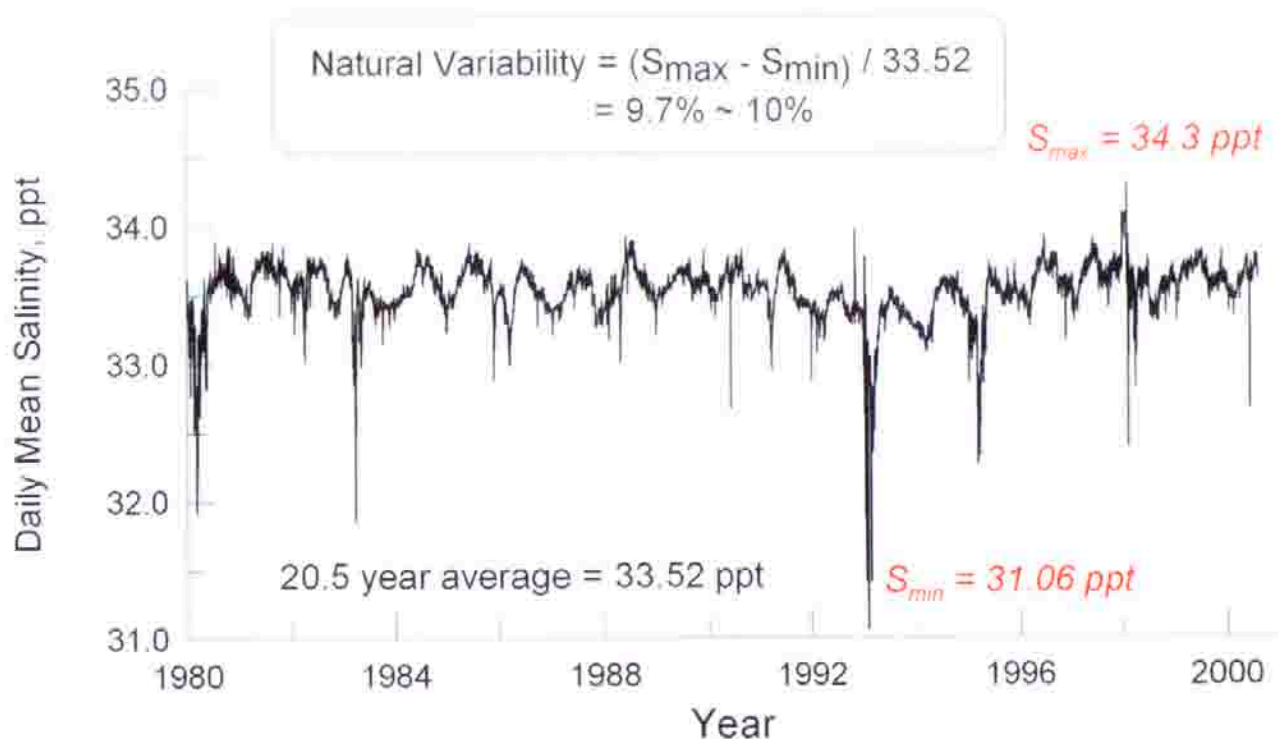


Figure 2a. Period of record for ocean water daily mean salinity, Huntington Beach, 1980-2000. [data from NPDES monitoring reports for AES and OCSD outfalls, in MBC, 1980-2001; OCSD, 1993, 2000]

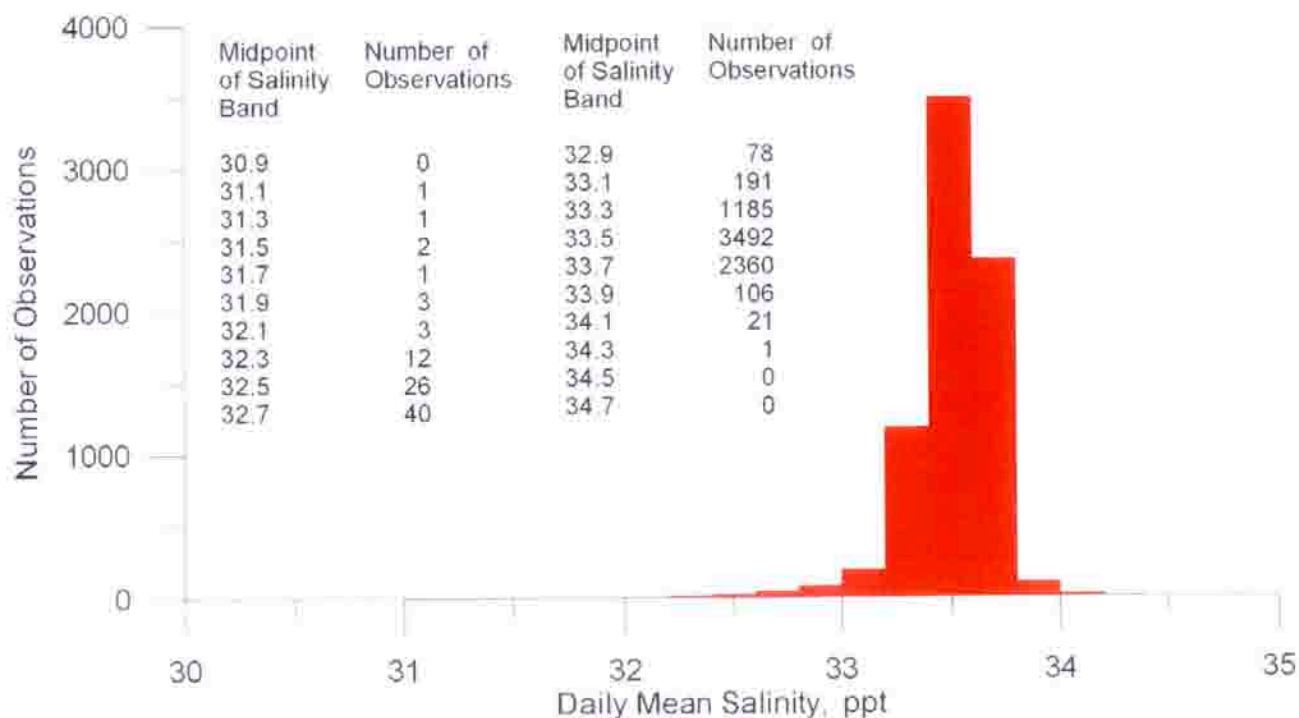


Figure 3.21. Histogram of ocean water daily mean salinity, Huntington Beach, 1980-2000. [from MBC, 1980-2001; OCSD, 1993, 2000]

days of the period of record and were below average during 1,543 days. Therefore above average salinities are more common than below average salinities. Average salinities were observed a total of 3,492 days of the period of record, or about 46% of the time. (These data are also confirmed by long term salinity monitoring at Scripps Pier NOAA Station #941-0230, and by 55 CalCOFI cruises in the Southern California Bight between 1984 and 1997, see SIO, 2001; Roemmich, 1989, and Bograd, et al, 2001).

H) Ocean Temperature

Ocean temperature effects the buoyancy of the combined discharge of the generating station and the desalination plant. The ocean temperature further effects the buoyancy of the discharge through the absolute temperature of the plant discharge, which is regulated under the NPDES permit by a ΔT limit relative to ocean temperature. This buoyancy effect is calculated by the specific volume change of the discharge relative to the ambient ocean water according to Equation (5). The buoyancy of the plume exerts a strong effect on the mixing and rate of assimilation of the excess heat and sea salts by the receiving waters.

We use the average of temperature records from NPDES monitoring data along the 8.5 meter depth contour at Stations 8a and 8g to characterize the temperature environment off AES Huntington Beach (see MBC 1980-2002, NPDES Monitoring Reports). We use the average of these 2 stations to avoid aliasing from the thermal plume emitted from the AES outfall at Station 8d. Gaps in the record derived from Stations 8a and 8g were preferentially filled with temperature data from the NPDES monitoring reports of the OCSD outfall (OCSD, 1993,2000). Any remaining gaps were filled from the Scripps Pier Shore Station (SIO, 2001). The

20.5 year record of daily mean ocean water temperatures is plotted in Panel-c of Figure 3.23 found at the end of this section, summarizing the complete set of boundary conditions. A pronounced seasonal variation in these temperatures is quite evident with the maximum recorded daily mean temperature reaching 25.1 °C during the summer of the 1993 El Niño and the minimum falling to 9.9 °C during the winter of the 1999-2000 La Niña. The 20.5 year mean temperature was found to be 17.6 °C. On a percentage basis, the natural variability of the temperature of coastal waters in the vicinity of AES Huntington Beach Generating station is significantly greater than that of salinity (on the order of $\Delta T = 86\%$ vs $\Delta S = 10\%$).

I) HBGS Operating Temperatures

California's Thermal Plan incorporates provisions of Section 316(a) of the Federal Water Pollution Control Act of 1972 and defines the relevant regulatory requirements for cooling water discharge from the AES Huntington Beach Generating station. Although certified to discharge thermal waste at as much as 30 °F (16.5 °C) above ambient ocean temperatures, ($\Delta T = \Delta T = 30$ °F), the AES plant operators have adopted operating procedures that discharge considerably below the maximum certified Delta-T. NPDES monitoring data from MBC (1980-2002) show that the plant discharge temperatures track the ambient ocean temperatures rather clearly with an average Delta-T of 18 °F (10 °C). This value is used for modeling marine environmental effects due to desalination during normal electrical generation activities. The discharge temperatures occasionally spike to as high as 113 °F (45 °C) during short term heat treatment cycles performed to remove bio-fouling from the cooling water circulation system. (NPDES permit constraints limit heat treatments to a maximum of 125 °F). Since the desalination plant will not

operate during heat treatments, the heat treatment temperature spikes are neglected in the analysis. Regardless, high discharge temperatures promote rapid mixing and assimilation of the excess sea salts from desalination by reducing the negative density anomaly caused by the heavy brine. Therefore, we include in this study model results for “cold water” discharges (Delta-T of 0 °F) during *standby mode* when two circulation pumps are operating but the generating station is not operating its boilers to produce electricity.

J) Plant Flow Rates and Concentrated Sea Water Discharge Salinity

Generating station flow rates determine the volume of water available in-the-pipe to dilute the concentrated seawater discharge from the desalination plant. For example, if the ocean salinity is an average of 33.52 ppt then the RO unit will increase the salinity of the plant discharge to as much as 55.37 ppt if only one generating unit is operational, or as little as 37.19 ppt if all four generation units are operating, (Jenkins and Wasyl, 2001). Hence, the operational patterns of the plant will be an important determinant of the variability of the salinity of the combined discharge once the desalination plant is added to the sea water circulation loop of AES Huntington Beach. For the present study we will use 2 historical flow rate databases; 1) the 20.5 year period from 1980 to mid 2000 that preceded the completion of re-powering of HBGS, and 2) the 1.6 year post re-powering period from 1 January 2002 to 30 July 2003. The operational patterns engendered in these two records reflect both historic user demand for electrical power as well as recent plant equipment up-grades.

There are a total of eight cooling water pumps at AES Huntington Beach, each with a capacity ranging from 44,000 gpm to 46,300 gpm. They are paired two

per power generation unit, and there are four power generation units at the site. Because the pumps are operated in pairs as generating units are brought on-line, the cascade of flow rate is as follows:

Unit 1

2 pumps@44,000 gpm each

Combined Capacity = 88,000 gpm = 126.7 mgd

Units 1 and 2

4 pumps@44,000 gpm each

Combined Capacity = 176,000 gpm = 253.4 mgd

Units 1, 2 and 3

6 pumps@44,000 gpm each

Combined Capacity = 264,000 gpm = 380.2 mgd

Units 1, 2, 3 and 4

8 pumps@44,000 gpm each

Combined Capacity = 352,000 gpm = 506.9 mgd

AES Huntington Beach provided plant flow rate data in daily increments.

Figure 3.22 gives the annual averages of daily flow rates for the period 1979 -2002.

The average flow rate for this 24 year period is 234 mgd and no value is less

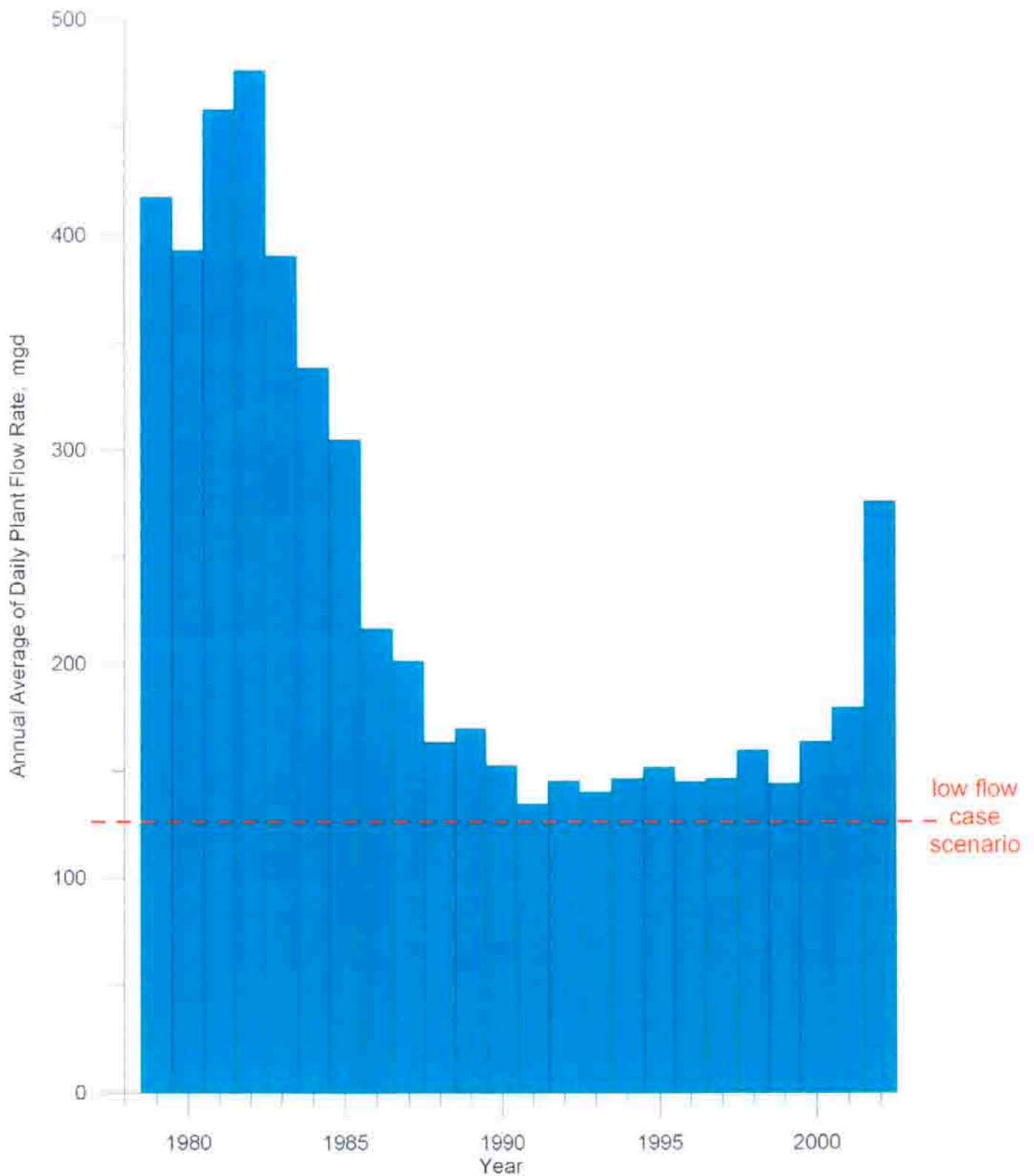


Figure 3.22. Annual average of the daily plant flow rate at AES Huntington Beach LLC generating station, 1979-2002. [from NDPES, 2002, courtesy of MBC Applied Environmental]

than the low flow case scenario of 126.7 mgd. The 20.5 year record of daily flow rates is plotted in Panel-a of Figure 3.23, summarizing the complete set of boundary conditions. Average daily flow rate for this model simulation period is 226 mgd. Both of these long term averages reflect a number of low production years from 1987-2000 when several of the generating units were down for equipment modernization. The closest operational scenario to either of these long term averages is 2 generation units to be on-line with cooling water circulation at 176,000 gpm or 253.4 mgd.

The cooling water pumping rate of seawater discharged through the offshore outfall may be supplemented by in-plant waste streams certified up to a maximum daily discharge of 1.66 mgd. These in-plant waste streams are primarily storm water draining off the site having fresh water salinities. The plant storm water is gravity fed into the discharge after the cooling water has past through plant condensers. The cooling water is typically heated to temperatures of 10°C above ambient seawater.

The proposed desalination plant will divert approximately 100 mgd of heated condenser water through a reverse osmosis system (RO) before in-plant waste streams are added to the cooling water discharge. The RO system will produce 50 mgd of product from approximately 100 mgd of cooling water diverted from the condenser cooling stream. The RO system will discharge 50 mgd of concentrated seawater by-product at twice ambient ocean salinity, which is subsequently diluted in the remaining cooling water discharge stream. Based on the pumping rate cascade stated above, the salinities and changes in specific volume of the combined generating station and desalination plant discharges are shown in Table 2. Here the discharge rates through the offshore outfall are listed

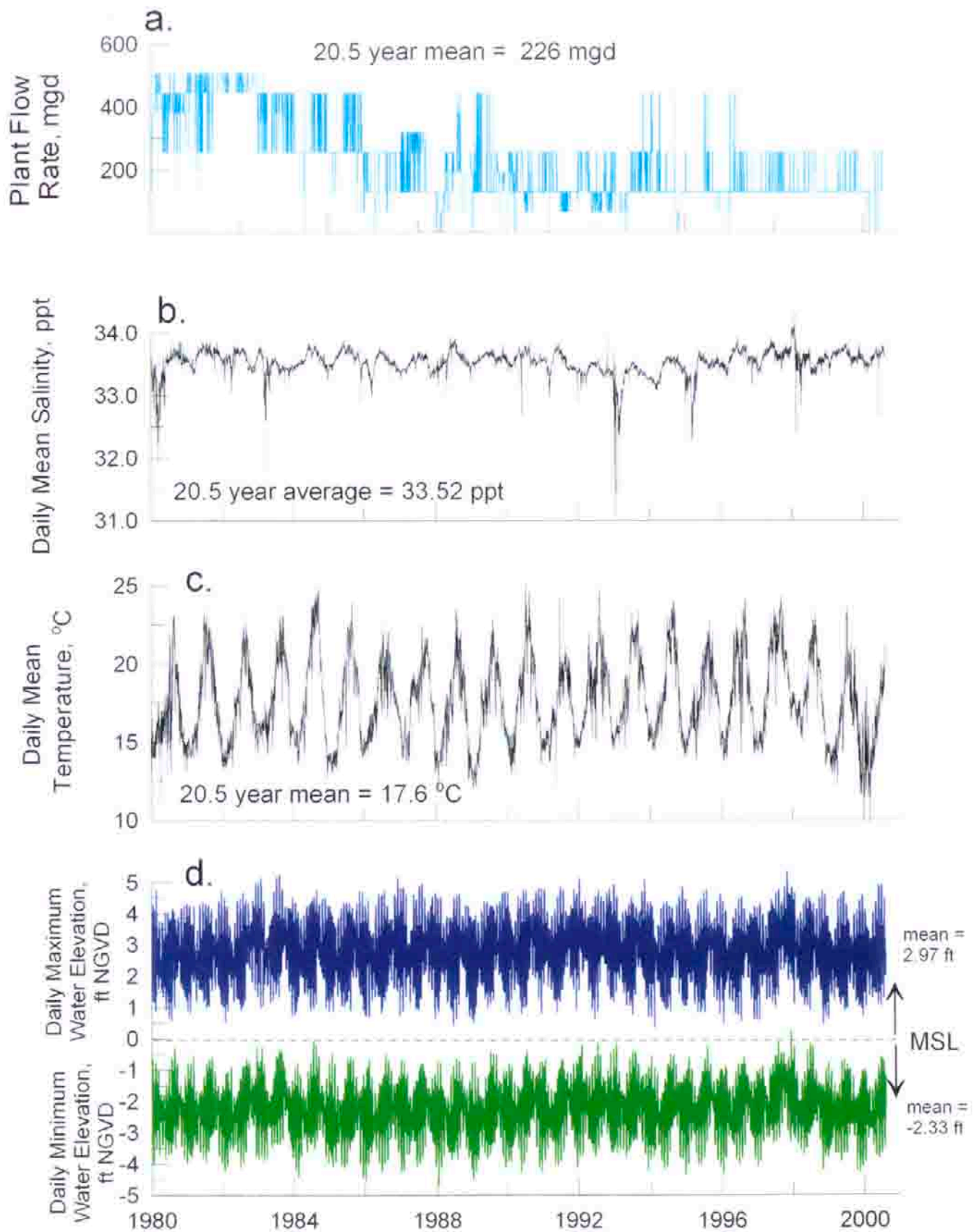


Figure 3.23. Controlling environmental variables for brine dilution, boundary conditions: a) plant flow rate b) daily mean salinity, c) daily mean temperature, and d) daily high and low water elevations. [data from MBC, 1980-2001; OCSD, 1993, 2000; SIO, 2001]

without and with supplemental in-plant waste streams in the first and second rows of the table, respectively. In the second row the addition of in-plant waste stream (primarily storm water) is computed at the maximum rate certified under the NPDES permit limits (1.66 mgd). The third row of Table 2 lists the salinity of the discharge if a 50 mgd RO production plant was retrofitted to the cooling water stream leaving the plant condenser. No additional in-plant streams are considered in the row 3 computation, typical of dry weather summer conditions. We find that the RO unit will increase the salinity of the plant discharge to a maximum of 55.37 ppt if only one generating unit is operational (or is in standby mode with 2 pumps on line), with a minimum saline elevation to 37.19 ppt if all four generation units are operating with 8 pumps on line. In row 5 of Table 2 we find that the addition of plant storm water to the combined discharge of the generating station and RO unit will lower the maximum salinities with one generating unit operation by about one part per thousand, or a combined discharge salinity maximum of 54.19 ppt. For all other levels of power generation, the plant storm water has little effect in diluting the concentrated seawater by-product of the RO plant. The end-of pipe discharge salinity for a 50 mgd RO production plant is shown in Figure 3.25 as a continuous function of generating station flow rate. Operating points for the various possible combinations of generating units are shown by the colored dots.

Regardless of whether or not plant storm water is added to the combined discharge of the generating station and RO unit, we find that the water discharged from the offshore outfall will be heavier than the ambient ocean water. For all levels of in-plant flow rate, Table 2 shows that the changes in the specific volume of the discharge due to the addition of the RO unit is always negative.

Table 2. AES Huntington Beach Discharge Rates and Effluent Physical Properties for Desalination Plant Retrofit

Generation Units On-Line	1 or standby	1, 2	1, 2, 3	1, 2, 3, 4
Cooling Water Flow Rate (mgd)	126.7	253.4	380.2	506.9
Combined Cooling Water & Plant Storm Water Discharge Maximum (mgd)	128.4	255.1	381.9	508.6
* Salinity (ppt) of Discharge@RO = 50 mgd Plant Storm Water = 0 mgd	55.37	41.76	38.57	37.19
* Specific Volume Change ($d\alpha / \alpha$)@RO = 50 mgd Plant Storm Water = 0 mgd $\Delta T = 10\text{ C}$	-0.01592	-0.00472	-0.00210	-0.00096
* Salinity (ppt) of Discharge@RO = 50 mgd Plant Storm Water = 1.66 mgd	54.19	41.42	38.38	37.05
* Specific Volume Change ($d\alpha / \alpha$)@RO = 50 mgd Plant Storm Water = 1.66 mgd $\Delta T = 10^\circ\text{C}$	-0.01494	-0.00444	-0.00194	-0.00085

* Based on an annual mean local ocean salinity of 33.52 ppt

Consequently, the discharge water will sink to the seafloor after the initial vertical momentum of the discharge has diffused into the water column. This has several positive implications: 1) it will increase initial dilution of the combined discharge, 2) it will remove the majority of the thermal footprint from the sea surface, and 3) it should diminish the size of the thermal footprint. Sinking of the discharge plume to the seafloor after the initial vertically upward discharge from the outfall tower will produce trajectories of the effluent that engage the entire water column in the

dilution process. These trajectories should increase initial dilution. Subsidence of the discharge plume to the seafloor following this higher initial dilution should isolate both the concentrated seawater and the waste field of the generating station from subsequent ingestion by the infall tower at mid-water column depths (the infall draws water from 4.8 m (15.8 ft) above the bottom). This is a favorable circumstance with respect to re-circulation. On the other hand, the heavier than seawater discharge plume will bring the elevated salinities into contact with the seafloor where there could be an effect on benthic biology. The extent of seabed effected in this way is studied in Section 4.

K) Event Scenarios Derived From Historical Data 1980-2000

Overlapping 20.5 year long records of the 4 primary boundary condition variables: generating station flow rates (Figure 3.23a), ocean salinity (Figure 3.23b), ocean temperature (Figure 3.23c), and ocean water levels (Figure 3.23d). Coincident records for the 3 primary forcing functions are shown in Figure 3.24 for waves, currents and winds. These records contain 7,523 consecutive days between 1980 and 2000. We adopt a commonly used approach in environmental sciences for bracketing the variability of long period records with event scenarios of historically worst day, average day, worst month and average month conditions. The criteria for a worst day and worst month was based on the simultaneous occurrence of seven variables having the highest combination of absolute salinity and temperature during periods of low plant flow rates concurrent with low mixing and advection in the local ocean environment. The worst day and worst month involve some potential situations for operating the desalination plant when the

generating station is not generating electricity in standby mode or when it is operating at very low production levels. We refer to these as “theoretical extreme low flow cases” because they are caused by extreme conditions occurring “in-the-pipe” in combination with extreme conditions in the ocean environment. These theoretical extreme low flow conditions (abbreviated “*low flow cases*”) are superimposed on the historic extreme combinations of the remaining 6 controlling variables in Figures 3.23 and 3.24. The resulting modeled response gives the expected impacts for a set of theoretical low flow cases that can not be reproduced from the historic records of all 7 controlling variables during last two decades (1980- July 2000). To establish a statistical comparison for these theoretical extreme cases, we subsequently develop 7523 alternative solutions in Section 5 for the modeled ocean response to the 50 mgd desalination plant, based on historically realized plant operations and ocean conditions. Criteria for low flow case conditions are summarized in Table 3 below.

In the low flow scenarios, brine concentration from the desalination plant is maximized when the AES flow rate is at the minimum operational level (sufficient for power generation) while the ocean salinity is maximum. The low flow case scenario is based on the minimum AES generating configuration or a standby mode with two circulation pumps on line. This configuration involves an in-plant flow rate of 126.7 million gallons per day (mgd). The desalination plant must have at least 100 mgd of in-plant flow available to make 50 mgd of product water, and no combination of HBGS pumps can meet this requirement at less than 126.7 mgd. Consequently, minimum operational flow rate for the desalination plant is limited to no less than 126.7 mgd, and production of product water would cease for any flow rate less than 126.7 mgd.

Table 3: Search Criteria and Ecological Significance for Low flow Case Combinations of Controlling Variables.

Variable	Search Criteria	Ecological Significance
Plant Flow Rate	Minimize	Lower flow rate results in less initial dilution in the pipe of the concentrated sea salts from desalination
Ocean Salinity	Maximize	Higher salinity leads to higher initial concentrations of sea salts in the pipe from desalination
Ocean Temperature	Maximize	Higher temperature leads to greater stress on resident marine biology
Ocean Water Levels	Minimize	Lower water levels result in less dilution volume in the nearshore and consequently slower dilution rates
Waves	Minimize	Smaller waves result in less mixing in surfzone and less inshore dilution
Currents	Minimize	Weaker currents result in less advection and less offshore dilution
Winds	Minimize	Weaker winds result in less surface mixing and less dilution in both the inshore and offshore

The minimum operational flow rate provides the least amount of “in-the-pipe” dilution and the highest brine concentrations that would be discharged from the desalination plant and consequently represents the worst *possible* case. The histogram in Figure 3.22 shows that AES Huntington Beach has not averaged daily flow rate less than the low flow case modeling condition during any year in the period of record.

Minimum ocean mixing levels were obtained from a computer search of 20 year long records of winds, waves and currents, (as detailed in Jenkins and Wasyl,

2001 and in the technical appendix of the EIR). The red dashed line in Figure 3.24 identifies the time in these records when waves, currents and winds were simultaneously at a minimum. However, the ocean salinity at this time was 33.52 ppt, not the salinity maximum of 34.3 ppt identified in Figure 3.21a. This is due to the fact that salinity maximums are mutually exclusive with mixing minimums. Salinity maximums are caused by vigorous southerly winds that create a well-mixed coastal ocean while pushing high salinity water masses into the Southern California Bight. A series of sensitivity analyses determined the salinity maximum would increase the concentration of brine discharge by 2%, but that the effects of this increase on brine dilution were smaller than the dilution impairment caused by the effects of retarded mixing during low energy conditions. In fact the dilution rates for the conditions are 99% smaller than the dilution rates during the salinity maximum in Figure 3.21a, (see Section 4). Therefore, minimal ocean mixing conditions became the dominant set of environmental variables in defining the low flow case scenario. Accordingly low flow case dilution modeling was based on the following set of parameters:

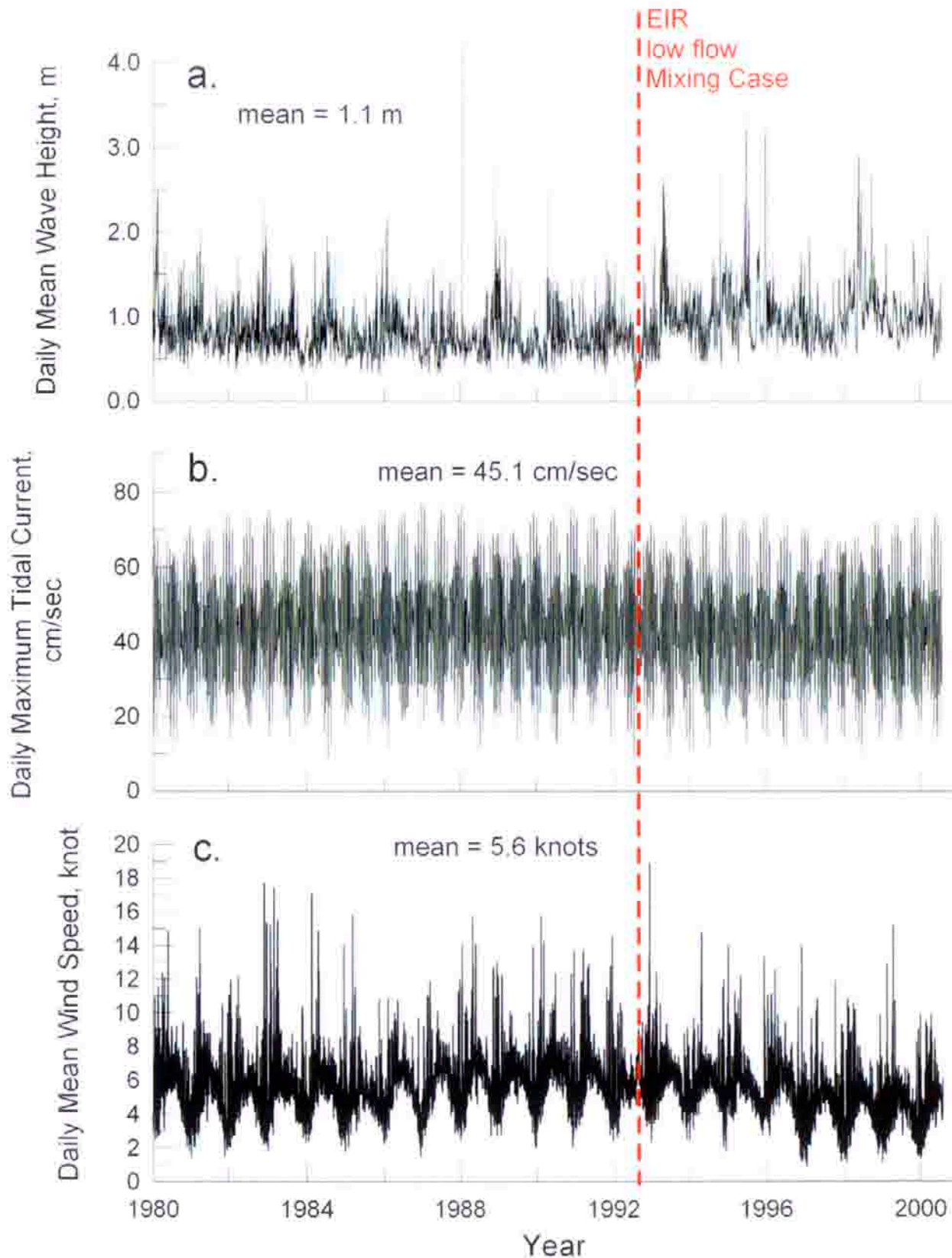


Figure 3.24. A 20.5 year record of forcing for the Newport Littoral Cell [centered at Huntington Beach, CA]. a) daily mean wave height (CDIP), b) daily maximum tidal current velocity (Station 8d), and c) daily mean wind (Station 8d). [data from CDIP, 2001; SIO, 2001; NCDC, 2004]

Table 4: Input Parameters for Low flow Case Simulations

- 1) AES intake flow rate = 126.7 mgd
- 2) Desalination production rate = 50 mgd
- 3) Combined discharge = 76.7 mgd
- 4) Ocean salinity = 33.52 ppt
- 5) End-of pipe combined discharge salinity = 55.37 ppt
- 6) Combined discharge temperature anomaly $\Delta T = 10^0$ C
- 7) Combine discharge density anomaly $\Delta \rho / \rho = 1.59$ %
- 8) Wave height = 0.16 m
- 9) Wave period = 8 sec
- 10) Wave direction = 255^0
- 11) Wind = 0 knots
- 12) Tidal range = Syzygian spring/neap cycle
- 13) Daily maximum tidal current = 8.7 cm/sec

Ocean conditions represented by these parameter assignments did not persist in the long term record of Figure 3.24 for more than a week. However, in the model simulations these conditions were perpetuated for 30 days to verify the stability of the computed results as well as specify a low flow month scenario. Historically, the recurrence of low flow case environmental extremes is about 1 week every 3 to 7 years, commensurate with the dominant ENSO frequencies. By perpetuating low flow case conditions in the model for 30 continuous days the recurrence interval is actually more rare, about 1 month every 13 to 31 years.

The average day and average month scenarios were found by a statistical search of these records for the average 24 hour and 30 day combinations

of the 7 variables occurring over the 20.5 year period of record. This procedure produced the model scenarios presented in the EIR. Based on analysis of the AES plant operations data (Figures 3.22) and the ocean monitoring data (Figures 3.23 & 3.24), the following parameter assignments were made for average case dilution modeling:

Table 5: Input Parameters for Average Case Simulations

- 1) AES intake flow rate = 253.4 mgd
- 2) Desalination production rate = 50 mgd
- 3) Combined discharge = 203.4 mgd
- 4) Ocean salinity = 33.52 ppt
- 5) End-of pipe combined discharge salinity = 41.42 ppt
- 6) Combined discharge temperature anomaly $\Delta T = 10^{\circ} \text{C}$
- 7) Combine discharge density anomaly $\Delta \rho / \rho = 0.44 \%$
- 8) Wave height = 1.1 m
- 9) Wave period = 11 sec
- 10) Wave direction = 267°
- 11) Wind = 5 knots
- 12) Tidal range = Syzygian spring/neap cycle
- 13) Daily maximum tidal current = 45.1 cm/sec

In Section 5 we augment the event analysis with continuous modeling simulations on the entire set of 7,523 daily combinations of the 7 controlling variables in the 1980-mid 2000 period of record. This is period was selected

because it is the longest length of time for which an uninterrupted record of directional wave data can be assembled in this region. The purpose of this long-term continuous modeling exercise was to both establish the viability of the EIR procedure as well as examine the persistence of all the intermediate outcomes occurring between low flow and average cases. In addition changes to the dispersion statistics of the hyper-saline plume are examined for cold water discharges from AES Huntington Beach, as a consequence of the generating station pumping seawater at 126.7 mgd with a $\Delta T = 0$.

L) Calibration

The coupled sets of models shown in Figure 2.1 were calibrated for end-to-end simulations of the salinity and temperature fields based on salinity and temperature depth profile measurements conducted over a nearshore sampling grid during November and December 2000 by MBC (2001). These measurements are listed in tabular form in Appendix H together with a sampling map and were collected as part of an NPDES compliance monitoring program for AES Huntington Beach. Wave and current forcing for the model were reconstructed for this two month period based on the wave data in Figure 3.9 and tidal current reconstructions like those in Figures 3.13 to 3.20. Free parameters in the subroutines were adjusted iteratively until a best fit was achieved between the measured and simulated salinity fields.

The subroutines of **SEDXPORT-f** contain seven free parameters which are selected by a calibration data set specific to the coastal type for which the hindcast simulation is run. These parameters are as follows according to subroutine:

BOTXPORT-f

*ak2 - stretching factor for vertical eddy diffusivity, ϵ

*ak - adjusts mixing lengths for outfalls

NULLPOINT.f

*ak7 - adjusts the asymmetry of the bedform distribution curve,
 μ

SURXPORT.f

*aks - adjusts the surf zone suspended load efficiency, K_s

ak4 - stretching factor for the horizontal eddy diffusivity, ϵ_x

RIVXPORT.f

*ak3_1 - adjusts the jetty mixing length and outfall mixing
lengths

*ak3 - stretching factor for the horizontal eddy diffusivity
of the river plume, ϵ_H

The set of calibration values for these parameters was used without variation or modification for all model scenarios contained in Sections 4-9.

**SECTION 4: EVENT ANALYSIS OF DILUTION AND
DISPERSION OF CONCENTRATED SEA WATER**

4) **Event Analysis of Dilution and Dispersion of Concentrated Sea Water**

In this section we solve for long term steady state solutions for the dispersion and dilution of the concentrated seawater by-product of the proposed desalination plant at AES Huntington Beach. The objective here is to determine persistent levels of disturbance to the ambient ocean salinity field. We consider a *low-flow case* model scenario in which maximum salinity levels are produced in-the-pipe as a consequence of minimum power generation (or standby with 2 pumps on line) and are subsequently discharged into a tranquil, summer-time ocean environment wherein ambient mixing is minimal. We also consider a *average case* in which saline levels of discharge for average power generation are evaluated in an ocean environment with mixing due to average annual wind, waves and currents. These two scenarios are run continuously in the model for 30 days, and then the solutions are time averaged. The purpose of running these event scenarios for 30 days was to provide a long enough simulation that would reveal any possible cumulative effects, ie to verify that the receiving waters were fully saturated and that a steady state was achieved. This is common practice for impact assessment modeling. Modeling for shorter periods of time tends to result in slightly lower salinities in the receiving waters. Our sensitivity analyses performed during the development of these solutions show that the receiving waters reach steady state within 5 days for the low flow case scenario, and within 3 days for the average case scenario. Thereafter, there are no significant changes in the event scenario solutions.

A) Description of Low flow-Case Conditions

We consider a low flow-case model scenario in which maximum salinity levels at minimum power generation are discharged into a tranquil, summer-time ocean environment wherein ambient mixing is minimal. The source loading for the low flow case dilution and dispersion model scenario is given by the set of operational conditions which produces the highest salinities for the combined discharges of the generating station and the desalination plant when the latter is producing 50 mgd of product water per day. This operational level will give the highest dose level to the benthic and pelagic biology. From Tables 2 & 3 in Section 3, we conclude that this low flow case arises when the generating station is operating only one generating unit and discharging no in-plant waste streams, producing a total discharge of 126.7 mgd from 2 pumps operating at 44,000 gpm each. The R0 unit would withdraw approximately 100 mgd and return 50 mgd of concentrated seawater to the discharge stream. The resulting combined discharge from the plant outfall would be 76.7 mgd at a salinity of 55.37 ppt. The change in specific volume of this effluent (including the thermal effects of the generating station) would be -1.59% relative to ambient seawater and consequently it will be heavier than the receiving water.

To study the minimum possible dilution rates of this low flow-case effluent in a sustained steady state, the 20-yr wave records, in Figure 3.23 & 3.24 were searched with a digital filter to obtain the precise model initialization for low flow case according to the search criteria set forth in Table 3 of Section 3. This search produced the initialization values for low flow case listed in Table 4 of Section 3. These condition are an extremely over-specified low flow-case scenario for a 30-day simulation. Because such benign ocean mixing conditions are typically

summer events when user demand for power is high, this low flow-case combination of environmental and operational conditions is highly unlikely for any protracted period of time. Historically, the recurrence of low flow case environmental extremes is about 1 week every 3 to 7 years, commensurate with the dominant ENSO frequencies. By perpetuating low flow case conditions in the model for 30 continuous days the recurrence interval is actually more rare, about 1 month every 13 to 31 year.

B) Findings for Low flow Month

The model simulation of the 30 day average of the salinity field in the middle of the water column is plotted in Figure 4.1 for an RO production rate of 50 mgd and a plant flow rate of 126.7 mgd during the low flow month conditions. The corresponding salinity distribution on the sea surface is plotted in Figure 4.2 and at the seabed in Figure 4.3. Contours of salinity are in parts per thousand (ppt), where the ambient background ocean salinity is 33.52 ppt. The distribution shown in Figure 4.1 gives the salinity field at approximately the depth of the “end of the pipe” of the infall and outfall, with a region of concentrated sea salts reaching 55.0 ppt found directly over the outfall. The combined discharge of the generating station and RO plant creates a jet of negatively buoyant fluid directed vertically upward at the sea surface with a flow rate of 76.7 mgd. Figure 4.2 shows that this jet broaches the sea surface, creating a “boil” of hyper-saline water with a salinity of 50.1 ppt in the core of the boil. However, this saline boil rapidly subsides in the water column as it is advected downcoast (towards the southeast) in the net tidal transport over a 30 day period. The subsidence of the discharge ultimately leads to a widely dispersed, weakly elevated, saline anomaly at the sea

floor throughout the farfield region downdrift of the outfall (Figure 4.3). In the nearfield of the outfall, there is a saline inversion, with bottom salinities at the tow of the outfall reaching only 48.3 ppt. This nearfield inversion is due to the dilution of concentrated seawater that occurs along the discharge trajectory, as it is initially propelled towards the surface and away from the bottom by the discharge flow momentum.

From the salinity fields calculated in Figures 4.1-4.3, the highest salinities are found to occur in the water column at mid-depth directly adjacent to the outfall tower. For low flow month conditions a total of 18.3 acres of pelagic habitat experience a 10% (or greater) increase in salinity. The benthic area effected by 10% increases in salinity is 15.6 acres. Again the smaller impacted area at the seabed is due to the nearfield saline inversion around the outfall tower. However, the footprint of the 1% saline anomaly is greater on the bottom than in the water column due to subsidence in the farfield. The benthic area experiencing a 1% (or greater) increase in salinity is 263 acres for low flow month conditions, while the pelagic area similarly effected is 151 acres.

The model simulation of the 30-day average of the salinity profile in a crossshore section passing through the outfall (Figure 1.1, Section-A) is plotted in Figure 4.4 during the low flow case conditions perpetuated over a 30-day period. The corresponding longshore section of the salinity profile (Figure 1.1, Section-B) is plotted in Figure 4.5. Both plots are scaled identically to Figures 4.1- 4.3 with contours of salinity in parts per thousand (ppt), where the ambient background ocean salinity is 33.52 ppt. The thin, white vertical rectangle rising 4.8 meters above the bottom in Figures 4.4 and 4.5 indicates the location of the outfall tower, where the discharge is directed vertically upward toward the surface from the

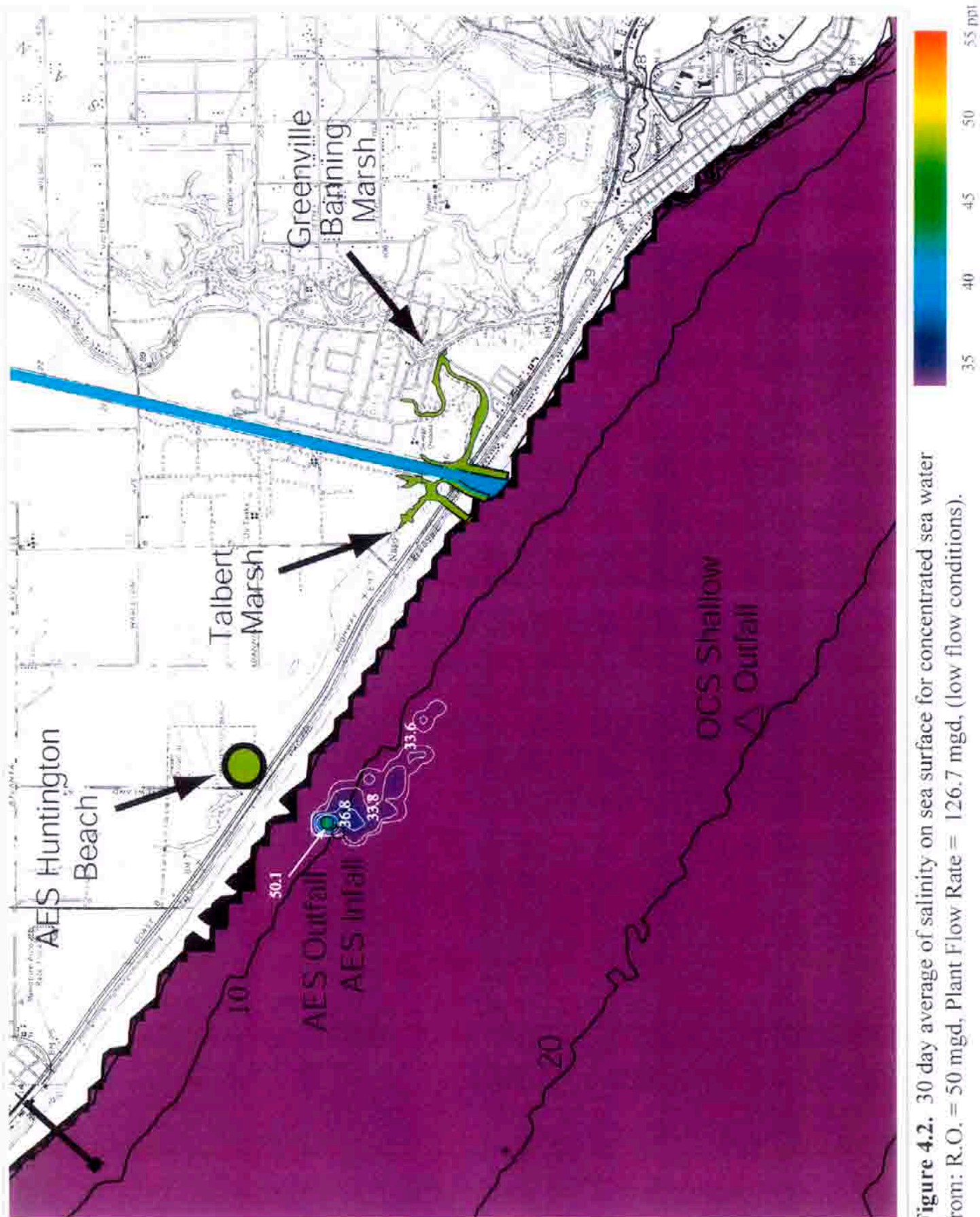


Figure 4.2. 30 day average of salinity on sea surface for concentrated sea water from: R.O. = 50 mgd, Plant Flow Rate = 126.7 mgd, (low flow conditions).

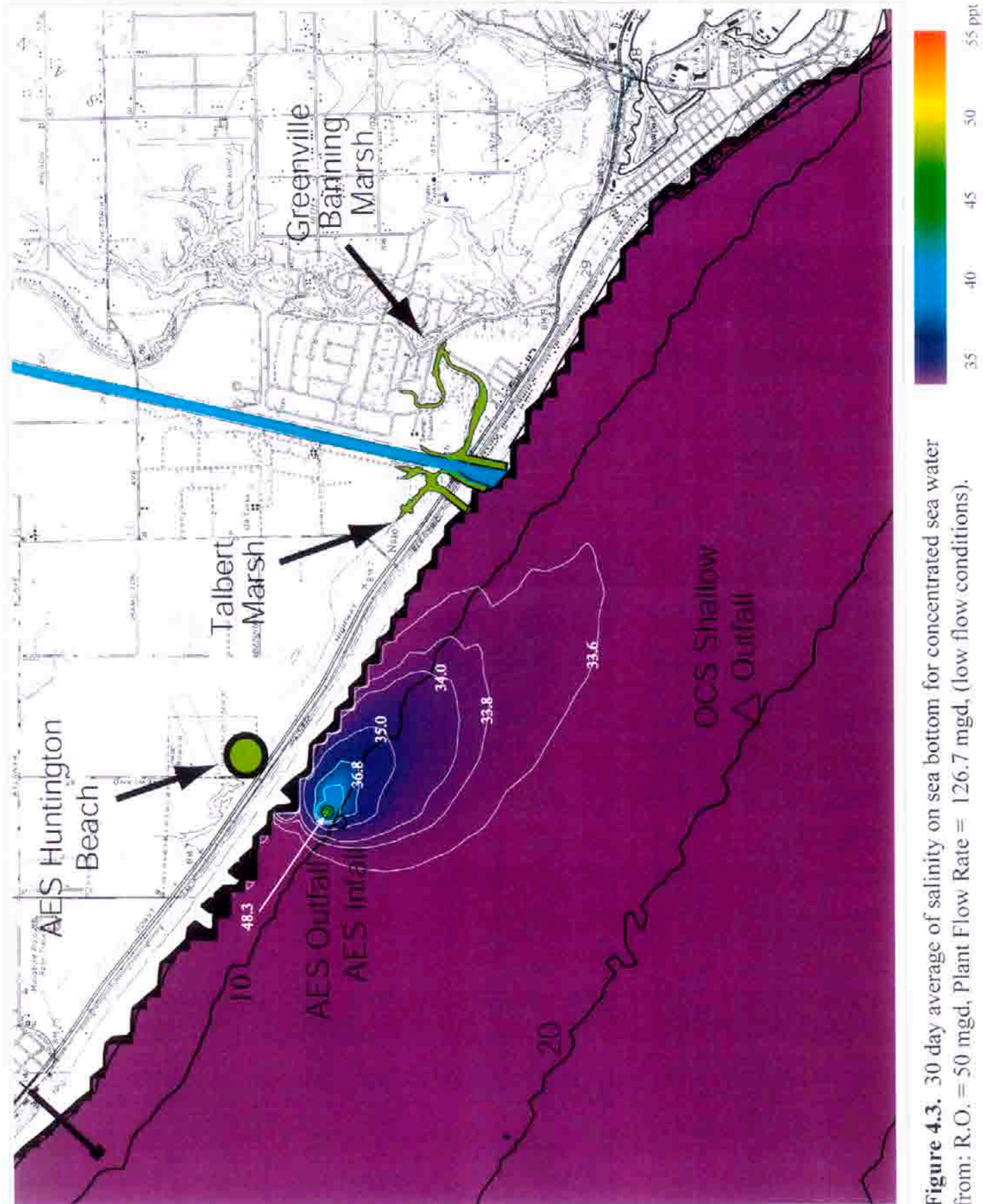


Figure 4.3. 30 day average of salinity on sea bottom for concentrated sea water from: R.O. = 50 mgd, Plant Flow Rate = 126.7 mgd, (low flow conditions).

top of the rectangle. In Figure 4.4 the cross-shore profile is exaggerated vertically by 40 to 1. In Figure 4.5 the longshore distances are greater so that the vertical exaggeration is increased to 60 to 1. In both plots this was done to delineate vertical structures in the discharge plume.

The cross-shore and longshore profiles shown in Figures 4.4 and 4.5 reveal that the discharge plume consists of two primary features: 1) a high-salinity core that forms a narrow column around the outfall tower, and 2) a broad-scale salt wedge spreading outward from the core in which the salinities are weakly hyper-saline. The core is formed by the initial discharge jet emanating from the top of the outfall tower at a flow rate of 76.7 mgd. The core has two distinct dynamical zones: an inner core comprised of an axi-symmetric turbulent jet whose momentum is directed vertically upward, and an outer core comprised of a collapsing inversion zone around the jet. The maximum salinity in the center of jet is 55.0 ppt immediately above the outfall tower, but the turbulence of the jet quickly dilutes salinities in the inner core to about 50 ppt, with sufficient residual momentum to broach the sea surface, creating a "surface boil" of hyper-saline water. In the outer core surrounding the jet, entrainment of water leads to formation of a vertical column of convective cells in which the salinity dilutes from 50 ppt to 38 ppt. The radius of the inner core varies between 40 and 50 meters (measured from the center of the outfall). The outer core is asymmetric, extending outward to a maximum distance of 150 meters from the outfall in the cross shore direction and 300 meters in the longshore direction toward the southeast (down-drift bias). The upward momentum of the initial jet discharge supports the weight of the core above the bottom which otherwise is "top heavy" relative to the surrounding water mass. Thus, along the outer edges of the core

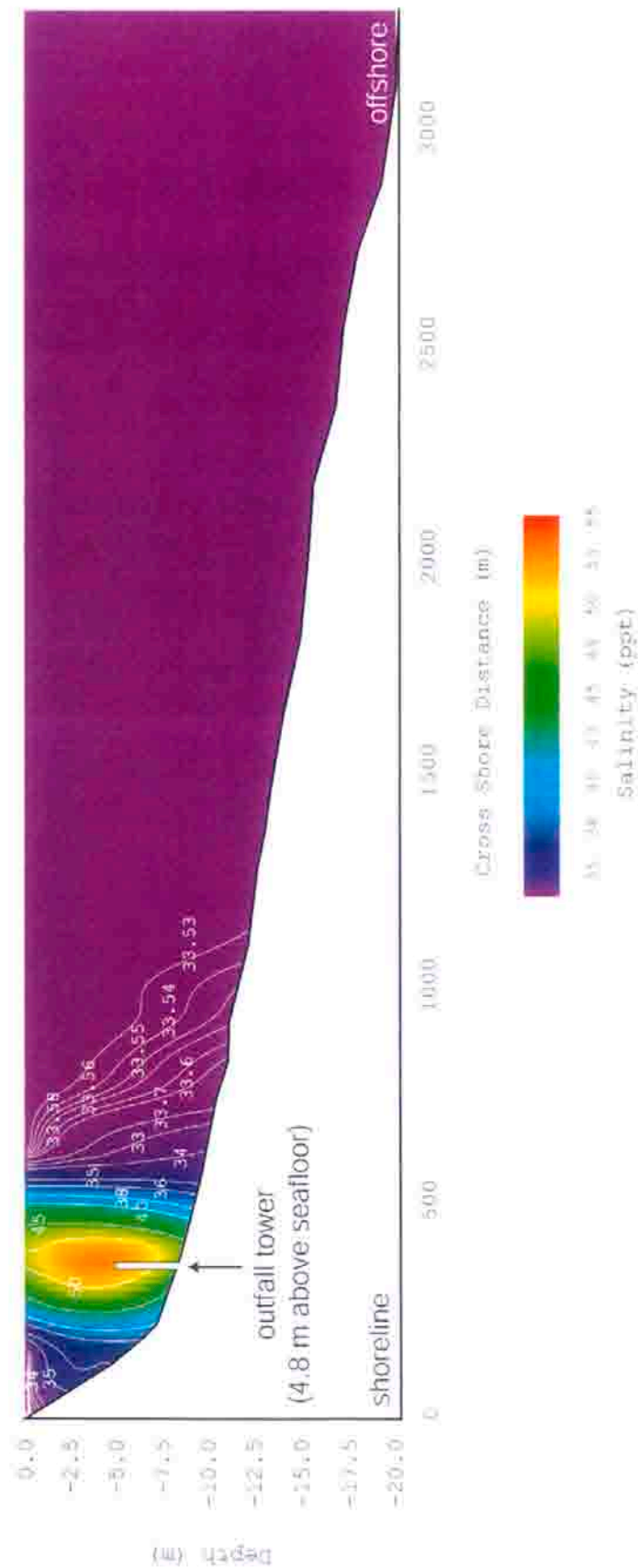


Figure 4.4. Cross shore salinity profile through the AES Huntington outfall along Section-A (see Figure 1). 30-day average of salinity for concentrated sea water discharge using: R.O. = 50 mgd, Power Plant Flow Rate = 126.7 mgd, (low flow conditions). (Profile corresponds to results in Figures 4.1 - 4.3.)

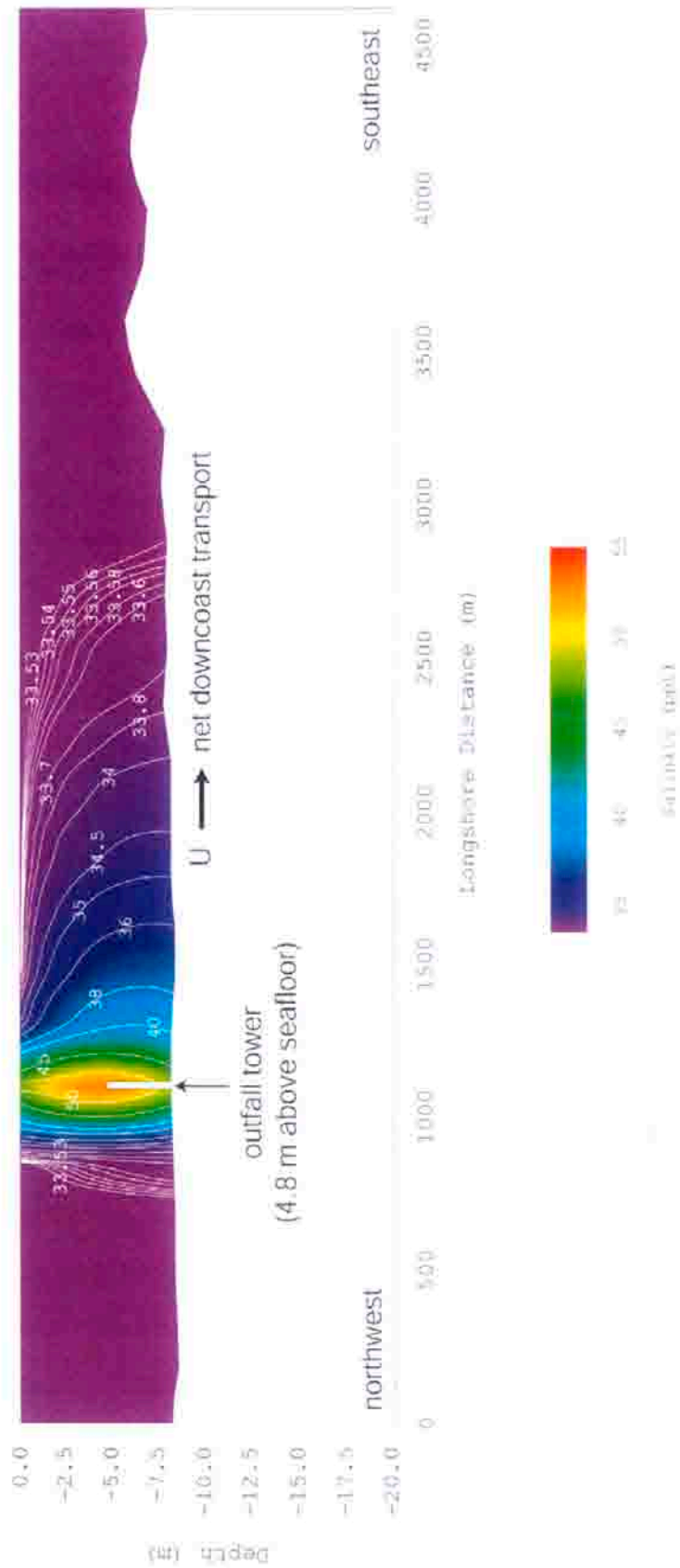


Figure 4.5. Longshore salinity profile through the AES Huntington outfall along Section-B (see Figure 1). 30-day average of salinity for concentrated sea water discharge using: R.O. = 50 mgd, Power Plant Flow Rate = 126.7 mgd, (low flow conditions). (Profile corresponds to results in Figures 4.1 - 4.3.)

where there is insufficient upward jet momentum to support the weight core water in a vertical column structure, the core collapses and subsides into the ambient water mass, forming a salt wedge that spreads outward as a slowly creeping density flow. The salt wedge spreads predominantly downslope (offshore) in the cross shore direction (Figure 4.4) under the influence of gravity, and downdrift in the alongshore direction (Figure 4.5) as it is advected towards the southeast by the net tidal transport. To a lesser degree, there is also some dispersion of the discharge plume shoreward and upcoast (towards the northwest) due to mixing of the salt wedge under the influence of shoaling waves. Salinities in the salt wedge nominally range from about 1.5 ppt above ambient (4‰ salinity anomaly) to only 0.01 ppt above ambient (0.1‰ salinity anomaly), well within the envelope of natural variability. The salt wedge is highly asymmetric, with a large offshore and downdrift bias toward the southeast. The salt wedge extends 800 meters offshore of the outfall and 1800 meters downdrift toward the Santa Ana River mouth.

The corresponding dilution fields of concentrated seawater in the middle of the water column, at the sea surface and on the seabed are plotted in Figures 4.6-4.8, respectively. Dilution contours are shown in a log-10 scale relative to the raw concentrate (at twice ambient ocean salinity). Inspection of Figure 4.6 (showing minimum nearfield dilution) indicates that the dilution of concentrated seawater is 31 to 1 at the plant infall. Thus, about 2% of the sea salts from reverse osmosis might become re-circulated back through the production unit for this 30 day low flow case scenario which has a return probability of between 0.27% and 0.64% depending on the length of ENSO cycles. Figure 4.7 shows that dilution in the saline boil at the sea surface is extremely rapid and sharp-edged due to the subsidence of the negatively buoyant combined effluent. Seabed dilution (Figure

4.8) is faster in the nearfield of the discharge tower than in the water column or at the sea surface, but slower in the farfield. Minimum dilution of concentrated seawater at the shoreline is 32 to 1. The recently completed CEC study (KOMEX, 2003; Jones and Major, 2003) found that dye discharged from the HBGS outfall is diluted by a minimum of 36 to 1 at the shoreline. Thus the model results presented in Figures 4.6- 4.8 (that were derived two years before the KOMEX field study) appear to be well confirmed. Given these dilution findings in combination with offshore measurements of indicator bacteria, both studies have concluded that the dilution associated with the AES outfall is sufficiently large that it can not account for the high bacteria levels measured at the shoreline.

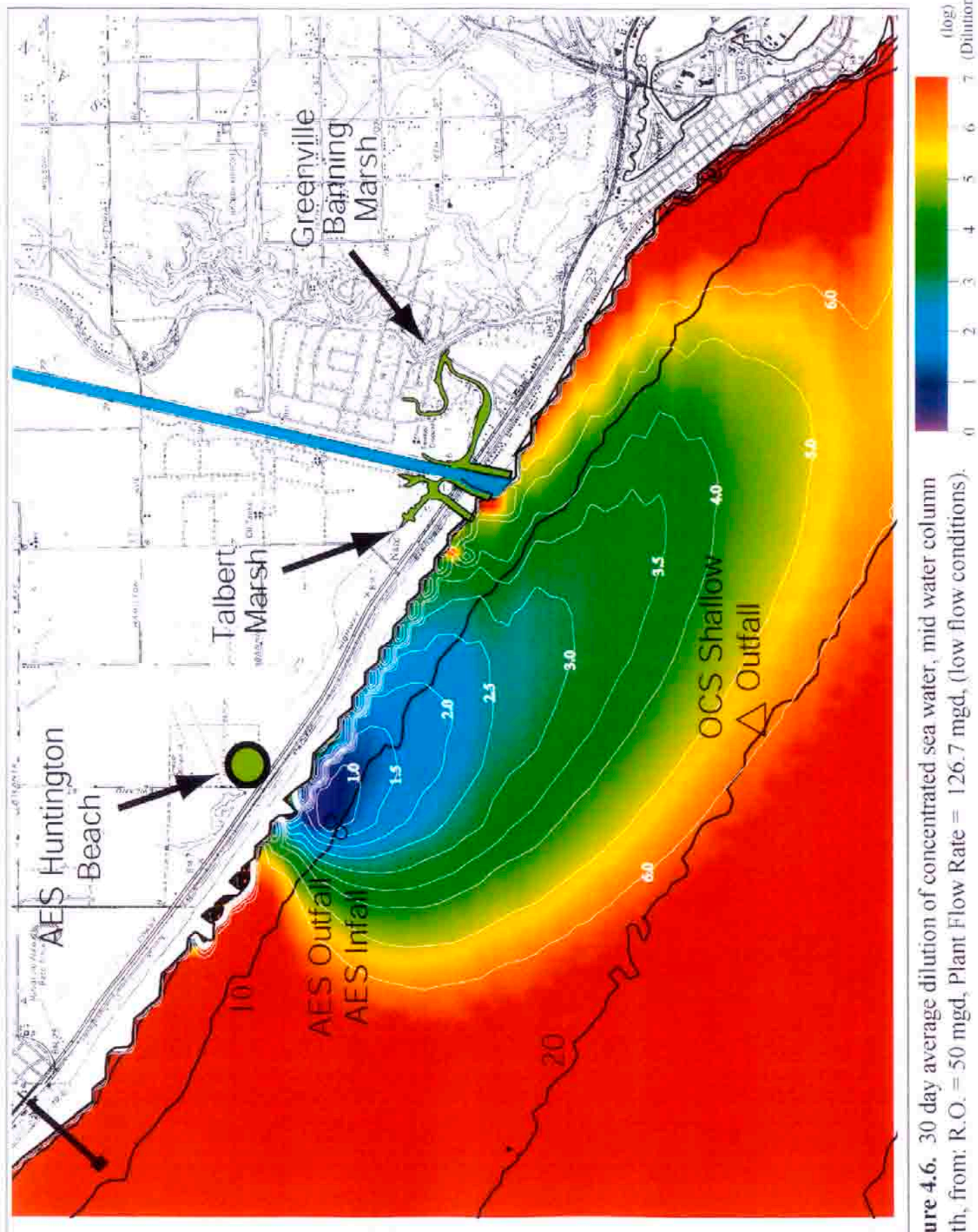


Figure 4.6. 30 day average dilution of concentrated sea water, mid water column depth, from: R.O. = 50 mgd, Plant Flow Rate = 126.7 mgd, (low flow conditions).

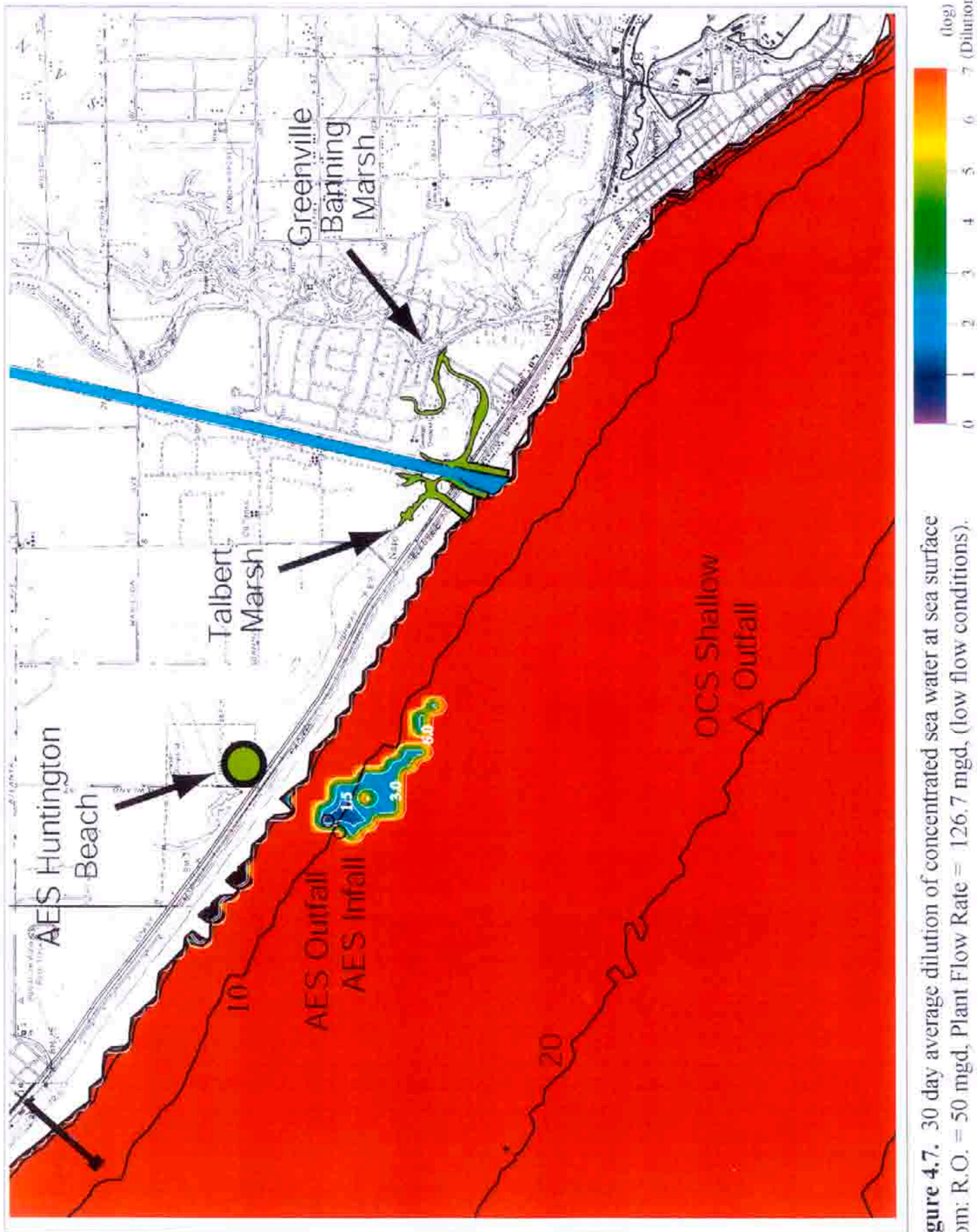


Figure 4.7. 30 day average dilution of concentrated sea water at sea surface from: R.O. = 50 mgd, Plant Flow Rate = 126.7 mgd, (low flow conditions).

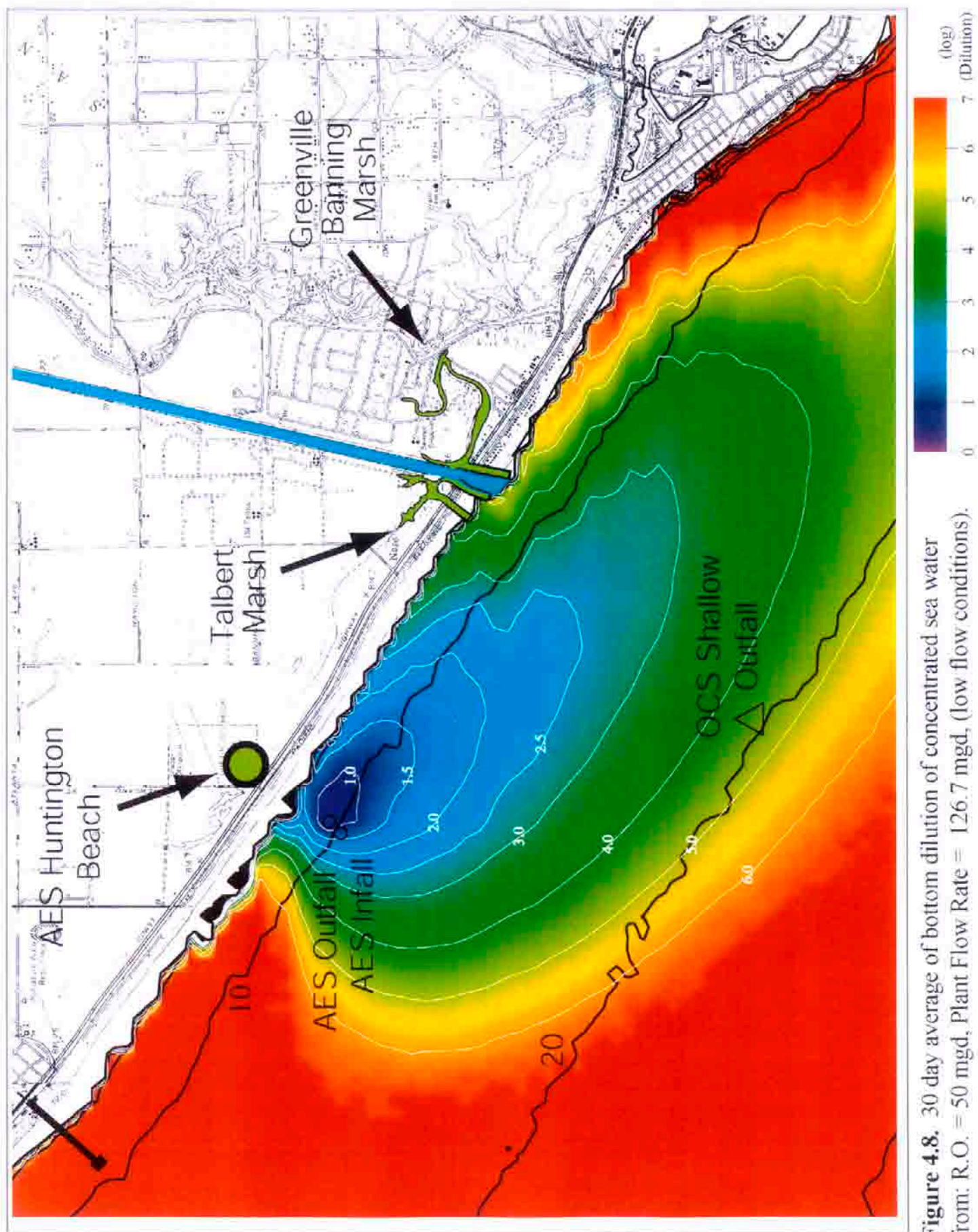


Figure 4.8. 30 day average of bottom dilution of concentrated sea water from: R.O. = 50 mgd, Plant Flow Rate = 126.7 mgd, (low flow conditions).

C) Description Average-Case Conditions

For the evaluation of dilution and saline impacts on the receiving body during more typical or nominal operating levels, we consider two generating units to be online. We assume no storm water discharge (summer conditions) so that the power plant flow rate is 253.4 mgd due to 2 generating units being on line with 4 operating circulation pumps and heating the seawater to discharge temperature of $\Delta T = 10^\circ \text{C}$, (Table 2). With the RO unit producing 50 mgd of product water, the effluent stream from the plant outfall will have an end-of-the-pipe salinity of 41.76 ppt and a combined flow rate (cooling plus RO concentrate) of 203.4 mgd (see Tables 2 & 5, Section 3). This gives the combined effluent (including thermal expansion) a -0.44% change in specific volume relative to ambient seawater, (i.e., lighter than the effluent of the low flow case scenario but still heavier than ambient seawater).

The average case scenarios were found by a statistical search of the records for the 7 variables occurring over the 20.5 year period of record (Figures 3.23 & 3.24). This procedure produced the selection of inputs to represent average case conditions listed in Table 5 in Section 3. Wave forcing for the bottom mixing action on this effluent is provided by the average annual wave whose properties were calculated from averaging the height, period, and direction of the 20-year wave record (Figure 3.24a). The statistical average wave was run continuously throughout the 30-day simulation of the normal operational impacts. The current mixing in the 30-day simulation was due purely to tidal flow and was provided by a mean range pair of spring neap cycles. The wind mixing was set for a diurnal sea breeze with a 5.6 knot 24 hr mean (Figure 3.24c).

D) Findings for Average Month

The model simulations for the 30 day average of the salinity fields at mid-depth, sea surface, and sea floor are plotted in Figures 4.9 - 4.13 for an RO production rate of 50 mgd and a plant flow rate of 253.4 mgd during the average month conditions. Contours of salinity are in parts per thousand (ppt), where the ambient ocean salinity is 33.52 ppt. The corresponding dilution fields of the concentrated seawater by-product are plotted in Figures 4.14-4.16. Dilution contours are in a log-10 scale relative to the raw concentrate. Comparing salinity fields in Figures 4.9-4.11 with the low flow month simulations in Figures 4.1-4.3, we find that the regions of elevated salinity in the water column are muted for average month conditions and that the footprint of the saline anomalies are smaller. In either case, the dispersion patterns over a 30 day period spread out downdrift towards the southeast due to the net tidal transport. The high salinity regions in the water column are reduced in intensity because the higher plant flow rates for an average month result in greater “in-the-pipe” dilution, (combined flow rate for power generation and RO production is 203.4 mgd). The increased dilution in the pipe is also combined with increased ambient ocean mixing for an average month, thereby increasing the rate of dilution in the receiving water and reducing the size of the footprints of the saline anomalies.

For an average month the maximum area of pelagic habitat subjected to a 10% (or greater) increase in salinity is reduced to only 8.3 acres, in which the maximum salinity is 41.7 ppt in the core of the discharge jet (Figure 4.9). Salinities in the surface boil reach a maximum of 38.3 ppt before subsidence ensues (Figure 4.10). Maximum seabed salinities (Figure 4.11) are only 37.6 ppt at the base of the outfall and the area of benthic habitat subjected to a 10% increase in salinity is 6.8

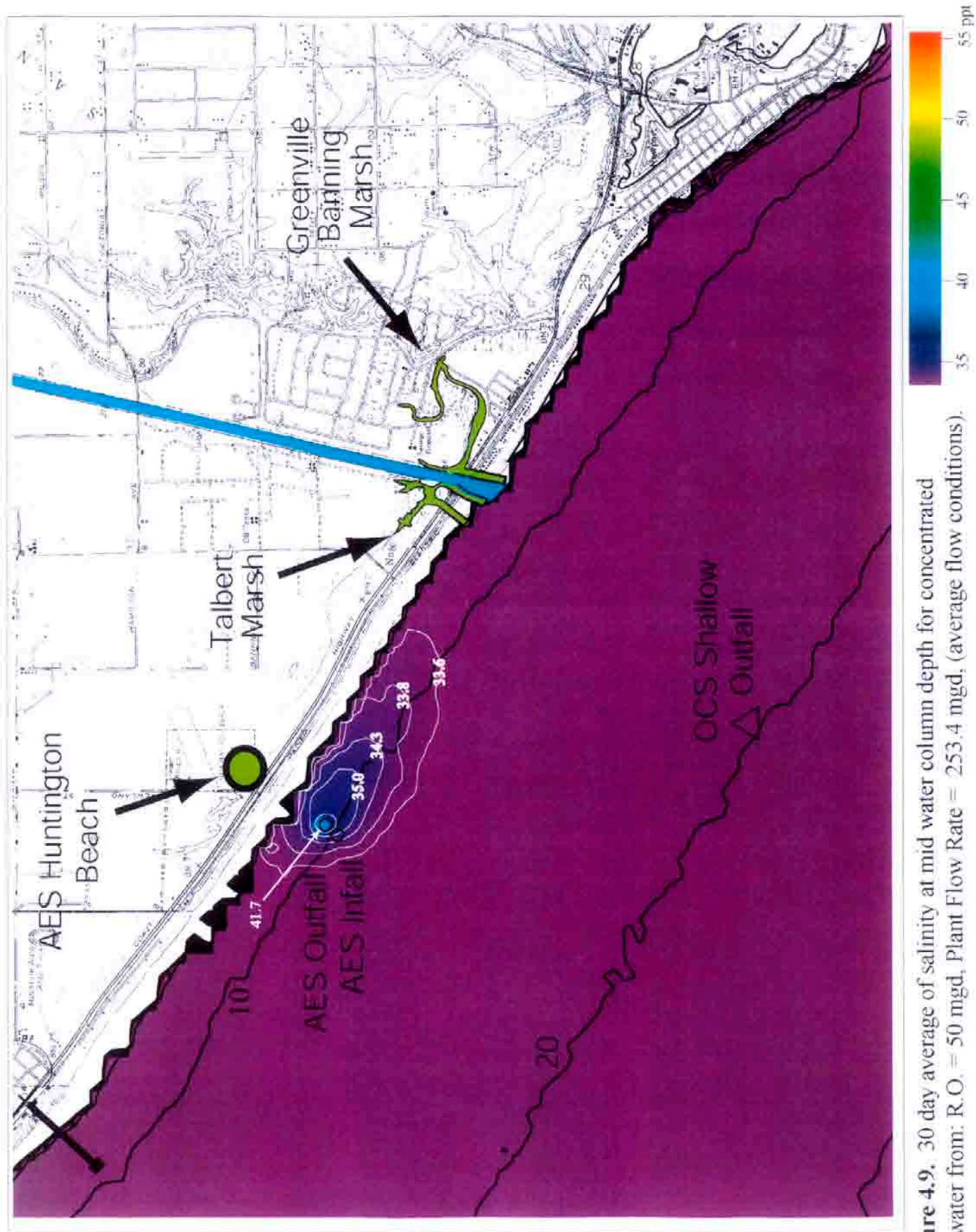


Figure 4.9. 30 day average of salinity at mid water column depth for concentrated sea water from: R.O. = 50 mgd, Plant Flow Rate = 253.4 mgd, (average flow conditions).

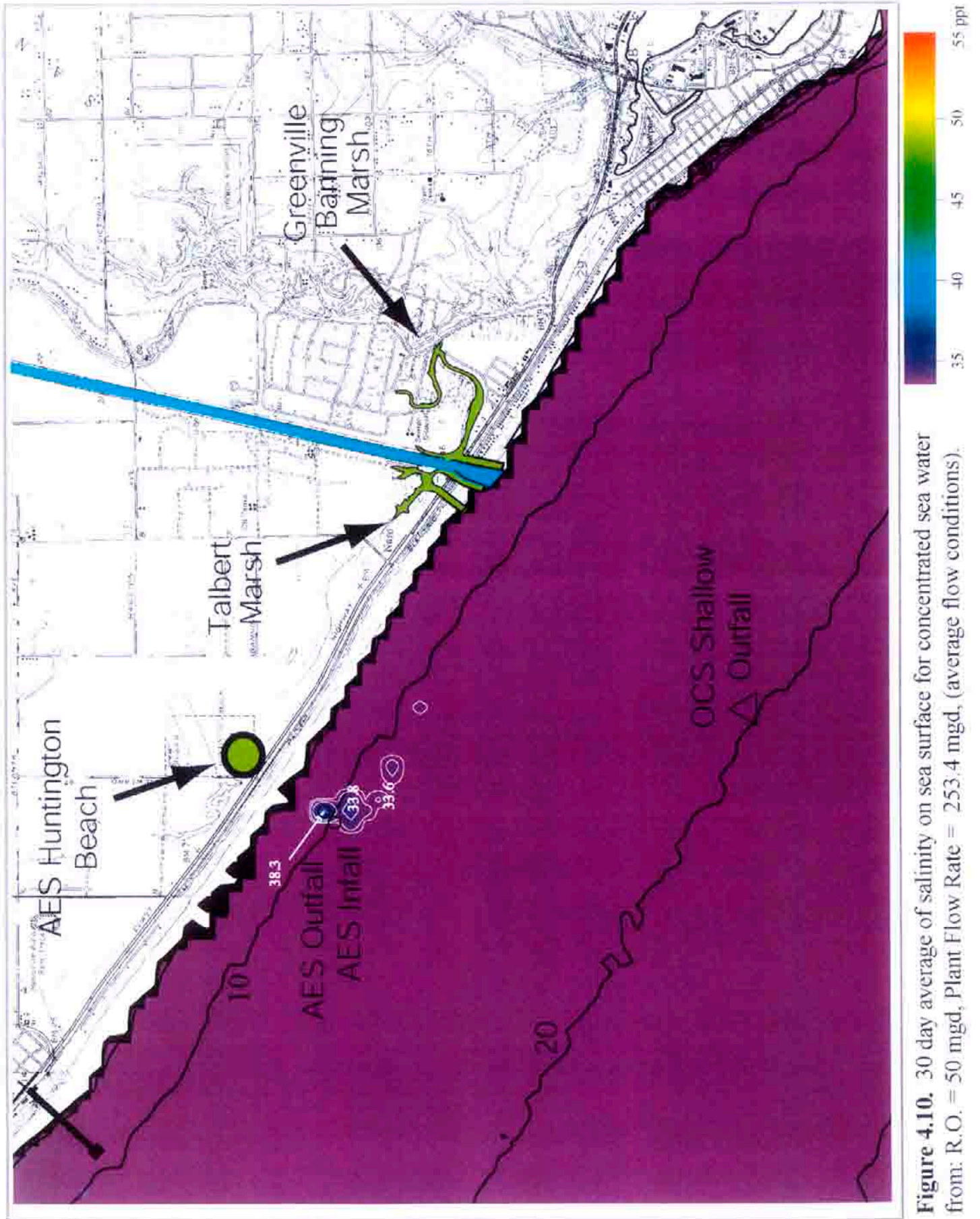


Figure 4.10. 30 day average of salinity on sea surface for concentrated sea water from: R.O. = 50 mgd, Plant Flow Rate = 253.4 mgd, (average flow conditions).

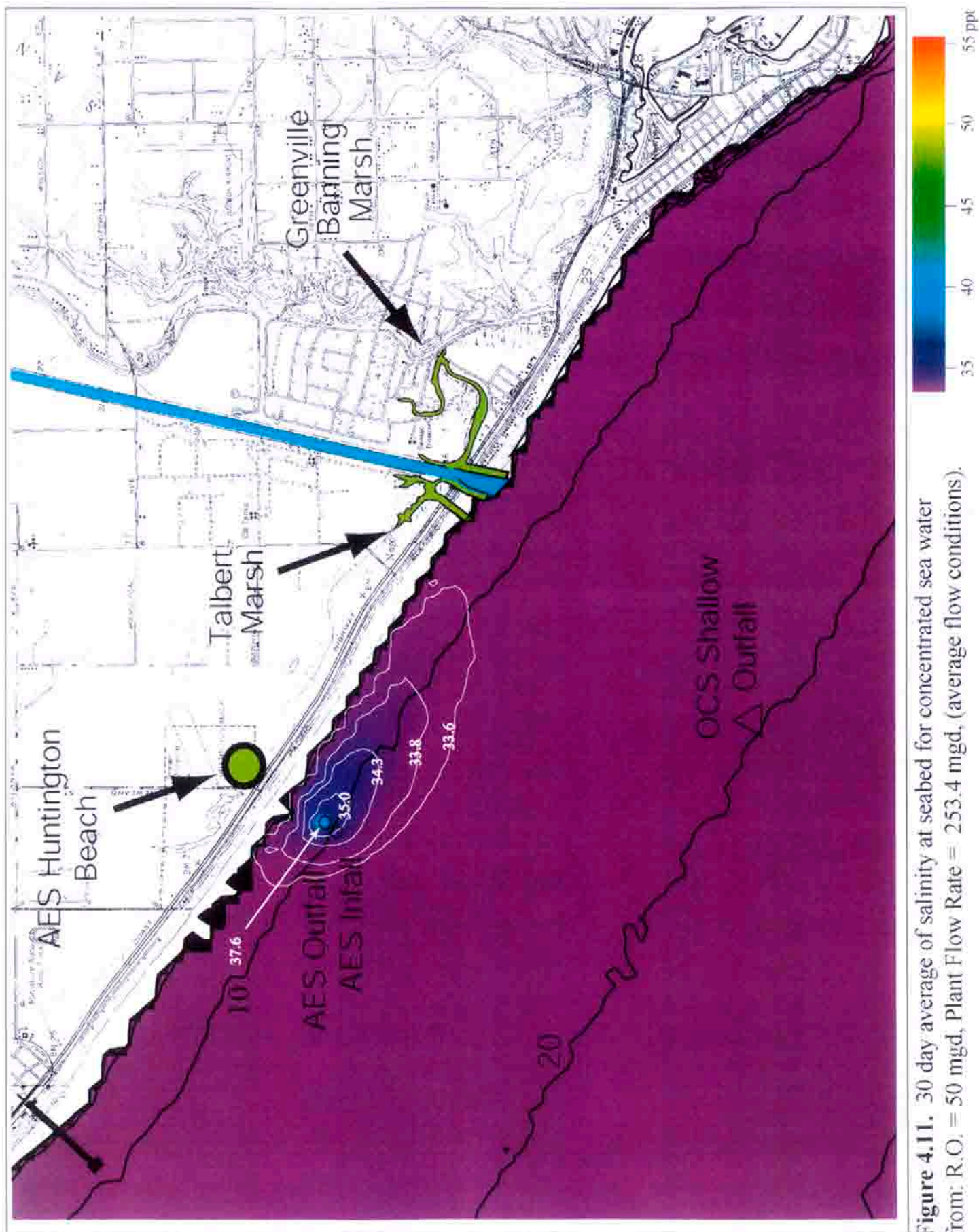


Figure 4.11. 30 day average of salinity at seabed for concentrated sea water from: R.O. = 50 mgd, Plant Flow Rate = 253.4 mgd, (average flow conditions).

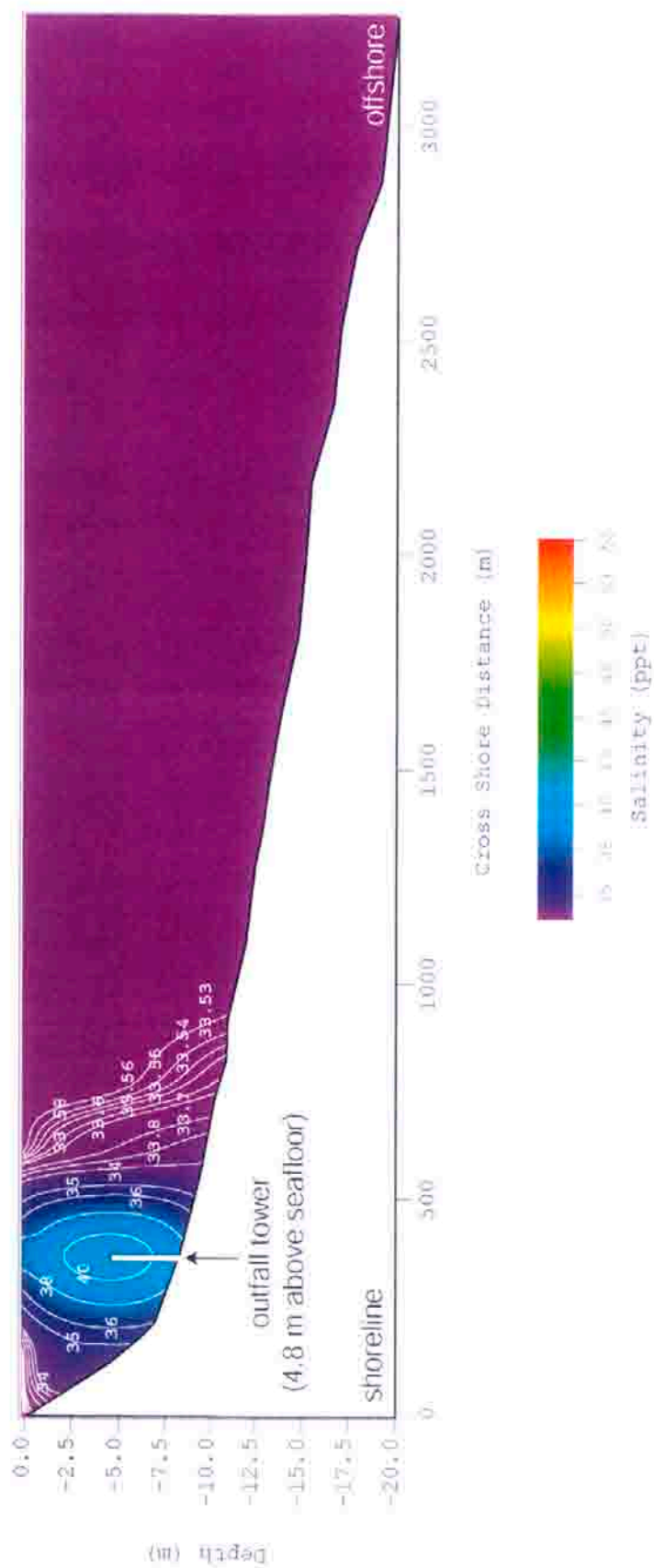


Figure 4.12. Cross shore salinity profile through the AES Huntington outfall along Section-A (see Figure 1). 30-day average of salinity for concentrated sea water discharge using: R.O. = 50 mgd, Power Plant Flow Rate = 253.4 mgd, (average flow conditions). (Profile corresponds to results in Figures 4.9 - 4.11.)

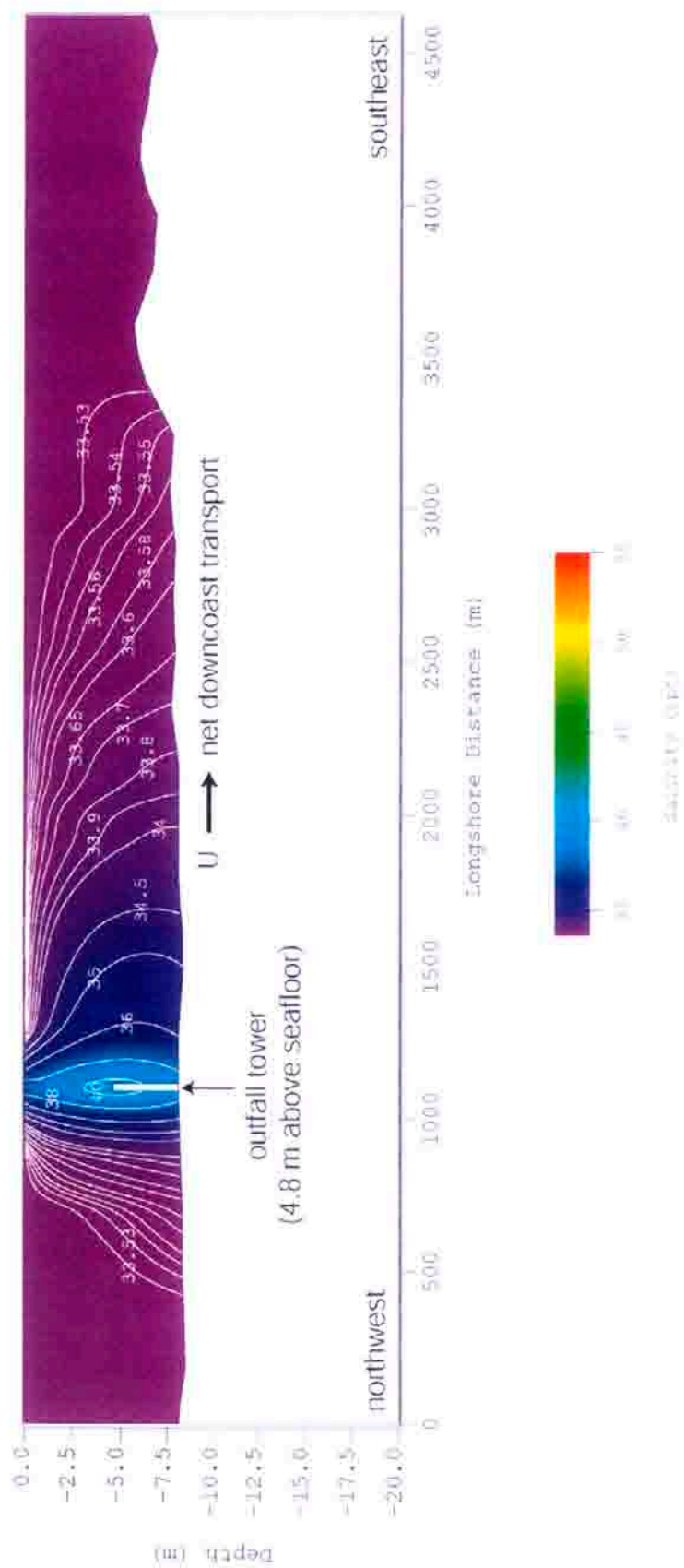


Figure 4.13. Longshore salinity profile through the AES Huntington outfall along Section-B (see Figure 1). 30-day average of salinity for concentrated sea water discharge using: R.O. = 50 mgd, Power Plant Flow Rate = 253.4 mgd, (average flow conditions). (Profile corresponds to results in Figures 4.9 - 4.11.)

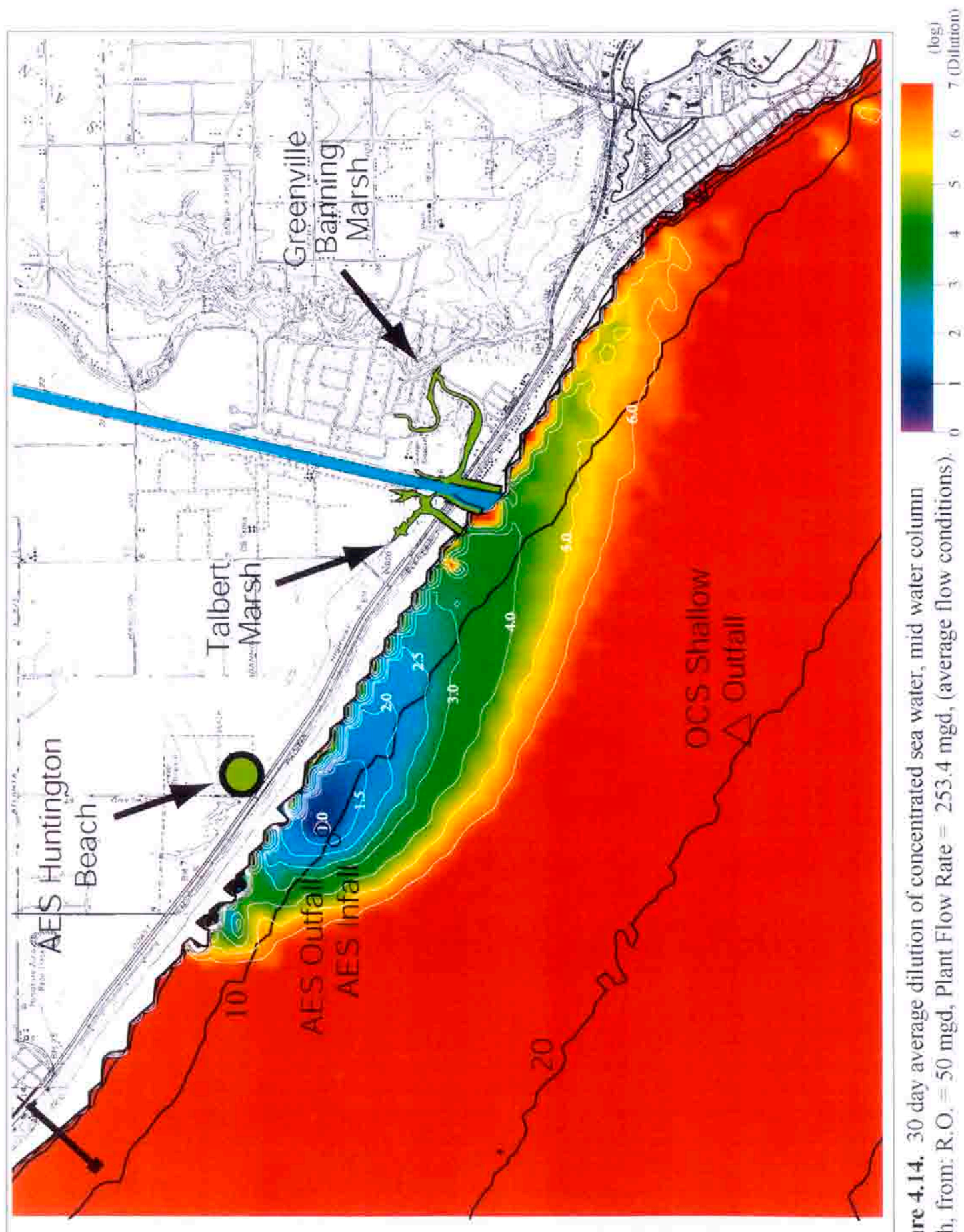


Figure 4.14. 30 day average dilution of concentrated sea water, mid water column depth, from: R.O. = 50 mgd, Plant Flow Rate = 253.4 mgd, (average flow conditions).

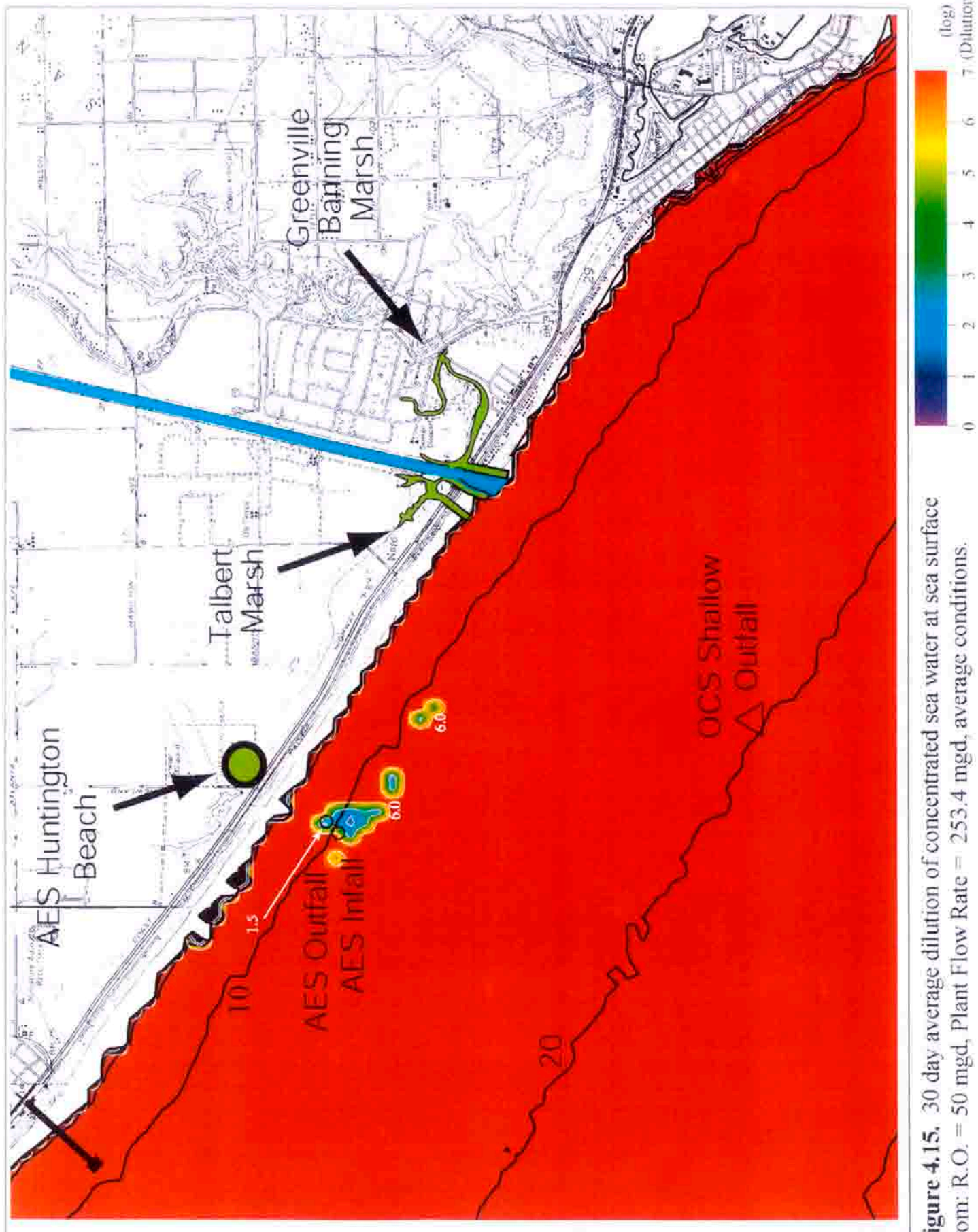


Figure 4.15. 30 day average dilution of concentrated sea water at sea surface from: R.O. = 50 mgd, Plant Flow Rate = 253.4 mgd, average conditions.

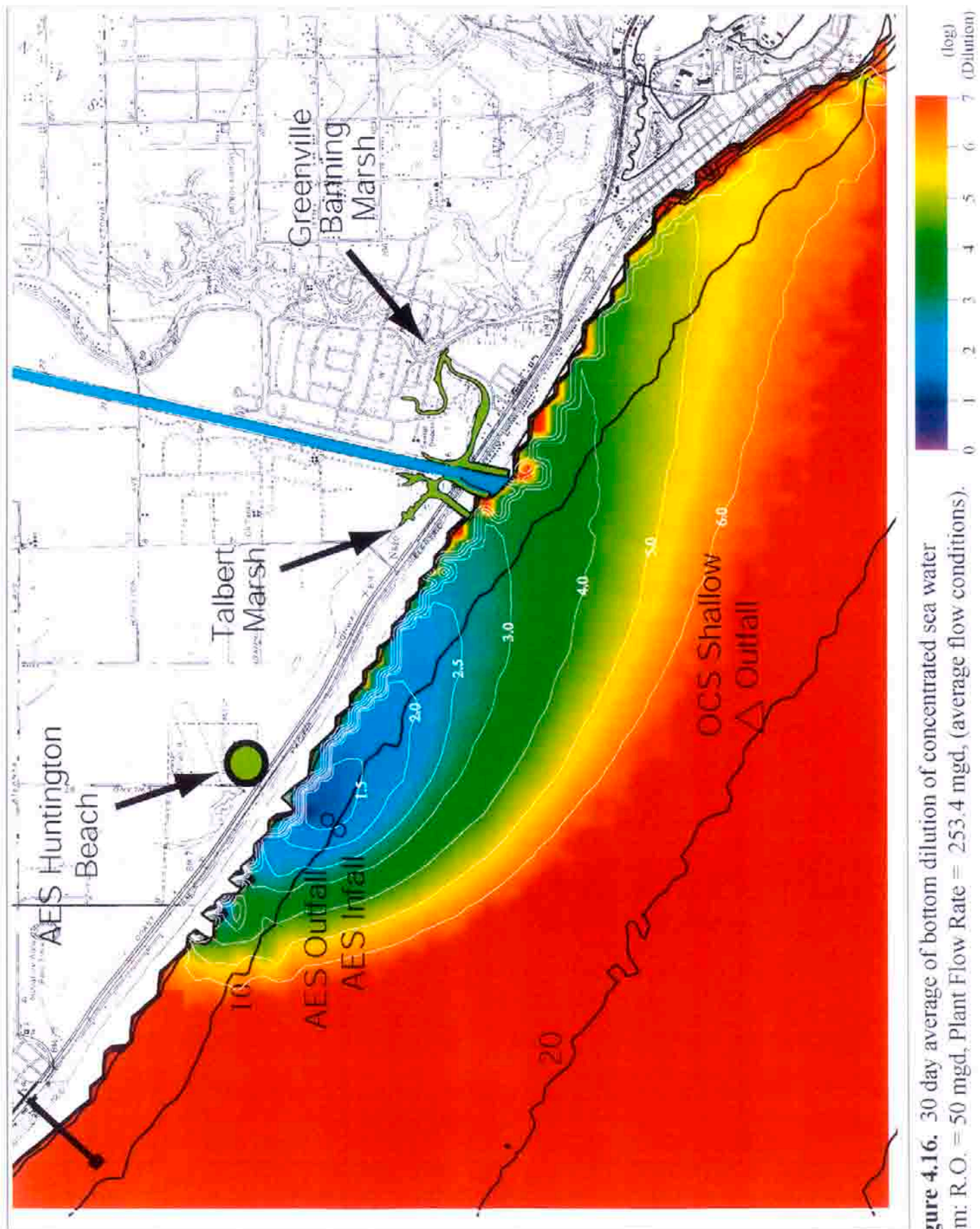


Figure 4.16. 30 day average of bottom dilution of concentrated sea water from: R.O. = 50 mgd, Plant Flow Rate = 253.4 mgd, (average flow conditions).

acres. The footprint of the 1% saline anomaly covers a maximum area of 130 acres in the water column and 172 acres at the seabed.

The model simulation of the salinity profile in a cross-shore section passing through the outfall (Section-A, Figure 1.1) is plotted in Figure 4.12 for an RO production rate of 50 mgd and a plant flow rate of 253.4 mgd during the average month conditions. The corresponding longshore section of the salinity profile (Section-B) is plotted in Figure 4.13. Both plots are scaled identically to Figures 4.9 - 4.11 with contours of salinity in parts per thousand (ppt), where the ambient background ocean salinity is 33.52 ppt. It is apparent that the core salinities are substantially diminished for average month conditions, reaching a maximum of only 41.7 ppt with a nominal value of 38 ppt in the inner core, and nominally 36 ppt in the outer core. However both the inner and outer cores are enlarged relative to low flow case, with a nominal radius of 90 - 115 meters for the inner core and 170-440 meters to the outer fringes of the outer core where salinities have declined to 35 ppt. The enlarged core structures with lower salinity anomalies are a result of higher "in-the-pipe" dilutions and more vigorous ocean mixing during average case operational and environmental conditions. The salt wedge is similarly enlarged along shore and more diffuse due to the higher net longshore currents during average month oceanographic conditions. Nominal salinities in the salt wedge are only 33.65 ppt (0.38% anomaly) with a maximum detectable limit spreading 570 meters offshore and 2,200 meters downdrift from the outfall. The offshore spreading of the plume is diminished for average conditions because the lower core salinities reduce the downslope gravitational forces acting to move the plume in that direction. Concurrent with diminished downslope gravity are larger waves with longer periods that exert a larger shoreward directed wave transport (Stokes Drift)

to counter downslope gravity.

The dilution of concentrated seawater at the generating station infall is 32 to 1 (Figure 4.14) and hence only 0.7% of the sea salts from reverse osmosis are potentially re-circulated during an average month. Minimum dilution of concentrated seawater at the shoreline is 190 to 1 (Figure 4.16) and minimum dilution at 1000 ft in any direction from the outfall is 20 to 1.

E) Summary of Dilution and Dispersion Results:

Low flow case dilution calculations are summarized in the first column of Table 6 for low-flow conditions and in the third column for standby mode. Simulations in Figures 4.1-4.8 indicate that the desalination project will result in a tear-drop-shaped saline plume around a jet of water discharged vertically upward toward the sea surface from the outfall tower. In the core of this jet, the highest salinity reaches 55.0 at mid depth in the water column for low flow conditions and 55.2 ppt for standby mode. The difference between the discharge salinity and the background seawater salinity rapidly decreases with increasing distance from the discharge outfall tower. Taking the average radius of the tear-drop-shaped plume, salinity in the water column decreases to 40 ppt (20 percent above background salinity) within 283 feet from the discharge outfall tower for low-flow conditions and within 360 ft for standby mode. Water column salinity decreases to 10 % above background seawater salinity (37 ppt) within 504 feet from the outfall tower for low-flow conditions and within 528 ft for standby mode. The total pelagic area of the plume within the 10% saline anomaly is 18.3 acres for low-flow and 20.1 acres for standby mode. The size and strength of the plume are a bit less on the seafloor than in the water column. On the seafloor, the highest salinity is at the base of the outfall tower and is 48.3 ppt for low-flow conditions . The

Table 6: Summary of Event Analysis of Dispersion and Dilution

Model Conditions	Composite Low-flow Month	Composite Average Month	Composite Standby Month
Recurrence Probability	0.27% - 0.64%	50.0%	0.04% - 0.1%
Maximum Seabed Salinity	48.3 ppt	37.6 ppt	50.4 ppt
Maximum Mid-Water Column Salinity	55.0 ppt	41.7 ppt	55.2 ppt
Maximum Surface Salinity	50.1 ppt	38.3 ppt	53.1 ppt
Maximum Benthic Area of 10% Saline Anomaly	15.6 acres	6.8 acres	18.2 acres
Maximum Pelagic Area of 10% Saline Anomaly	18.3 acres	8.3 acres	20.1 acres
Maximum Benthic Area of 1% Saline Anomaly	263 acres	172 acres	284 acres
Maximum Pelagic Area of 1% Saline Anomaly	151 acres	130 acres	163 acres
Dilution of Concentrated Seawater at Plant Infall ^a	100 to 1	500 to 1	90 to 1
Minimum Saline Dilution 305 m from Discharge Structure ^a	10 to 1	20 to 1	8 to 1
Minimum Saline Dilution at Shoreline ^a	32 to 1	190 to 1	30 to 1

^a Dilution of Raw Concentrate from RO Process

bottom salinity maximum is 50.4 ppt at the base of the tower for standby mode.

The bottom salinity drops to 40 ppt within 236 feet from the discharge for low flow conditions, and within 300 ft for standby mode. The bottom discharge salinity is reduced to 10 % of the background salinity within 465 feet from the

outfall tower for low-flow conditions, and within 502 ft for standby mode. This 10 % bottom salinity anomaly covers 15.6 acres of the seafloor for low-flow conditions and 18.2 acres for standby mode.

Dispersion and dilution contours of sea salts for the theoretical extreme of the standby mode are very similar to those shown in Figures 4.1 through 4.8. The absence of power plant heat produces a heavier combined discharge that is more slowly assimilated by the receiving waters. As a result, the high salinity inner core of the standby mode discharge plume collapses earlier under larger forces of gravity, entraining less ambient water during subsidence and diluting more slowly. Dilution is also impeded by less thermal agitation in the unheated discharge.

Under average conditions, the maximum salinity anywhere is at mid water column depth in the core of the discharge jet, and reaches 41.7 ppt, which is only 25 percent higher than the background salinity. Along the long-axis of the tear-drop-shaped plume (Figures 4.9 & 4.13), the discharge salinity in the water column decreases to 38.5 ppt (15 percent above background salinity) within 200 feet from the discharge outfall tower. Within 339 feet from the outfall tower, the average discharge salinity in the water column will be only 10 percent higher than the background seawater salinity (37 ppt) over an area of 8.3 acres. On the seafloor, salinity never reaches 40 ppt (20% over ambient) due to entrainment by the collapsing inner core as it subsides. The highest salinity on the seafloor for average conditions is found at the base of the outfall tower and is 37.6 ppt (only 12 % above background salinity). The bottom salinity drops to less than 10 % above the background salinity over an average distance 307 feet away from the discharge, subjecting no more than 6.8 acres of seabed to salinity on the order of 37 ppt.

F) Drift Rates and Exposure Time

Pelagic organisms drifting in the nearshore currents can be carried through the discharge plume along trajectories governed by the *Lagrangian drift* (Batchelor, 1970). The Lagrangian drift is the mean motion of a particle that would be observed by following that particle along its drift trajectory. The concept of Lagrangian mean motion is particularly important in the problem at hand because the water velocity in and around the plume varies from point to point due to the cross shore variation in the wave and tidal currents and the local velocity variation due to the discharge of the outfall. (Such variations in the local velocity field are referred to as *velocity gradients*, and were resolved by the model over the entire nearshore domain by the wave and current algorithms described Sections 2 and 3. The drift rates of organisms passing through these velocity gradients are not the same as the mean current speed measured by a fixed current meter located near the outfall. The current meter will have an error in drift rate estimates due to the effects of velocity gradients acting on the organism at places away from the current meter location. A hydrodynamic model can correct for such errors because it can reconstruct the entire velocity gradient structure that is required to calculate the actual drift rate of a particle moving in a variable velocity field. The drift rate of an organism passing through the plume is calculated as described below subject to the assumption that the organism is represented by a neutrally buoyant particle.

The maximum exposure time to elevated salinity for a drifting pelagic organism is plotted as a red line in Figure 4.17 for low flow case conditions. The salinity bins used for the drift trajectory calculations are indicated by red crosses. Exposure to the maximum salinity of the inner core (53-55 ppt) occurs for at most 7 minutes, while about 35 minute exposure could occur along the fringes of the

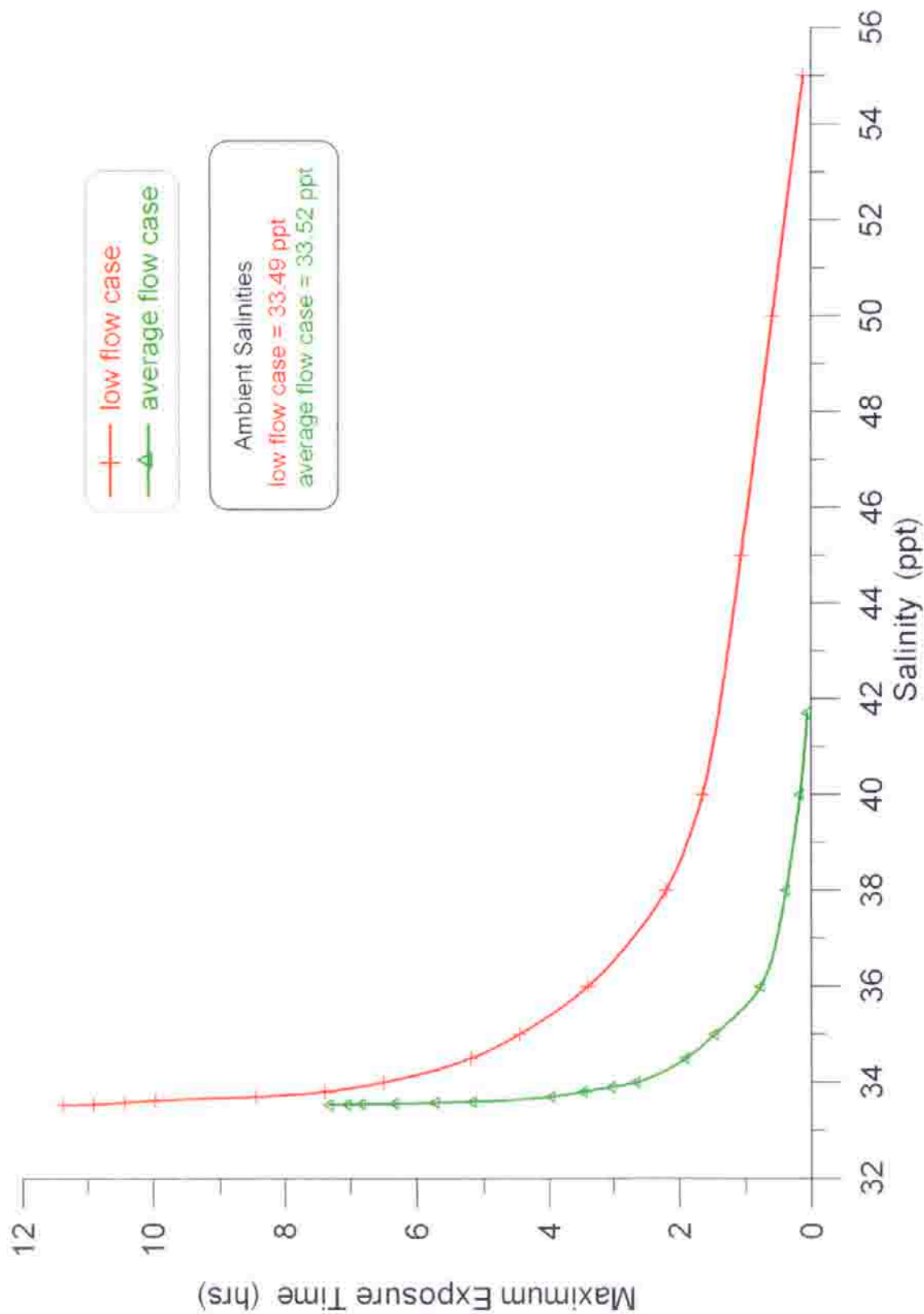


Figure 4.17. Maximum exposure time of a drifting organism passing through the discharge plume of concentrated seawater from the AES Huntington Beach outfall for low flow case conditions (red, plant flow rate = 126.7 mgd) and average case conditions (green, plant flow rate = 253.4 mgd).

inner core (40-50 meters from the outfall) where salinities are 50 ppt. In the outer core where salinities are nominally 45 ppt, the exposure time of a drifting organism would be about 1 hour, and about 2.2 hours along the outer fringes of the outer core where salinities decline to 38 ppt. In the salt wedge where salinities are nominally 34 ppt (equivalent to the seasonal maximum during the 1998 El Nino), the exposure time would be 6.5 hrs. At the outer limit of the salt wedge where the effect of the discharge from desalination is barely detectable above ambient mean salinities, the exposure time would be 11.4 hours.

The maximum exposure time to elevated salinity for a drifting pelagic organism is plotted as a green line in Figure 4.17 for average month conditions. The salinity bins used for the drift trajectory calculations are indicated by green triangles. Exposure to the maximum salinity of the inner core (40- 41.7 ppt) occurs for at most 10 minutes, while about 23 minute exposure could occur along the fringes of the inner core (90-115 meters from the outfall) where salinities are 38 ppt. In the outer core where salinities are nominally 36 ppt, the exposure time of a drifting organism would be about 46 minutes, and about 1.5 hours along the outer fringes of the outer core where salinities decline to 35 ppt. In the salt wedge where salinities are nominally 33.65 ppt (equivalent to the seasonal maximum of an average year), the exposure time would be 4.5 hrs. At the outer limit of the salt wedge where the effect of the discharge from desalination is barely detectable above ambient mean salinities, the exposure time would be 7.3 hours.

While passive exposure of pelagic organisms to the discharge plume is limited by the Lagrangian drift rates in the water mass around the outfall, the benthic organisms will experience exposure to low flow case conditions for as long as the environmental and operational conditions contributing to low flow case

persist. (In the model those conditions are perpetuated artificially for 30 consecutive days when in fact these conditions are likely to occur only 0.27% to 0.64 % of the time). The red curve in Figure 4.18 gives the variation in the bottom salinity for low flow-case conditions in a cross-shore section through the outfall (Figure 4.4) and in a longshore section (Figure 4.5). The highest bottom salinity found anywhere is 48.3 ppt at the base of the outfall tower, rapidly falling to 41 ppt at the outer fringes of the inner core. In the outer core and salt wedge, bottom salinities are slightly in excess of those in the water column for a given distance from the outfall. At the outer fringes of the outer core, bottom salinities are 38 ppt, while the structure of the salt wedge affords weakly elevated salinities out to greater distances along the bottom than in the water column. The total longshore expanse of the detectable presence of the salt wedge along the seabed is about 2,150 meters but the bottom salinities over most of this distance are no greater than the inter-annual maximum occurring naturally during a strong El Nino.

The green curve in Figure 4.18 gives the variation in the bottom salinity during average month conditions in a cross-shore section through the outfall (Figure 4.12) and in a longshore section (Figure 4.13). The highest bottom salinity found anywhere is about 37.6 ppt at the base of the outfall tower, rapidly falling to 35 ppt at the outer fringes of the core. Though out the preponderance of the salt wedge, bottom salinities are typically elevated no more than 0. 1 to 0.3 ppt above ambient. The total longshore expanse of the detectable presence of the salt wedge over the seabed is about 3000 meters but the bottom salinities over most of this distance are no greater than the inter-annual. maximums of an average year.

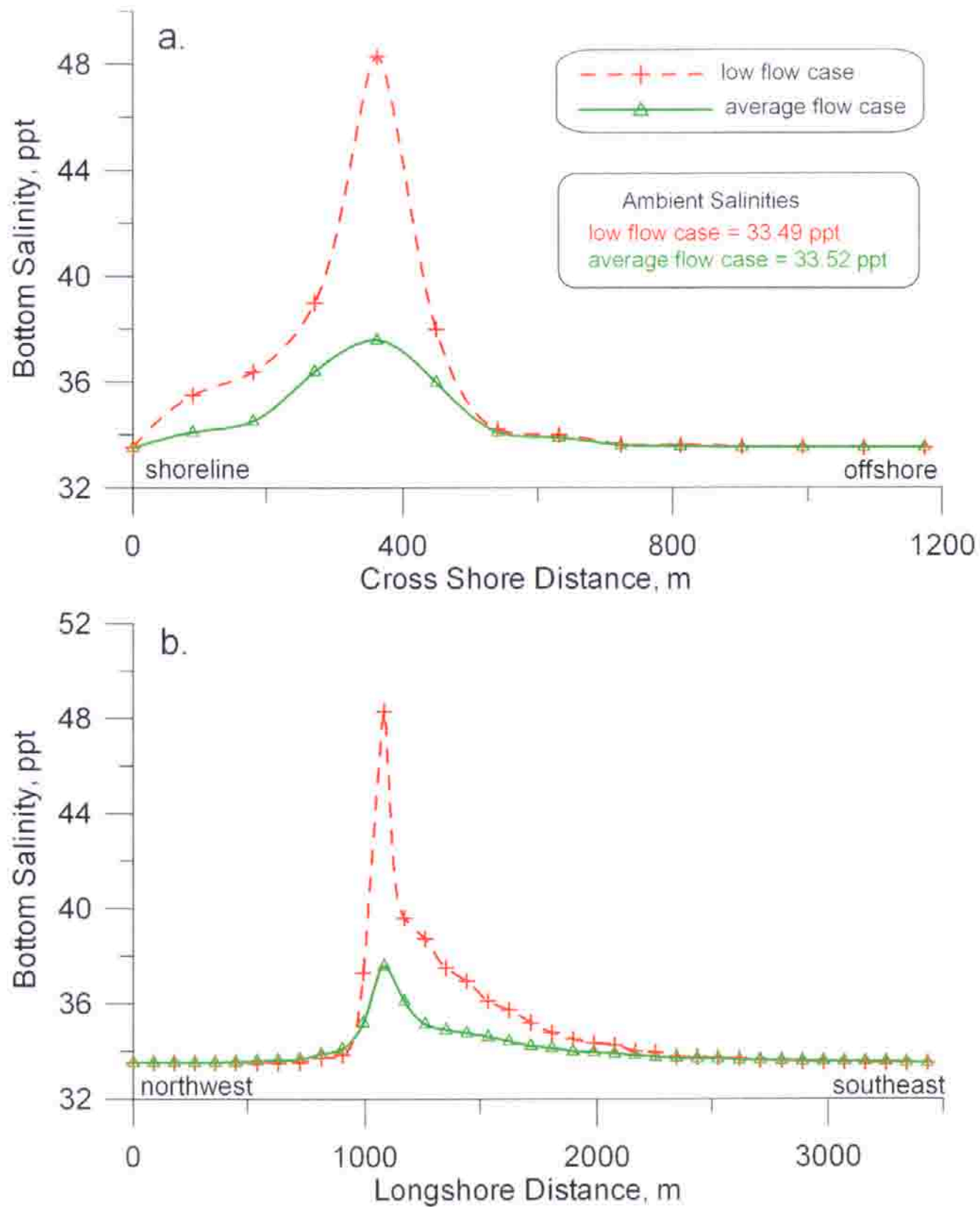


Figure 4.18. Thirty day average of bottom salinity for low flow and average flow case months along: a) crossshore profile (Section A), b) longshore profile (Section B).

SECTION 5: LONG TERM ANALYSIS OF DILUTION OF CONCENTRATED SEA WATER

5) Long-Term Analysis of Dilution of Concentrated Sea Water

In this section we perform modeling simulations on the entire set of 7,523 daily combinations of the 7 controlling variables presented in Figures 3.23 and 3.24 for the period of record from 1980 through mid-2000. This period was selected because it is the longest length of time for which an uninterrupted record of directional wave data can be assembled in this region. The purpose of this long-term continuous modeling exercise was to both establish the viability of the event analysis presented in Section 4 for characterizing low flow and average case, as well as exploring the persistence of all the intermediate outcomes occurring between low flow and average cases. In addition changes to the dispersion statistics of the hyper-saline plume are examined for cold water discharges from AES Huntington Beach, as a consequence of the generating station pumping seawater with a $\Delta T = 0$.

The marine environment around the AES Huntington Beach Generating station has both short-term and long-term variability due to an interplay between climatic variability and certain local features due to physical setting and generating station operations. El Niño events cause significant warming and stratification of the coastal ocean around AES Huntington Beach over recurrence periods of 3 to 7 years. These warm El Niño events are superimposed on seasonal warming cycles. The salinity field shows similar variability due to the same sets of climatic, and seasonal mechanisms. El Niño events bring floods causing river discharges of fresh water which depress the salinities of the coastal oceans in the vicinities of river mouths. Similar variations occur inter-annually as seasonal changes in wind patterns move different water masses with different salinities into and out of the

Southern California Bight. Therefore, the local environment already has a natural degree of variability in temperature and salinity on which the activities of the generating station and desalination plants are superimposed. In addition the ocean forcing functions that will mix and carry away the heat and concentrated seawater resulting from these two activities are likewise modulated by El Niño events, seasonal changes in weather patterns and by diurnal and semi-diurnal changes in tidal stage. Even the generating station's production is effected by climatic, seasonal, and daily changes in user demand, with corresponding adjustments in the volume of sea water consumed by the plant and the amount of waste heat introduced into the coastal waters. We will explore the potential effect on the discharge of concentrated sea water from the desalination plant associated with the interplay between the operational variability of the host generating station and the environmental variability of the receiving water by computing each possible outcome among the 7,523 separate combinations of potential inputs contained Figures 3.23 and 3.24.

The historic boundary conditions from Figure 3.23 and the forcing functions from Figure 3.24 were sequentially input into the model, producing daily solutions for the salinity field discharged from the AES Huntington Beach outfall due to the combined operations of the generating station and the desalination plant. The input stream of seven controlling variables from Figures 3.23 & 3.24 produced 7,523 daily solutions for the salinity field around the outfall. A numerical scan of each of these daily solutions searched for the maximum salinity at distances of 0, 50, 100, 150, 300, 500, 1,000 and 2,000 meters away from the outfall in all directions. These increments of search radii were selected to resolve both the high saline core of the discharge plume as well as the extent of the associated broad-scale salt wedge

feature having weakly elevated salinities. The solution scans searched for salinity maximums in both the water column and along the seafloor. For each search radius, the largest salinity found in any direction away from the outfall was entered into a histogram bin for ultimately assembling a probability density function and cumulative probability from the 7,523 outcomes. Histogram bins were constructed at salinity increments of 0.4 ppt. The bins were then summed to calculate the cumulative probability distribution. The histogram recurrence analysis was repeated for both warm water discharges at a Delta-T of $\Delta T = 18^\circ\text{F}$ (10°C) and a cold water discharge at a Delta-T of 0° .

When reading the histogram plots in this section (Figures 5.2 - 5.15 and 5.21 - 5.34), the following conventions are used:

- 1) In the water column, vertical red bars are the histogram bins for a discharge Delta-T of $\Delta T = 18^\circ\text{F}$ (10°C), while the vertical blue bars are the histogram bins of cold water discharge at $\Delta T = 0^\circ\text{C}$.
- 2) On the sea floor, vertical green bars are the histogram bins for a discharge Delta-T of $\Delta T = 18^\circ\text{F}$ (10°C), while the vertical blue bars are the histogram bins of cold water discharge at $\Delta T = 0^\circ\text{C}$.
- 3) For both water column and sea floor histograms, only those histogram bins for cold water outcomes ($\Delta T = 0^\circ\text{C}$) that exceed the salinity of the normal warm water discharges ($\Delta T = 10^\circ\text{C}$) are shown.
- 4) For both water column and sea floor plots, the calculation of the cumulative probability (blue line) is based on the highest salinity outcomes, regardless of whether they are due to warm or cold water discharges. Thus the cumulative probability distribution always includes ultimate worst case. For reference, the maximum salinity from the low flow case scenario from

Section 4 is shown as a dashed, black vertical line.

A) Saline Anomalies at the Outfall

Figure 5.1 gives the histogram and cumulative probability of daily maximum salinities at mid depth directly over the outfall (0 meters from outfall). These results are in the core of the discharge jet directed vertically upward toward the sea surface (see Figures 4.4, 4.5, 4.12 & 4.13). These salinities are nearly the same as end-of-pipe values other than for the mixing that occurred over the short distance between the top of the outfall and the middle of the water column. Hence the statistical character of these salinities are controlled by the interplay between historic plant flow rates and historic ocean salinities between 1980 and July 2000. Inspection of the post-1987 portion of the flow rate record in Figure 3.23a reveals that plant operations have been limited primarily to only two modes: either one generating unit operating at 126.7 mgd or 2 generating units at 253.4 mgd. Figure 5.1 shows that when the flow rate history in Figure 3.23a is applied to the ocean salinity variation in Figure 3.21 or 3.23b, the resulting end-of-pipe salinity variation from the combined discharge of the desalination plant and generating station will have a bi-modal probability density distribution. This bi-modal behavior is a direct consequence of the historic 2-mode production levels of the generating station. Although there were instances of the plant operating with three and four generating units in the first seven years of the 1980- July 2000 period of record (see Figure 3.22 and 3.23a) the preponderance of the record shows that the plant supplied only 2 different flow rates (127.6 or 253.4 mgd) most of the time. In the long term desalination simulations based on this historic operating record, this

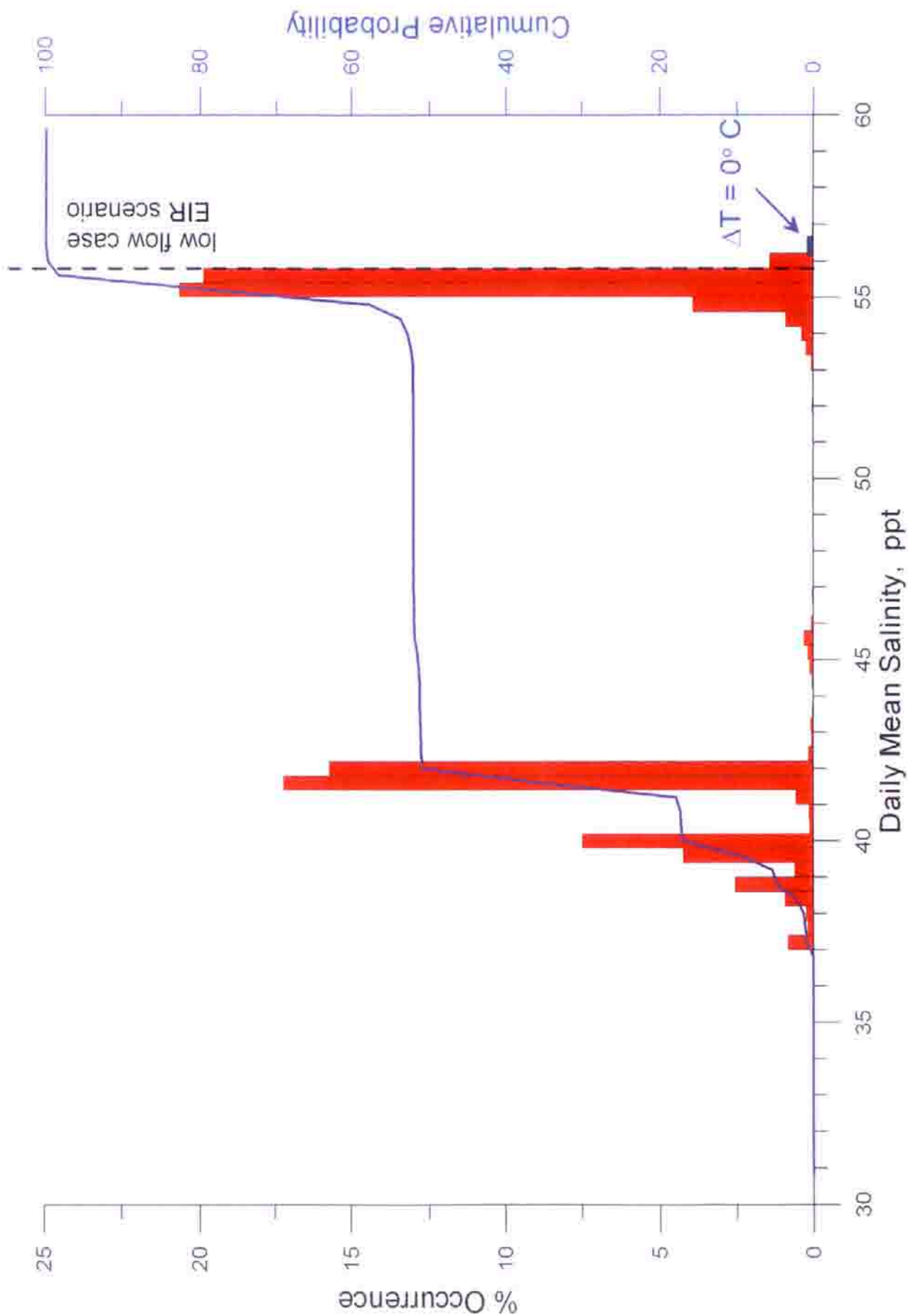


Figure 5.1. Histogram of daily maximum salinity at mid-depth and 0 meters from the AES outfall for desalination production rate of 50 mgd. Percent occurrence based on historic observations of ocean mixing and water mass mass properties, and AES daily plant flow rates, 1980-2000.

gives only 2 different flow rates for diluting the 50 mgd stream of concentrated sea salts from the desalination plant. Consequently there are only two preponderant discharge salinities, because the natural variability in ocean salinity (10%) is small compared to 100% variability (127.6 vs 253.4 mgd) in plant flow rate.

Figure 5.1 also shows that the combined end-of-pipe salinity will vary from a minimum of 37 ppt to a maximum of 56.4 ppt for cold water discharges ($\Delta T = 0$ °C). The two predominantly recurring peaks in the probability density function for end-of-pipe salinity are centered at 41.6 ppt and 55.2 ppt, consistent with the average and low flow case values, respectively, as assigned to end-of-pipe sea salt concentrations (see Table 6, Section 3). The median (50% cumulative probability) salinity is actually 42.0 ppt. The maximum salinity of the warm water discharge ($\Delta T = 10$ °C) is 55.4 ppt, also in line with the low flow case scenario presented in the EIR. However the cumulative probability of the Section 4 low flow case salinity turns out to be only 82%. The discrepancy is due to the low flow rate bias in the flow rate statistics during the plant re-fitting of the 1990's. The absence of thermal agitation in the cold water discharge results in an increase of one part per thousand (1 ppt) in the salinity at mid depth of the water column directly over the outfall. The cold water exceedence of 1 ppt occurs about 20% of the time throughout the 20.5-year period of record. However, we will show in the subsequent sections that this initially higher water column salinity at the outfall is quickly suppressed with increasing depth or distance away from the outfall. This occurs because the cold water discharge is heavier in the absence of thermal expansion from the waste heat. The heavier discharge subsides more rapidly from its initial upward trajectory after leaving the outfall chimney. The subsidence is itself a mixing mechanism, engaging the full water column in the dilution volume. The more rapid the subsidence, the

more vigorous the vertical stirring of that dilution volume becomes.

Figure 5.2 gives the histogram and cumulative probability of daily maximum salinities on the sea floor at the base of the outfall (0 meters from outfall). The median (50% cumulative probability) salinity is 38.8 ppt, about 1.2 ppt higher than with the average case scenario presented in Section 4; but the maximum warm water discharge salinity is 48.2 ppt, on par with the low flow case scenario in Section 4. The cold water discharge salinities exceed the Section low flow case scenario by 0.3 ppt but, are a less than 1% occurrence events for which the cumulative probability greater than 99%.

While the water column and sea floor salinities above and at the foot of the outfall appear to be in-line with the average and low flow case results in Section 4, the frequency of occurrence of the low flow case extremum are not negligible. In the water column above the outfall, 55 ppt is found about 22 % of the time from the 1980- July 2000 records, and all the outcomes in the high flow rate peak of the probability density distribution around 55ppt account for 48% of the outcomes. While 48.3 ppt is found on the seafloor less than 1 % of the time, 47.6 ppt would occur about 28 % of the time, and all of the collection of sea floor realizations in the low flow rate peak centered at 47.5 ppt account for 48% of the outcomes; but again, based on the historic plant operating patterns during the 1980- July 2000 time frame. However, at the outfall salinity is controlled by in-the -pipe conditions rather than by ambient mixing or advection by ocean processes. Because the plant operated very close to the low flow case scenario flow rate throughout the 1990's (see Figure 3.22), the salinity extremes at the outfall in both the water column and

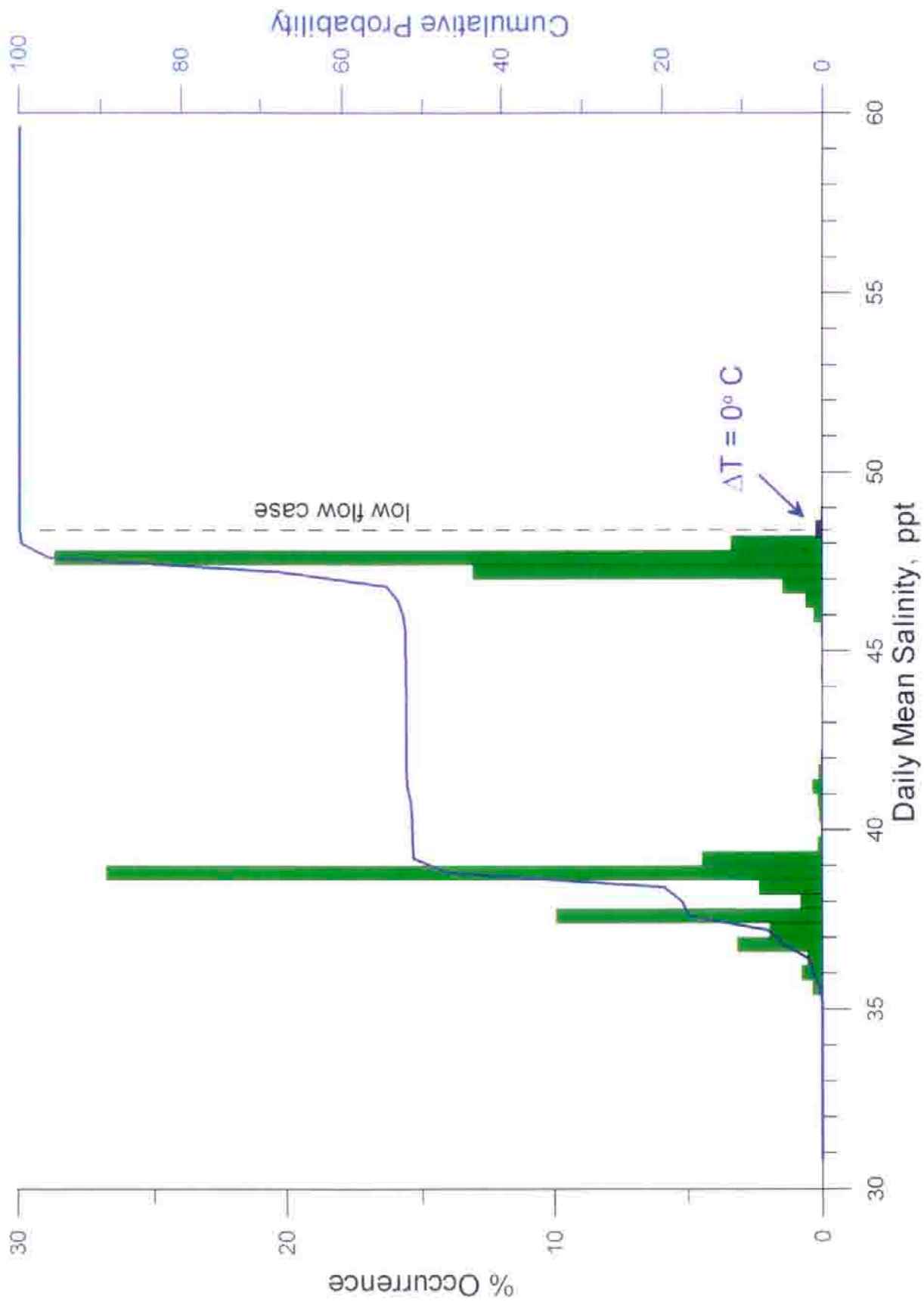


Figure 5.2. Histogram of daily maximum salinity at the bottom and 0 meters from the AES outfall for desalination production rate of 50 mgd. Percent occurrence based on historic observations of ocean mixing and water mass mass properties, and AES daily plant flow rates, 1980-2000.

on the sea floor are also at or near low flow case values a disproportionately high percentage of the time. We will find in subsequent sections that as we get further away from the outfall, the occurrence statistics of the ocean processes will begin dominate the recurrence behavior of the salinity extremes.

B) Saline Anomalies 50 meters from the Outfall

Figure 5.3 shows that a substantial amount of dilution of the salinity maximums and means occurs in the water column over the first 50 meters away from the outfall due to the mixing occurring in the inner core of the discharge plume. The dynamical effect of this mixing shifts the two primary peaks of the probability density to lower salinity values and to broaden those peaks over a wider salinity range. Mixing reduces the median salinity to 38.2 ppt and the maximum salinity to 47 ppt, both consistent with the results presented in Section 4 for average and low flow case. There were no cold water outcomes ($\Delta T = 0^\circ\text{C}$) that exceeded the Section 4 low flow case scenario. The probability density distribution 50 meters from the outfall remains bi-modal with a low flow rate peak centered on 45.4 ppt that accounts for 48% of the outcomes and a mid-flow rate peak centered at 37.4 ppt accounting for 52 % of the outcomes. The low flow rate peak is associated with only one operational generating unit while the mid-flow rate peak is due to two generating units on line.

In Figure 5.4 we find similar bi-modal histograms of probability density and cumulative probability on the sea floor 50 meters away from the outfall. The salinity peaks and maximums are less due to the additional dilution that occurs as the plume sinks from mid-depth to the bottom. For warm water discharges, the

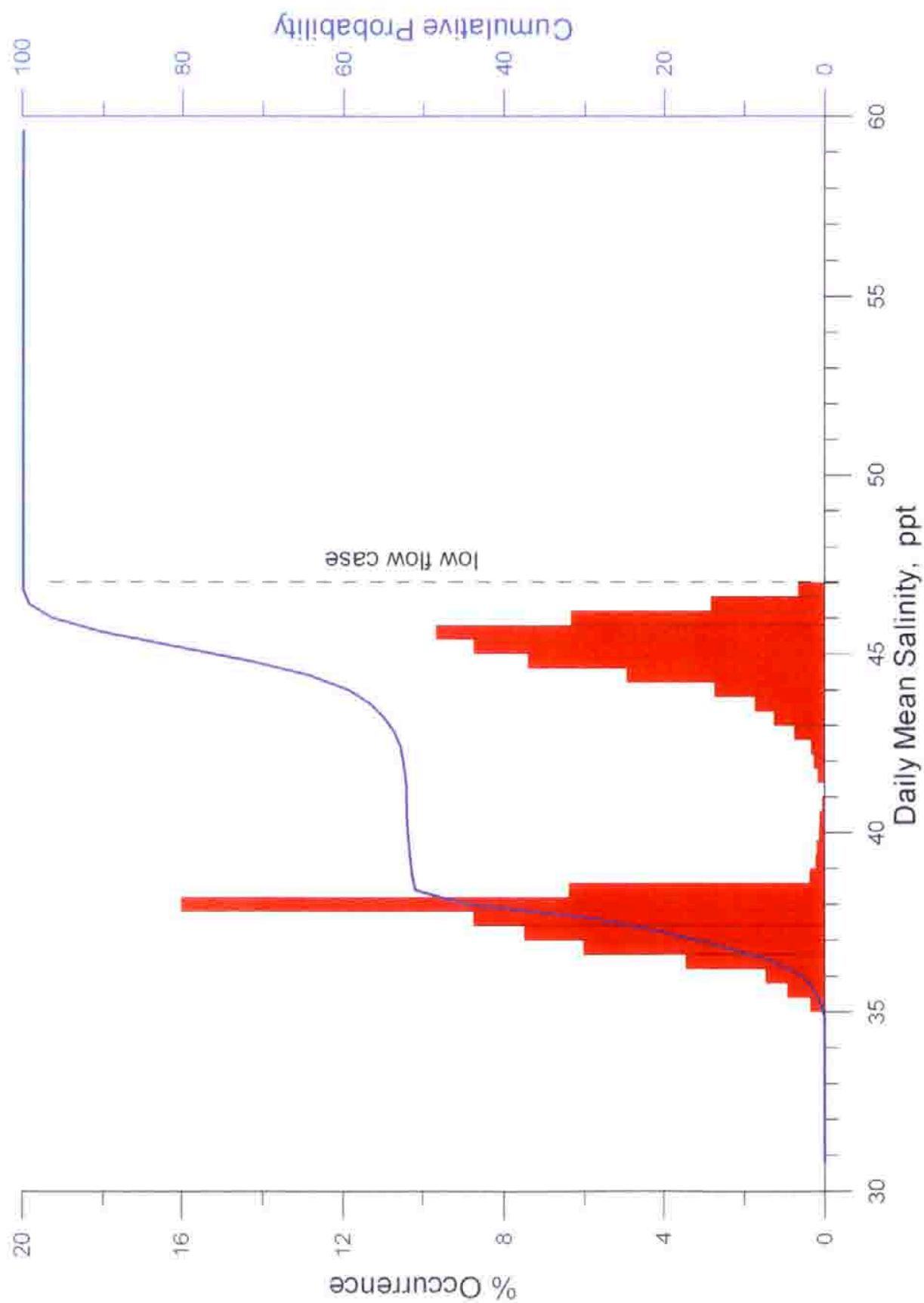


Figure 5.3. Histogram of daily maximum salinity at mid-depth and 50 meters from the AES outfall for desalination production rate of 50 mgd. Percent occurrence based on historic observations of ocean mixing and water mass mass properties, and AES daily plant flow rates, 1980-2000.

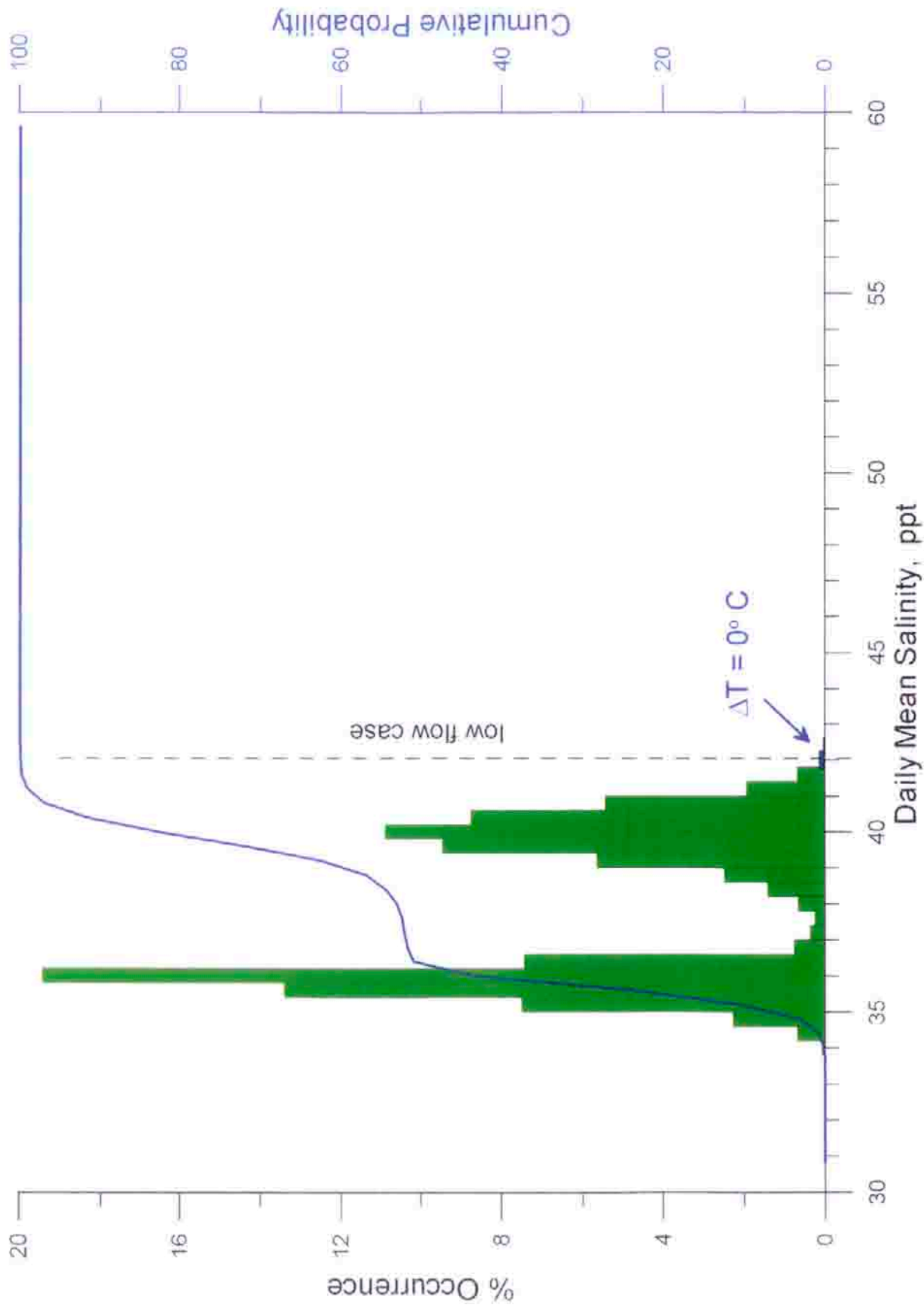


Figure 5.4. Histogram of daily maximum salinity at the bottom and 50 meters from the AES outfall for desalination production rate of 50 mgd. Percent occurrence based on historic observations of ocean mixing and water mass mass properties, and AES daily plant flow rates, 1980-2000.

salinity maximum is 41.8 ppt, while the cold water discharge reaches 42 ppt, both in line with the Section 4 low flow case scenario. The median salinity here on the outer edge of the inner core is 36.2 ppt, also comparable to the Section 4 average case scenario. The low flow rate recurrence peak in the sea floor probability density function is centered at 40 ppt and accounts for about 48% of the outcomes in the 1980-July 2002 record. The mid-flow rate recurrence peak is centered at 36 ppt and accounts for about 52% of the outcomes.

C) Saline Anomalies 100 meters from the Outfall

Here we enter the outer core of the discharge plume where advective entrainment of surrounding water by the residual upward momentum of the discharge jet causes further dilution (see Figures 4.4, 4.5, 4.12 & 4.13). As a result, further shifts towards lower salinities occur in both the low and mid-flow rate peaks of the water column probability density function (histogram) in Figure 5.5. The low flow rate peak is broader and is centered at about 43 ppt, accounting for about 47 % of the outcomes. Maximum salinity in the water column 100 meters from the outfall is 46 ppt, consistent with the Section 4 low flow case scenario and independent of warm vs cold water discharges. The mid- flow rate peak is shifted down to 36.6 ppt and accounts for 53% of the outcomes. The median water column salinity is 37 ppt. Comparing Figures 5.5 and 5.3 indicates that the advective entrainment effects in the inner portion of the outer core are not especially vigorous, reducing salinity maximums and means by about 1ppt, but significantly broadening the low and high flow rate peaks and thereby reducing the degree of sorting between them.

Figure 5.6 gives the histogram (probability density) and cumulative

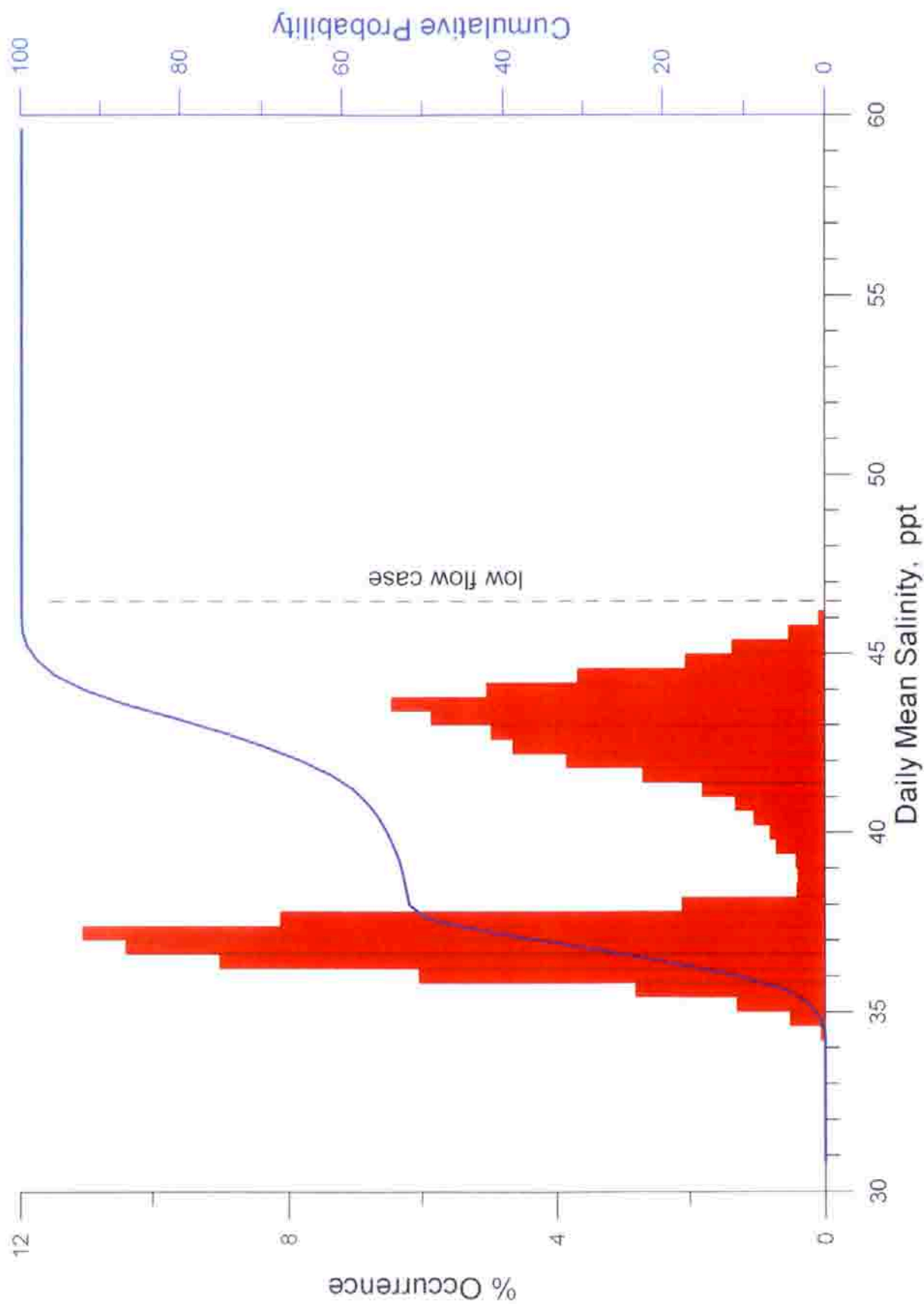


Figure 5.5. Histogram of daily maximum salinity at mid-depth and 100 meters from the AES outfall for desalination production rate of 50 mgd. Percent occurrence based on historic observations of ocean mixing and water mass mass properties, and AES daily plant flow rates, 1980-2000.

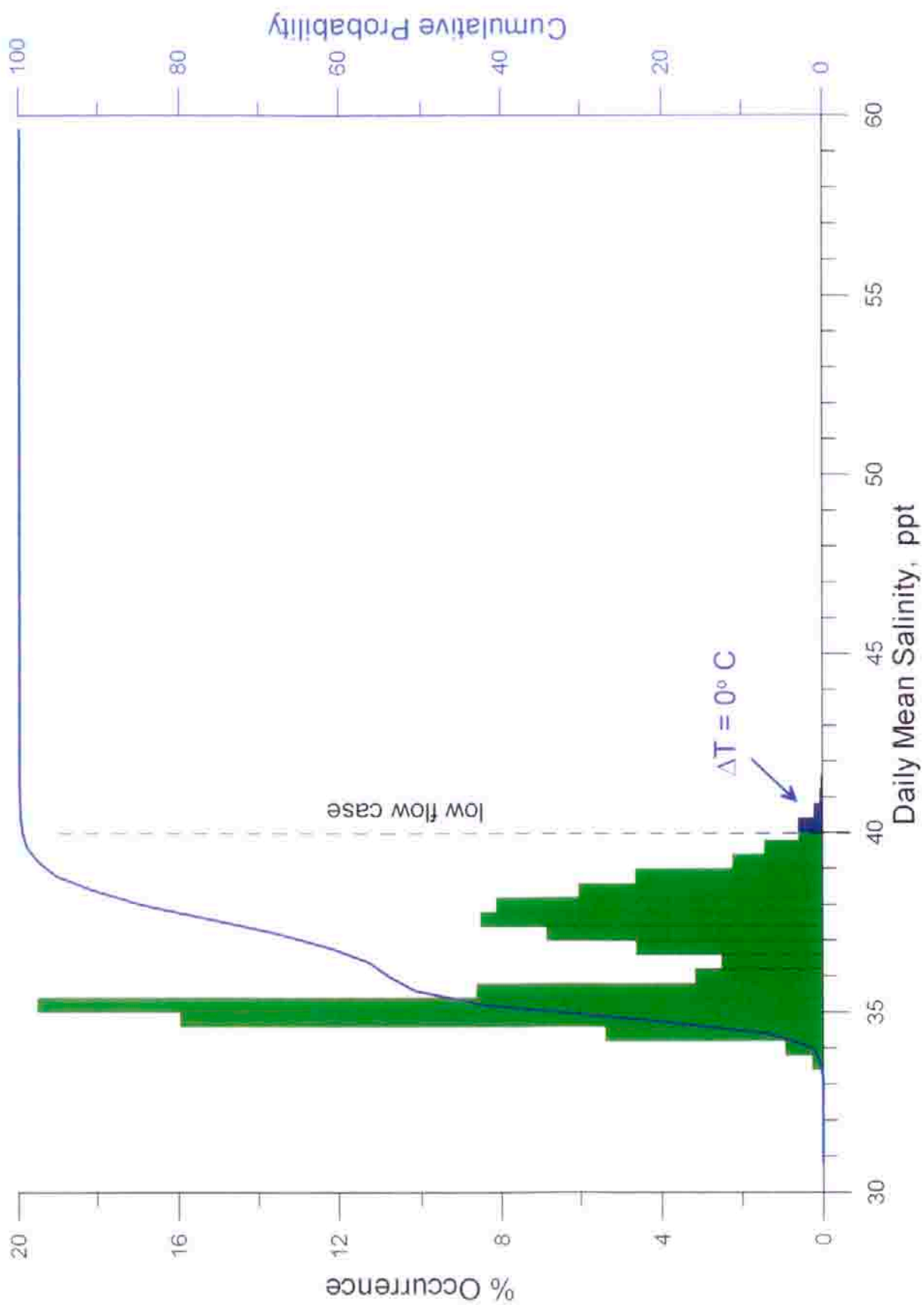


Figure 5.6. Histogram of daily maximum salinity at the bottom and 100 meters from the AES outfall for desalination production rate of 50 mgd. Percent occurrence based on historic observations of ocean mixing and water mass mass properties, and AES daily plant flow rates, 1980-2000.

probability of daily maximum salinities on the sea floor at 100 meters away from the base of the outfall. Here the median sea floor salinity is 35.5 ppt, and the maximum warm water discharge salinity is 40 ppt both consistent with the average and low flow case scenarios presented in Section 4. However the, the heavier cold water discharge produces salinity extremes reaching 41.3 ppt about 3% of the time during the 1980- July 2000 record. The low- flow rate peak centered on 37.8 ppt accounts for 43% of the outcomes, while the mid-flow rate peak centered on 35 ppt accounts for 57%. In both Figures 5.4 and 5.5 it is noted that the low flow rate peak is broader. This is due to the higher salinity of the low flow rate peak which results in larger concentration gradients relative to the surrounding ambient water mass, thereby yielding larger diffusive fluxes than for the mid-flow rate peak.

D) Saline Anomalies 150 meters from the Outfall

At this distance from the outfall we are in about the middle of the outer core in the down drift direction and at the outer edge in the cross shore direction (see Figures 4.4, 4.5, 4.12 & 4.13). The reason for this directional asymmetry is the along shore stretching of the plume by the ebb-dominated tidal currents that have a net drift downcoast towards the Santa Ana River over any given 24 hour period (see Figures 4.1 - 4.3 and 4.10 - 4.12).

Figure 5.7 gives the histogram (probability density function) and cumulative probability of daily maximum salinities at mid depth in the water column at a distance of 150 meters from the outfall. The continued broadening of the low flow rate peak of the probability density function is becoming more apparent at increasingly larger distances away from the outfall. In fact the low-flow and mid-

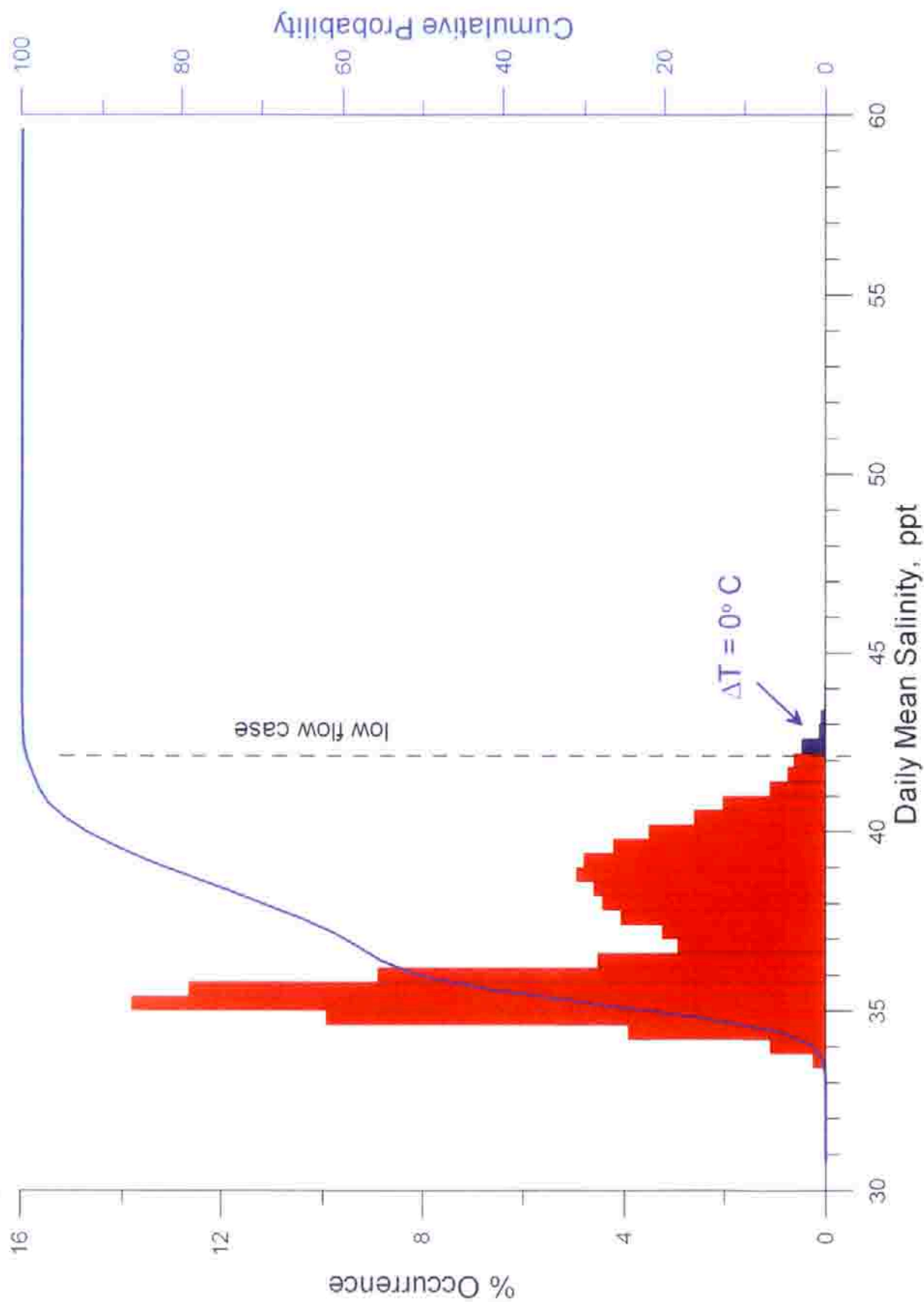


Figure 5.7. Histogram of daily maximum salinity at mid-depth and 150 meters from the AES outfall for desalination production rate of 50 mgd. Percent occurrence based on historic observations of ocean mixing and water mass mass properties, and AES daily plant flow rates, 1980-2000.

flow rate peaks of the probability density function are beginning to merge. The low flow rate peak is centered on 39 ppt and accounts for 42% of the outcomes, but extends to maximum warm water discharge salinities as high as 42.2 ppt. The highest warm water salinity matches the Section 4 low flow case scenario, but cold water discharges reach an ultimate maximum salinity of 43.4 ppt and account for about 3% of the outcomes. The median water column salinity (50% cumulative probability) is 36 ppt. The mid-flow rate peak in the probability density distribution is centered on 35.2 ppt and makes up 58% of the total realizations.

Figure 5.8 gives the histogram (probability density) and cumulative probability of daily maximum salinities on the sea floor at 100 meters away from the base of the outfall. The median sea floor salinity is 35.0 ppt, and the highest warm water discharge salinity is 39 ppt, again both consistent with the average and low flow case scenarios presented in Section 4. The cold water discharge that results in greater density stratification produces highest salinities of 39.8 ppt that occur about 3 % of the time during the 1980- July 2000 record. The low- flow rate peak in the probability density distribution is centered on 37.0 ppt accounts for 42% of the outcomes, while the mid-flow rate peak centered on 34.8 ppt accounts for 58% of the modeled realizations. Comparing Figure 5.8 against Figure 5.7 it is interesting to note that the density stratification within the saline plume at a distance of 150 meters from the outfall is unstable, with higher salinities in the water column than on the sea floor. This indicates that subsidence is underway in the middle of the outer core, and that the mid-depth portion of the plume is in a state of overturning, thereby promoting vertical stirring and mixing. This effect is greatest for the low-flow rate portion of the probability distribution for which salinities are highest and the subsidence rates are greatest.

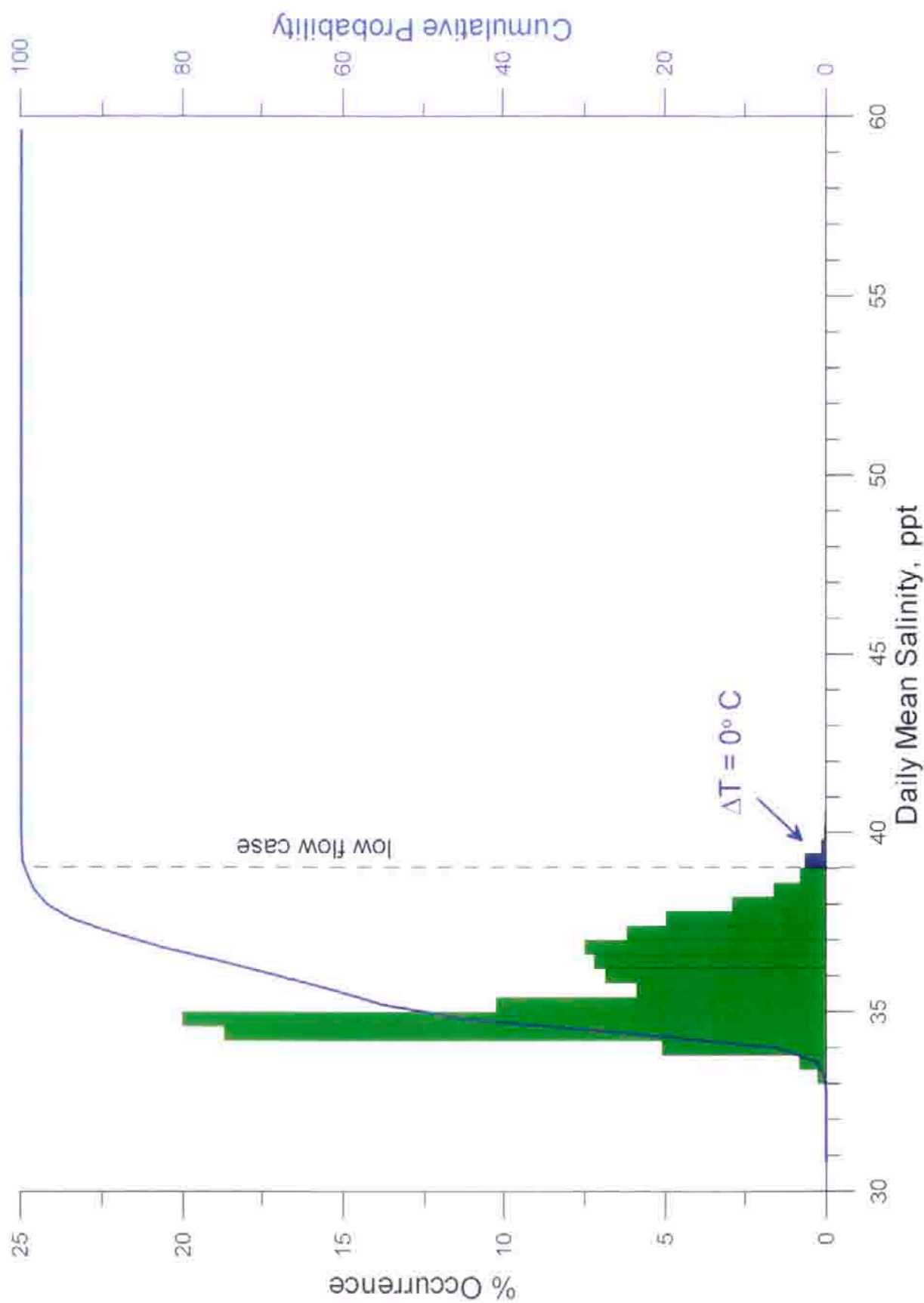


Figure 5.8. Histogram of daily maximum salinity at the bottom and 150 meters from the AES outfall for desalination production rate of 50 mgd. Percent occurrence based on historic observations of ocean mixing and water mass mass properties, and AES daily plant flow rates, 1980-2000.

E) Saline Anomalies 300 meters from the Outfall

At this distance from the out fall we are now at the outer edge of the outer core of the plume. The subsidence effects from the inverted salinity distribution in the outer core have now accelerated the mixing, particularly of the heavier low-flow rate salinity peak where salinities are highest, and have nearly homogenized the vertical salinity contrasts of the plume. Inspection of the probability density functions (histograms) of both the daily maximum salinities in the water column (Figure 5.9) and on the sea floor (Figure 5.10) show that low-flow rate peak has merged with the mid-flow rate peak, forming an asymmetric uni-modal distribution with a shoulder on the on the high-salinity side of the distribution. Furthermore, both water column and sea floor distribution are very similar with only minor differences on a bin-by-bin comparison, indicating that the inverted salinity distribution that was characteristic of the plume closer to the outfall has been smeared nearly uniformly by mixing and subsidence. Since the bi-modal character of the histogram has been lost, we shall refer to its characteristics from here on as the *mid-flow rate peak and the low-flow rate shoulder*.

For the water column at 300 meters from the outfall (Figure 5.9) the median salinity is 34.6 ppt while the highest salinity for warm water discharges reaches 39 ppt, commensurate with the low flow case scenario results in Section 4. Cold water discharges increase the extreme water column salinity to 40.2 ppt. These cold water exceedence outcomes account for only 2% of the 7,523 number of realizations. The mid-flow rate peak of the distribution appears to be centered on 34.6 ppt and account for about 60% of the outcomes. Half of the outcomes in the low-flow rate shoulder are found either side of 36.2 ppt and altogether account for

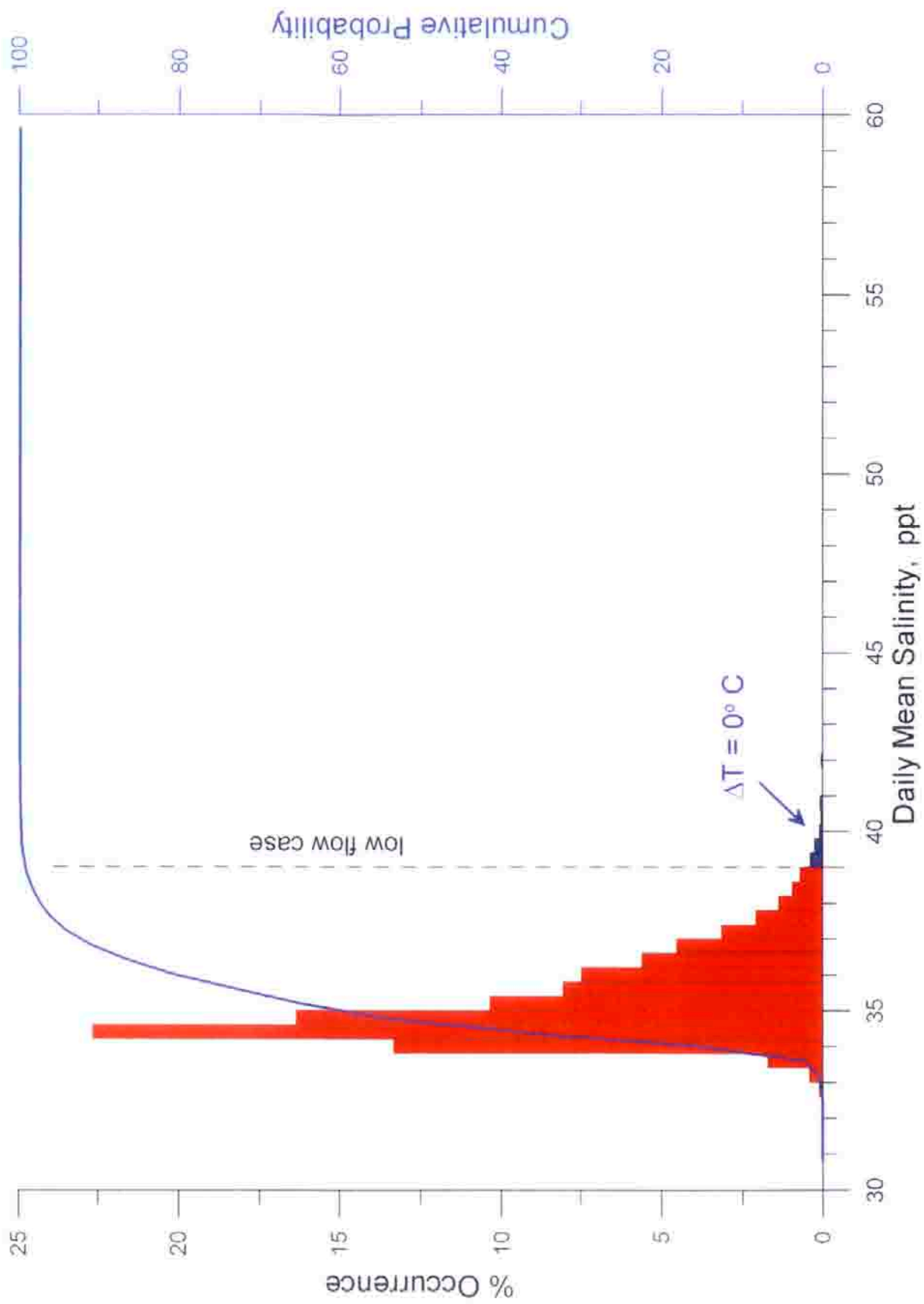


Figure 5.9. Histogram of daily maximum salinity at mid-depth and 300 meters from the AES outfall for desalination production rate of 50 mgd. Percent occurrence based on historic observations of ocean mixing and water mass mass properties, and AES daily plant flow rates, 1980-2000.

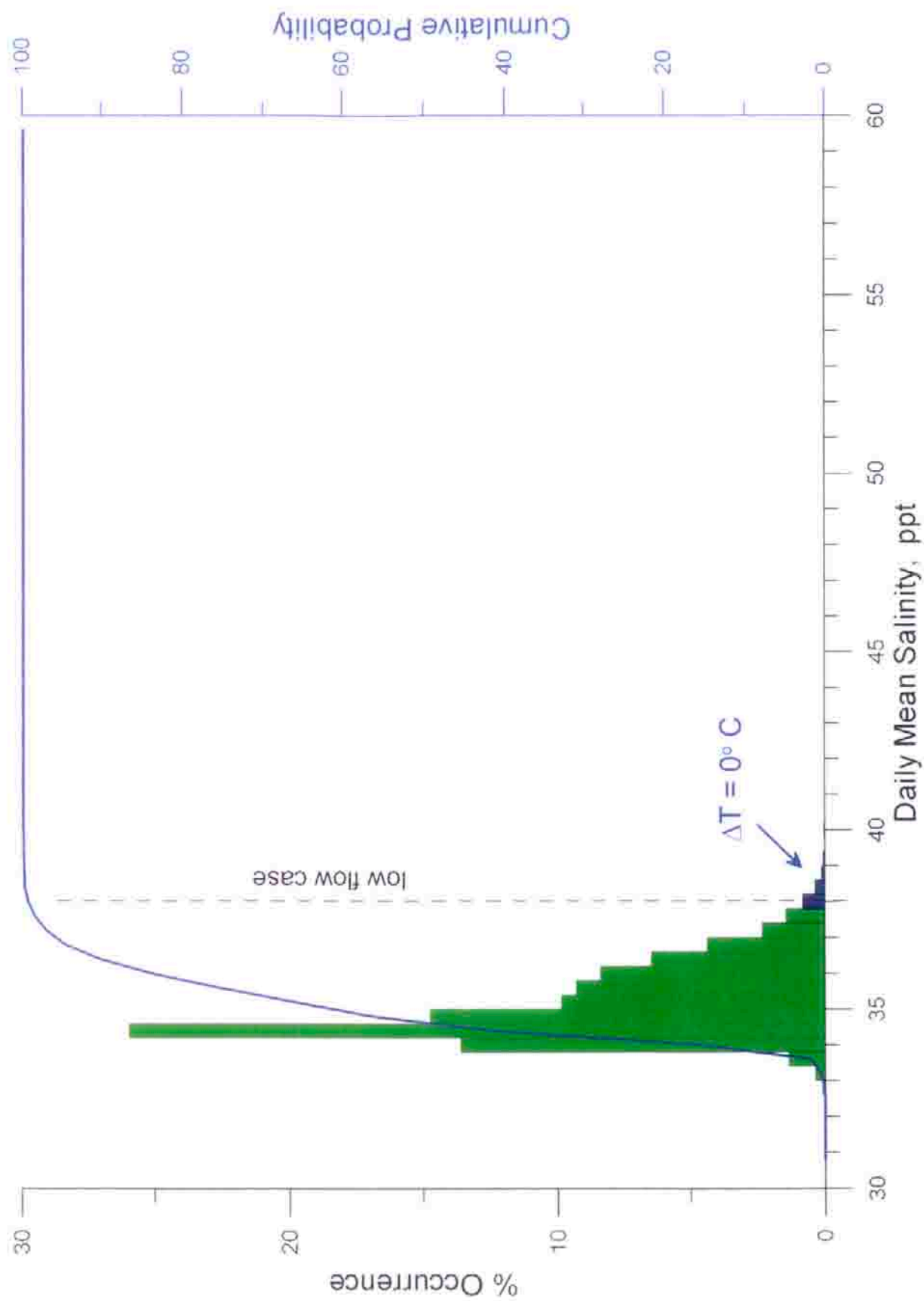


Figure 5.10. Histogram of daily maximum salinity at the bottom and 300 meters from the AES outfall for desalination production rate of 50 mgd. Percent occurrence based on historic observations of ocean mixing and water mass properties, and AES daily plant flow rates, 1980-2000.

40 % of the modeled realizations. For the sea floor salinities in Figure 5.10, the median salinity is also 34.6 ppt; the highest salinity for warm water discharges reaches 38.8 ppt; and cold water discharges reach a high of 40 ppt and exceed the warm water values about 3 % of the time. The mid-flow rate peak of the distribution also appears to be centered on 34.6 ppt accounting for about 60% of the outcomes. Half of the outcomes in the low-flow rate shoulder are found either side of 36.0 ppt and account for 40% of the realizations.

F) Saline Anomalies 500 meters from the Outfall

At 500 meters away from the outfall we are in the inner portions of the salt wedge region of the discharge plume. Here ambient ocean mixing by wind waves and currents takes over from discharge turbulence, entrainment and subsidence as the dominant dilution mechanisms. However, subsidence still continues throughout the salt wedge, but at slower rates as salinities come closer to ambient ocean water. The continuation of these subsidence effects causes the salt wedge to progressively become more stably stratified with increasing distance from the outfall. Comparison of the probability density functions (histograms) of the daily maximum salinities in the water column (Figure 5.11) versus those on the sea floor (Figure 5.12) show that the plume has become stably stratified on the low-flow rate shoulder of the distribution, with more outcomes of higher salinities occurring on the sea floor than in the water column. The other notable feature of these histograms, is that the uni-modal probability density distribution has become more narrow and shifted closer to the ambient ocean water distribution in Figure 3.21b. These traits become more pronounced at greater and greater distances from the outfall as will be shown in following sections. What they indicate is that

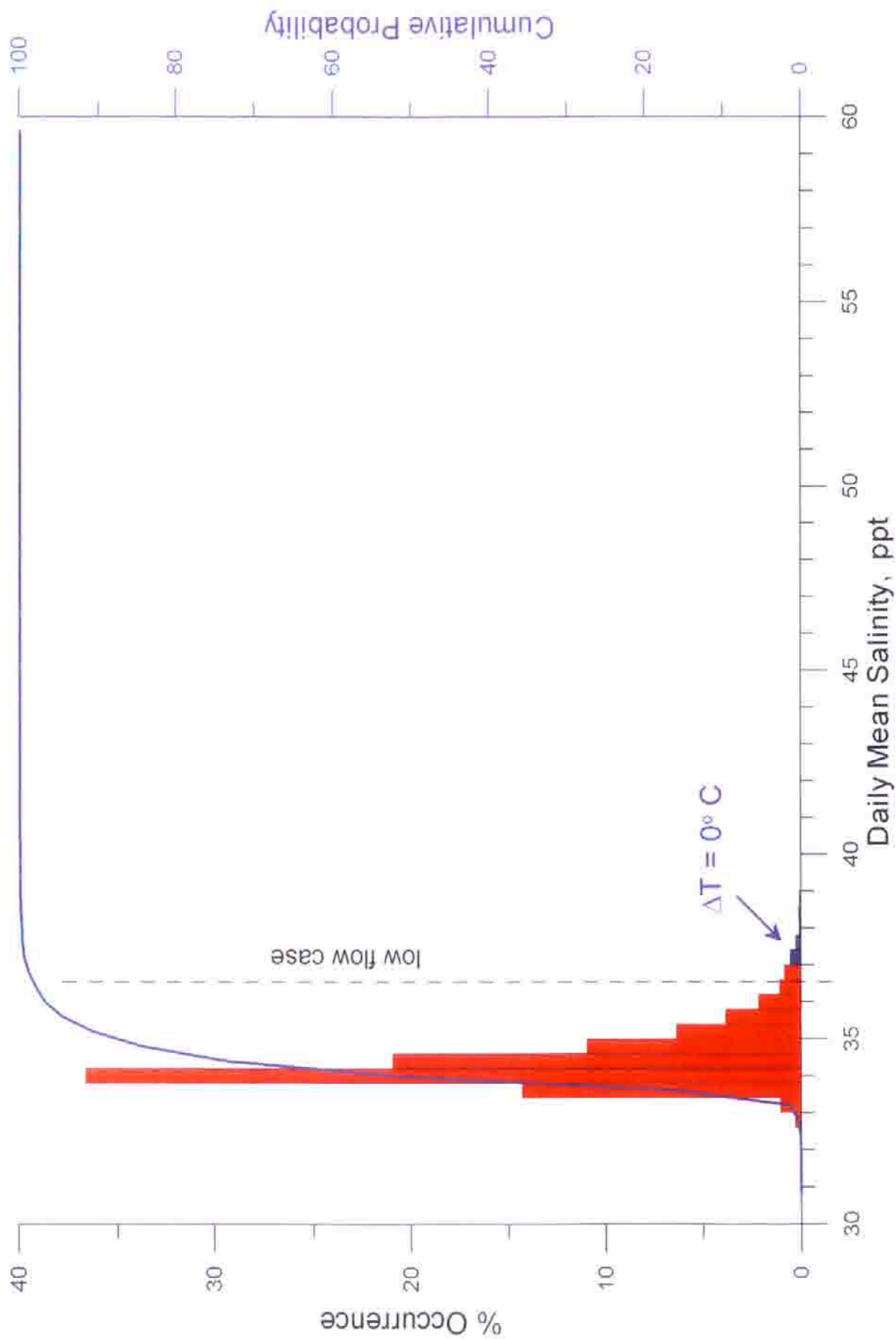


Figure 5.11. Histogram of daily maximum salinity at mid-depth and 500 meters from the AES outfall for desalination production rate of 50 mgd. Percent occurrence based on historic observations of ocean mixing and water mass mass properties, and AES daily plant flow rates, 1980-2000.

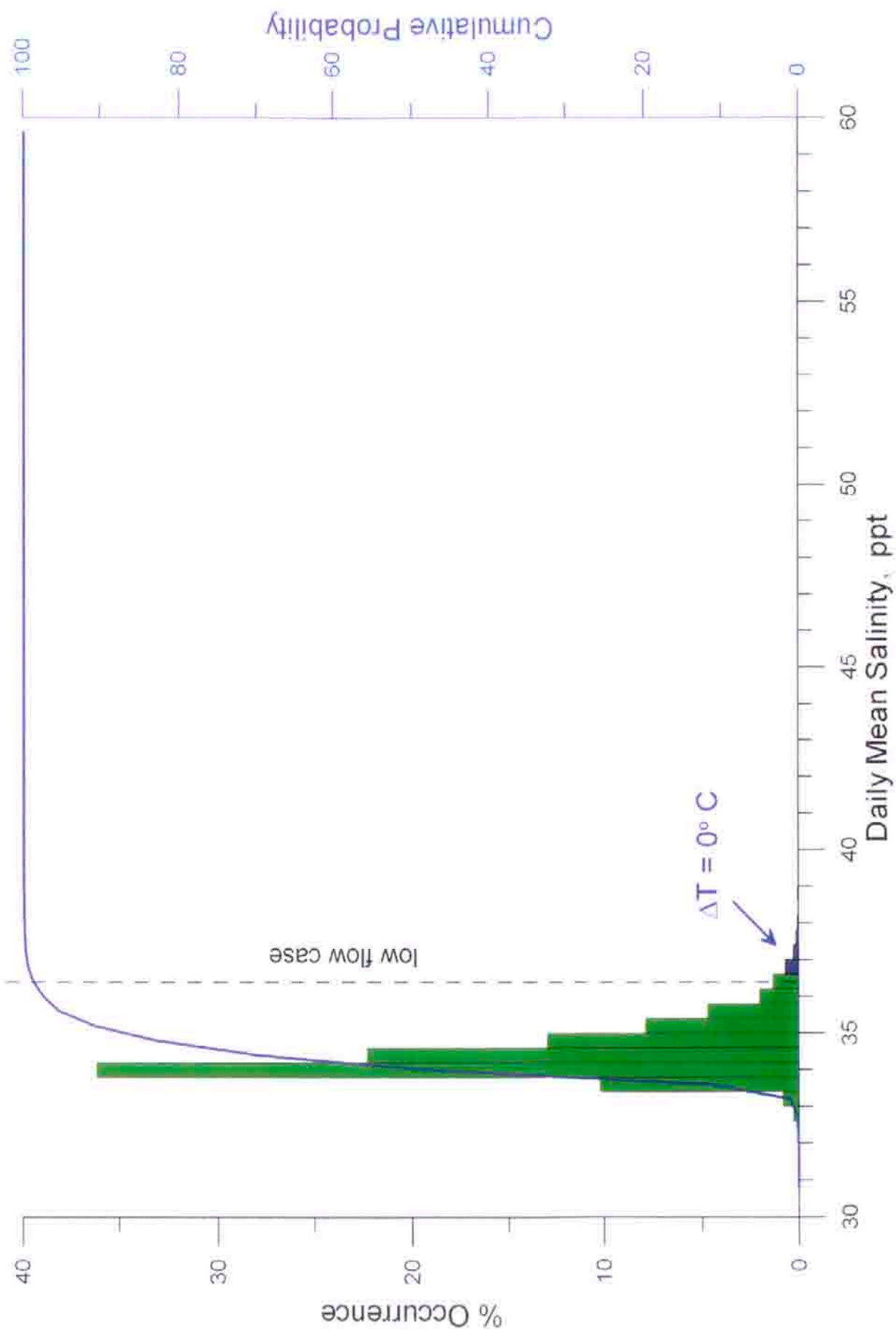


Figure 5.12. Histogram of daily maximum salinity at the bottom and 500 meters from the AES outfall for desalination production rate of 50 mgd. Percent occurrence based on historic observations of ocean mixing and water mass mass properties, and AES daily plant flow rates, 1980-2000.

differences in the salinity plume caused by different plant operating levels became less and less important in the salt wedge portion of the plume, as ambient ocean mixing dilutes the plume closer and closer to ambient ocean salinity.

At 500 meters from the outfall (Figure 11) the median water column salinity is 34.0 ppt while the highest salinity for warm water discharges reaches 36.6 ppt, consistent with results reported for the low flow case scenario results of Section 4. Cold water discharges increase the extreme water column salinity to 36.8 ppt. These cold water outcomes account for only 3% of the total number of realizations. The mid-flow rate peak of the distribution appears to be centered on 34.0 ppt and accounts for about 75% of the outcomes. Half of the outcomes in the low-flow rate shoulder are found either side of 35.0 ppt and altogether account for 25% of the modeled results. For the sea floor results in Figure 5.12, the median salinity is also 34.0 ppt; the highest salinity for warm water discharges reaches 36.2 ppt; and cold water discharges reach a high of 38.2 ppt. The number of cold water outcomes that exceed the highest warm water discharge occur about 4 % of the time. The mid-flow rate peak of the distribution also appears to be centered on 34.0 ppt accounting for about 70 % of the outcomes. Half of the outcomes in the low-flow rate shoulder are found either side of 35.2 ppt and account for 30% of the realizations.

G) Saline Anomalies 1000 meters from the Outfall

At 1,000 meters from the outfall, maximum daily salinities are always found in the long shore cross section of the salt wedge portion of the discharge plume (see Figure 4.13). Inspection of the probability density functions (histograms) of the daily maximum salinities in the water column (Figure 5.13) and on the sea floor

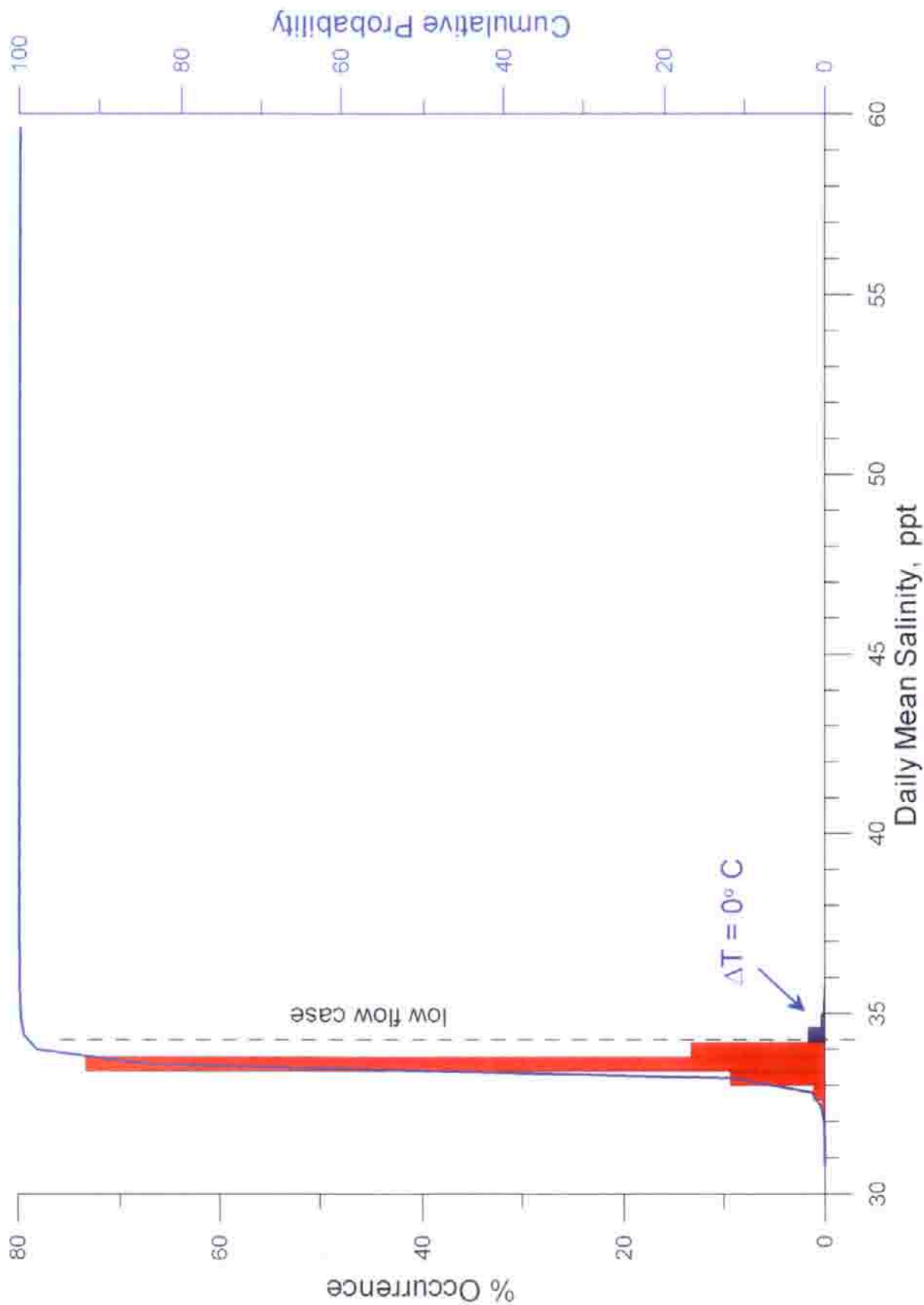


Figure 5.13. Histogram of daily maximum salinity at mid-depth and 1000 meters from the AES outfall for desalination production rate of 50 mgd. Percent occurrence based on historic observations of ocean mixing and water mass mass properties, and AES daily plant flow rates, 1980-2000.

(Figure 5.14) show that the uni-modal probability density distribution has become exceedingly narrow banded to the point that the low-flow rate shoulder is hardly recognizable. Both water column and sea floor distributions are very close to the ambient ocean water distribution in Figure 3.21b, indicating that dilution is nearly total (but not quite complete). In Figure 5.13, the median water column salinity is 33.6 ppt while the highest salinity for warm water discharges reaches 34.2 ppt, slightly less than results reported for the low flow case scenario results of Section 4. Cold water discharges increase the extreme water column salinity to 35.0 ppt. These cold water outcomes account for only 2% of the total number of realizations. The mid-flow rate peak of the distribution appears to be centered on 33.6 ppt and accounts for about 8% of the outcomes. Half of the outcomes in the low-flow rate shoulder are found either side of 34.0 ppt and altogether account for 18% of the model realizations. For the sea floor results in Figure 5.14, the median salinity is also 33.6 ppt; the highest salinity for warm water discharges reaches 34.6 ppt; and cold water discharges reach a high of 35.4 ppt. The number of cold water outcomes that exceed the highest warm water discharge occur about 1.5 % of the time. The mid-flow rate peak of the distribution also appears to be centered on 33.6 ppt accounting for about 82% of the outcomes. Half of the outcomes in the low-flow rate shoulder are found either side of 34.2 ppt and account for 18% of the realizations.

H) Saline Anomalies 2,000 meters from the Outfall

At 2,000 meters from the outfall, the discharge plume can be hardly distinguished from ambient ocean water, and dilution may be considered for all practical purposes, complete. Comparison of the probability density functions

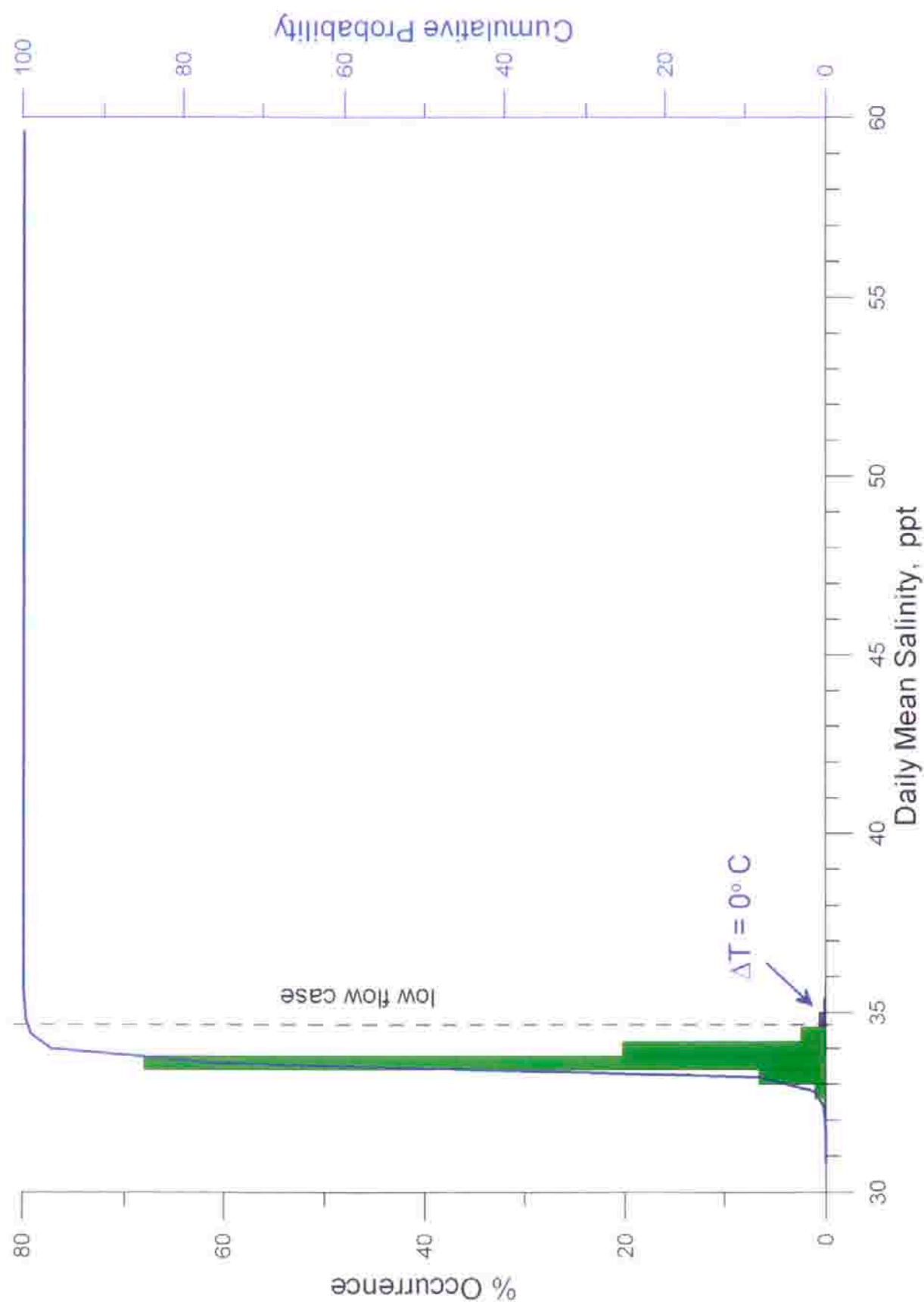


Figure 5.14. Histogram of daily maximum salinity at the bottom and 1000 meters from the AES outfall for desalination production rate of 50 mgd. Percent occurrence based on historic observations of ocean mixing and water mass mass properties, and AES daily plant flow rates, 1980-2000.

(histograms) of the daily maximum salinities in the water column (Figure 5.15) and on the sea floor (Figure 5.16) versus the ambient ocean water distribution in Figure 3.21b shows virtually no difference other than for a an enhancement of about 1.5% of the salinity bin centered on 34 ppt, largely the result of cold water discharge effects. Statistics for the water column and sea floor distributions are identical and essentially the same as ambient ocean water: median water column salinity is 33.5 ppt; maximum salinity is 34.3 ppt; minimum salinity is 31.1 ppt. The only change in the discharge plume 2,000 meters from the outfall is that salinities between 34.0 ppt and 34.3 ppt happen 2% of the time in the plume versus 0.3% of the time in ambient ocean water.

I) Summary of Long-Term Dilution Analysis:

An intensive set of hydrodynamic model runs produced 7,523 outcomes for the dispersion of the saline plume discharged from the AES Huntinton Beach outfall, as a result of piggy-backing a 50 mgd desalination plant on the back end of the generating station cooling loop. The modeled outcomes were the result of 20.5 year long continuous time series of daily records for seven controlling operational and environmental inputs. The period of record for these simultaneous sets of seven inputs was 1980 to July 2000. We were constrained to this particular historic period based on the availability of wave monitoring data. However, this period was probably atypical from the operational stand point because the generating station was under going re-fit and equipment modernization. These capital improvements limited plant production to either one or two generating units for much of the time, providing only 126.7 mgd or 253.4 mgd with which to

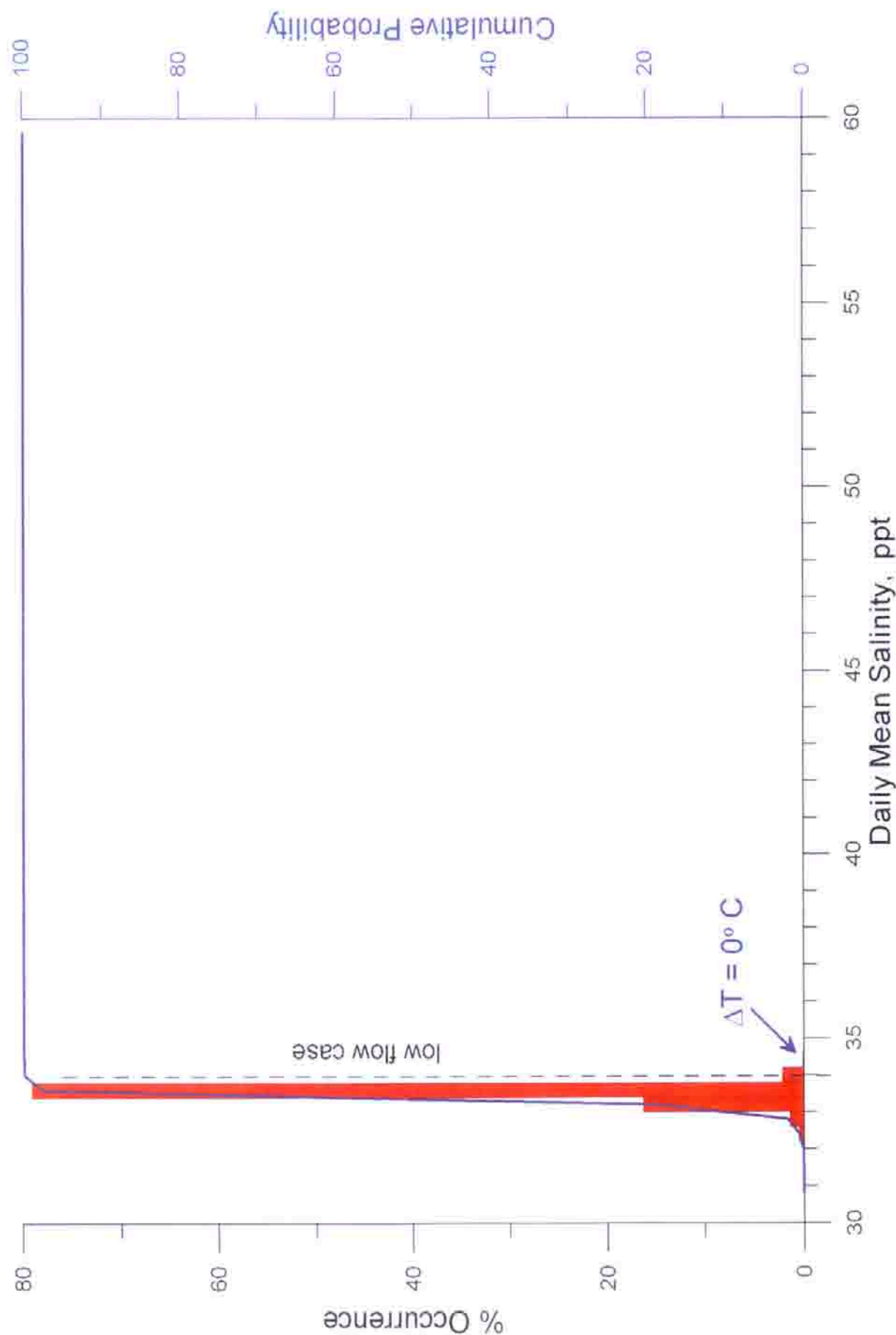


Figure 5.15. Histogram of daily maximum salinity at mid-depth and 2000 meters from the AES outfall for desalination production rate of 50 mgd. Percent occurrence based on historic observations of ocean mixing and water mass mass properties, and AES daily plant flow rates, 1980-2000.

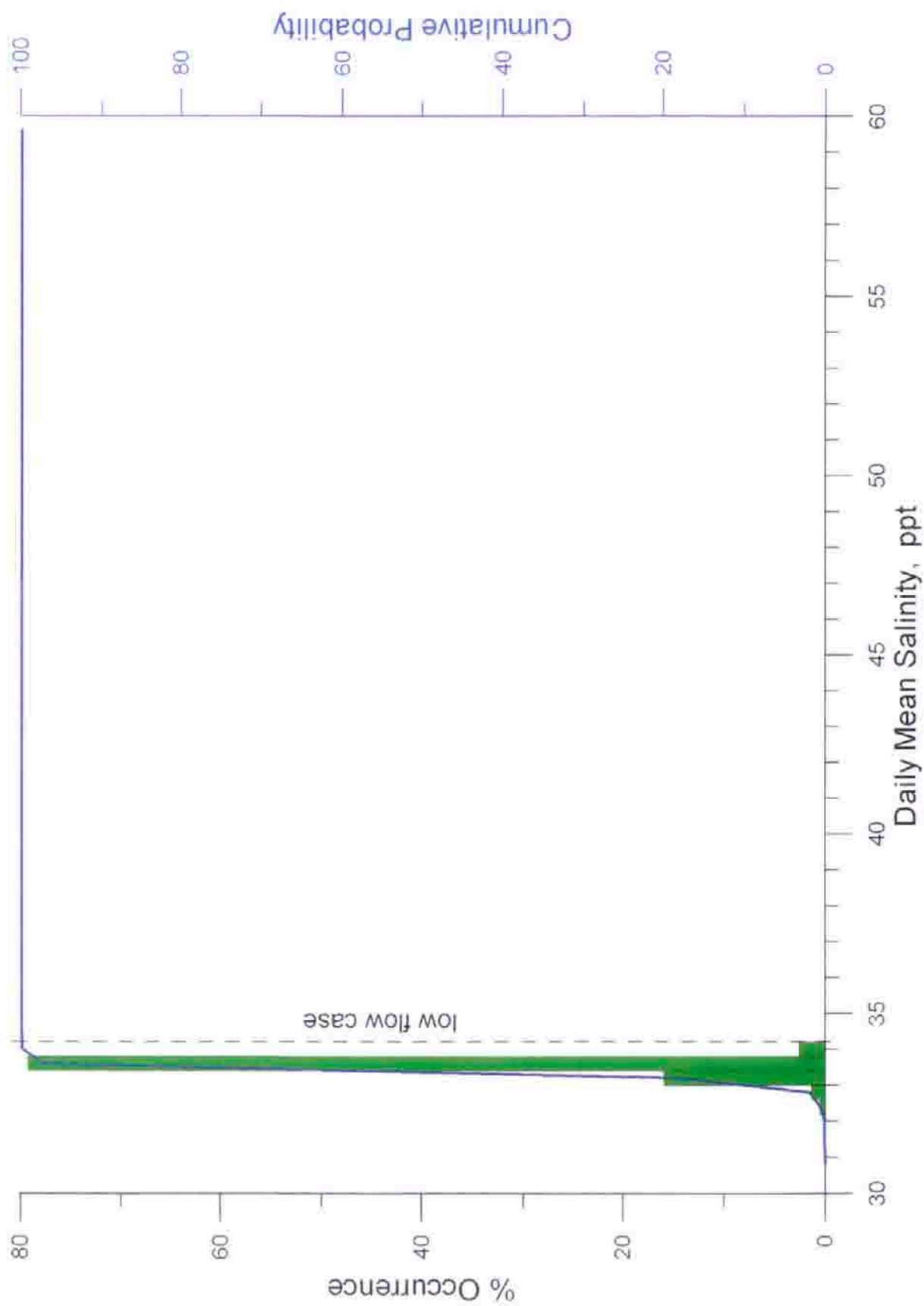


Figure 5.16. Histogram of daily maximum salinity at the bottom and 2000 meters from the AES outfall for desalination production rate of 50 mgd. Percent occurrence based on historic observations of ocean mixing and water mass mass properties, and AES daily plant flow rates, 1980-2000.

dilute the 50 mgd of concentrated sea water from the desalination plant. This historic 2 mode operational pattern introduced a bimodal statistical pattern into the model results of this study and a probable bias for persistence of low plant flow rate conditions.

The results of this study are summarized in Table 7. Entries are given for the characteristic daily maximum salinities that can be expected for various distances away from the out fall extending as far as 2,000 meters (1.2 miles). Characteristic salinities were identified in the peaks of the probability density distributions (histograms); and two well defined peaks were identified with the two predominant operational modes of the generating station giving a bi-modal distribution. Outcomes for those peaks in the bi-modal probability density distribution are indicated in red in Table 7. One peak (low-flow rate peak) was attributed to the operation of only one generating unit, and give the highest salinities in the discharge plume. These are listed in the second and third columns of Table 7. The third and fourth columns of Table 7 give the outcomes for the other peak in the probability density distribution (mid-flow rate peak) resulting from operation of two generating units. The salinities of the low-flow rate peak start out at 55 ppt in the water column above the outfall and fall off to 39 ppt at 150 meters away, accounting for between 42% and 48% of the modeled outcomes. On the sea floor, the low-flow rate operational condition (one generating unit) produces salinities that typically range from 47.5 ppt at the foot of the outfall to 37.0 ppt at 150 meters from the outfall with the same recurrence rates as found in the water column. During times when two generating units(or more) were operated (mid-flow rate peak), salinities varied in the water column from 41.6 ppt at the outfall to 35.2 ppt at 150 meters away with a recurrence rate of 52% to 58%.

Table 7. Generalized Salinity Plume from 7,523 outcomes, 1980- July 2000

Distance from Outfall (m)	One Generating Unit ^a		Two Generating Units	
	Characteristic Salinity (ppt)	Recurrence Rate (%)	Characteristic Salinity (ppt)	Recurrence Rate (%)
0 Mid-depth	55.2	48%	41.6	52%
0 Bottom	47.5	48%	38.6	52%
50 Mid-depth	45.4	48%	37.4	52%
50 Bottom	40.0	48%	36.0	52%
100 Mid-depth	43.0	47%	36.6	53%
100 Bottom	37.8	43%	35.0	57%
150 Mid-depth	39.0	42%	35.2	58%
150 Bottom	37.0	42%	34.8	58%
300 Mid-depth	36.2	40%	34.6	60%
300 Bottom	36.0	40%	34.6	60%
500 Mid-depth	35.0	25%	34.0	75%
500 Bottom	35.2	30%	34.4	70%
1000 Mid-depth	34.0	18%	33.6	82%
1000 Bottom	34.2	18%	33.6	82%
2000 Mid-depth	33.5	100%	33.5	100%
2000 Bottom	33.5	100%	33.5	100%

^a includes cold water discharges, $\Delta T = 0^{\circ}\text{C}$

^b red indicates values associated with bimodal probability density distributions

^c green indicates values associated with uni-modal probability density distributions

On the sea floor, 2 generating unit operation (mid-flow rates) causes salinity to range from 38.6 ppt at the foot of the outfall to 34.8 ppt at 150 meters away with the same recurrence rate as for the water column.

Beyond 150 meters from the outfall, the probability density distribution for the discharge plume salinities no longer exhibits bi-modal character. Because the salinity contrast with the ambient water is greater for the low-flow rate peak, it becomes smeared by higher mixing rates promoted along stronger concentration gradients and it merges with the mid-flow rate peak in the distribution to form an asymmetric uni-modal distribution. The characteristics of this distribution are mid-flow rate peak at lower salinities with a low-flow rate shoulder extending into higher salinity ranges. The outcomes that exhibit this uni-model probability density distribution are listed in green in Table 2. Salinities in the mid-flow rate peak of this distribution range from 34.6 ppt at 300 meters from the outfall and decay down to ambient ocean salinity at 2,000 meters from the outfall with a recurrence rate of 60% to 82% before reaching ambient ocean salinity levels. Salinities are only a fraction of a ppt greater on the bottom than in the water column over this range. For the low flow rate shoulder of the probability density distribution, salinities vary from 36.2 ppt 300 meters from the outfall to ambient salinity 2000 meters away, with recurrence rate of 40% down to 18% before reaching ambient ocean salinity levels.

The bi-modal statistical bias imprinted on the model results by the historical plant flow rates throughout the re-fitting period appears to exhibit itself only in the nearfield of the outfall. The recurrence pattern of two distinct outcomes of approximately equal likelihood, one of high salinity and the other of more moderate salinity, is only apparent in the inner and outer core of the discharge plume,

extending out to about 150 meters from the out fall. This is an area of about 17.5 acres. In the salt wedge portion of the plume from 500 meters out and beyond, operational patterns do not appear to alter the results by more than about 1 ppt, with salinities occurring between 34 ppt and 35 ppt or less regardless of historic operational tendencies. In the intermediate zone between 150 and 500 meters from the outfall, there is some residual effect of operational pattern. Here operational patterns can mean the difference between 36 ppt or about 34.5 ppt, that is the difference between exceeding the upper limit of the natural ocean salinity range for this region or not. In spite of the historical patterns there were no outcomes involving generation of electrical power that resulted in discharge salinities exceeding those of the Section 4 low flow case scenario. Only for the particular non-generating scenario of "Zero Delt-T" ($\Delta T = 0\text{ }^{\circ}\text{C}$) did higher salinities occur, and these exceeded the Section low flow case by no more than 1 ppt and accounted for only 1% to 6% of all possible outcomes.

Now that re-powering of the AES Huntington Beach generating station is complete, it is sensible to expect that it will be operated at higher production levels than those observed for the late 1980's and throughout the 90's. This is evident from the plant flow rate history for the post re-fit period, from 2002 to July of 2003 as shown in Figure 5.17. Average flow rates of the plant during this period was 265 mgd and the operational pattern involved a balanced proportion of all four generating units. This most recent plant flow rate average exceeds the average for the model simulation period when the plant operated close to the Section 4 low flow case conditions throughout the 1990's. Consequently the persistence analysis of Sections 5 A-H was likely biased towards a low- flow rate operational pattern that may not be representative of the future conditions in which

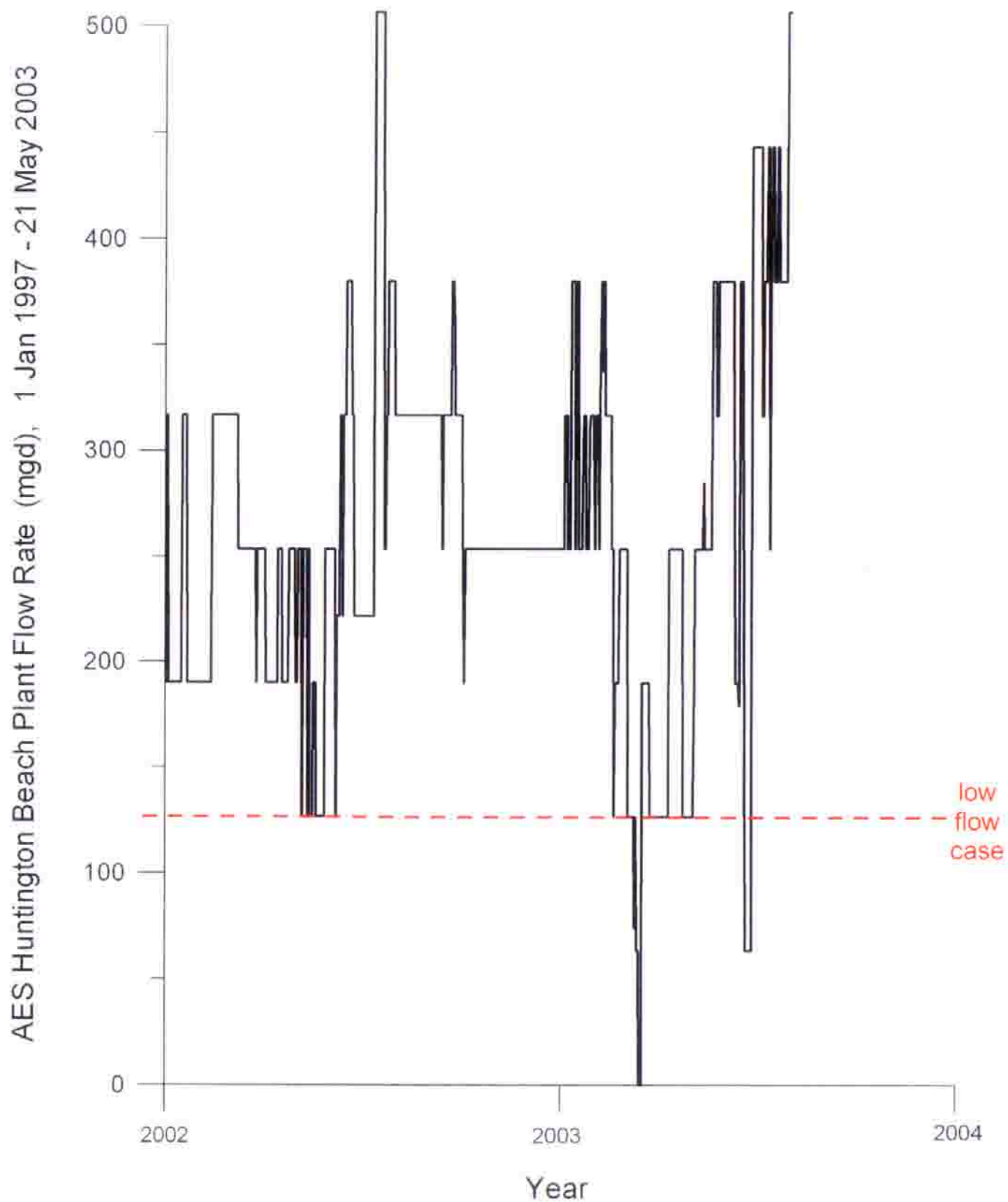


Figure 5.17. Most recent history of AES Power Plant flow rate 1 January 2002 - 30 July 2003 (19 Months). Value for "worst case" modeling scenario shown in red.

the desalination plant is built. This bias will tend to over-estimate the intensity and persistence of the saline anomalies induced by the desalination plant, but should also provide a more cautious assessment of potential saline impacts to the marine environment. To prove this hypothesis, we repeat the long-term analysis methodology on the 7 controlling variables for the post re-powering period, 2 January 2002 - 30 July 2003 as plotted in Figures 5.18 and 5.19. The results are summarized in Table 8 and the histogram solution set is presented in Figures 5.20 through 5.34. Inspection of the end-of pipe salinities in Figure 5.20 shows that the low flow rate peak at 55 ppt is greatly reduced and represents only about 5% of the 578 daily outcomes in the post re-powering period. Even within 50 meters of the outfall (Figures 5.21 and 5.22) the histogram distribution is predominantly unimodal and centered on 35 ppt with 92% of the outcomes giving salinities elevated less than the 10% above ambient. Beyond 150 meters away from the outfall, no outcomes from the 7 controlling variables during the post re-powering period give rise to salinities exceeding 40 ppt anywhere in the water column or along the seabed. Furthermore, no outcomes at any distance from the outfall during post re-powering conditions reach give salinities as high as the low flow case events evaluated in Section 4. Thus, the operation of a 50 mgd desalination plant at AES Huntington Beach is unlikely to ever match or exceed the low flow case outcomes during the foreseeable future.

Table 8. Generalized Salinity Plume from 578 outcomes, January 02- July 03

Distance from Outfall (m)	Low Flow Rate Condition ^a		Nominal Flow Rate Condition	
	Characteristic Salinity (ppt)	Recurrence Rate (%)	Characteristic Salinity (ppt)	Recurrence Rate (%)
0 Mid-depth	55.2	9%	43.0	91%
0 Bottom	47.5	9%	39.0	91%
50 Mid-depth	45.4	9%	38.0	91%
50 Bottom	40.0	9%	35.0	91%
100 Mid-depth	42.8	8%	37.4	92%
100 Bottom	37.8	6%	35.6	94%
150 Mid-depth	38.0	6%	35.4	94%
150 Bottom	37.2	6%	35.2	94%
300 Mid-depth	36.0	3%	34.6	97%
300 Bottom	36.0	3%	34.6	97%
500 Mid-depth	35.0	1%	34.0	99%
500 Bottom	35.2	1%	34.2	99%
1000 Mid-depth	33.6	100%	33.6	100%
1000 Bottom	33.8	100%	33.8	100%
2000 Mid-depth	33.5	100%	33.5	100%
2000 Bottom	33.5	100%	33.5	100%

^a includes all operating conditions pumping 126.7 mgd or less.

^b red indicates values associated with bimodal probability density distributions

^c green indicates values associated with uni-modal probability density distributions

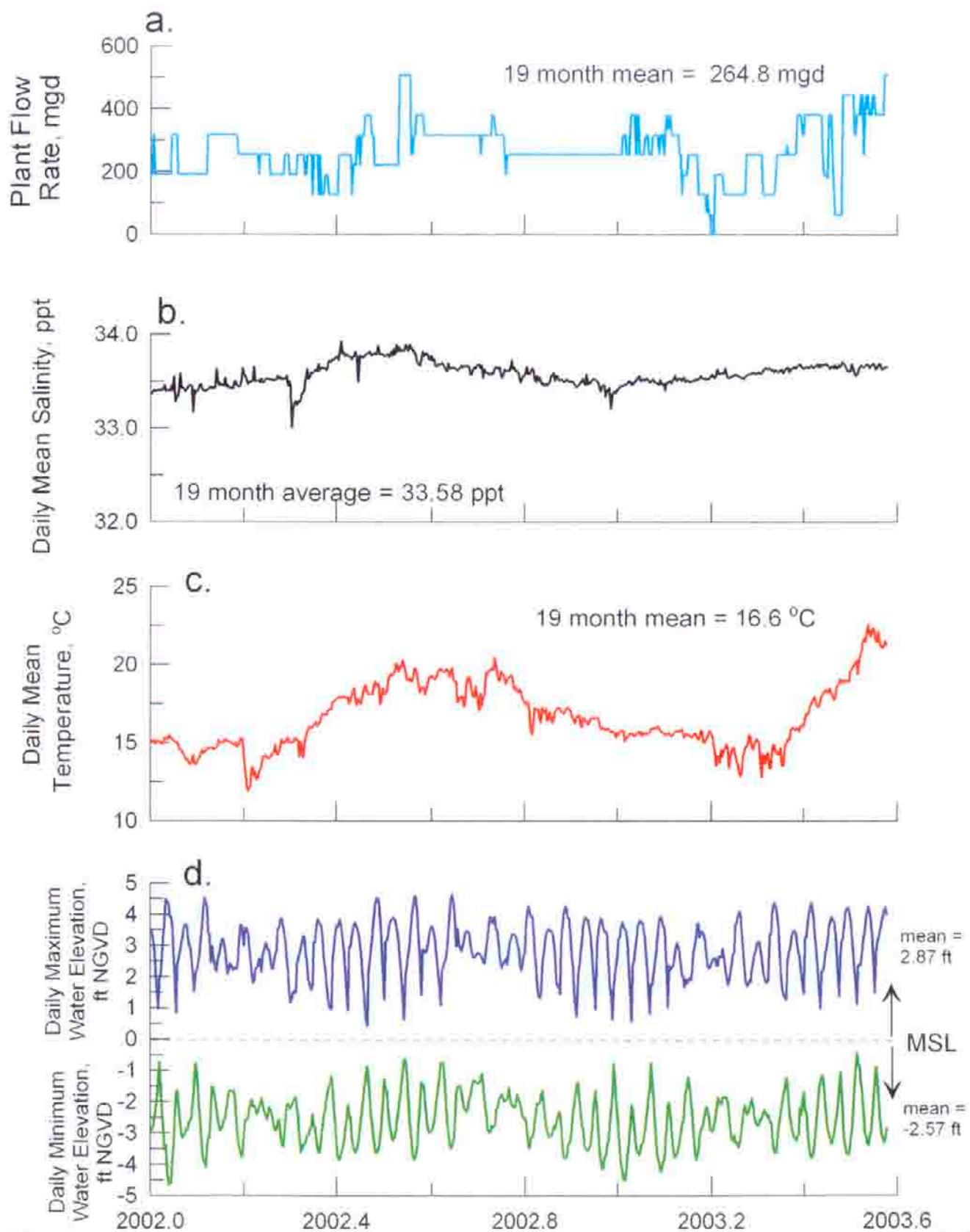


Figure 5.18. Controlling boundary condition variables for the post re-powering period of AES Huntington Beach, Jan 2, 2002 - July 30, 2003. a) plant flow rate b) daily mean salinity, c) daily mean temperature, and d) daily high and low water elevations. [data from MBC, 2002-03; CDIP, 2002-03; SIO, 2002-03]

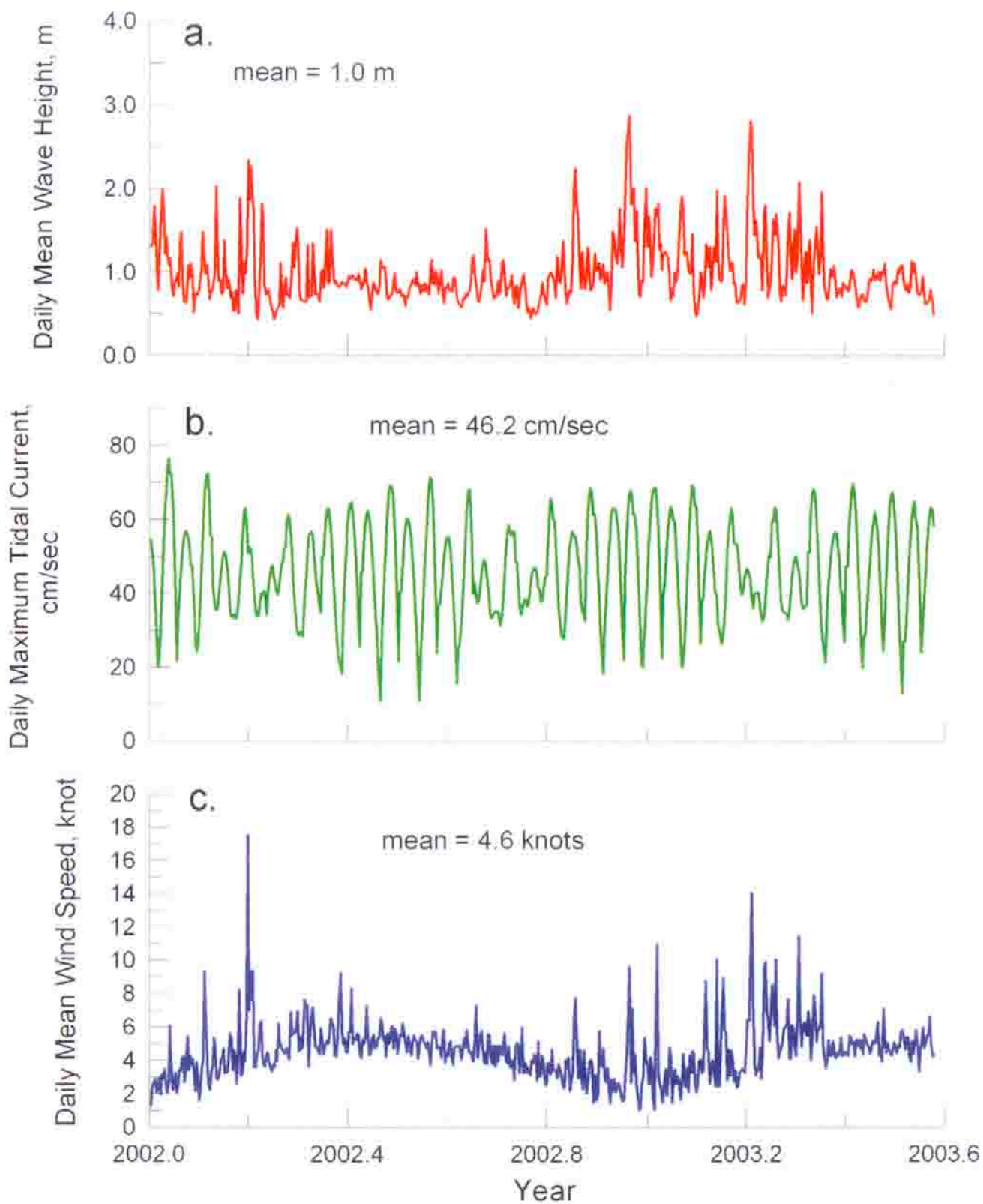


Figure 5.19. Controlling forcing function variables for the post re-powering period of AES Huntington Beach, Jan 1, 2002 - July 30, 2003. a) wave height; b) tidal currents; c) daily mean wind speed; [data from MBC, 2002-03; CDIP, 2002-03; UCAR, 2002-03]

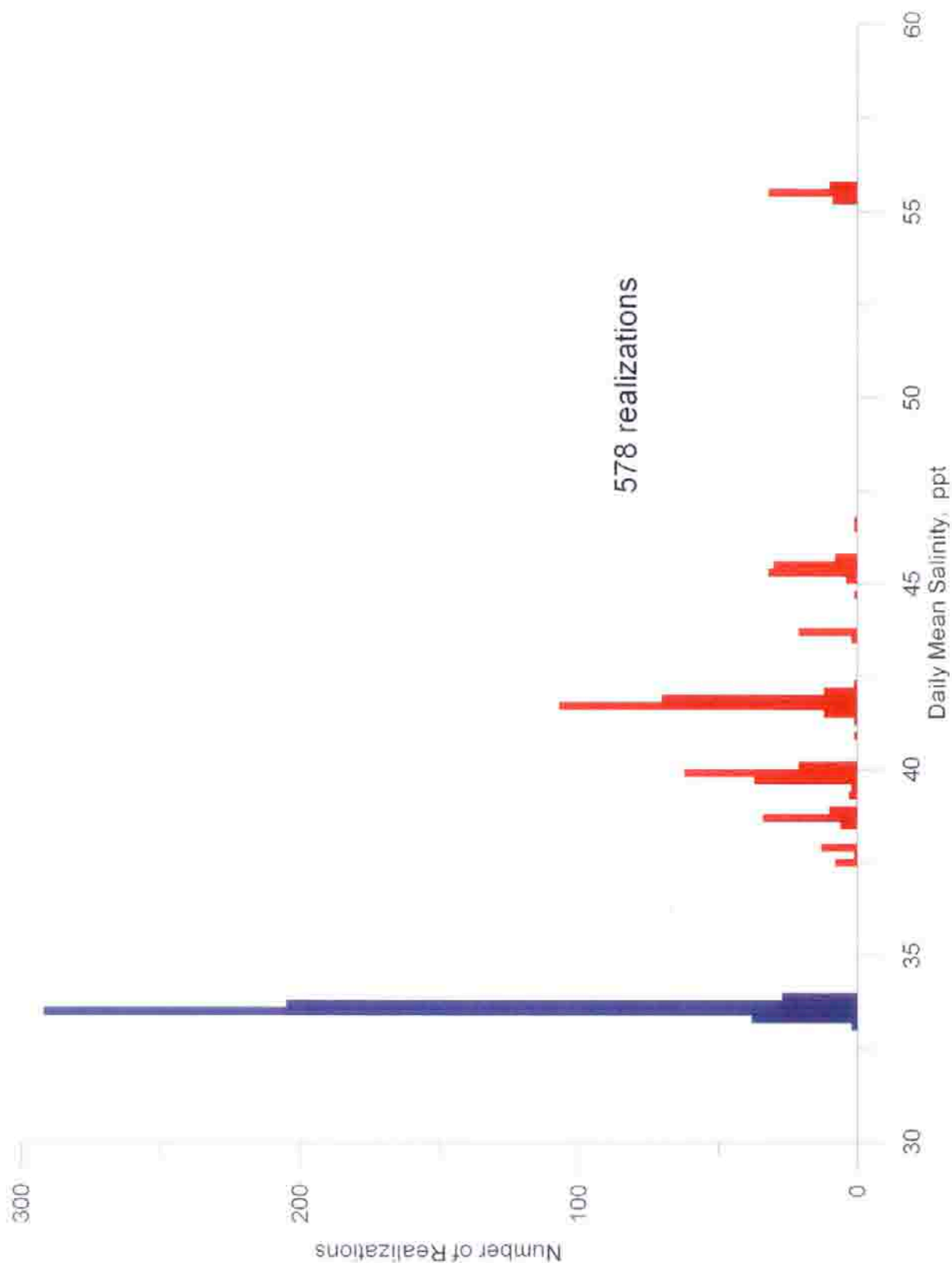


Figure 5.20. Histogram of daily mean salinity for the post re-powering period based on historic observations and AES daily plant flow rates, 1 Jan 2002-30 July 2003. Ocean salinity off Huntington Beach (blue) and end-of-pipe combined discharge salinity for desalination plant producing at 50 mgd (red).

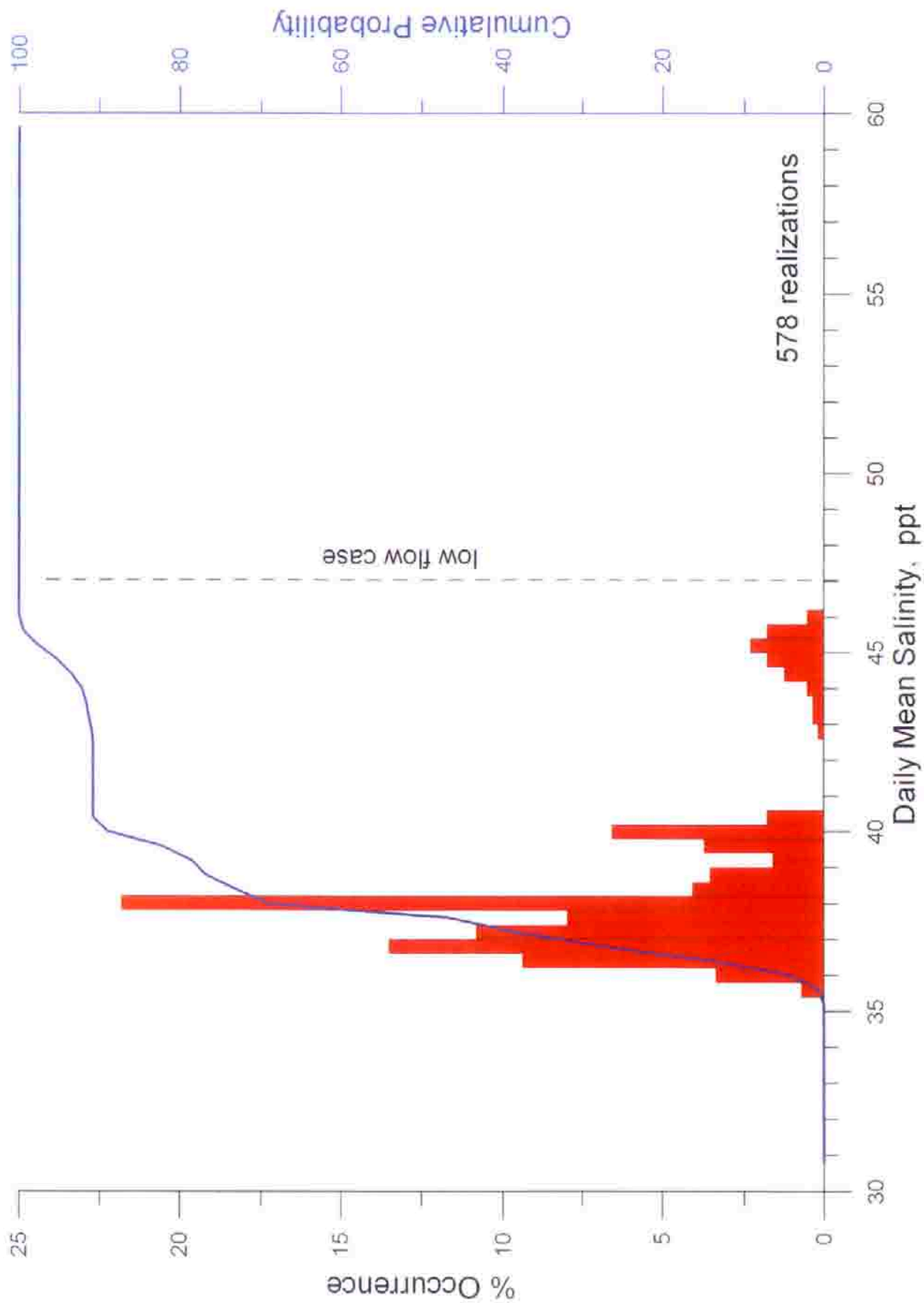


Figure 5.21. Histogram of daily maximum salinity at mid-depth and 50 meters from the AES outfall for desalination production rate of 50 mgd. Percent occurrence based on historic observations of ocean mixing and water mass mass properties, and AES daily plant flow rates for the post re-powering period, 1 Jan 2002 - 30 July 2003.

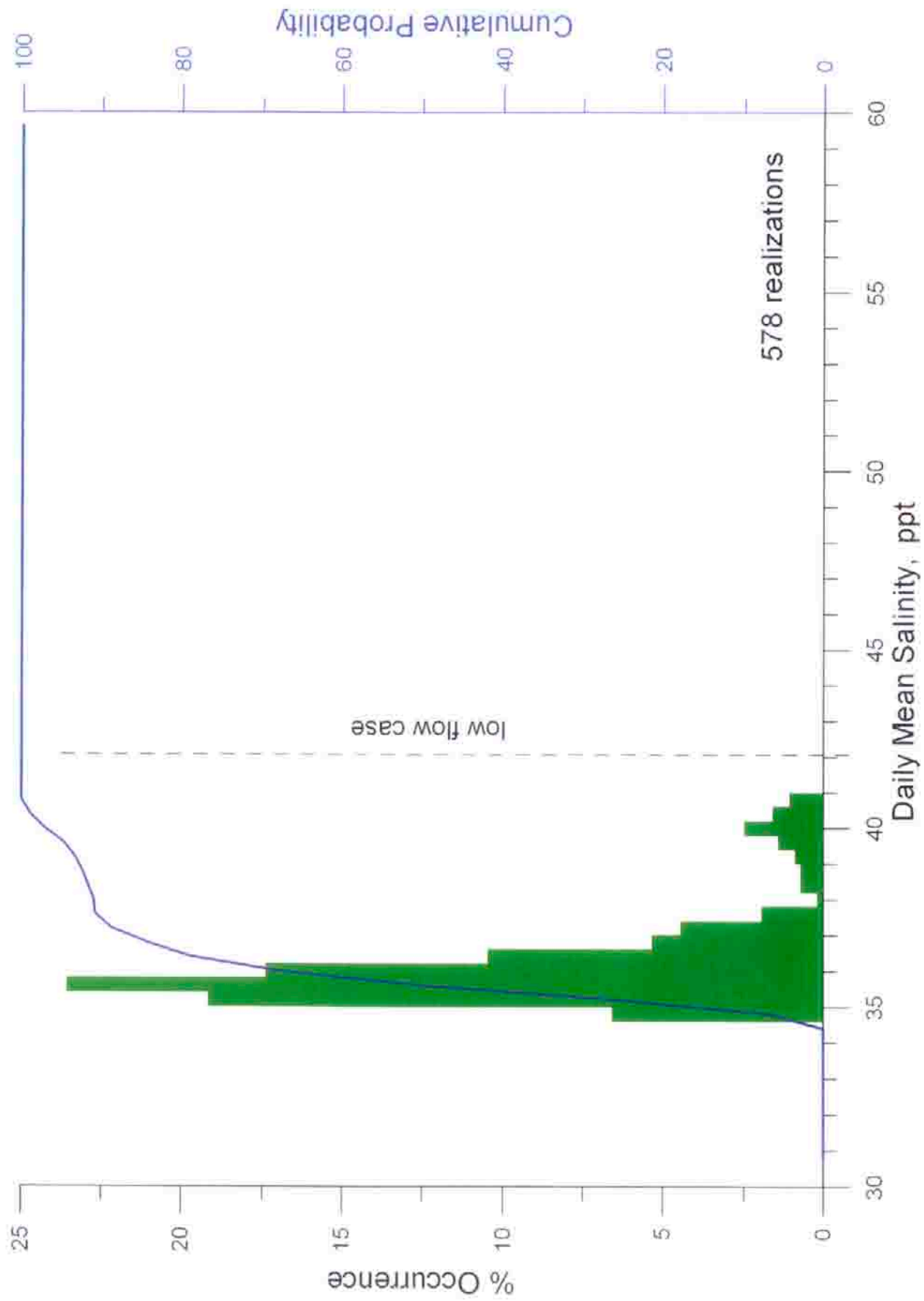


Figure 5.22. Histogram of daily maximum salinity at the bottom and 50 meters from the AES outfall for desalination production rate of 50 mgd. Percent occurrence based on historic observations of ocean mixing and water mass mass properties, and AES daily plant flow rates for the post re-powering period, 1 Jan 2002 - 30 July 2003.

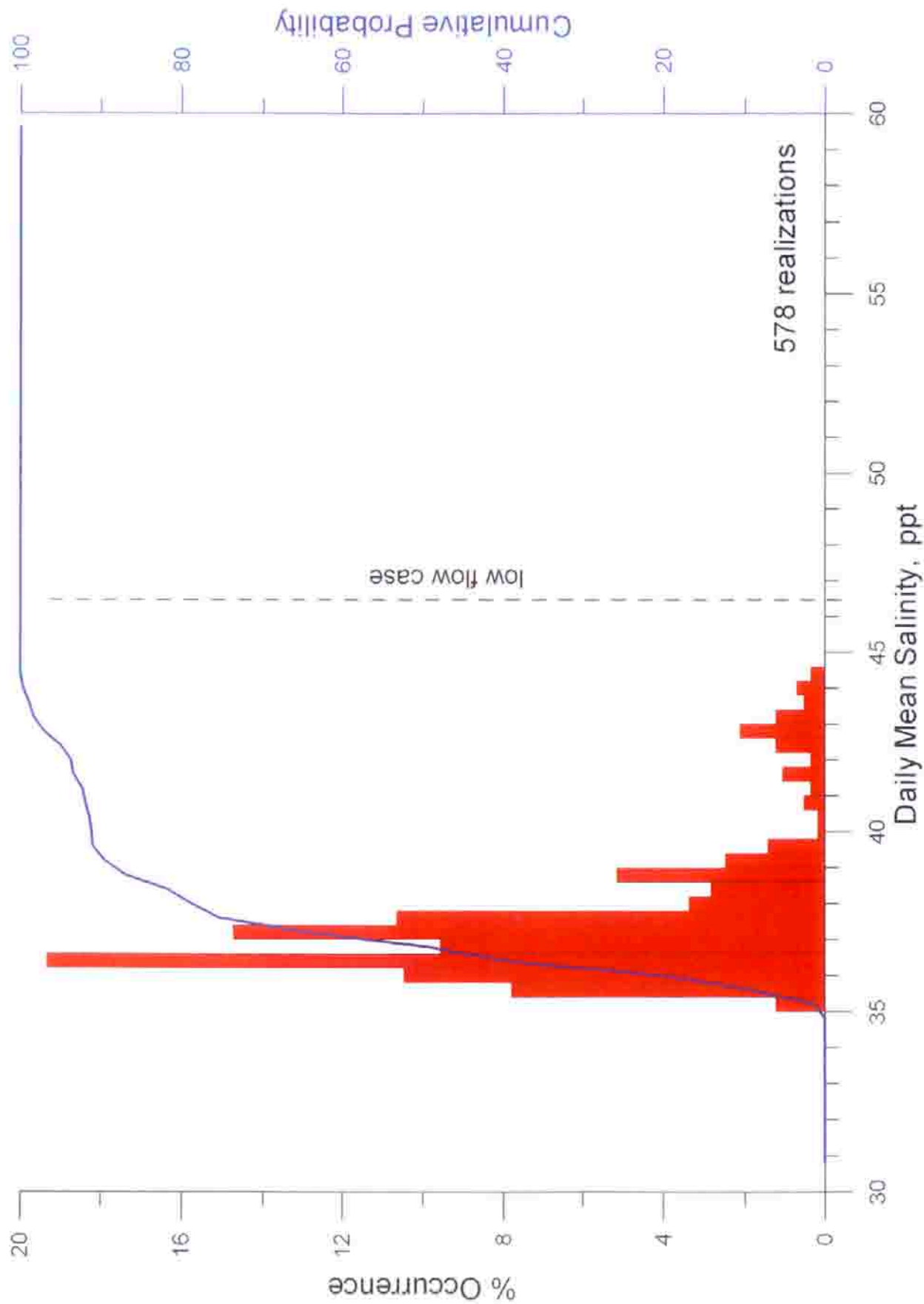


Figure 5.23. Histogram of daily maximum salinity at mid-depth and 100 meters from the AES outfall for desalination production rate of 50 mgd. Percent occurrence based on historic observations of ocean mixing and water mass properties, and AES daily plant flow rates for the post re-powering period, 1 Jan 2002 - 30 July 2003.

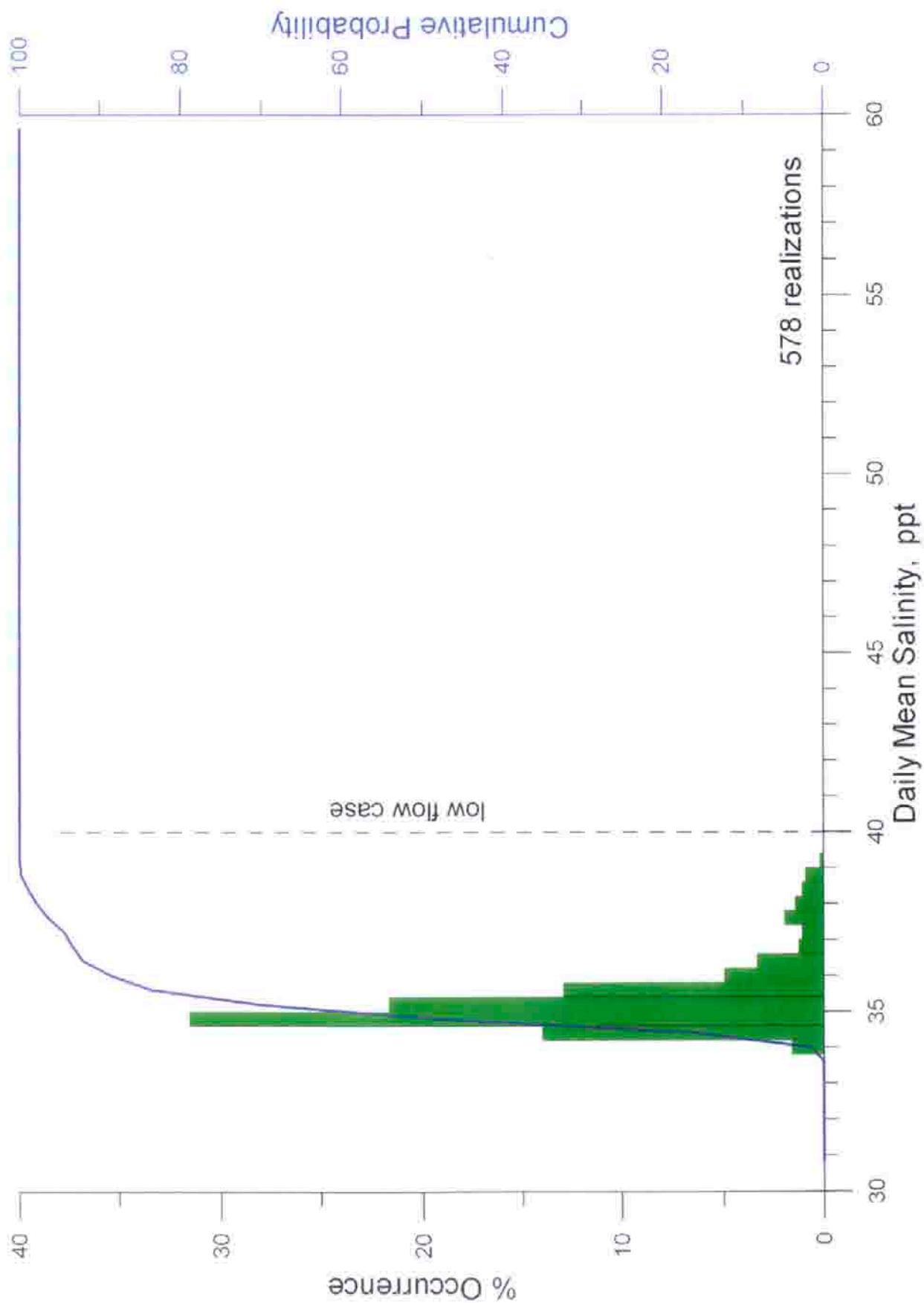


Figure 5.24. Histogram of daily maximum salinity at the bottom and 100 meters from the AES outfall for desalination production rate of 50 mgd. Percent occurrence based on historic observations of ocean mixing and water mass mass properties, and AES daily plant flow rates for the post re-powering period, 1 Jan 2002 - 30 July 2003.

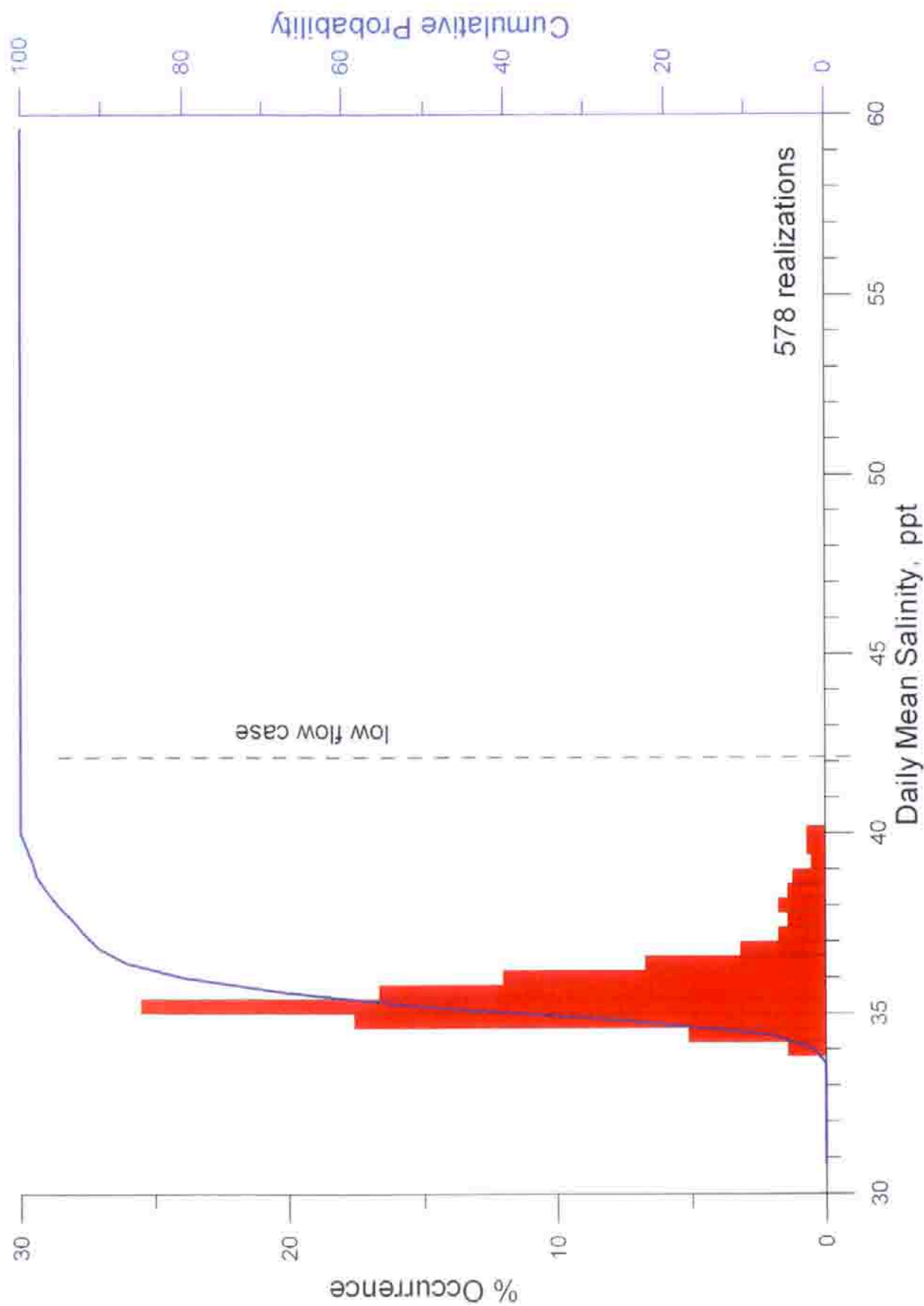


Figure 5.25. Histogram of daily maximum salinity at mid-depth and 150 meters from the AES outfall for desalination production rate of 50 mgd. Percent occurrence based on historic observations of ocean mixing and water mass properties, and AES daily plant flow rates for the post re-powering period, 1 Jan 2002 - 30 July 2003.

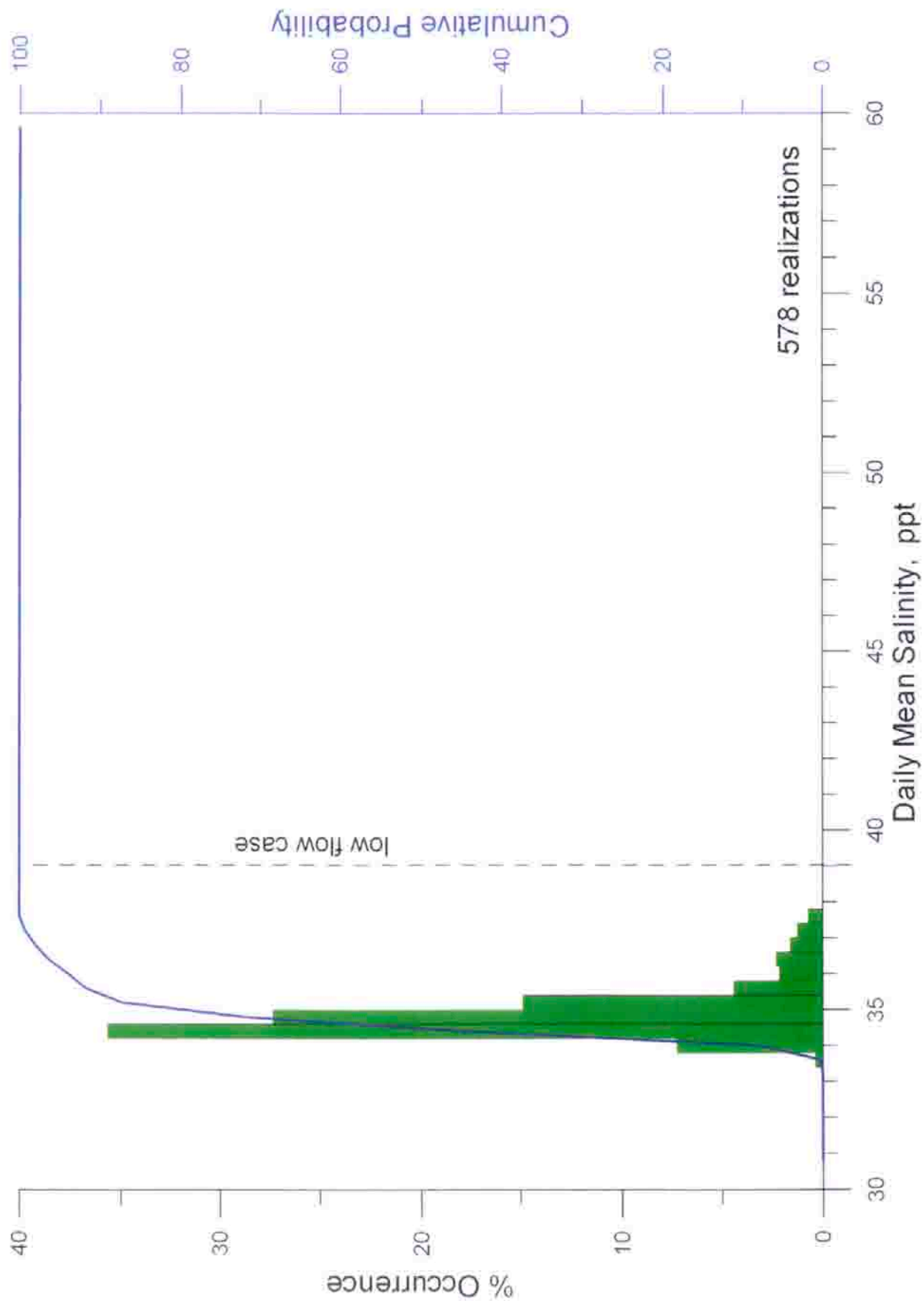


Figure 5.26. Histogram of daily maximum salinity at the bottom and 150 meters from the AES outfall for desalination production rate of 50 mgd. Percent occurrence based on historic observations of ocean mixing and water mass properties, and AES daily plant flow rates for the post re-powering period, 1 Jan 2002 - 30 July 2003.

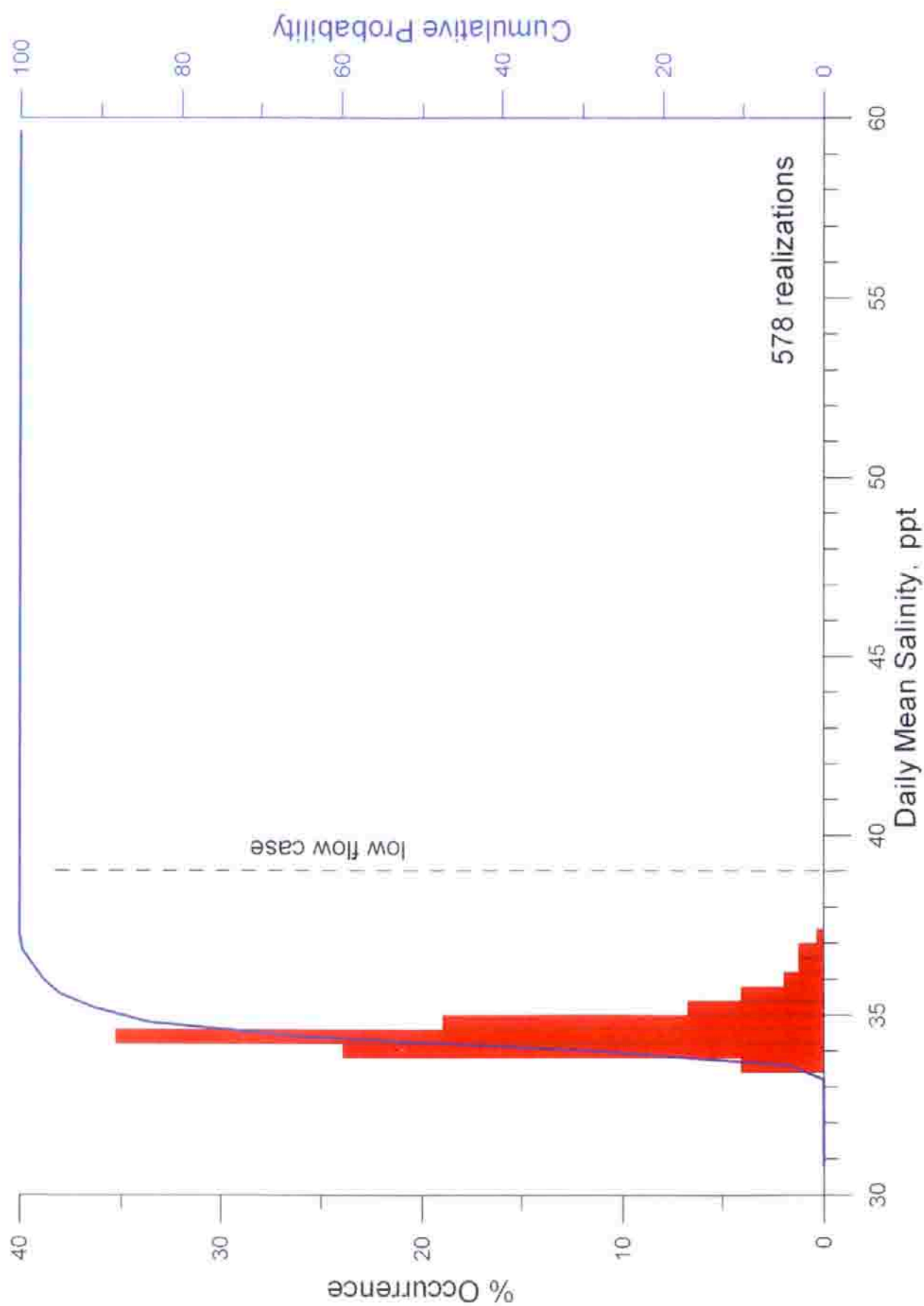


Figure 5.27. Histogram of daily maximum salinity at mid-depth and 300 meters from the AES outfall for desalination production rate of 50 mgd. Percent occurrence based on historic observations of ocean mixing and water mass properties, and AES daily plant flow rates for the post re-powering period, 1 Jan 2002 - 30 July 2003.

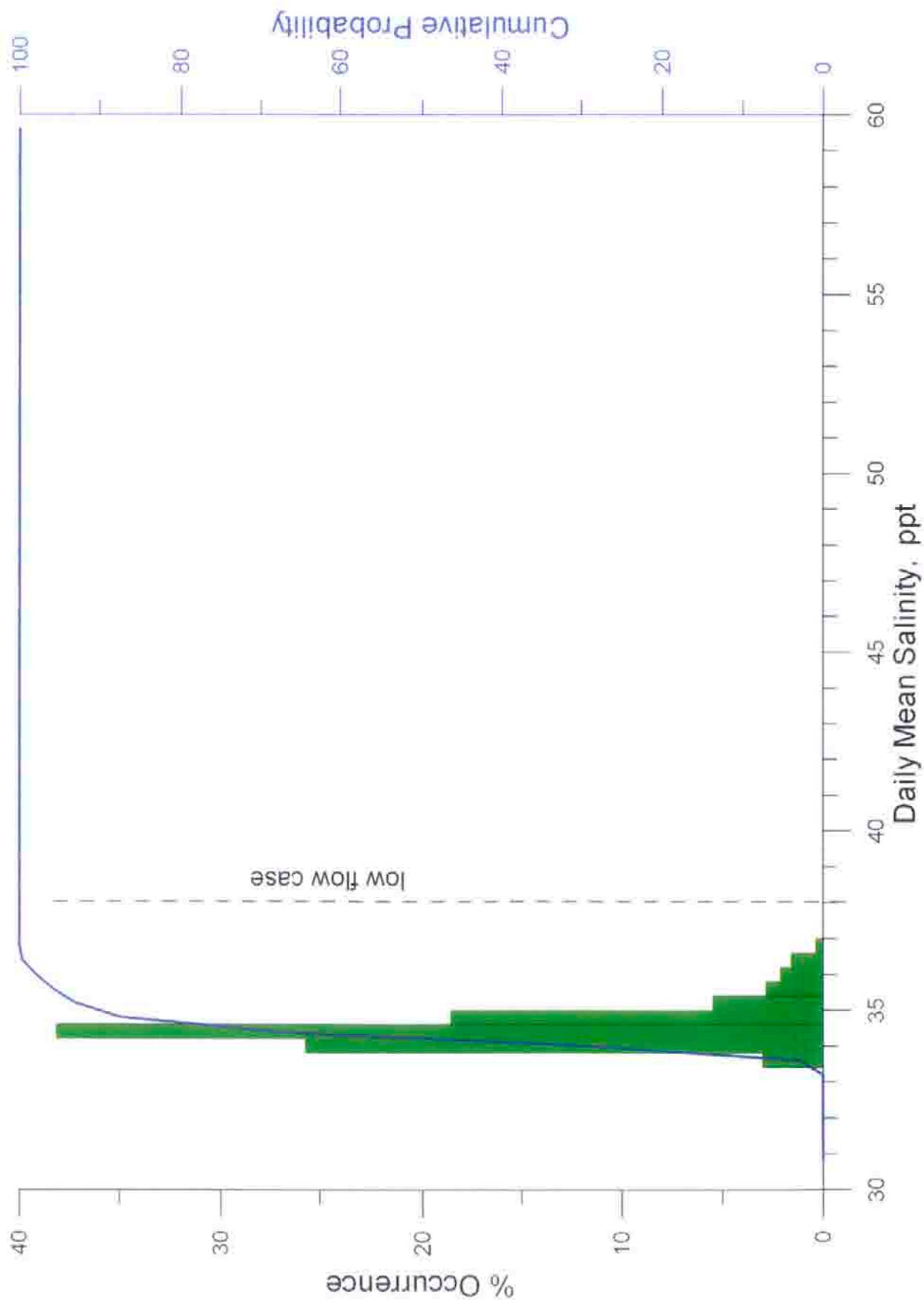


Figure 5.28. Histogram of daily maximum salinity at the bottom and 300 meters from the AES outfall for desalination production rate of 50 mgd. Percent occurrence based on historic observations of ocean mixing and water mass mass properties, and AES daily plant flow rates for the post re-powering period, 1 Jan 2002 - 30 July 2003.

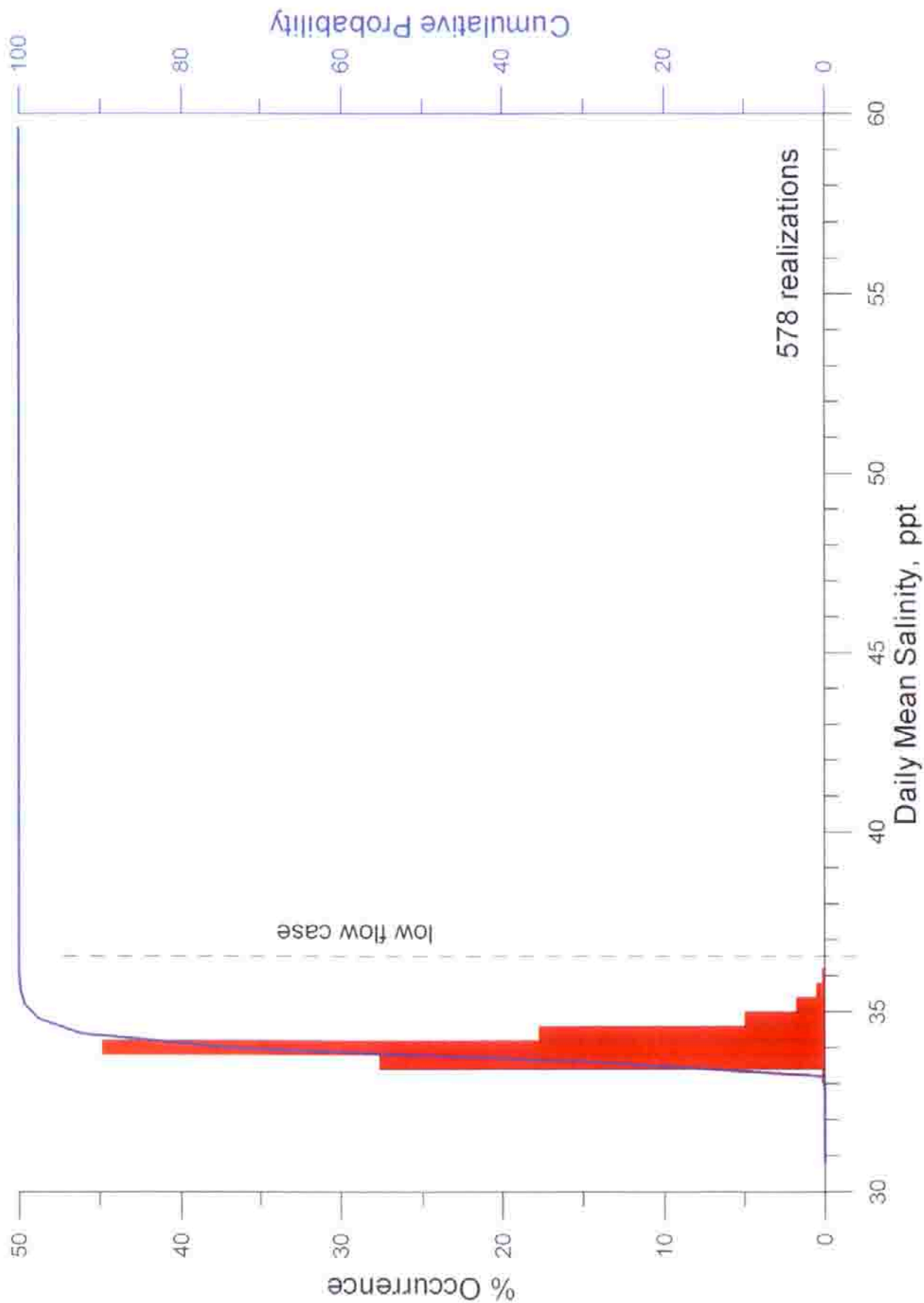


Figure 5.29. Histogram of daily maximum salinity at mid-depth and 500 meters from the AES outfall for desalination production rate of 50 mgd. Percent occurrence based on historic observations of ocean mixing and water mass mass properties, and AES daily plant flow rates for the post re-powering period, 1 Jan 2002 - 30 July 2003.

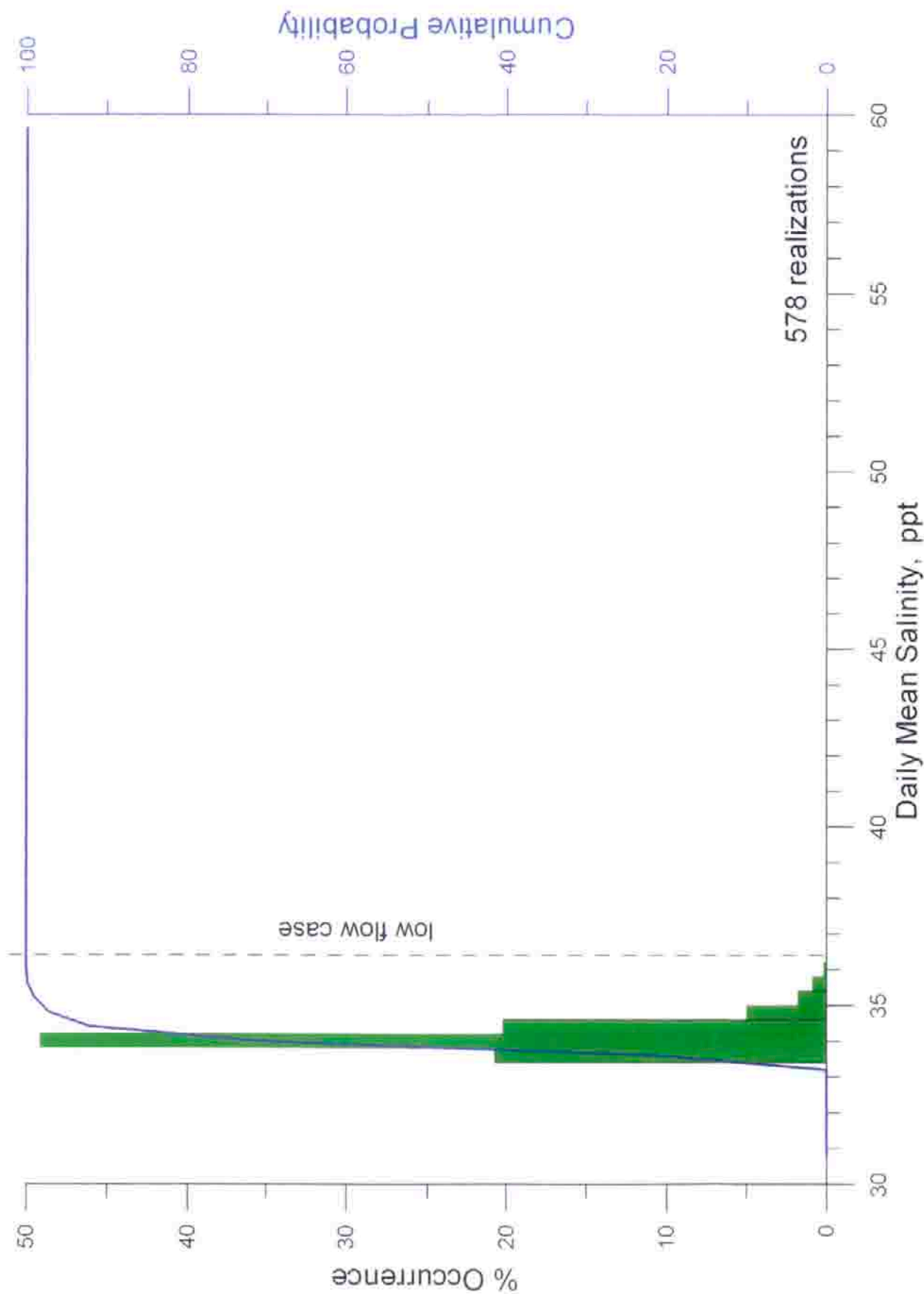


Figure 5.30. Histogram of daily maximum salinity at the bottom and 500 meters from the AES outfall for desalination production rate of 50 mgd. Percent occurrence based on historic observations of ocean mixing and water mass properties, and AES daily plant flow rates for the post re-powering period, 1 Jan 2002 - 30 July 2003.

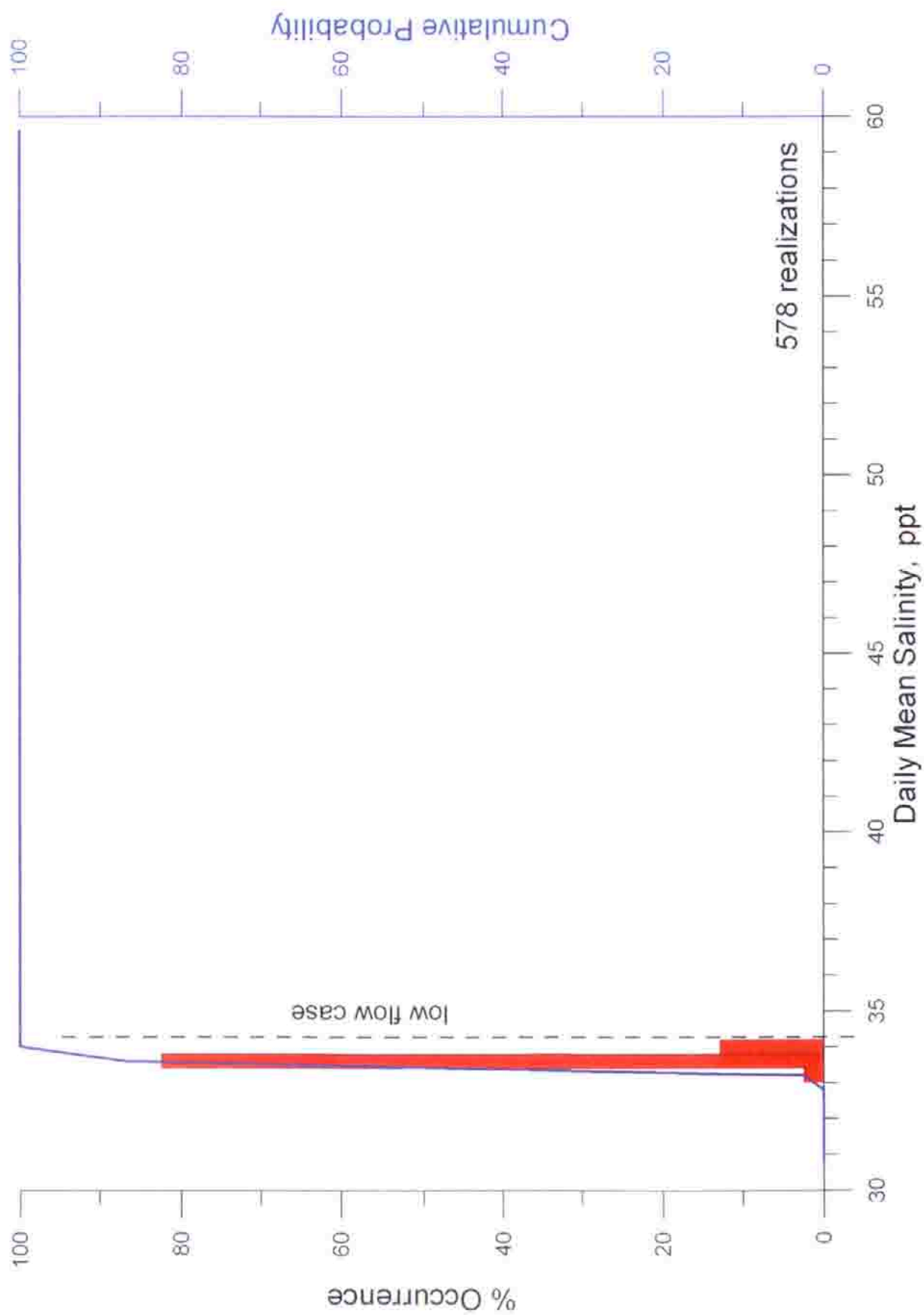


Figure 5.31. Histogram of daily maximum salinity at mid-depth and 1000 meters from the AES outfall for desalination production rate of 50 mgd. Percent occurrence based on historic observations of ocean mixing and water mass mass properties, and AES daily plant flow rates for the post re-powering period, 1 Jan 2002 - 30 July 2003.

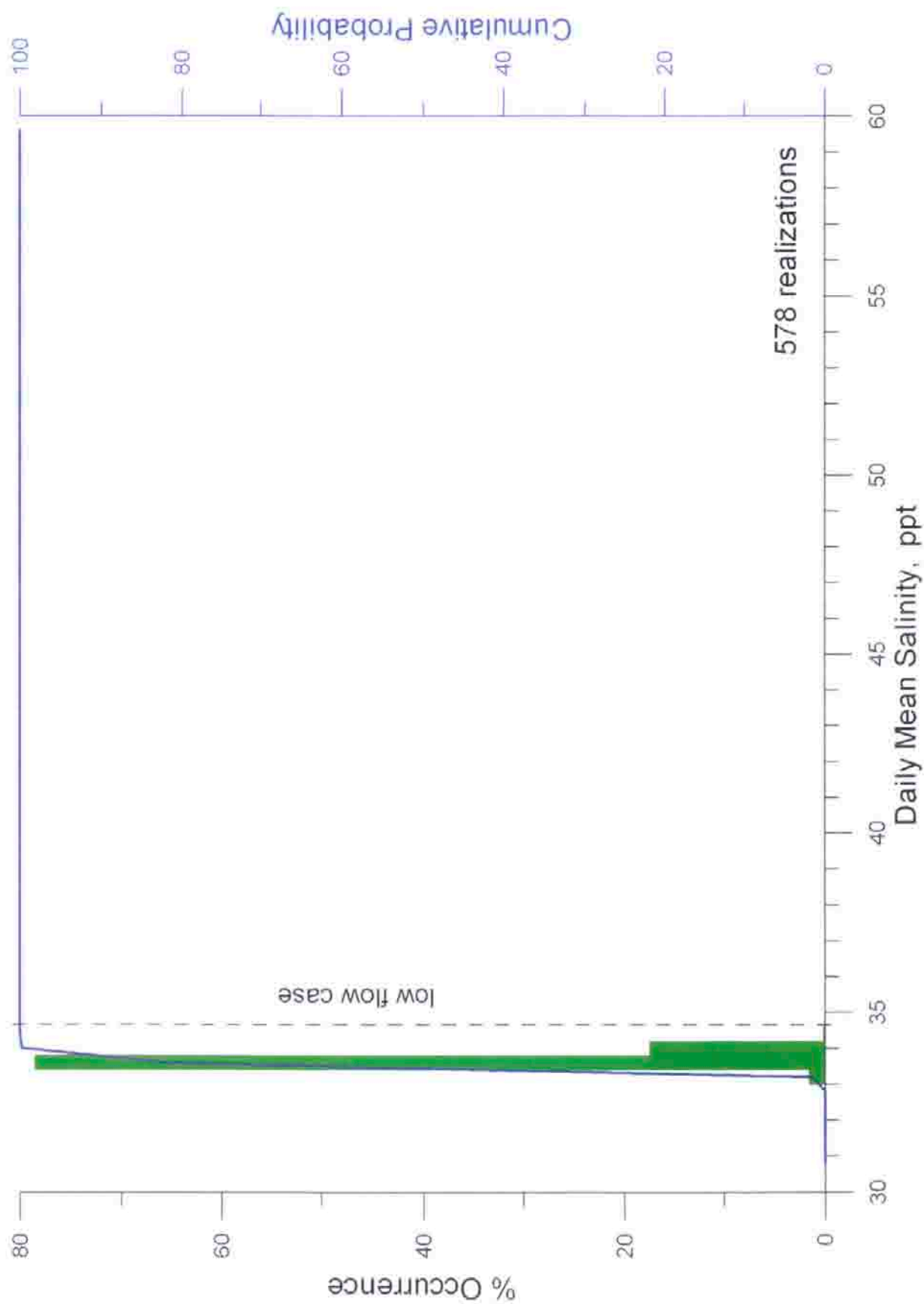


Figure 5.32. Histogram of daily maximum salinity at the bottom and 1000 meters from the AES outfall for desalination production rate of 50 mgd. Percent occurrence based on historic observations of ocean mixing and water mass properties, and AES daily plant flow rates for the post re-powering period, 1 Jan 2002 - 30 July 2003.

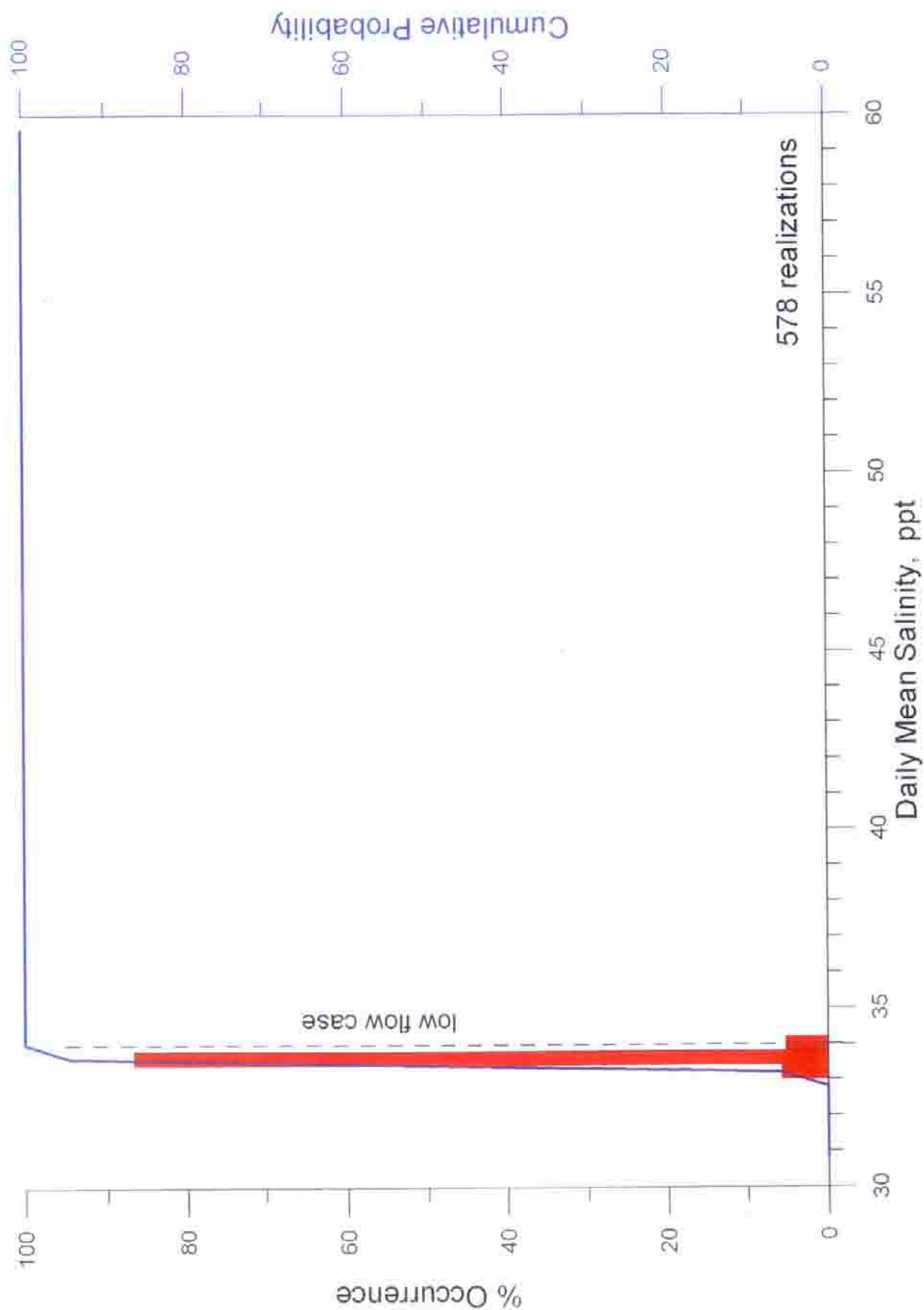


Figure 5.33. Histogram of daily maximum salinity at mid-depth and 2000 meters from the AES outfall for desalination production rate of 50 mgd. Percent occurrence based on historic observations of ocean mixing and water mass properties, and AES daily plant flow rates for the post re-powering period, 1 Jan 2002 - 30 July 2003.

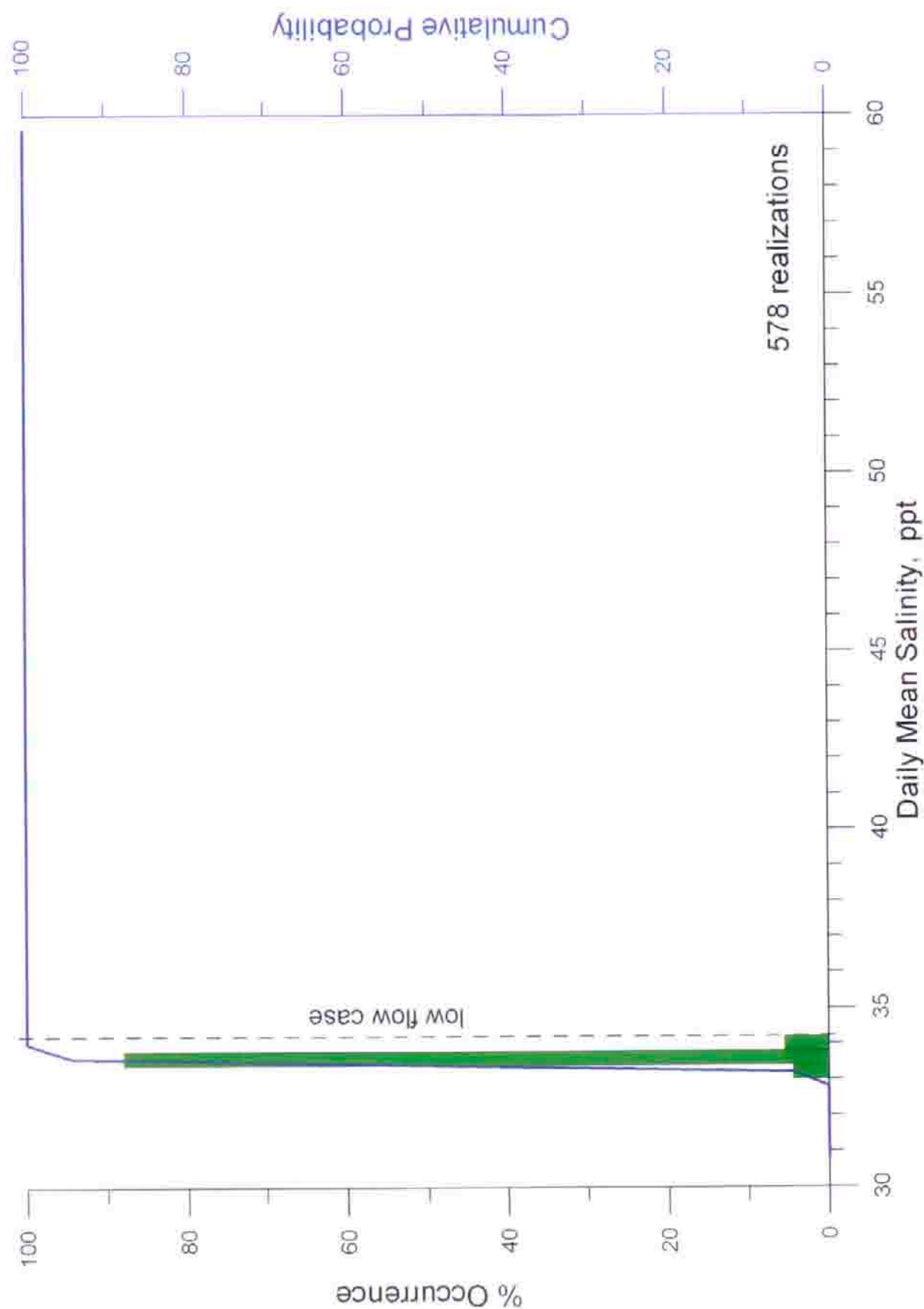


Figure 5.34. Histogram of daily maximum salinity at the bottom and 2000 meters from the AES outfall for desalination production rate of 50 mgd. Percent occurrence based on historic observations of ocean mixing and water mass properties, and AES daily plant flow rates for the post re-powering period, 1 Jan 2002 - 30 July 2003.

SECTION 6: In-Plant Waste Stream From AES Huntington Beach

6) In-Plant Waste Stream From AES Huntington Beach

A) Initialization

Under NPDES permit restrictions, the AES Huntington Beach Generating station can discharge up to 1.66 mgd of in-plant waste water. NPDES monitoring data in Appendix A indicates that maximum daily plant waste water discharges have not reached this limit in recent years, and that the highest discharges occur during wet weather conditions due to surface water runoff from plant facilities. The highest recorded daily discharge was 0.727 mgd (or 44% of certified limit) and occurred in February 1998 due to runoff from the El Niño storms studied in previous sections. The preponderance of in-plant waste water is therefore storm water runoff from the impervious surfaces of the plant facility.

In this section we evaluate the possible degree of recirculation of plant storm water between the plant outfall and infall while the proposed RO unit is producing 50 mgd of product water. We evaluate this recirculation potential using the oceanographic forcing for the storm series of late February 1998 as an extreme wet-weather model problem. However, rather than use the below certified limit data for in-plant waste streams recorded during that period, we will use the maximum certified discharge limit of 1.66 mgd to provide a low flow case assessment of recirculation potential. Furthermore we examine recirculation for both ends of the envelope of generation capacity, providing two separate model scenarios: 1) recirculation with 1 generating unit on-line with RO production at 50 mgd, and 2) recirculation with 4 generating units on-line with RO production at 50 mgd. We evaluate both of these scenarios for continuous plant operation over a 7 day period using 22-28 Feb 98 oceanographic forcing data.

From Table 2 in Section 3, we find that in the first of these two model scenarios that the generating station discharges 126.7 mgd of cooling water and 1.66 mgd of in-plant waste stream (storm water) for a combined plant discharge of 128.4 mgd. The RO unit removes 100 mgd of cooling water prior to the addition of the in-plant waste stream and returns 50 mgd of concentrated seawater by-product at 67.04 ppt (twice ambient seawater salinity). The resulting end-of-the-pipe effluent, (consisting of the plant cooling water, storm water, and of RO concentrated seawater by-product) is 78.36 mgd at 54.19 ppt. For the second recirculation model scenario, the generating station discharges 506.9 mgd of cooling water and 1.66 mgd of storm water for a combined discharge of 508.6 mgd. With the activity of the RO unit producing 50 mgd of product water, the resulting end-of-the-pipe effluent (cooling water, storm water, concentrated seawater) is 458.66 mgd at 37.05 ppt salinity. The specific volume of the cooling water discharge was based on a operating temperature of 10° C over ambient receiving water. Monitoring data for 22-28 February 1998 indicates that receiving water temperature averaged 17.5° C.

B) Results

Because the generating station infall draws source water from about the middle of the water column (4.8 meters above the bottom and 5.6 meters below the mean sea surface) we evaluate the recirculation at the depth of the infall velocity cap. The 7-day average of the dilution factor for the combined effluent with 1 generating unit operational is shown in Figure 6.1. The dilution of the effluent at the plant infall is 316 to 1, (where dilution factors are contoured on a log-10 scale). This implies that 0.32% (round off to 0.3%) of the combined plant effluent is recirculated to the infall, of which 2.1% is plant storm water. Hence 0.0066%

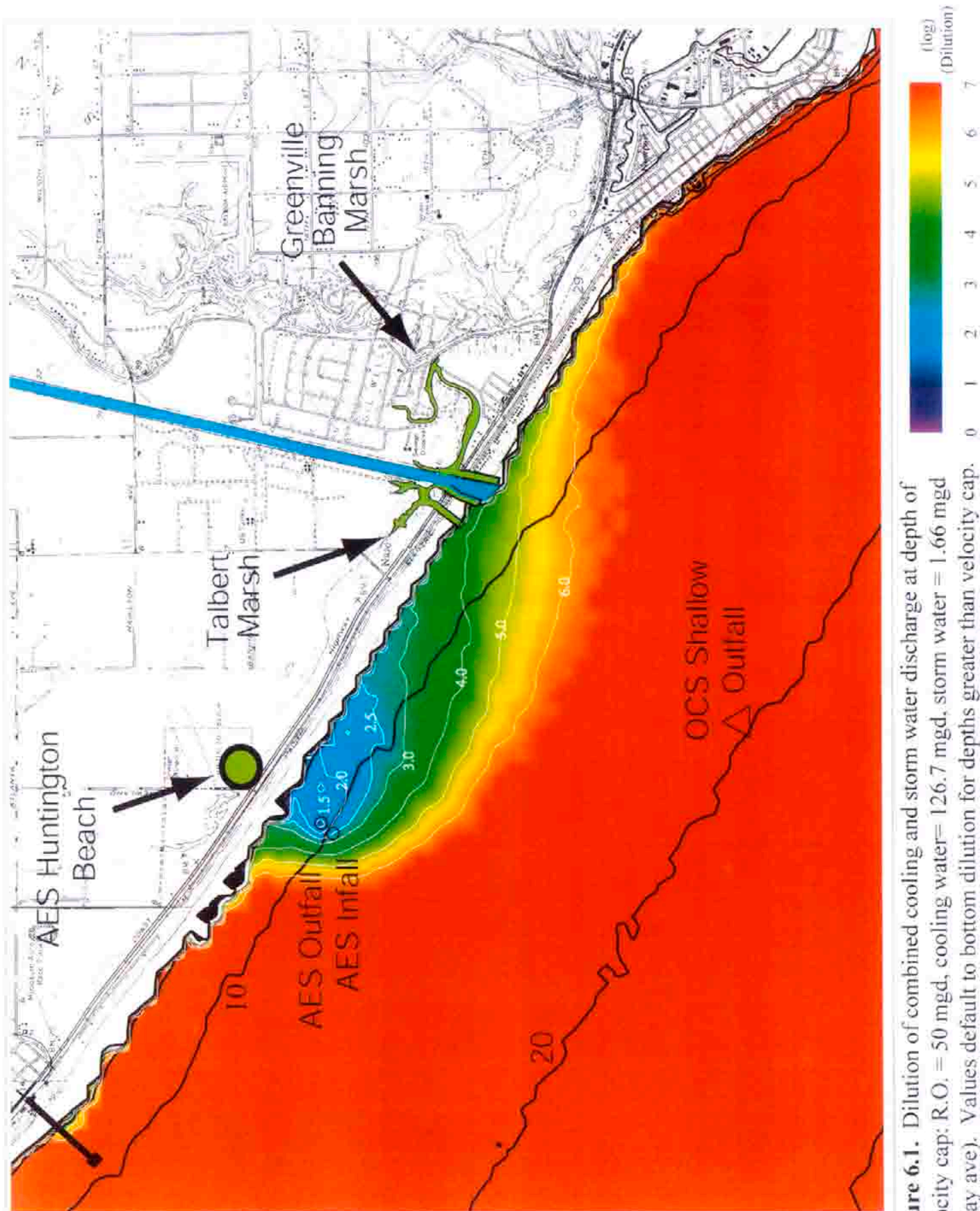


Figure 6.1. Dilution of combined cooling and storm water discharge at depth of velocity cap: R.O. = 50 mgd, cooling water= 126.7 mgd, storm water = 1.66 mgd (7 day ave). Values default to bottom dilution for depths greater than velocity cap.

(round off to 0.007%) of the source water uptake is plant storm water during a 7-day period of extreme wet weather conditions with only one generation unit on-line.

In Figure 6.2 the depth averaged dilution field is shown for all four plant generation units in operation continuously over a 7-day wet weather period. The dilution of the combined effluent is 1000 to 1 over the plant infall. Consequently 0.1% of the plant effluent is recycled through the infall of which 0.36% is plant storm water. This reduces the plant storm water constituent to only 0.00036% (round off to 0.0004%) of the source water uptake at the infall.

There are two factors which contribute the reduction in the recirculation of plant storm water as generation levels increase above the minimal levels modeled in Figure 6.1. The first is that the 1.66 mgd of storm water discharge experiences about 4 times more initial dilution in the pipe when all 4 generation units are operational versus the minimum generation configuration in Figure 6.1. The second is that the change in specific volume of the combined effluent relative to ambient seawater is less when all four generating units operate in tandem with the RO unit. With only one generating unit on-line, the change in specific volume of the effluent relative to seawater is -1.49% (Table 2 in Section 3) making it considerably heavier than seawater. In this case the effluent sinks immediately to the seafloor and dilutes relatively slowly on the bottom as a stable stratified bottom boundary layer. On the other hand the specific volume change of the effluent with all 4 units on-line is only -0.08% relative to ambient seawater, allowing it to be more readily overturned by wave mixing in the bottom boundary layer and thereby more rapidly diluted into the complete water column. The combined effect of higher-in-the-pipe dilutions and diminished specific volume

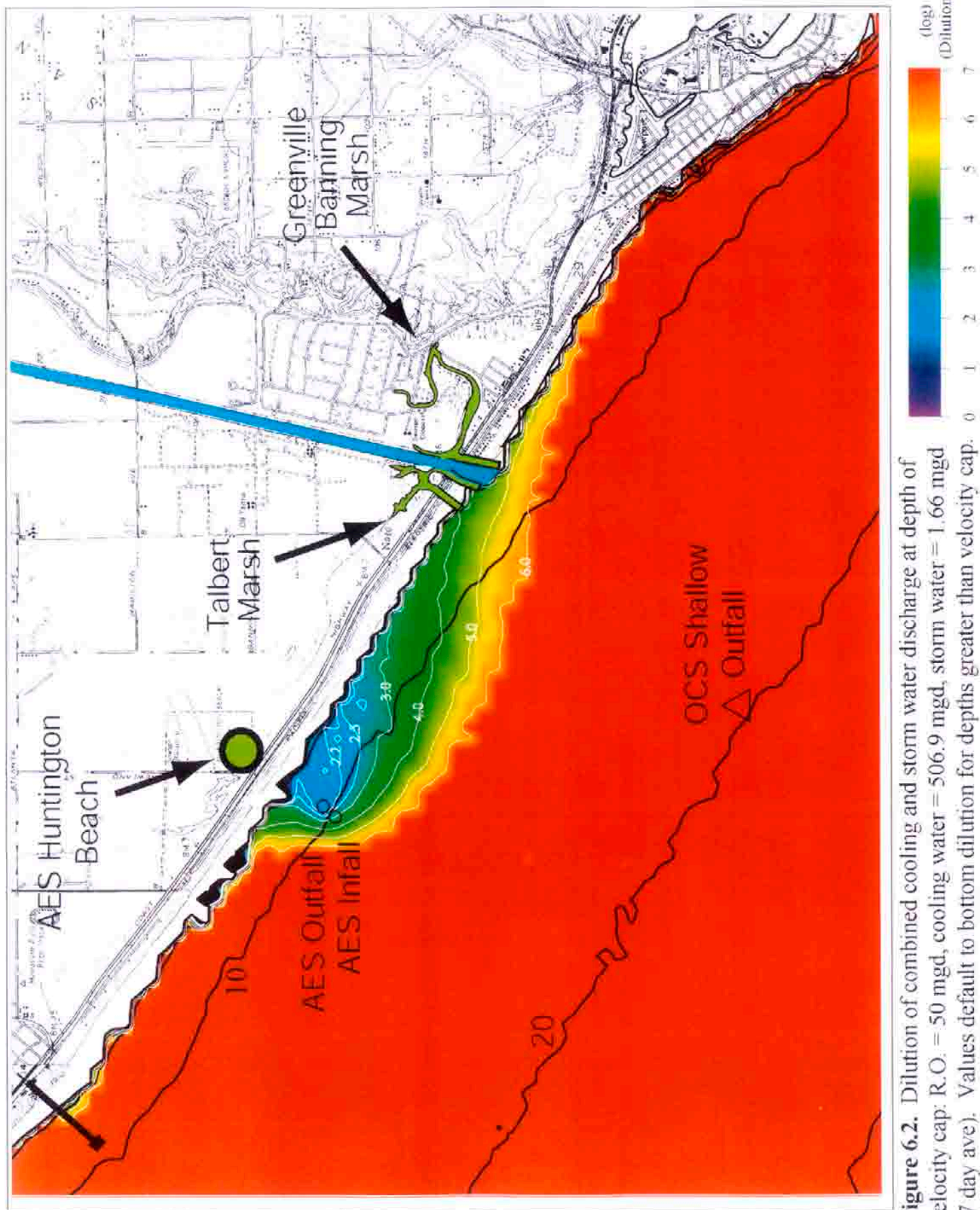


Figure 6.2. Dilution of combined cooling and storm water discharge at depth of velocity cap: R.O. = 50 mgd, cooling water = 506.9 mgd, storm water = 1.66 mgd (7 day ave). Values default to bottom dilution for depths greater than velocity cap.

contrast with receiving waters allows the plant storm water to be diluted significantly faster with all generating units on-line and thereby contribute a negligible fraction to recirculation in the source water. These results indicate that for normal plant operations with 2 generating units on-line that recirculated plant storm water would constitute 0.003% of the source water make-up.

Figure 6.3 maps the temperature for the combined effluent of cooling water, storm water, and concentrated sea water from RO production as computed in the middle of the water column. The simulation is based on a $\Delta T = 10^\circ \text{C}$ for the generating station thermal effluent. The plant generation was assumed to be at nominal operation levels with 2 generating units on line and a combined discharge of 255.1 mgd. The footprint of the thermal plume has been averaged over a 7 day period for ambient ocean conditions of 22-28 February 1998. Because thermal diffusivity is several orders of magnitude greater than mass diffusivity, the temperature anomaly of the combined plant discharge decays rapidly in the direction of net transport (toward the southeast). The largest temperature anomalies are found in the immediate neighborhood of the outfall tower, where a maximum temperature in the mid-water column is found to reach 26.7°C , ($\Delta T = 9.2^\circ \text{C}$). Once the discharge broaches the sea surface, the maximum temperature in the core of the surface boil falls to 25.0°C , ($\Delta T = 7.5^\circ \text{C}$), see Figure 6.4. The discharge plume then subsides around the perimeter of the surface boil, engaging the entire water column in the thermal dilution process as it sinks to the seafloor. This discharge trajectory leads to greatly increased rates of heat dissipation. This increased heat dissipation is augmented by the effluent heat lost to the exported stream of product water (50 mgd) from the desalination plant. In general the thermal plume in Figure 6.3 shows that the temperature anomaly is reduced to

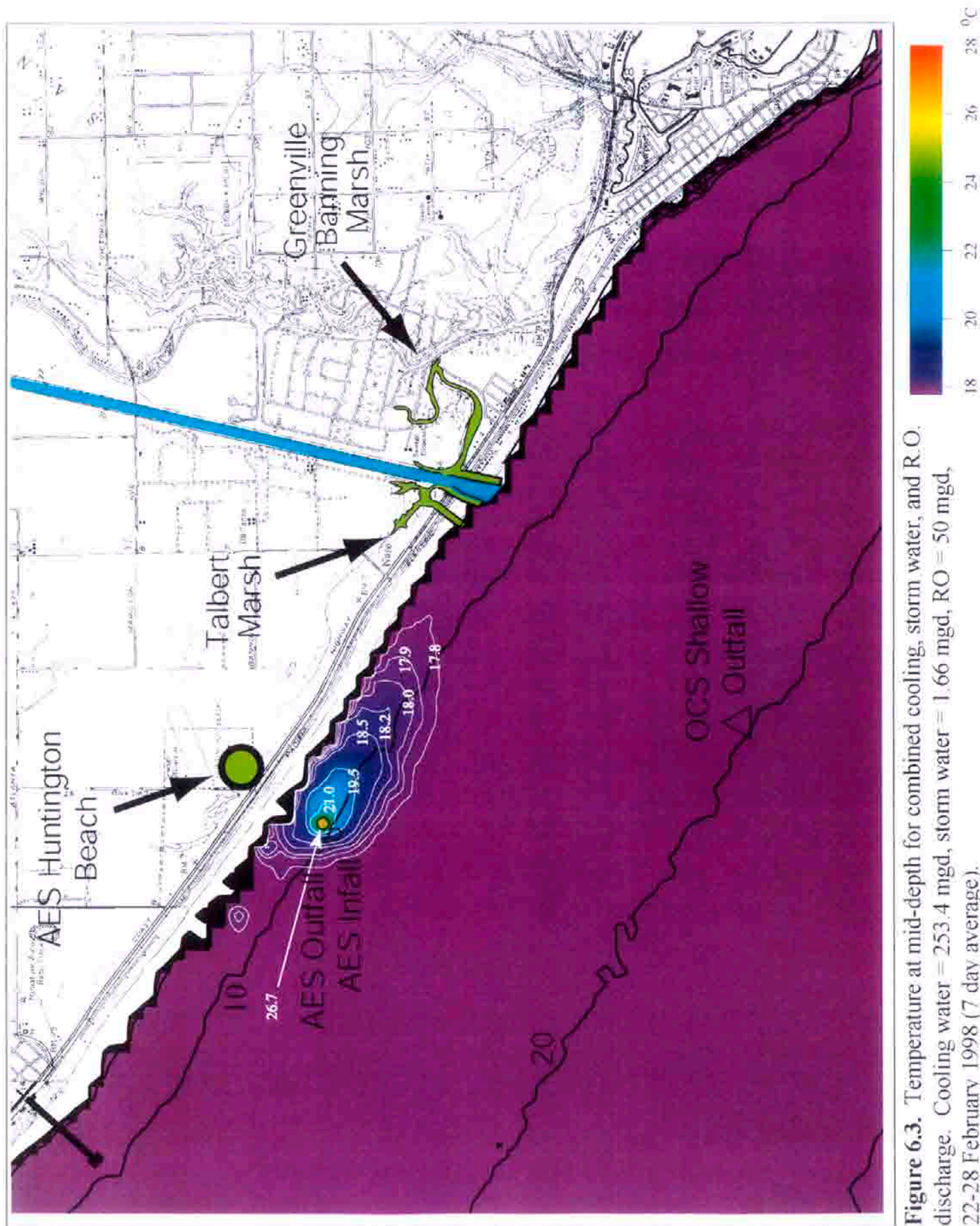


Figure 6.3. Temperature at mid-depth for combined cooling, storm water, and R.O. discharge. Cooling water = 253.4 mgd, storm water = 1.66 mgd, RO = 50 mgd, 22-28 February 1998 (7 day average).

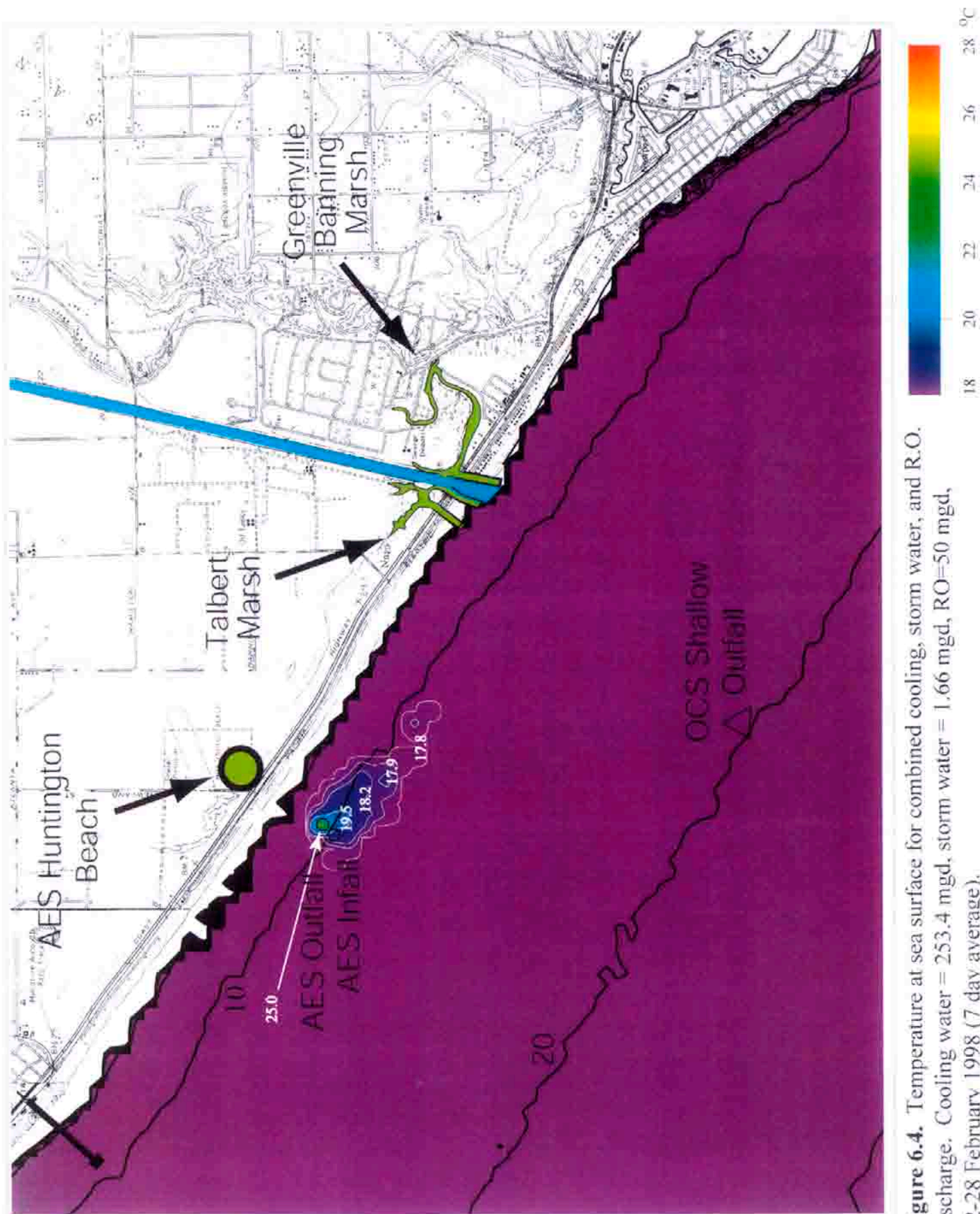


Figure 6.4. Temperature at sea surface for combined cooling, storm water, and R.O. discharge. Cooling water = 253.4 mgd, storm water = 1.66 mgd, RO=50 mgd, 22-28 February 1998 (7 day average).

$\Delta T = 1.5^{\circ} \text{C}$ above ambient in the water column over an area of about 6-8 acres surrounding the outfall tower. Applying the standards of the Thermal Plan, the foot print of the $\Delta T = 2.0^{\circ} \text{F}$ (1.1°C) temperature anomaly is only 74.6 acres anywhere in the water column. At the bottom (Figure 6.5) the combined effluent remains heavier than ambient seawater due to the presence of the by-product from RO production. This further promotes dilution because turbulence in the wave and current boundary layer increases mixing while greater dilution volume is provided by the overlying water column (as opposed to a thermal plume that floats on the sea surface in the absence of the concentrated seawater from RO production). The bottom foot print of the 2.0°F (1.1°C) temperature anomaly is 101 acres while the footprint of the 4.0°F (2.2°C) temperature anomaly is only 13.1 acres (Figure 6.5). These footprints represent about a 46% reduction in the average planar area of the thermal plume under existing conditions (MBC 1978-2003). Thus, the reduction in buoyancy of the thermal plume caused by the RO concentrated seawater has increased the dilution of the thermal plume of the AES cooling water effluent.

Thermal plan objectives give particular attention to temperatures on ocean substrate. Figure 6.5 shows a maximum bottom temperature of 24.1°C (6.6°C temperature anomaly). This occurs only on the rock footing of the outfall tower and not on the soft bottom benthic habitat. The seasonal temperature maximums of the ambient ocean waters at Huntington Beach commonly reach 25°C (Figure 3.23, Panel C).

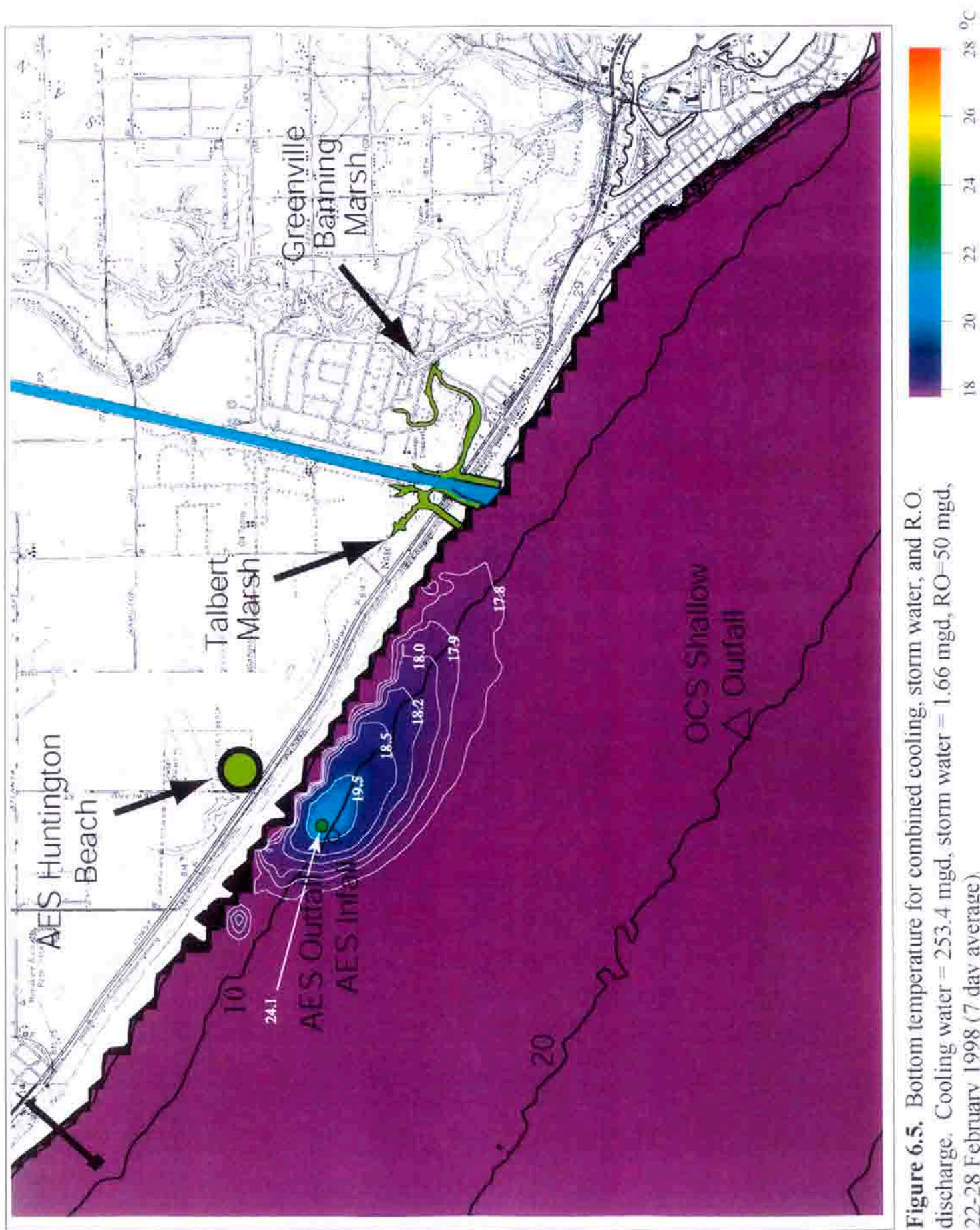


Figure 6.5. Bottom temperature for combined cooling, storm water, and R.O. discharge. Cooling water = 253.4 mgd, storm water = 1.66 mgd, RO=50 mgd, 22-28 February 1998 (7 day average).

**SECTION 7: Storm Water From Santa Ana River and Talbert
Channel**

7) Dilution and Dispersion of Storm Water From Santa Ana River and Talbert Channel

A) Initialization

To determine the source water make-up, the model was run for solutions to 24 hour, 7 day and 30 day average contribution of seawater and storm water at the AES Huntington Beach in fall during extreme runoff conditions. For all simulations, AES Huntington Beach was initialized for maximum cooling water flow rate (506.9 mgd), to determine the maximum amount of potential entrainment of storm water. The extreme runoff conditions were derived from the 1998 El Niño for the month of February as detailed in Section 3.

B) Results

Because the generating station outfall has no velocity cap, the combined discharge of the generating station and RO plant creates a jet of negatively buoyant fluid directed vertically upward at the sea surface at a flow rate of 456.9 mgd in the absence of any plant storm water. Figure 7.1 shows that this jet broaches the sea surface, creating a boil of high salinity water with a core at 36.7 ppt directly above the outfall. This result excludes any storm water discharge from the Santa Ana River or Talbert Channel. When those storm water discharges are superimposed, the surface boil acts to displace and dilute those runoff constituents on the surface and in the upper water column. Figure 7.2 gives the 24-hour average of the salinity at the sea surface during the peak flow day of the El Niño storm of 24 February 1998. The plume is due to the combined discharge of the Santa Ana River and Talbert Channel which averaged 8890 cfs over this 24 hour period (Figure 3.2). The hyper-saline surface boil produces a small hole in the river plume around the outfall (Figure 7.3), where local surface salinities exceed

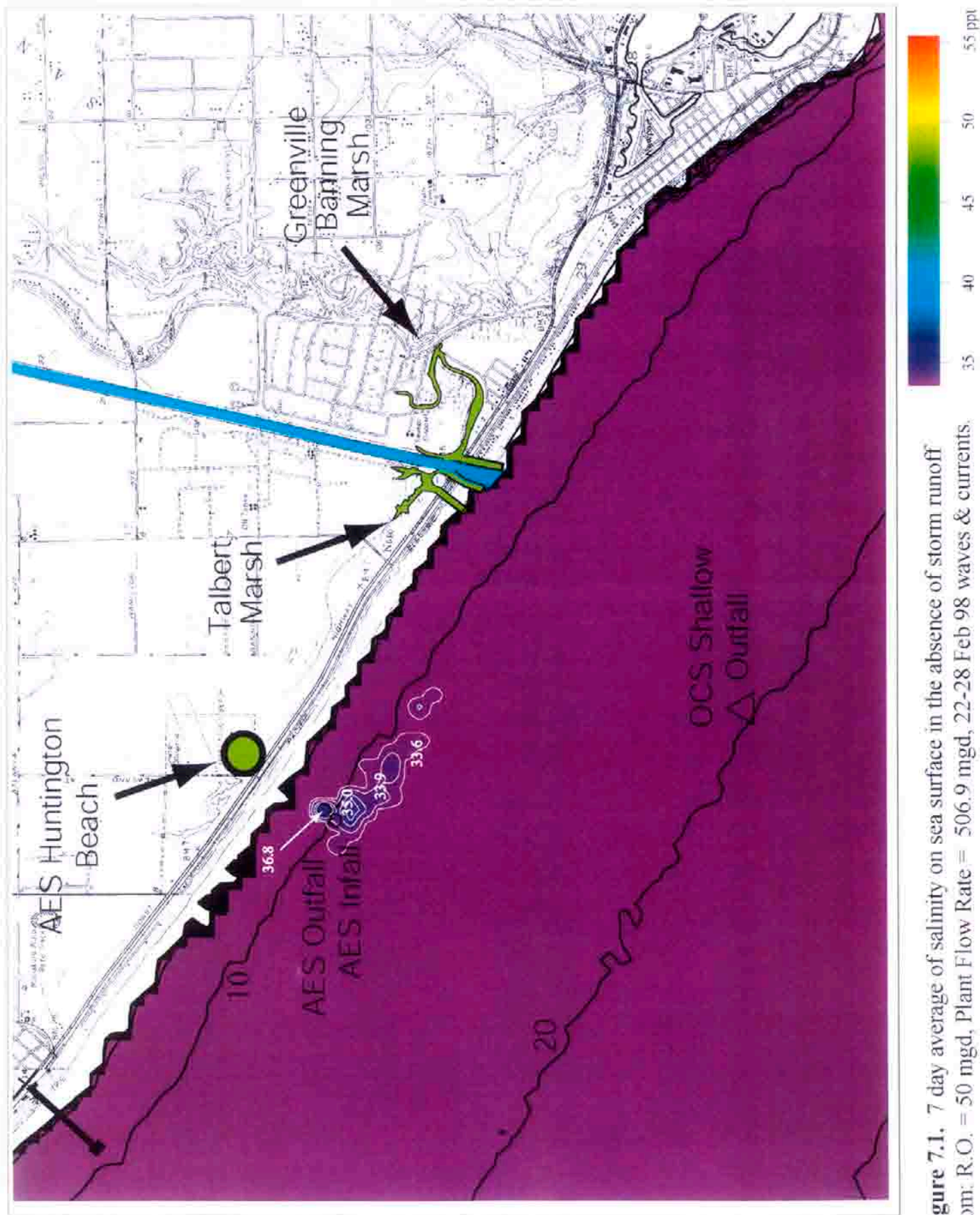


Figure 7.1. 7 day average of salinity on sea surface in the absence of storm runoff
from: R.O. = 50 mgd, Plant Flow Rate = 506.9 mgd, 22-28 Feb 98 waves & currents.

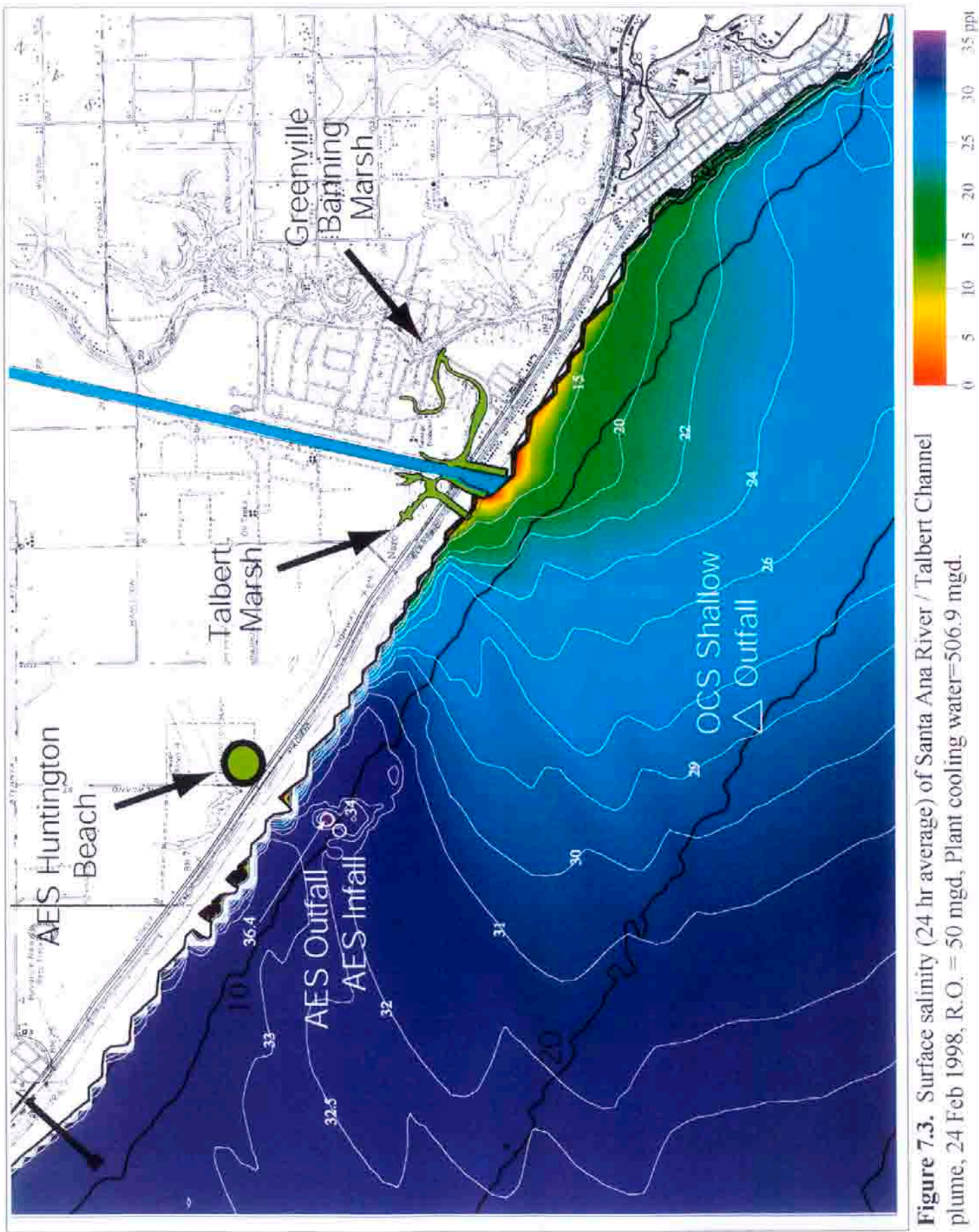


Figure 7.3. Surface salinity (24 hr average) of Santa Ana River / Talbert Channel plume, 24 Feb 1998, R.O. = 50 mgd, Plant cooling water=506.9 mgd.

the ambient deep water ocean salinity. Figure 7.4 shows the corresponding dilution field averaged over 24 hours on a log-10 scale. The AES Huntington Beach infall is denoted by a square symbol with an X through the center located near the 10 meter depth contour. The ebb dominance of the current field over a 24 hour period deflects the low salinity surface water mass in a downcoast direction toward the southeast. Inspection of the salinity and dilution contours in Figures 7.2 through 7.4 indicate that the storm water on the sea surface over the infall is diluted by a factor of 32 to 1. If the generating station infall were able to entrain water directly from the sea surface, the source water make-up would be 97% seawater and 3% storm water from the Santa Ana River and Talbert Channel. However the velocity cap of the infall tower is located 5.6 m below mean sea level. The dilution field at the depth from which the infall is drawing source water is calculated in Figure 7.5. At this depth (-5.6 m MSL) we find that the dilution of Santa Ana and Talbert Channel storm water is 316 thousand to 1. Because infall velocities are vanishingly small at the sea surface (CWQCB, 1993), the infall is more likely to entrain the preponderance of source water from depths near the depth of the velocity cap. Hence, the source water make-up for worst case floods is probably closer to being 99.9997% seawater and 0.0003% storm water according to dilutions shown in Figure 7.5.

Over a 7-day period that encompassed the peak runoff event and several following storms between 22-28 February 1998, the Santa Ana River and Talbert Channel averaged a combined discharge of 5,798 cfs. The 7-day average of the surface salinity over this period delineates the plume shown in Figure 7.6. Like the 24-hour average case in Figure 7.2, ebb dominance prevails in the current pattern over this 7 day period (Figure 3.18) and causes the plume to elongate in

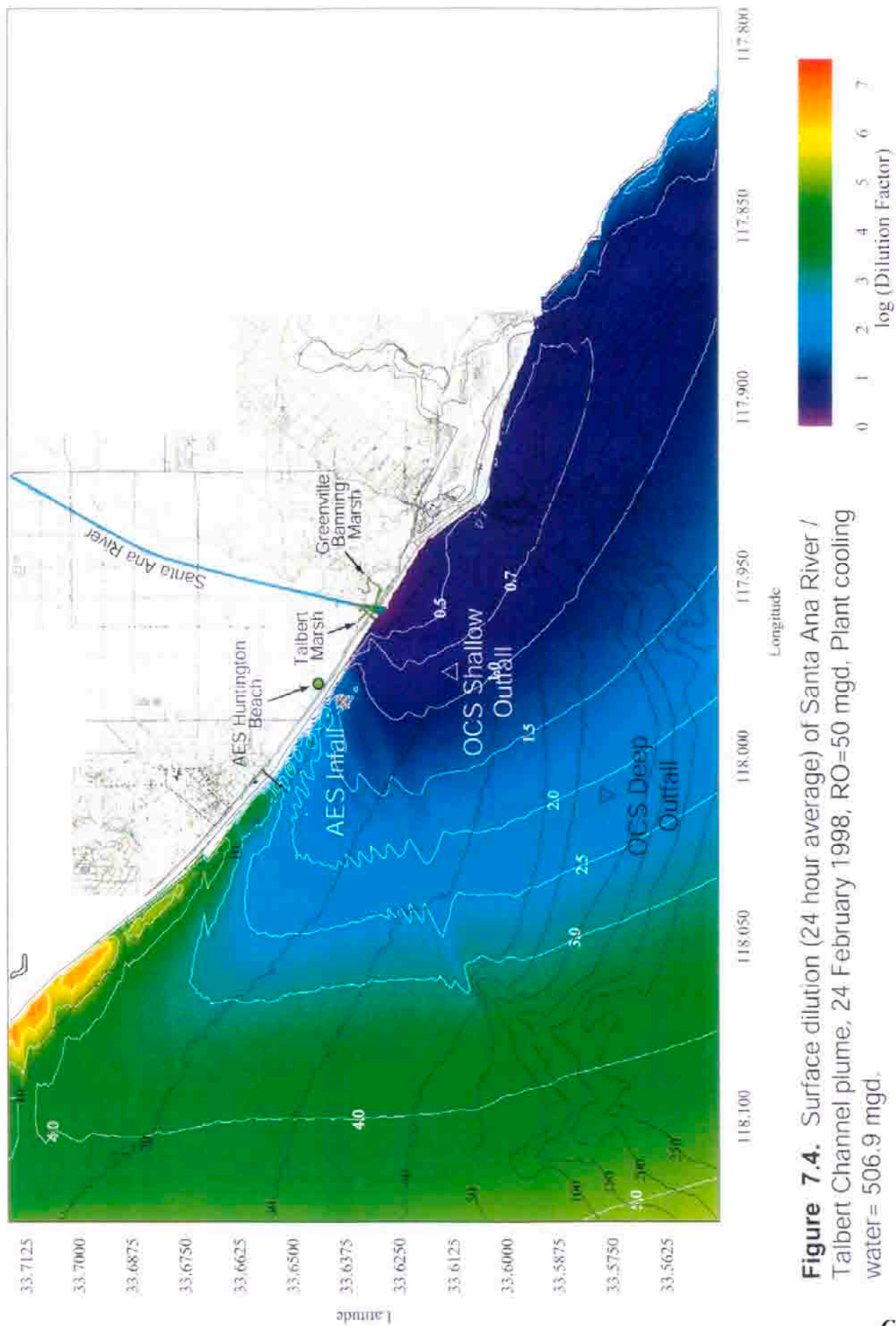


Figure 7.4. Surface dilution (24 hour average) of Santa Ana River / Talbert Channel plume, 24 February 1998, RO=50 mgd, Plant cooling water= 506.9 mgd.

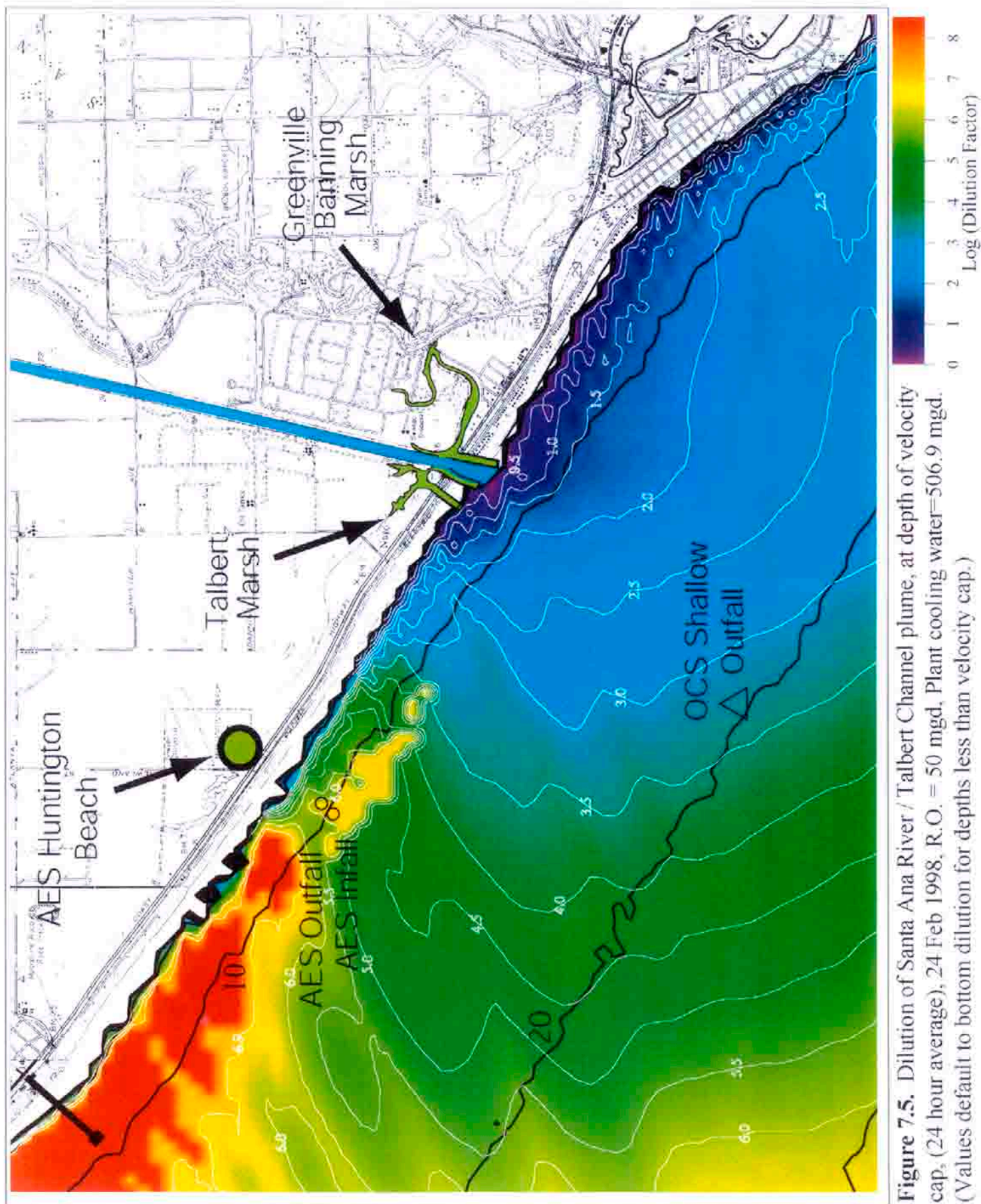


Figure 7.5. Dilution of Santa Ana River / Talbert Channel plume, at depth of velocity cap, (24 hour average), 24 Feb 1998, R.O. = 50 mgd, Plant cooling water=506.9 mgd. (Values default to bottom dilution for depths less than velocity cap.)

the downcoast direction towards Newport Harbor and Crystal Cove State Beach. The corresponding 7-day average of the surface dilution field in Figure 7.7 shows that the storm water is diluted 50 to 1 on the sea surface over the plant infall. Therefore, over a 7-day period surrounding peak runoff, the sea surface water make-up is at most 2% storm water and 98% seawater. But entrainment velocity due to the outfall vanishes at the sea surface, and the source water is instead drawn from below the surface at depths comparable to the infall velocity cap. The dilution factor at the velocity cap of the infall is shown in Figure 7.8 to average at least 1 million to 1 over a 7-day period around peak runoff. Thus the source water make-up is likely to be as little as 0.0001% storm water and 99.9999% seawater.

Over a 30-day period encompassing the peak runoff month of February 1998, the combined flow of the Santa Ana River and Talbert Channel averaged 2,732 cfs. This discharge produced a 30-day average of the sea surface salinity computed in Figure 7.9. Again the ebb dominance of the current system produces a net downcoast dispersion of the salinity anomaly of the discharge plume. The corresponding surface dilution field in Figure 7.10 indicates that the storm water on the sea surface over the infall is diluted to 100 to 1. Consequently surface water comprises only 1% storm water in a 30 day wet weather period, and that figure represents an upper bound limit on the source water. At the depth of the infall velocity cap, the 30-day average dilution factor in Figure 7.11 drops to 10 million to 1. In essence, the storm water becomes non-detectable in source water at the velocity cap over 30-day wet weather time scales.

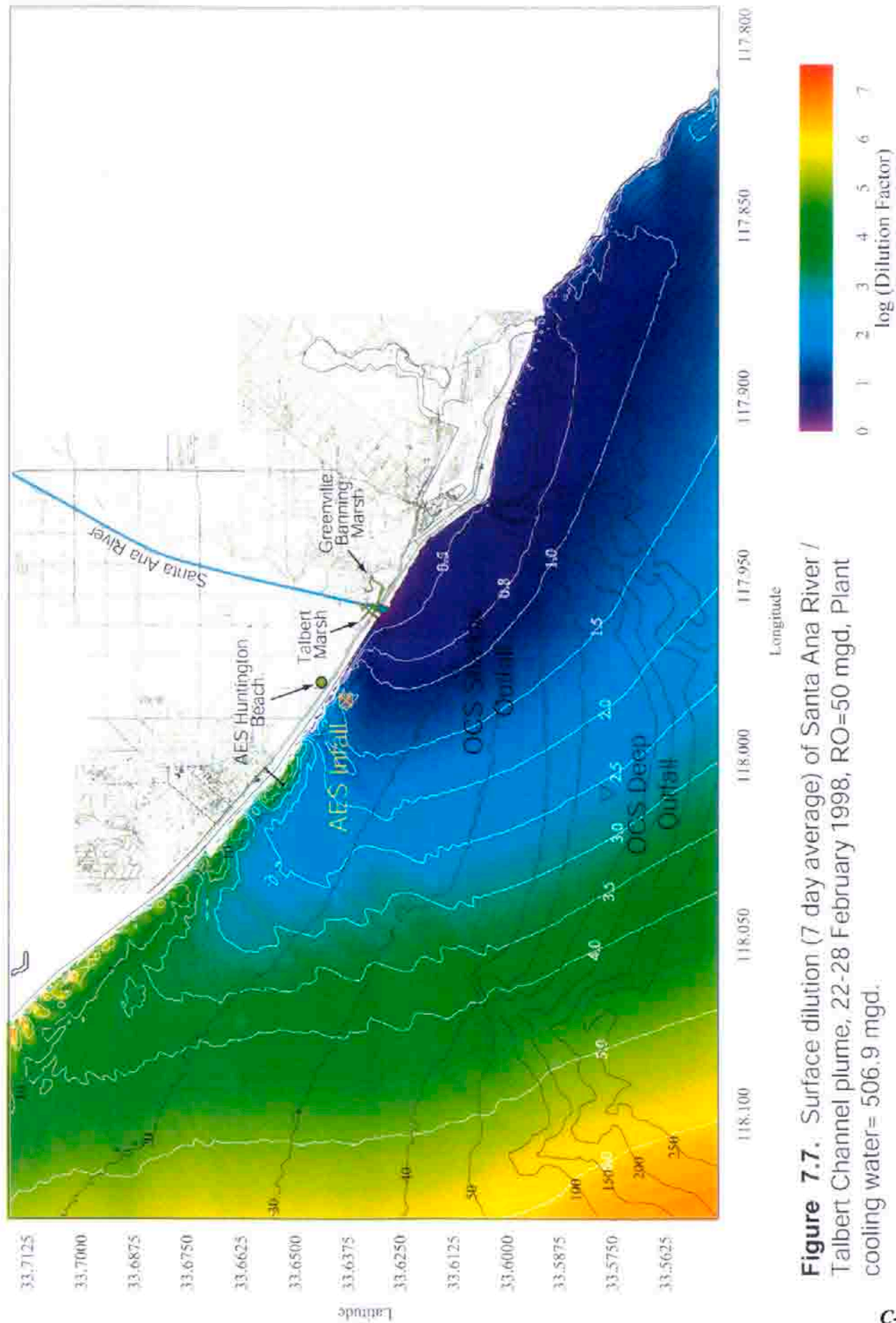
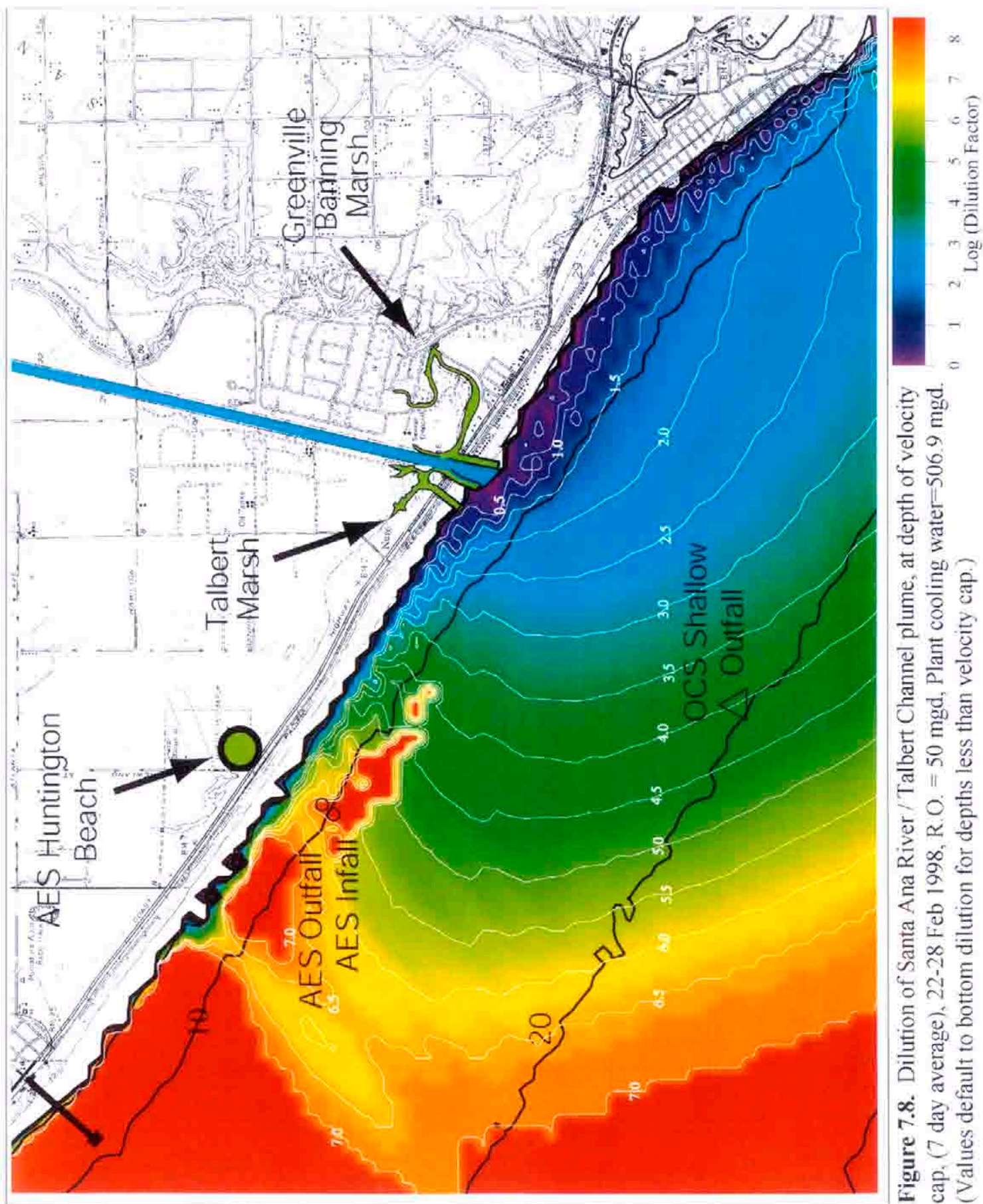


Figure 7.7. Surface dilution (7 day average) of Santa Ana River / Talbert Channel plume, 22-28 February 1998, RO=50 mgd, Plant cooling water= 506.9 mgd.



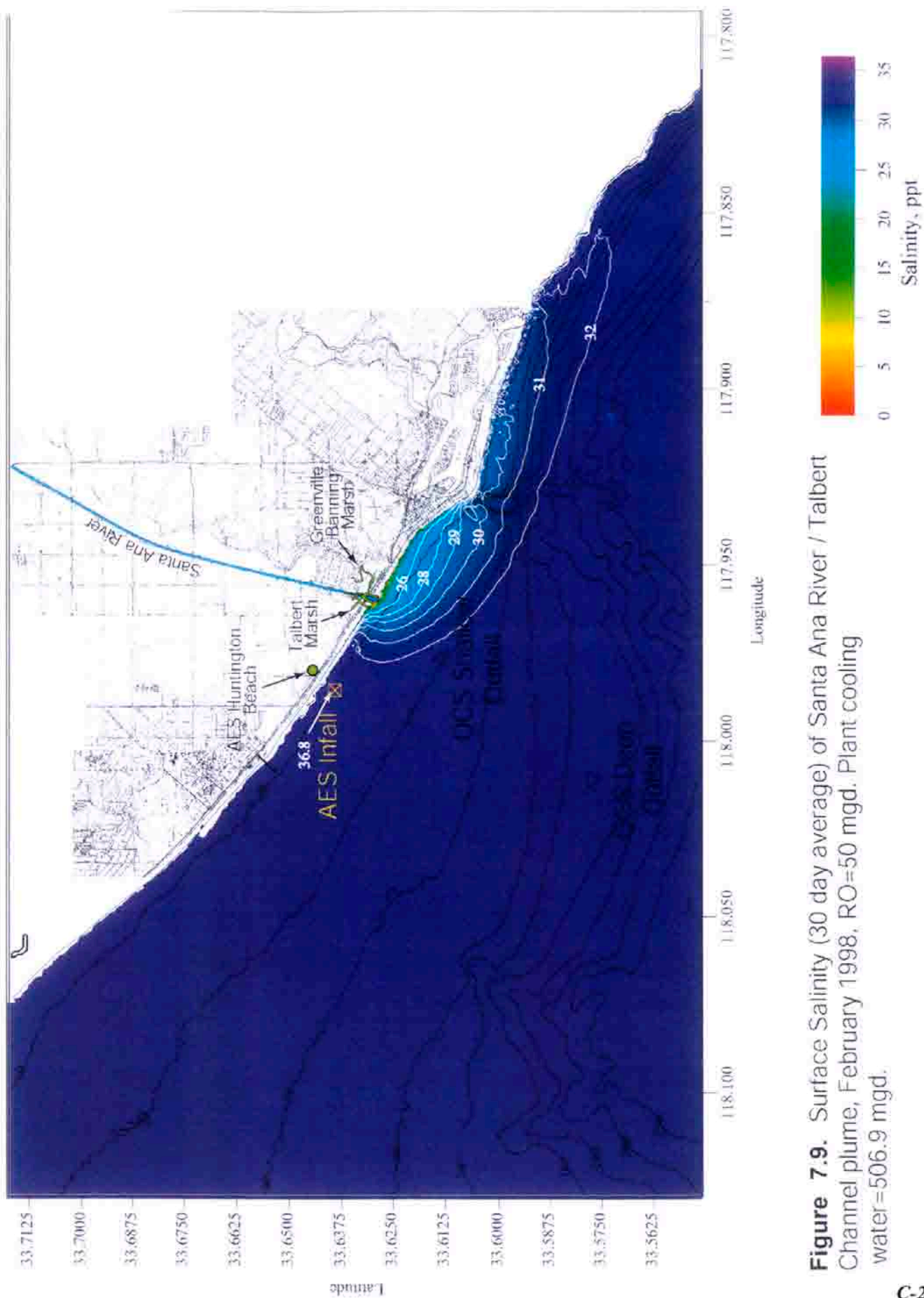
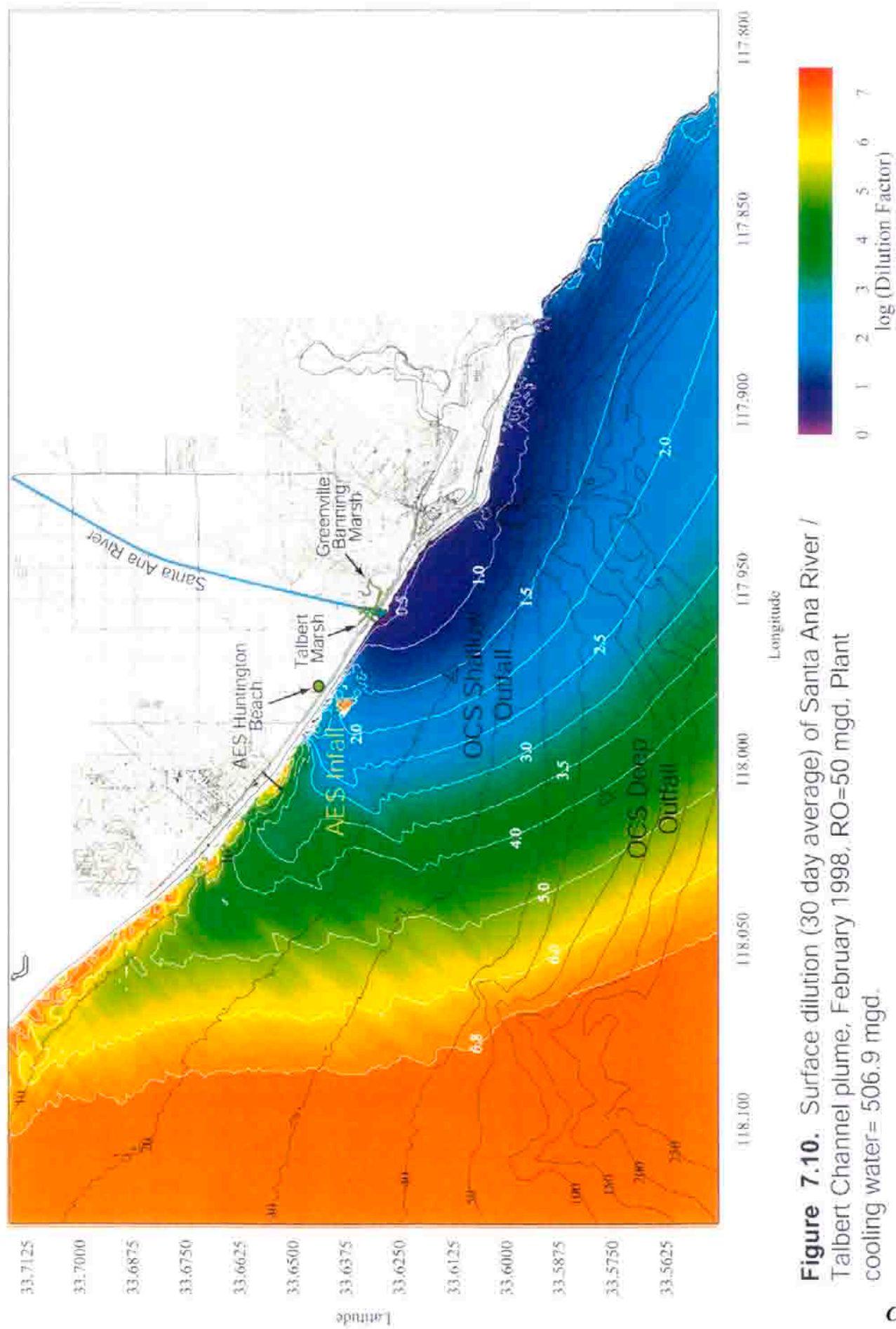


Figure 7.9. Surface Salinity (30 day average) of Santa Ana River / Talbert Channel plume, February 1998, RO=50 mgd. Plant cooling water=506.9 mgd.



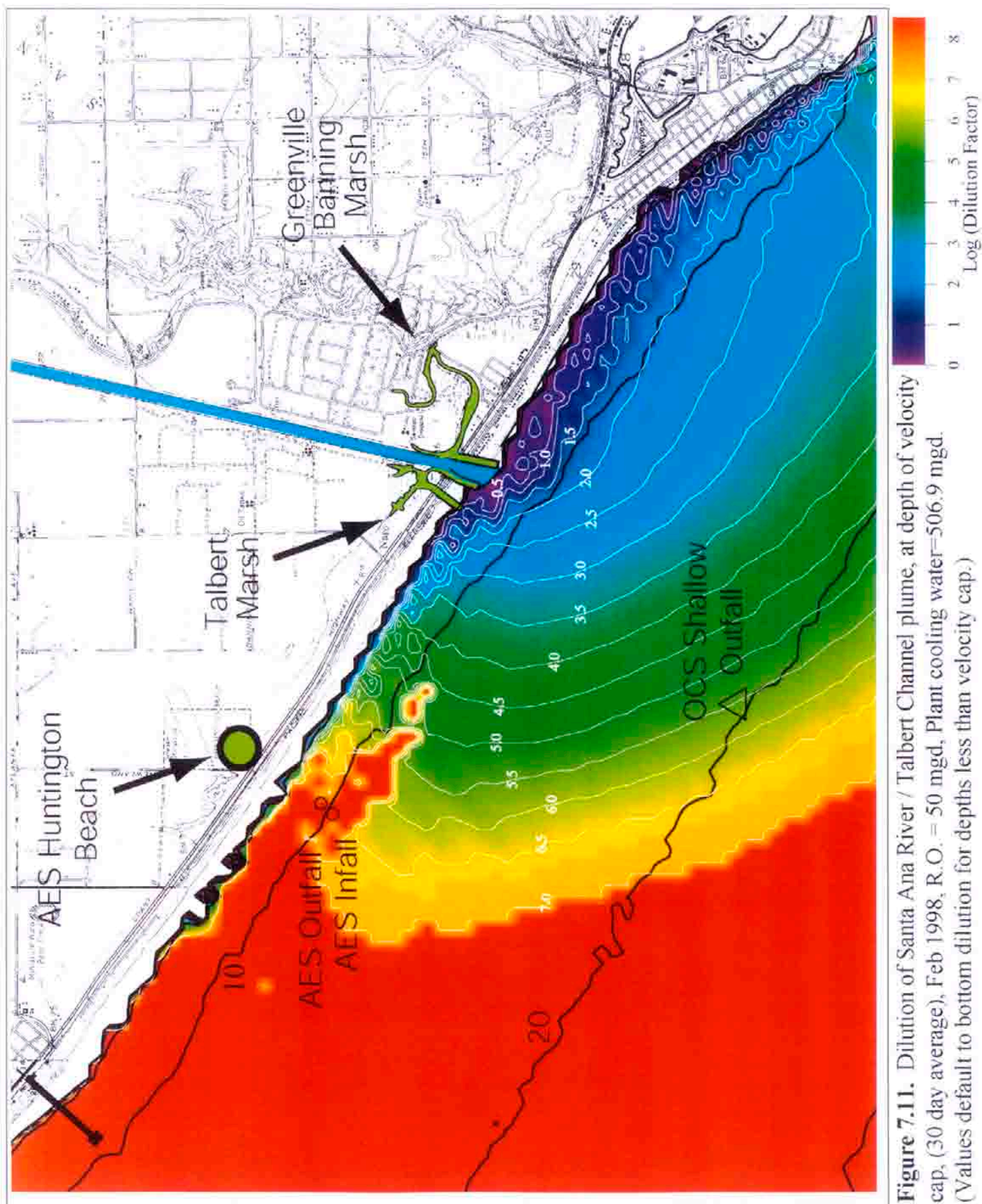


Figure 7.11. Dilution of Santa Ana River / Talbert Channel plume, at depth of velocity cap, (30 day average), Feb 1998, R.O. = 50 mgd, Plant cooling water=506.9 mgd. (Values default to bottom dilution for depths less than velocity cap.)

SECTION 8: Tidal Discharge From Talbert Marsh

8) Dilution and Dispersion of Tidal Discharge From Talbert Marsh

A) Initialization

The Talbert Marsh has a mean tidal prism of $3.0 \times 10^5 \text{ m}^3$ (79.3 million gallons) and a storage volume of about $7.6 \times 10^5 \text{ m}^3$ (200 million gallons), see Liedersdorf, et al. (1992). It discharges into the ocean through a pair of short, non-surf zone piercing jetties immediately to the northwest of the Santa Ana River jetties (Figure 1.1). The jetties stop at about the mean tide line about 275 m seaward of the Pacific Coast Highway. During dry summer weather with low waves, a sand spit builds across the inlet in the interior region of the jetties, periodically closing the inlet and arresting tidal exchange between the marsh and the ocean. While the inlet is closed, the marsh continues to receive dry weather flows from the Talbert Channel, draining the City of Huntington Beach. The dry weather runoff progressively raises water levels in the marsh behind the barrier spit, creating a kind of perched pond. This runoff is typically laden with nutrients and bacteria which incubate in the marsh while the inlet remains closed.

The sand spit blocking the inlet is episodically breeched when large summer south swells from Mexican hurricanes and southern hemisphere storms erode the beach and overtop the barrier. Breeching initially cuts a pilot channel through the barrier sand spit, releasing the perched water behind the spit in a single flush of between 80 and 100 million gallons. The flush of marsh water is introduced directly into the surf zone along with the high bacteria levels that have incubated in the marsh waters during the period of inlet closure. Because the marsh waters are close to ambient seawater salinities, the contaminated water quickly infiltrates the surfzone and moves longshore with the littoral drift as shown schematically by the upper panel in Figure 8.1. Following spit breeching and the initial tidal flush

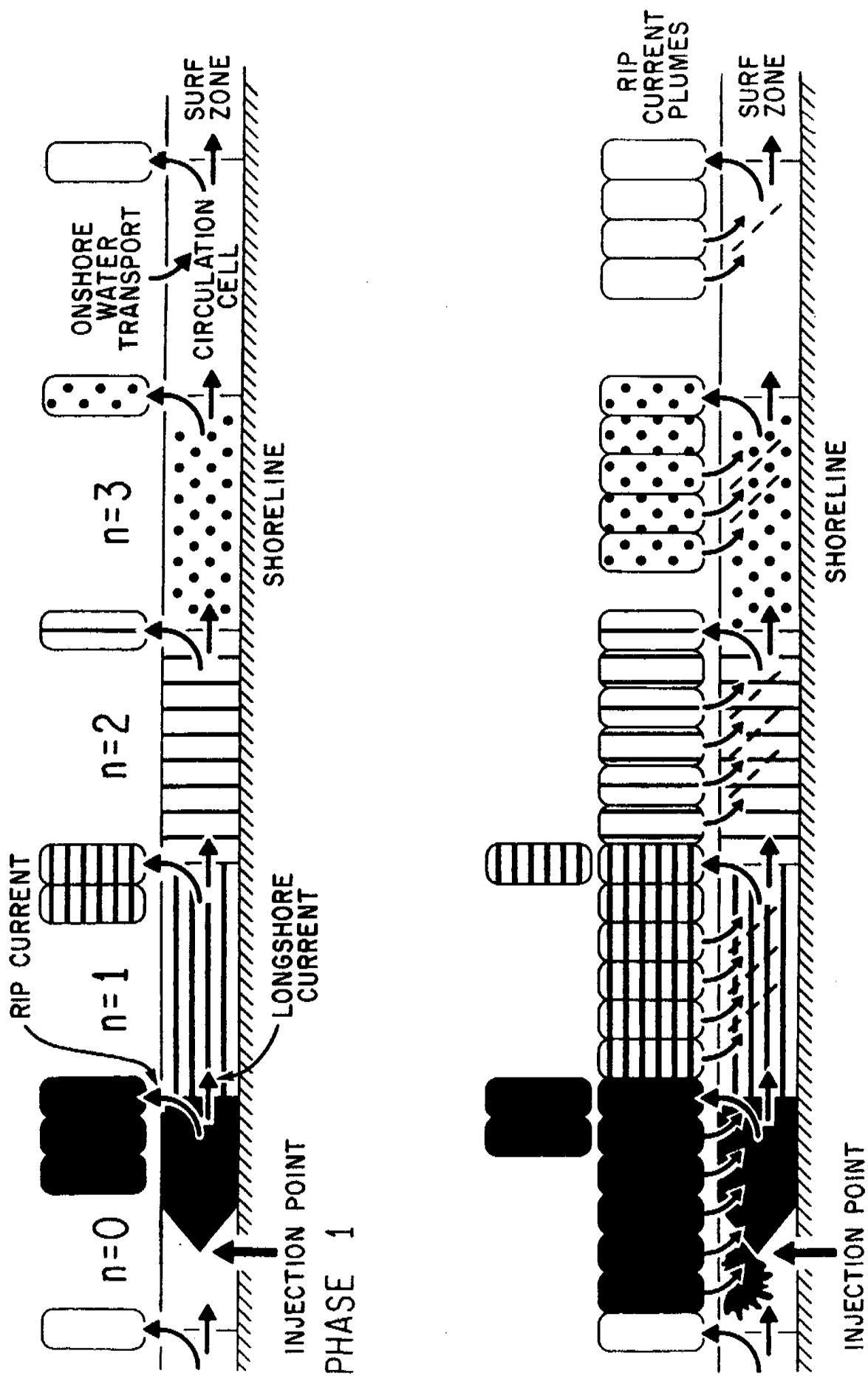


Figure 8.1. Schematic of dilution by rip cell mass transport of pollutants entering the surf zone from a shoreline source [after Inman et al., 1971].

of marsh water, bacteria remain largely confined near the shoreline by the rip current circulation cells. The rip current cells trap the contamination in recirculation loops between the offshore rip heads and the surfzone as shown by lower panel in Figure 8.1. Each rip cell extends only a few surfzone widths seaward of the break point. Consequently, the contamination disperses primarily in the longshore direction and mixes seaward over distances of no more than 3 or 4 surfzone widths (Inman et al., 1971).

Orange County Sanitation District monitors bacteria levels in Talbert Marsh and adjacent beaches in Huntington and Newport Beach (OCSD, 2001). The maximum recorded total coliform counts in the marsh are on the order of 10^5 mpn/100 ml. We use this bacteria level in a worst case modeling scenario that will consider the release of 100 million gallons from the marsh in a single tidal flush during dry weather summer conditions. We further consider ocean conditions for a summer El Niño with large south swells and nearshore transport directed northwestward toward AES Huntington Beach. For this purpose we use the historic wave and currents conditions for the southern swell event of 7-10 August 1997 (Figures 3.12, 3.19, 3.20 in Section 3). We calculate the dispersion of the total coliform bacteria over a 3-day period assuming no mortality in the bacteria population, to give a worst case assessment of the possibility for being ingested by the AES infall. The bacteria are treated as a neutrally buoyant micron-sized particle in the subroutine **NULLPT** of the model (Figure 2.1 in Section 2).

B) Results

Figure 8.2 through Figure 8.4 give the depth averaged dilution factors for the marsh water over the effected coastline surrounding the Talbert Marsh during a 3 day period following the initial breach of the inlet barrier spit by the south swells

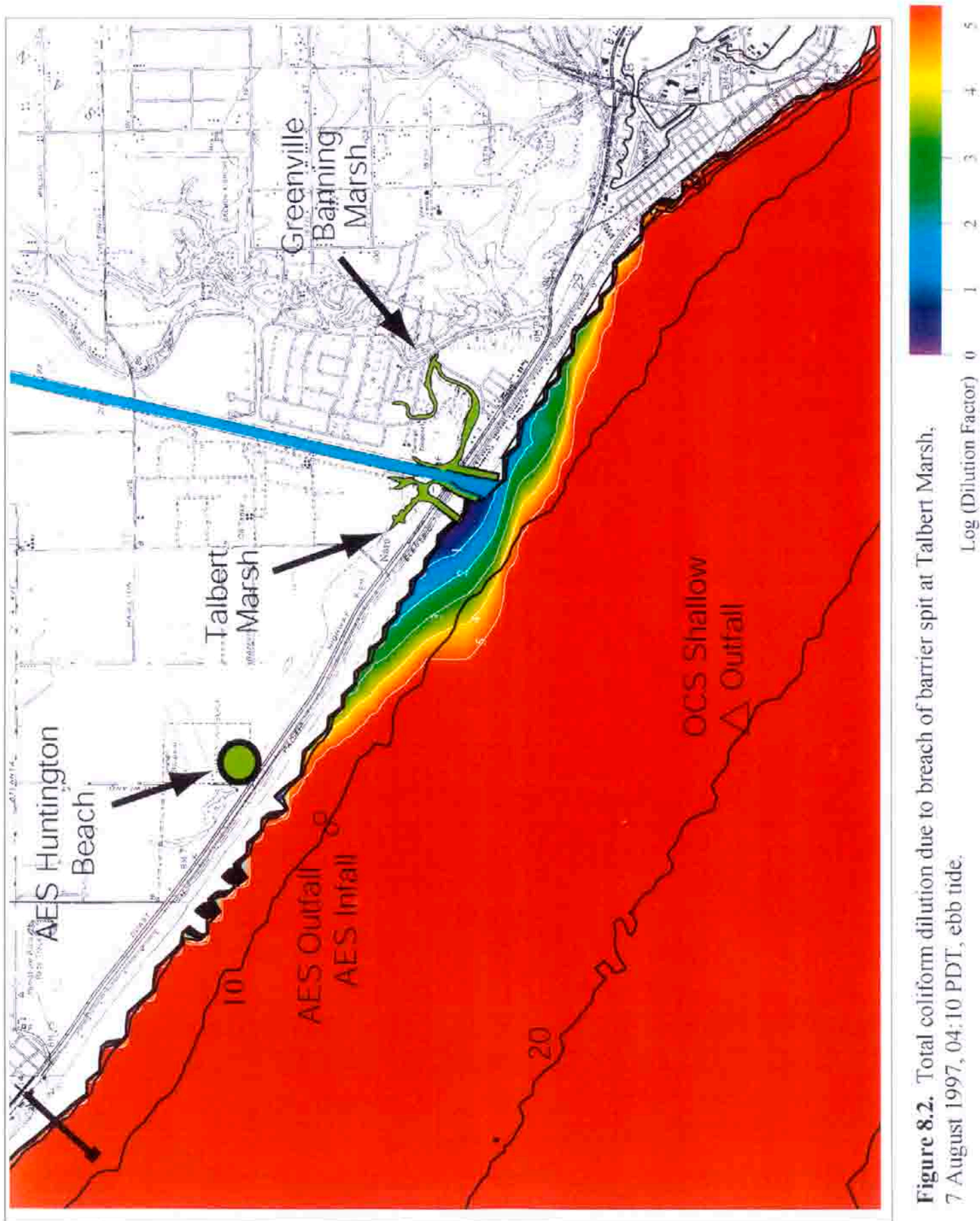


Figure 8.2. Total coliform dilution due to breach of barrier spit at Talbert Marsh, 7 August 1997, 04:10 PDT, ebb tide.

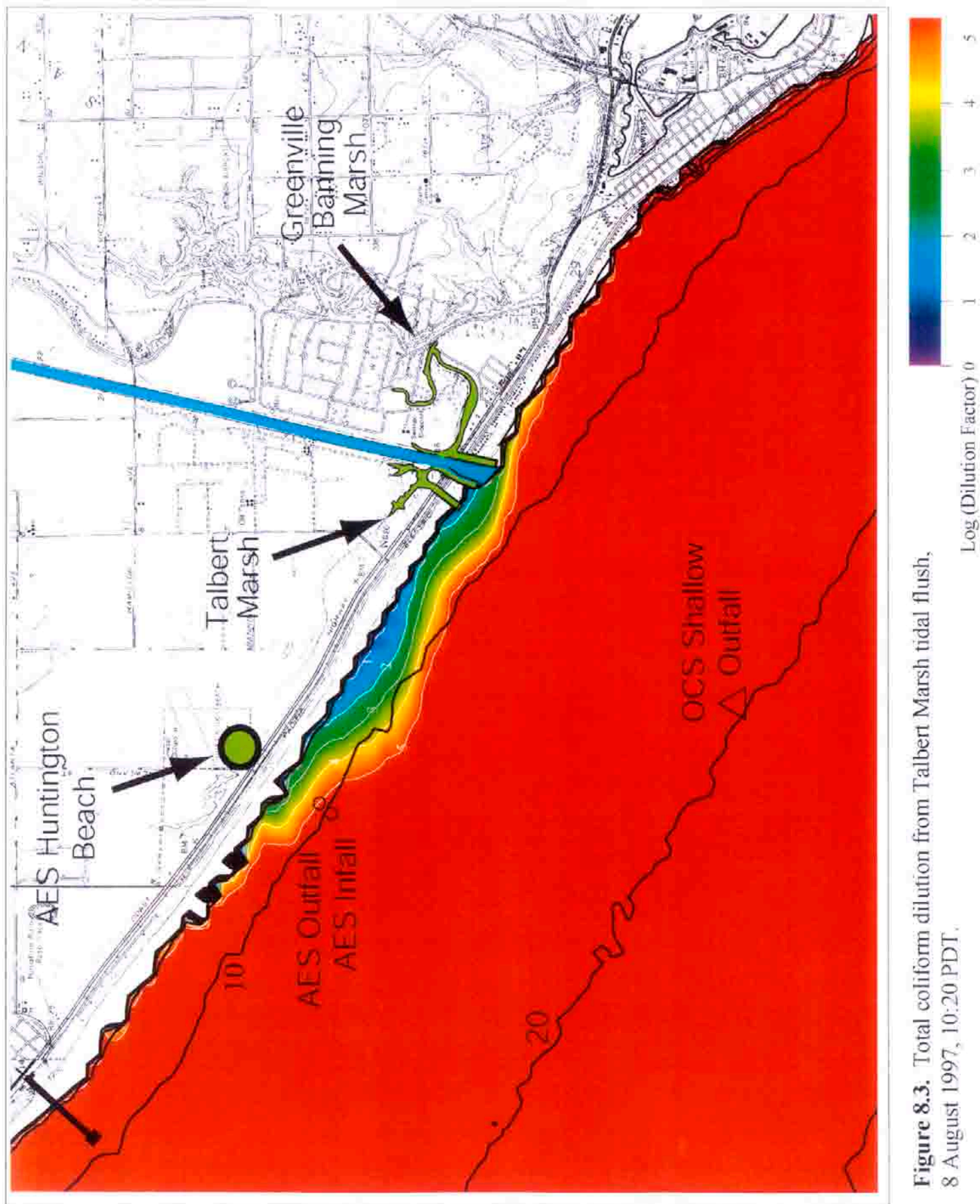


Figure 8.3. Total coliform dilution from Talbert Marsh tidal flush, 8 August 1997, 10:20 PDT.

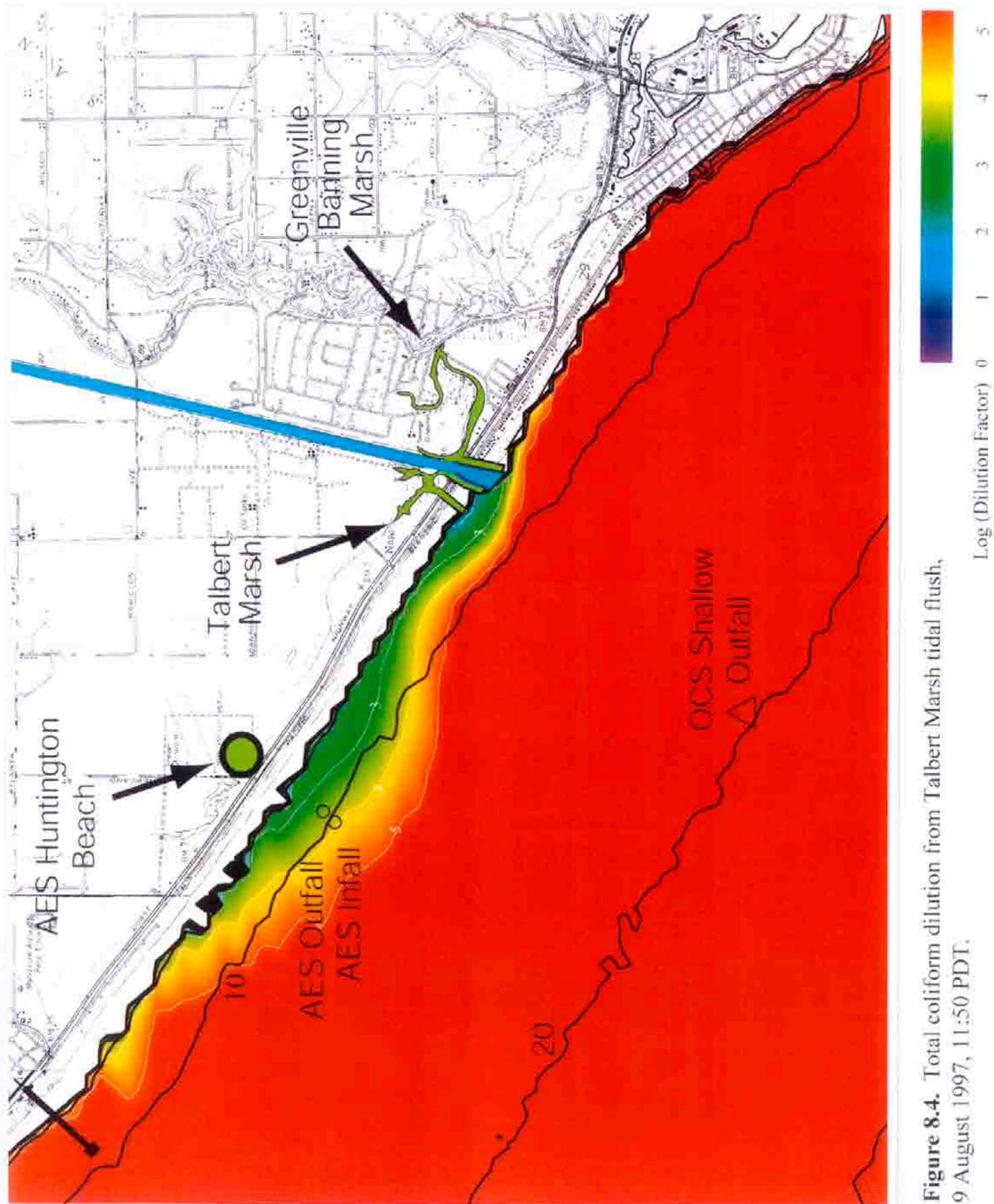


Figure 8.4. Total coliform dilution from Talbert Marsh tidal flush, 9 August 1997, 11:50 PDT.

of 7 August 1997 (Figure 3.12 in Section 3). The marsh water disperses progressively upcoast over the following 3 days as the discharge moves with the north-westward flowing littoral drift induced by the south swells. We find at the offshore location of the AES infall that the contaminated marsh water is diluted by at least 20,000 to 1 over this period. These high dilution factors are a consequence of three factors: 1) the infall is located offshore where deeper water depths afford large dilution volumes, 2) the infall is at a sufficiently large distance from the marsh source, and 3) the onshore fluxes of wave energy and re-circulation by rip cells keep the marsh water confined to the shallow water of the surf zone where dilution volumes remain low. Because the marsh discharges directly into the surf zone, the latter factor explains why coliform counts remain highest in the shallowest water nearshore.

The corresponding total coliform counts caused by the release of 100 million gallons of marsh water having total coliforms of 10^5 mpn/100 is shown in Figure 8.5 thru Figure 8.7. We find that total coliforms released by the marsh reach counts a maximum of 8 mpn/100 ml at the AES Huntington Beach infall during the 3 day period after the initial breaching of the inlet. However in the inshore domain, total coliform counts can range from 10^2 to 10^4 along the shoreline between the generating station and the Talbert Channel. This inshore patch of high coliform counts moves progressively north-westward with the most persistent hotspot in the dispersion occurring at the OCSD sample station #9N near the AES powerplant. The high total coliform counts decay rapidly in the downcoast direction (toward Newport) due to the net transport in the nearshore being directed north-westward during summer El Niño conditions (Figure 3.19 in Section 3). The results in Figures 8.5-8.7 are consistent with total coliform counts

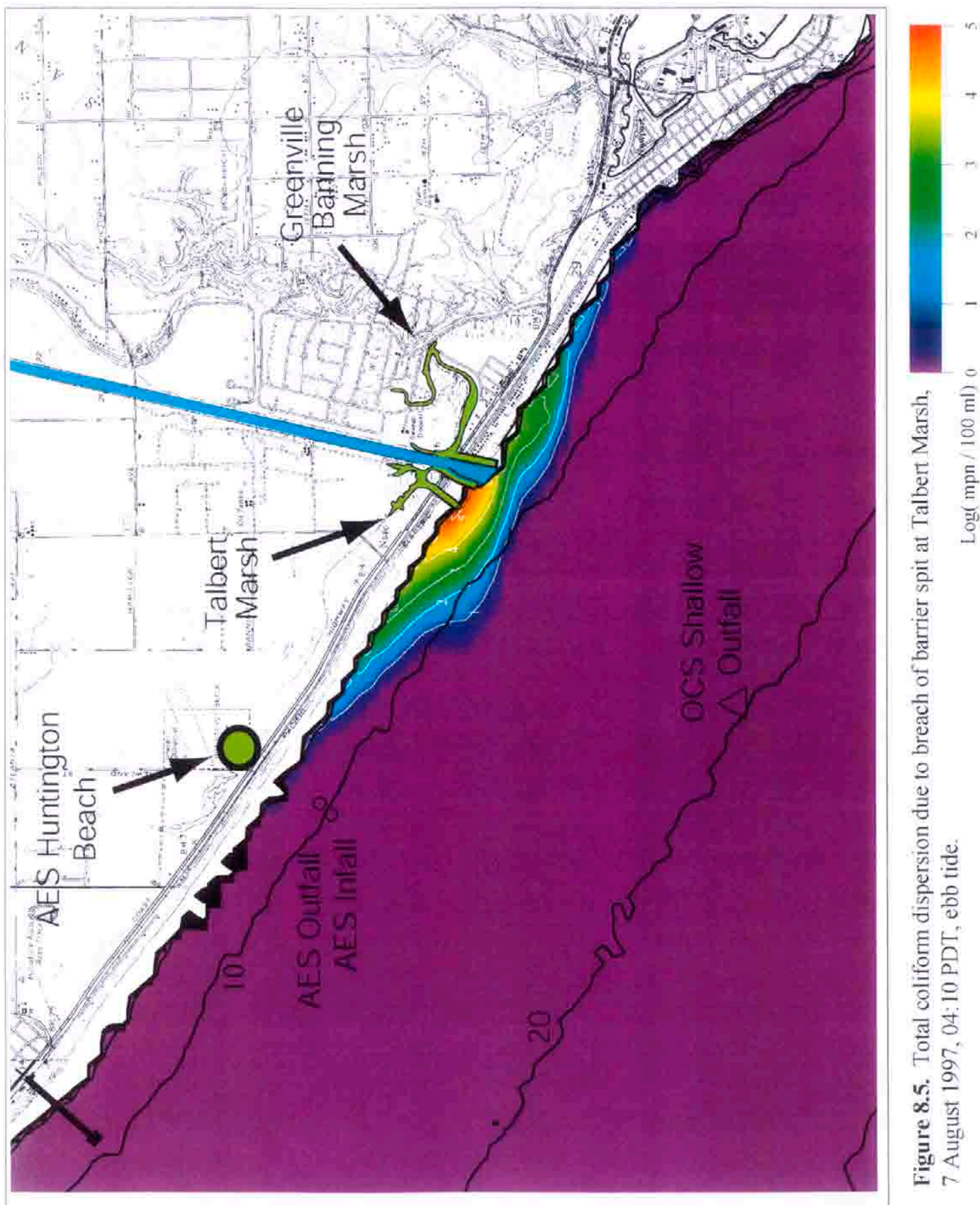


Figure 8.5. Total coliform dispersion due to breach of barrier spit at Talbert Marsh, 7 August 1997, 04:10 PDT, ebb tide.

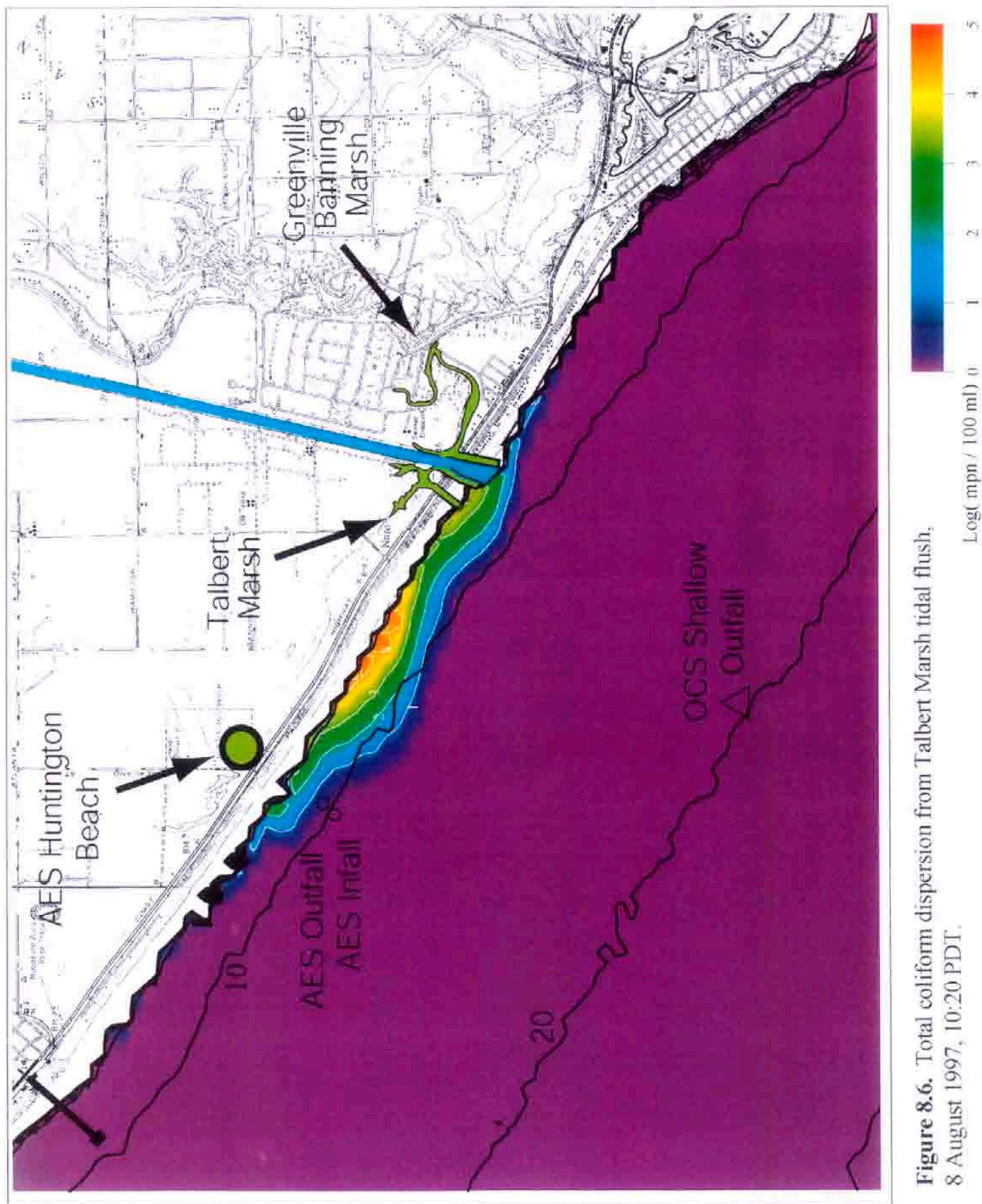


Figure 8.6. Total coliform dispersion from Talbert Marsh tidal flush, 8 August 1997, 10:20 PDT.

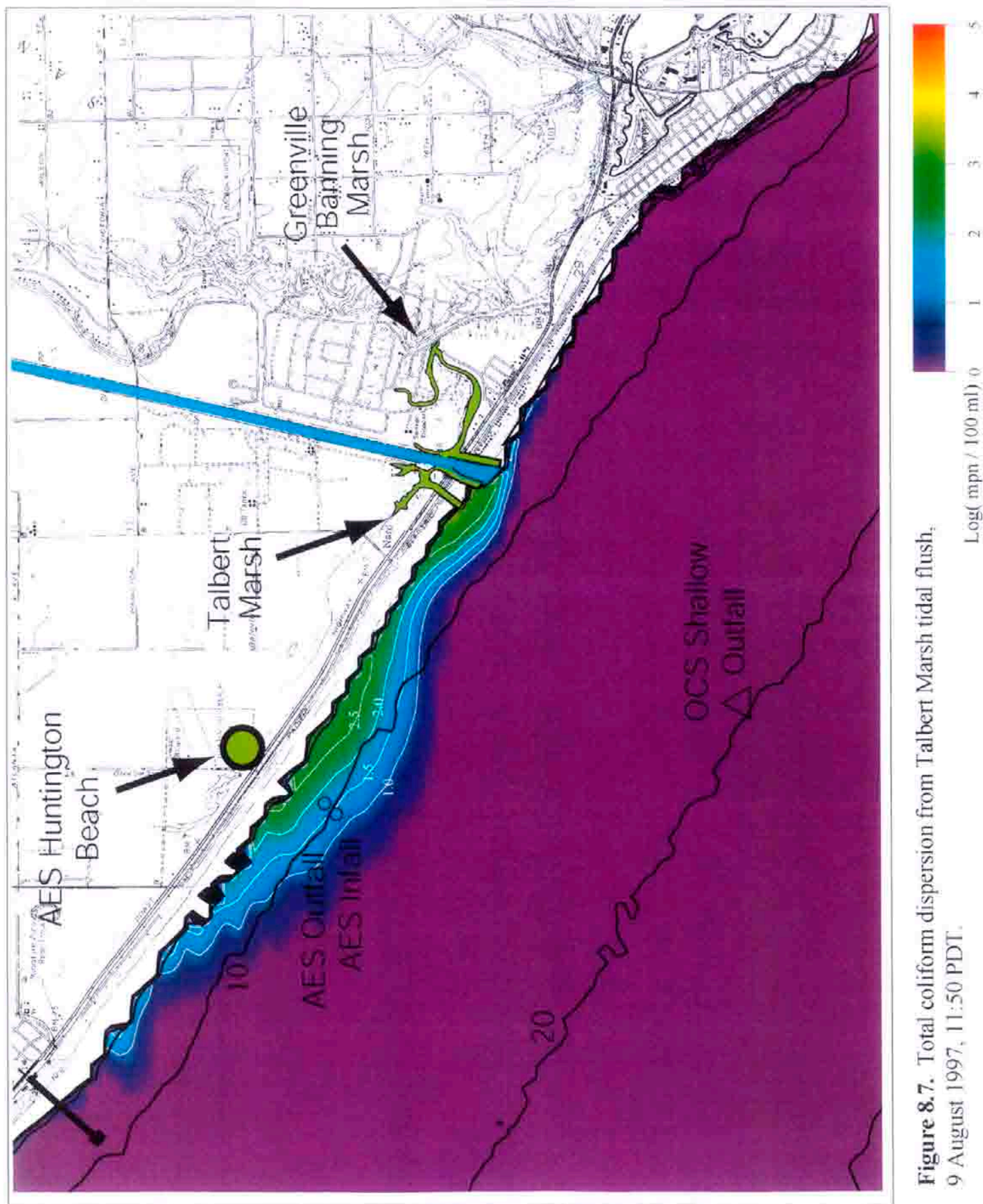


Figure 8.7. Total coliform dispersion from Talbert Marsh tidal flush, 9 August 1997, 11:50 PDT.

measured along these beaches during summer months by Orange County Sanitation District (OCSD, 2001). These findings have more recently been confirmed by high sample rate field measurements of dye and indicator bacteria released at the Talbert Channel and Santa Ana River jetties (Grant, et.al., in press).

Figures 8.5 thru 8.7 show that high coliform counts in the shallow wading depths of the surf zone do not imply high coliform counts in the offshore waters around the infall and discharge of the AES Huntington Beach generating station. It must be emphasized that the AES outfall is not in the surfzone. The water depth around the outfall is about -28 ft MSL, which could only be the surfzone if the waves were 36 ft high. Plant-induced currents decay rapidly with distance and are too weak to push water all the way to the shoreline. This does not mean that there is absolutely no exchange of water by other (natural) processes, in particular: wind drift, wave and tidal current mixing, rip cell circulation, mass transport in the wave boundary layers and shoaling internal waves. However, none of these processes are very effective shoreward transport mechanisms. The reasons for this are that the on/off-shore directed fluxes from these processes are discontinuous between the surfzone and the offshore and all shoreward directed motion has to stop at the beach. There is no current system that provides an uninterrupted pathway between the shoreline and the offshore area around the AES outfall. The onshore directed mass transport of the wave boundary layers is weak (second order) and is arrested near the break point by the action of wave breaking and by opposing under-tow currents in the surfzone; while the rip-cell currents extend only a few surfzone widths beyond the wave breakpoint. The AES outfall is well seaward of the surfzone and mixing or wind drift are the only persistent process that can bridge the gap in the discontinuous on/off-shore current pathways. Shoaling internal waves

that reach the surfzone are episodic and relatively rare, and when they do occur, the longshore current typically flows downcoast (toward the southeast) transporting AES discharge away from the chronic hot spots at 9N. As a result the exchange of water between the AES outfall and the shoreline is small (but not zero) and the dilution that occurs during that exchange is rather substantial. The recently completed CEC study (KOMEX, 2003; Jones and Major, 2003) found that dye discharged from the AES outfall is diluted by a minimum of 36 to 1 at the shoreline. Minimum dilution of AES discharge calculated by the hydrodynamic model study (low flow case in Section 4) was found to be 32 to 1 at the shoreline (see Figures 4.6 & 4.8). Thus the model results derived two years before the KOMEX field study appear to be well confirmed. Both studies conclude that even for worst case scenarios, the dilution associated with the AES outfall is sufficiently large that it can not account for the high bacteria levels measured at the shoreline. Moreover, typical shoreline dilutions of AES effluent average 190 to 1, (Figure 4.8 and Table 6, Section 4), making the generating station effects on surf zone pollution even more unlikely.

SECTION 9: Wastefield From OCSD Deep Outfall

9) Wastefield From OCSD Deep Outfall

A) Initialization

The outfalls for the Orange County Sanitation District Treatment Plant No. 2 are located offshore of the mouth of the Santa Ana River. The deep outfall is at 33°34'36"N, 118°00'36" W indicated by the inverted triangle in Figure 1.3 (OCSD, 1999). The shallow 78" emergency outfall is indicated by the regular triangle in Figure 1.3 located at 33°36'56"N, 117°58'13"W. The emergency outfall has never been operated since construction of the deep outfall, and will therefore be omitted from any analysis herein. The deep outfall of the OCSD Treatment Plant No. 2 is located on the broad shelf region of the Newport Coast at a depth of 195 ft (59 m). This discharge depth is well below the inter-annual maximum depth excursions of the surface mixed layer. The 120" diameter deep outfall has a certified maximum discharge rate of 480 MGD, and achieves an initial dilution at its diffusers of 148 to 1 (see OCSD, 1999).

For these initial dilutions, effluent from the deep outfall will rise vertically in the water column no higher than the pycnocline (thermocline), where the discharge plume will subsequently “pancake,” spreading laterally but unable to rise into the warmer, more buoyant waters of the surface mixed layer (Figure 9.1). Ocean temperature monitoring of the nearshore waters around the outfall indicate that the typical inter-annual variation in the mean thermocline depth is between -15 m and -30 m MSL (OCSD, 1993, 2000). On the other hand the infall for the Huntington Beach Generating Station is located 5.6 m below the mean ocean surface and is therefore usually above the thermocline in the surface mixed layer. Under normal oceanographic conditions the generating station infall and OCSD deep outfall remain segregated in two different water masses by ocean

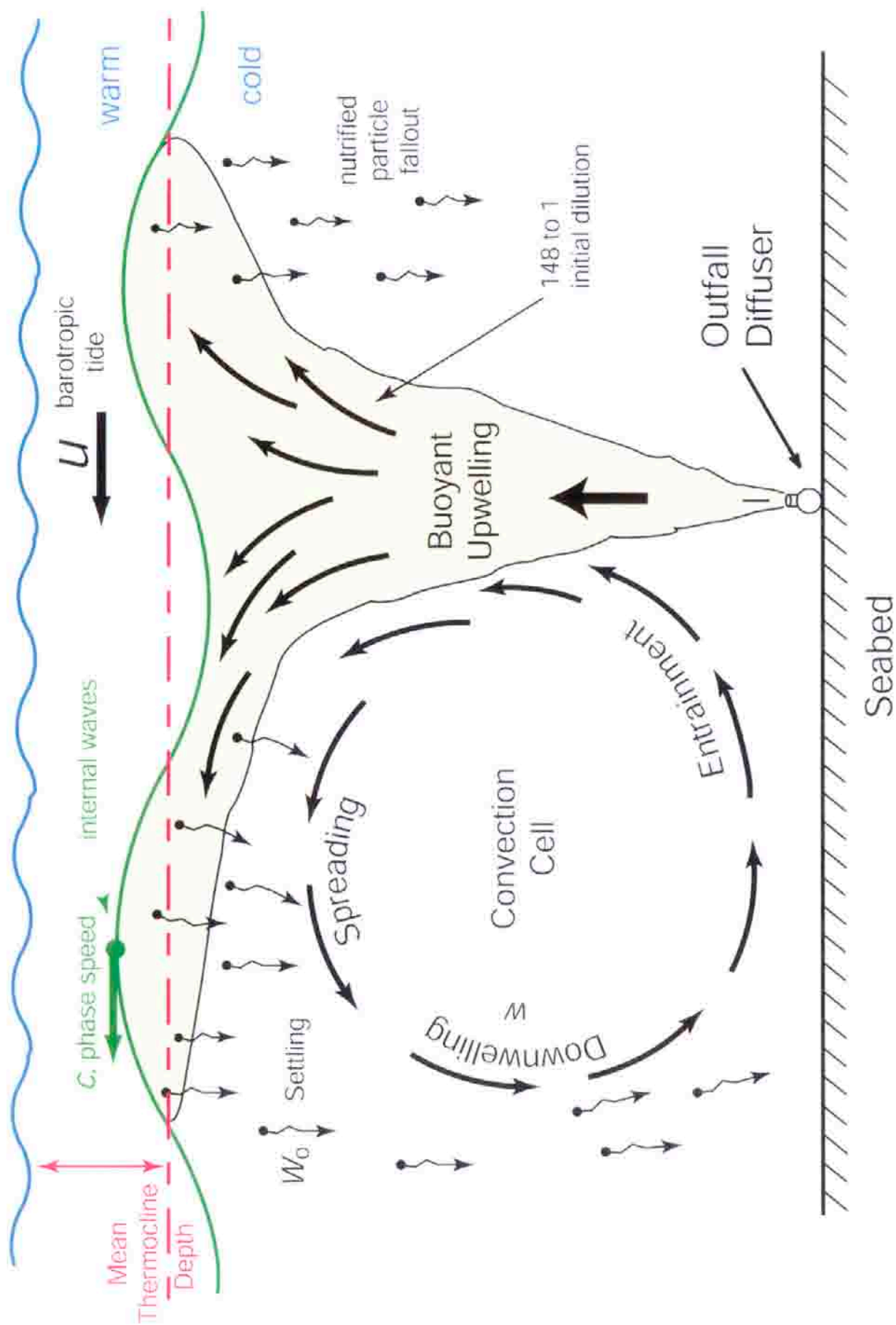


FIGURE 9.1. Schematic diagram of convection cell set up by the rising buoyant plume of treated sewage effluent from the OCS deep outfall diffuser.

stratification with no appreciable exchange between those water masses.

Furthermore, currents over the middle shelf are typically ebb dominated with a net mass transport downcoast to the southeast (Figure 3.16 in Section 3). Therefore discharges from the outfalls of the OCSD Treatment Plant No. 2 are normally advected **away** from the infall of the Huntington Beach Generating Station by the predominant wave and tidal transport.

In this section we simulate a combination of atypical conditions that would provide the maximum likelihood scenario for the dispersion of the OCSD wastefield toward the AES infall. These conditions include:

- 1) Discharge from the OCSD deep outfall at maximum rate certified under NPDES permit restrictions (480 mgd);
- 2) A shallow thermocline depth such that the velocity cap of the AES infall is periodically below the thermocline in the presence of internal waves;
- 3) A current regime with net transport directed upcoast toward the northwest;
- 4) End of pipe total coliform counts at the mid to high end of operational ranges prior to OCSD disinfection resolution, (OCSD, 2002)

5) AES Infall operating at maximum flow rate (506.9 mgd), with maximum certified intake velocity of 2 ft/sec (NPDS Permit, CRWQCB, 1993). Conditions (1) and (4) maximize source loading and bacterial emissions from the OCSD outfall, (even though OCSD has been disinfecting its discharge since 2002). Condition (2) allows the infall to draw from the same water mass as the wastefield by placing the infall under the density discontinuity that caps the rise of wastefield. Condition (3) provides for current advection from the OCSD outfall toward the AES infall. The

simultaneous occurrence of these atypical conditions is extremely rare because they tend to be mutually exclusive. For instance, the reversal of the net coastal transport (3) is more common during an El Niño, while the shallow thermocline depth is a summer La Niña condition (Section 3). The operation of the outfall at the maximum certified discharge rate of 480 mgd (1) is primarily a wet weather, winter time procedure resulting from the infiltration of surface runoff into the sewer conveyance system, (OCSD, 1999). On the other hand, coliform levels in the discharge typically reached maximum values (prior to adopting the disinfection resolution) in the summer when discharge rates and in-the-pipe dilution volumes are lowest. If we treat these factors as independent variables with the El Niño and La Niña return periods of 3 to 7 years and the remaining factors as annual, then the simultaneous occurrence of these atypical conditions is no less than a once in 9 year event, and perhaps as rare as a once in 49 year event. Because the probability for these conditions all happening together is low, the persistence of this combination is also probably quite low. In addition, the maximum flow rate condition for the AES infall (5) is a hot weather, high user demand condition and is specified concurrent with conditions (1-4) to examine if there is any likelihood of the suction flow of AES entraining or drawing the OCSD wastefield towards the shoreline. We stress that the intent here of evaluating these often mutually exclusive aggravating conditions is to determine if under any conceivable circumstance the wastefield from the OCSD might be ingested by the AES generating station infall and thereby impact the log-r requirements of the RO membranes to be used by the desalination plant.

To initialize the model for the simultaneous occurrence of these atypical conditions, we use wave and tidal currents from the El Niño summer events of

August 1997. The south swells of 7 August 1997 with 2.2 m deep water wave heights from 190° (Figure 3.12 in Section 3) are combined in the model problem with the Perigean Spring tides of 17 August 1997 (Figure 3.20 in Section 3). Together this combination of events produces the strongest possible reversal of net transport toward the northwest in both the nearshore and middle shelf regions surrounding the OCSD outfall and the city of Huntington Beach. The mean thermocline depth was set at -10 m MSL. Temperature above the thermocline was set in the model at 20° C and at 15° C below the thermocline. This assignment poses a strongly stratified two-layer system in which mass transport by internal waves will be maximized (Figure 9.1). The OCSD outfall was set to discharge at 480 mgd with end-of-the-pipe total coliform counts varied between 10^7 to 10^8 mpn/100 ml. Ambient ocean background coliform levels were set at 0 mpn/100 ml.

B) Results:

Figure 9.2 shows the suction velocity at the depth of the infall velocity cap (-5.6 m MSL) induced by the AES infall while operating at maximum flow rate (506.9 mgd). Intake velocities are 61 cm/sec at the velocity cap of the infall. However, suction velocity decays rapidly with increasing distance away from the infall tower (where the decay rate is proportional to the inverse of the square of the distance from the infall). Consequently, suction velocity decays to 0 (0.1 cm/sec) beyond the 15 meter depth contour, and is only 0.0015 cm/sec at the OCSD outfall. On the other hand the onshore velocity component of induced by internal waves was found to range from 5 to 10 cm/sec while the longshore velocity component of the barotropic tides ranges from 10 cm/sec to 50 cm/sec depending on cross-shore position on the shelf (see Figure 3.20 in Section 3). Therefore, at

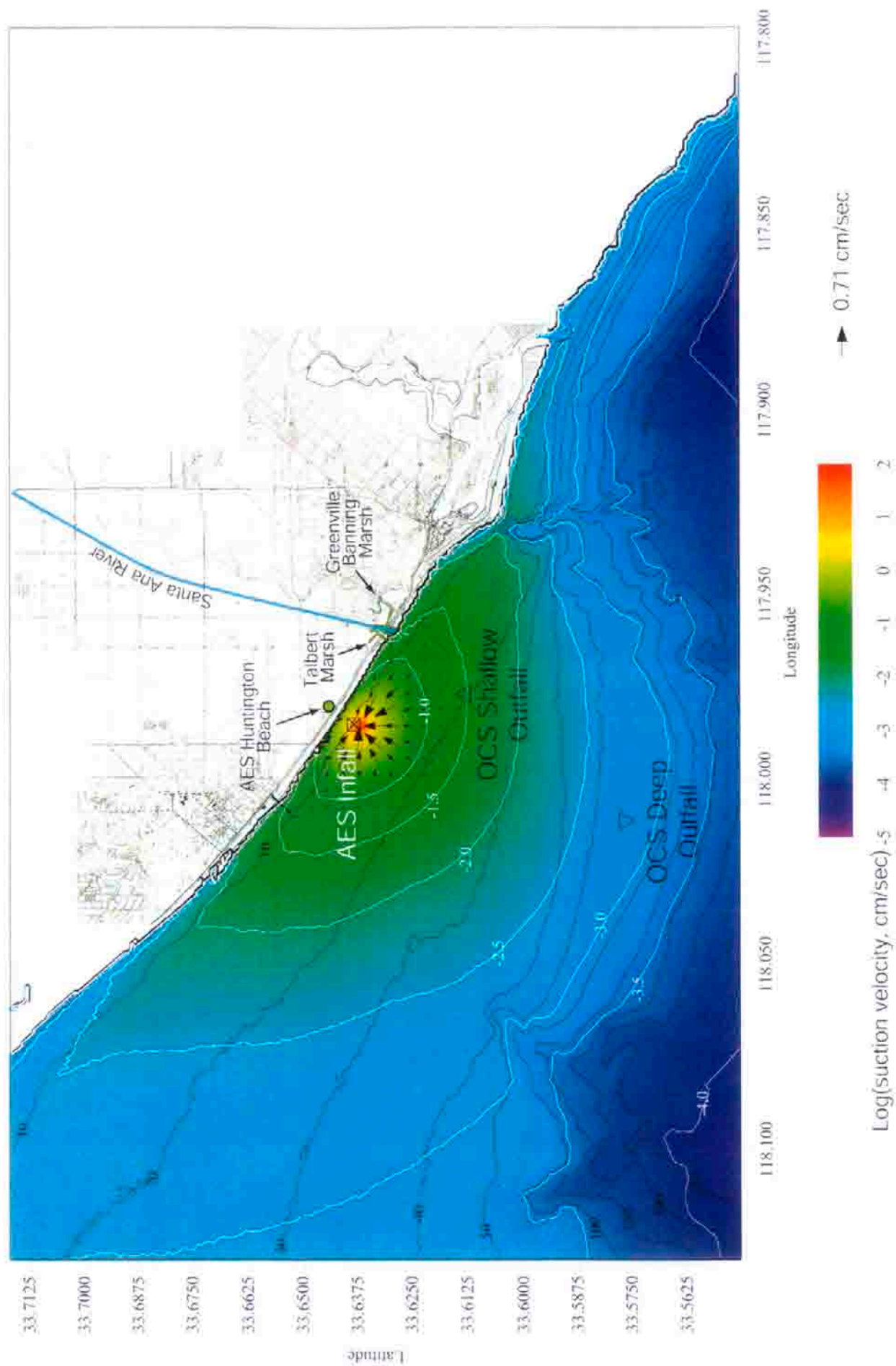


Figure 9.2. Suction velocity field due to AES Infall at maximum flow rate (506.9 mgd). Contours of Log (suction velocity) in cm/sec with progressive vectors relative to scale arrow (lower right corner).

any distance beyond 50 m from the infall, the AES suction velocity is insignificant in comparison to natural transport by the internal waves and barotropic tides.

Figure 9.3 gives a 6 hour average during flood (rising) tide of the dilution field of the OCSD wastefield for these worst case conditions derived from combining the south swells of 7 August 1997 with the spring flood tides of 17 August 1997. The dilution factors for the wastefield are plotted at the depth of the infall velocity cap (-5.6 m MSL). Dilution factors are contoured on a log10 scale. Inspection of Figure 9.3 indicates that the wastefield is diluted to about 30 million to 1 at the AES infall. In general, the shape of the dilution field in Figure 9.3 suggests that the wastefield predominantly moves parallel to the depth contours in the direction of transport of the barotropic tide during the flood tide phase (towards the northwest). This result is consistent with OCSD (1993). In the mid to inner shelf regions, the dilution field shows a rather complex structure associated with the refraction pattern of the shoaling internal waves computed by parabolic equation methods applied to the mild slope equations, (see discussion of the **OCEANRDS** model in Section 2). These waves produce shoreward directed transport during flooding tide with amplitudes that were found to vary typically from 3-5 m. In regions where refraction induced locally higher wave amplitudes, the wastefield is raised higher in the water column resulting in a zone of diminished dilution. Similarly in regions where internal wave refraction produces locally small wave amplitudes, the thermocline remains below the depth of the AES infall velocity cap and the dilution factor at infall depth is high. A particularly active area for shoaling of these internal waves is the Newport Canyon, where internal wave amplitudes were found to be as large as 8 m, raising the thermocline to within 2 m of the sea surface and forming a band of low

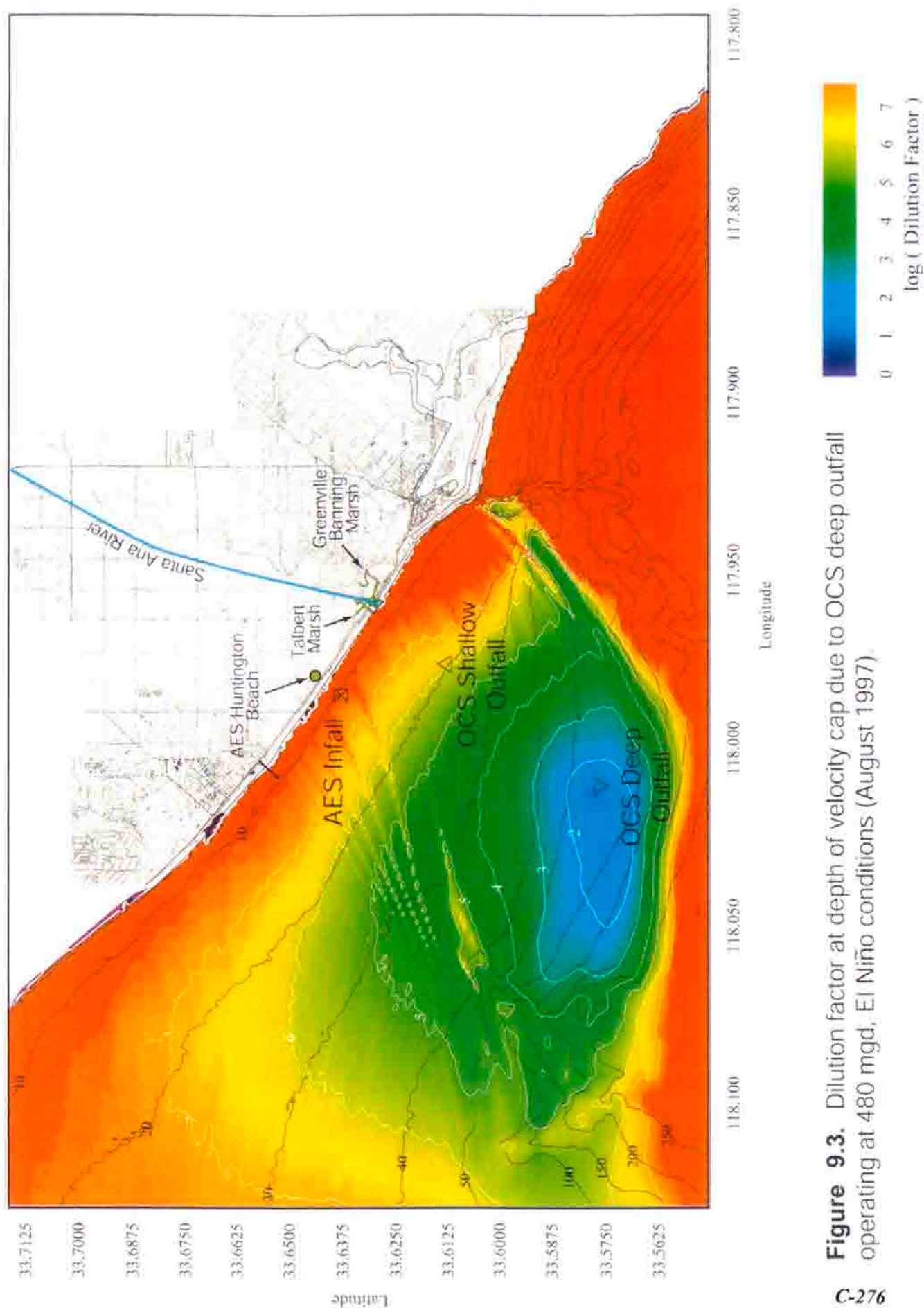


Figure 9.3. Dilution factor at depth of velocity cap due to OCS deep outfall operating at 480 mgd, El Niño conditions (August 1997).

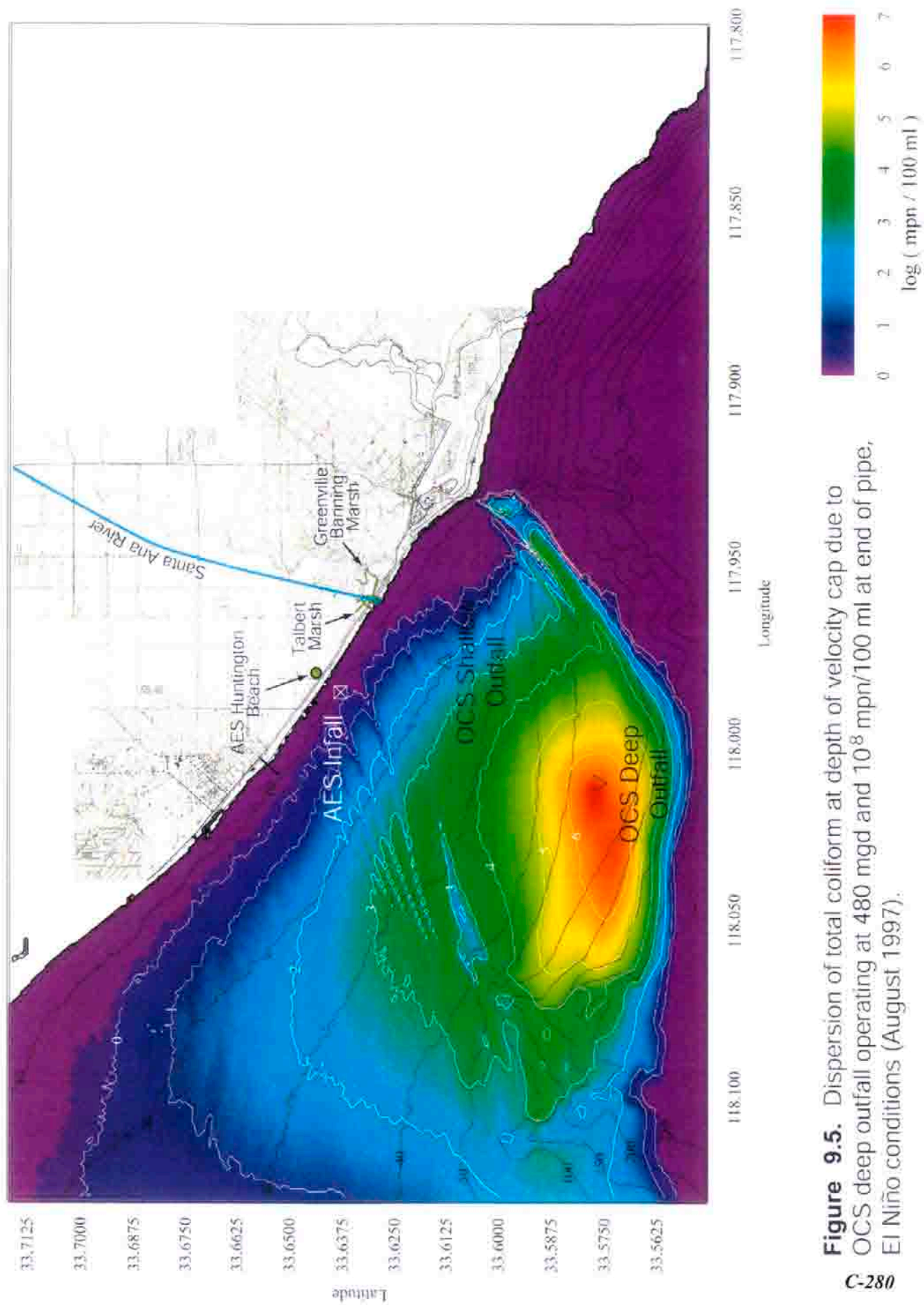
dilution contours $0(10^4)$.

The dispersion of total coliform bacteria from the OCSD outfall (assuming no disinfection) is contoured in Figure 9.4 based on mid-range end-of-the-pipe concentrations of 10^7 mpn/100 ml. Because it is not sensible to count a fraction of an organism, the edge of the wastefield is found in Figure 9.4 to advance no closer to the shoreline than the 15 meter depth contour in front of the AES Huntington Beach generating station, consistent with OCSD (2000). Total coliform counts at the AES infaill are found to be non-detectable. We note that the closest the wastefield gets to the shoreline is at the head of the Newport Canyon, about 500 m (1500 ft) from the shoreline.

When the OCSD outfall discharges at maximum flow rates without disinfection at the high-end total coliform levels (10^8 mpn/100 ml), see Figure 9.5, we find that the edge of the wastefield is just offshore of the AES infaill. In this case, perhaps 1-3 mpn/100ml total coliforms from the OCSD outfall might be found at the AES infaill. However, these counts would be indistinguishable from the ambient ocean background and are therefore neither significant nor detectable. Furthermore, this outcome is not persistent, having a duration of 1/2 of a semi-diurnal tidal cycle (6 hr 12.5 min). With the ensuing ebb tide, the longshore currents of the barotropic tides reverse from what is shown in Figure 3.20 in Section 3 and begin flowing downcoast to the southeast while the crossshore component of the internal waves flows offshore, thereby advecting the wastefield away from the AES infaill.

Shoreward transport of micro-organisms by internal waves has been reported in the literature (Pineda, 1991 and 1999). However, these observations have not demonstrated transport reaching the shoreline from an offshore deep-water point

source as distant as 7 km, such as the OCSD outfall.



SECTION 10: CONCLUSIONS

10) Conclusions

Hydrodynamic modeling of water mass dilution and dispersion was performed in a nearshore domain surrounding the HBGS which extends seaward to the edge of the continental shelf and alongshore from Seal Beach to Crystal Cove State Beach. (The model was developed at Scripps Institution of Oceanography for the US Navy's Coastal Water Clarity Program, was thoroughly peer reviewed, and has been calibrated and validated in numerous applications throughout the Southern California Bight). The model studied the ocean response to the proposed 50 mgd desalination plant using two separate modeling approaches: 1) event analyses of theoretical extreme cases, and 2) continuous long term simulations using the historical sequence ocean and plant operating variables. The latter approach was applied to two distinct historical periods: one resulting in 7,523 modeled solutions between 1980 and mid 2000 that characterized the period before HBGS was re-powered; the other involving 578 modeled solutions that characterized the post re-powering period using data collected between 1 January 2002 and 30 July 2003.

The event analysis involved some potential situations for operating the desalination plant when the generating plant is in *standby* mode and not producing electricity, or when it is operating at very low generating levels. We refer to these as "*low flow cases*" and they produce the highest in-the-pipe concentrations of sea salts from the desalination process. The most extreme of these low flow cases occurs when the generating plant is in *standby* mode and is providing no heating of the discharge water. The term "standby mode" broadly refers to a condition when the generating station is spinning an arbitrary collection of pumps with unheated discharge. But, not all possible combinations of pumps during "standby mode" are

adequate for the desalination plant to produce product water at a rate of 50 mgd. We consider only those cases of standby mode when at least two circulation pumps are on-line (producing 126.7 mgd), because a minimum flow of 100 mgd is required to produce 50 mgd of product water. (No other pump combinations are available within the hydraulic architecture of the generating station that will provide flow rates between 100 mgd and 126.7 mgd). These low flow and standby mode cases are evaluated in combination with extreme conditions in the ocean environment involving tranquil, dry weather, La Niña type summer climate. By superimposing two conditions that seldom occur together (low plant flow cases and a calm ocean) the maximum potential impact of the desalination plant on the local ocean environment can be assessed because the dose level of sea salts is highest when the dilution of those salts by mixing and ventilation is lowest. The event analysis also evaluated an “*average case*” based on seasonal mean ocean conditions and average plant flow rates to determine the most likely degree of dilution of desalination plant discharge in nearshore waters.

Numerical modeling of the dilution and dispersion of concentrated seawater discharge from the proposed desalination plant has found that salinities of the receiving water become elevated above mean seawater salinities near the bottom in the immediate neighborhood of the outfall, and only then, when a number of extreme environmental and plant operating conditions occur simultaneously. Between 1980 and mid 2003, the low flow case resulting from only one generating unit being on line occurred 37% of the time while the unheated standby mode accounted for less than 1% of the occurrences. On the other hand, the occurrence of the ultra-benign environmental extremes is about 1 week every 3 to 7 years, primarily in summer during strong La Niña conditions. The joint probability for the

simultaneous occurrence of these operating and environmental extremes is between 0.27% and 0.64% for the low-flow cases involving active power generation, and between 0.04% and 0.1% for the standby mode, depending on the length of ENSO cycles. In the model simulation of low flow case, these conditions were extended over 30 days, so that the recurrence interval for the low-flow results of this study are actually about 1 month every 13 to 31 years. The extreme operational conditions of the generating plant (low power generation and cooling water consumption) are mutually exclusive with these extreme environmental conditions. Because of this, dilution and dispersion of the concentrated seawater by-product were repeated using more nominal plant operating conditions and average climate conditions. Based on historical data representative of these conditions, the study made the following findings regarding dilution and dispersion of concentrated seawater by-product.

Dilution and Dispersion Before Completion of HBGS Re-Powering:

The dilution and dispersion results for the vent analyses are summarized in Table 6. Maximum event impacts during the low flow conditions produce an initial vertical jet of high salinity water that breaches the surface and subsequently sinks to the seafloor, spreading outward from the base of the outfall tower. The highest salinities in the core of the discharge jet are 55.0 ppt at mid-depth (Figure 4.1), falling to 50.1 ppt on the sea surface directly above the outfall tower (Figure 4.2). The highest salinities on the seafloor are 48.3 ppt at the base of the outfall tower, rapidly decreasing with increasing distance from the tower (Figure 4.3). At most, 15.6 acres of benthic area are impacted by an increase in salinity that exceeds 36.9 ppt, that is 10% above the average ambient level of 33.5 ppt. Bottom salinities

exceed ambient levels by more than 1% over an area of 263 acres. These elevated salinities effect only sandy, soft bottom habitat with no low relief exposed rocky substrate, and no surf grass or eel grass beds. The maximum area of pelagic habitat subjected to elevated salinity exceeding 10% of ambient is 18.3 acres while 151 acres of pelagic habitat experience an increase in salinity exceeding ambient by more than 1%. Minimum dilution of the concentrated seawater by-product at the shoreline is 32 to 1, (Figure 4.6) consistent with dye measurements from the recent study commissioned by the California Energy Commission (KOMEX, 2003). Two percent of the concentrated seawater by-product may be re-circulated in a sustained low flow case.

Dispersion and dilution contours of sea salts for the theoretical extreme of the standby mode are very similar to those shown in Figures 4.1 through 4.6. The absence of power plant heat produces a heavier combined discharge that is more slowly assimilated by the receiving waters. As a result, Table 6 indicates that the impacted benthic area around the outfall is marginally increased during standby mode to 18.2 acres, while the impacted pelagic area increases to 20.1 acres.

For average case events, the salinity in the water column directly above the discharge tower reaches 41.7 parts per thousand, (Figure 4.9), dropping to 38.3 ppt on the sea surface above the outfall tower (Figure 4.10). Maximum salinity on the sea bed is 37.6 ppt at the base of the outfall structure (Figure 4.11). The maximum area of benthic habitat subjected to a 10% increase in salinity is only 6.8 acres, while the area of pelagic habitat experiencing a similar increase is 8.3 acres. The benthic footprint of the 1% saline anomaly is 172 acres and the pelagic footprint is 130 acres. Except for the initial core of the discharge jet salinities under average conditions are everywhere within the range of natural variability. The percentage

of re-circulated concentrated seawater by-product under average conditions is only 0.7%. Minimum dilution of the raw concentrate at the shoreline is 190 to 1 (Figure 4.14).

In vertical cross sections through the outfall in the cross-shore and longshore directions, the numerical hydrodynamic model finds that the saline plume emitted from the combined flows of the generating plant cooling water and the concentrated seawater of the desalination plant consists of a higher saline core between the surface and the bottom surrounded by a broad-scale salt wedge feature with weakly elevated salinities. The high-salinity core is formed in the immediate vicinity of the outfall by a jet of combined effluent discharged vertically upward from the top of the outfall tower. The core typically extends 40-50 meters away from the outfall with salinities of about 50 parts per thousand (ppt) for low flow-case conditions and 38 ppt for average case conditions. Maximum core salinity reaches 55.0 ppt in the discharge jet immediately above the outfall tower for low flow case and 41.7 ppt for average case. In the salt wedge surrounding the core, salinities vary from a couple to only a fraction of a ppt over ambient mean ocean salinities. Salt wedge salinities for both low flow and average case are within the envelope of natural variability. The salt wedge extends offshore for about 800 meters seaward of the outfall for low flow case and about 600 meters for average case. The total along shore dispersion of the detectable limits of the salt wedge is 2,150 meters for low flow case and 3,000 meters for average case, both with a downdrift bias toward the southeast. The predominant net current around the outfall is alongshore directed toward the southeast. Organisms drifting with this current will pass through the saline plume and be exposed to elevated salinities for varying periods of time depending on whether they pass through the narrow, high

salinity core or the broad-scale salt wedge with its weakly elevated salinities. In a low flow case scenario drifting organisms would be subjected to maximum salinities of the core (53-55 ppt) for at most 7 minutes, but may linger in the salt wedge at 0.1 ppt above ambient ocean salinities for as long as 10 hours (Figure 4.17). Exposure times at salinities 10 % above ambient levels would be 2.7 hours for the low flow case and 30 minutes under average conditions. Exposure to maximum core salinities under average conditions (40- 41.7 ppt) would be no more than 10 minutes while exposure to the weakly elevated salt wedge salinities would be no more than 7 hours.

In the long-term analysis, the hydrodynamic model solves for 7,523 daily outcomes from the uninterrupted monitoring data of ocean conditions and plant operating conditions that have occurred between 1980 and mid 2000. The objective of this portion of the analysis is to resolve all the intermediate cases that are possible between the low flow and average case event scenarios. In addition, the long term analysis examines the changes to the dispersion of the saline plume resulting from cold water discharges from HBGS occurring during standby mode when the *Delta-T* (ΔT) of the discharge stream is zero. (ΔT is the temperature difference between ocean water and plant discharge).

The modeled long-term outcomes were the result of 20.5 year long continuous time series of daily records for seven controlling operational and environmental inputs. These seven variables may be organized into *boundary conditions* and *forcing functions*. The boundary conditions control the source strength (concentrated sea salts) and background conditions and include: ocean salinity, generating plant flow rates, ocean temperature, and ocean water levels. The period of record from 1980 until July 2000 was the longest period for which

an unbroken record of all seven variables could be obtained and wave data was the limiting data base. However, the latter portion of this period was probably atypical from the present operational stand point because the generating station was under going re-fit and equipment modernization. Although there were instances of the plant operating with three and four generating units in the first seven years of the 1980- July 2000 period of record the preponderance of the record shows that the plant seldom supplied other than 2 different flow rates (127.6 or 253.4 mgd) most of the time. This historic 2 mode operational pattern introduced a *bimodal* statistical pattern into the model results (Figure 5.7).

Over the 20.5 year simulation period, the combined end-of-pipe salinity was found to vary from a minimum of 37 ppt with all 4 generating units on line, to a maximum of 56.4 ppt for cold water discharges during standby mode ($\Delta T = 0^{\circ}\text{C}$). The two predominantly recurring peaks in the probability density function for end-of-pipe salinity are centered at 41.6 ppt and 55.2 ppt, consistent with the average and low flow case values, respectively. The results are summarized in Table 7. The high salinity peak (low-flow rate peak) was attributed to the operation of only one generating unit, while the lower salinity peak (mid-flow rate peak) resulted from operation of two generating units. The salinities of the low-flow rate peak start out at 55 ppt in the water column above the outfall and fall off to 39 ppt at 150 meters away (the approximate outer limit of the 10 % salinity anomaly), accounting for between 42% and 48% of the modeled outcomes (Figure 5.7). On the sea floor, the low-flow rate operational condition (one generating unit) produces salinities that typically range from 47.5 ppt at the foot of the outfall to 37.0 ppt at 150 meters from the outfall (Figure 5.8) having the same recurrence rates as found in the water column. During times when two generating units (or more) were operated (mid-

flow rate peak), salinities varied in the water column from 41.6 ppt at the outfall to 35.2 ppt at 150 meters away with a recurrence rate of 52% to 58%. On the sea floor, 2 generating unit operation (mid-flow rates) causes salinity to range from 38.6 ppt at the foot of the outfall to 34.8 ppt at 150 meters away with the same recurrence rate as for the water column.

Beyond 150 meters from the outfall, the probability density distribution for the discharge plume salinities no longer exhibits bi-modal character. Because the salinity contrast with the ambient water is greater for the low-flow rate peak, it becomes smeared by higher mixing rates promoted along stronger concentration gradients and it merges with the mid-flow rate peak in the distribution to form an asymmetric uni-modal distribution. The characteristics of this distribution are a mid-flow rate peak at lower salinities with a low-flow rate shoulder extending into higher salinity ranges. Salinities in the mid-flow rate peak of this distribution range from 34.6 ppt at 300 meters from the outfall and decay down to ambient ocean salinity at 2,000 meters from the outfall with a recurrence rate of 60% to 82% before reaching ambient ocean salinity levels. Salinities are only a fraction of a ppt greater on the bottom than in the water column over this range. For the low-flow rate shoulder of the probability density distribution, salinities vary from 36.2 ppt at a distance of 300 meters from the outfall, decaying to ambient salinity 2,000 meters away, with recurrence rate of 40% down to 18% before reaching ambient ocean salinity levels.

The bi-modal statistical bias imprinted on the model results by the historical plant flow rates throughout the re-fitting period appears to exhibit itself only in the nearfield of the outfall. The recurrence pattern of two distinct outcomes of approximately equal likelihood, one of high salinity and the other of more moderate

salinity, is only apparent in the inner and outer core of the discharge plume, extending out to about 150 meters from the out fall (Figures 5.7 & 5.8). This is an area of about 17.5 acres. In the salt wedge portion of the plume from 500 meters out and beyond, operational patterns do not appear to alter the results by more than about 1 ppt, with salinities occurring between 34 ppt and 35 ppt or less regardless of historic operational tendencies. In the intermediate zone between 150 and 500 meters from the outfall, operational patterns cause salinity variations between 36 ppt or about 34.5 ppt. Such variations mean the difference between exceeding the upper limit of the natural ocean salinity range for this location, or not. In spite of the historical patterns there were no outcomes involving generation of electrical power that resulted in discharge salinities exceeding those of the low flow event scenario. Only for the relatively rare standby mode occurrences ($\Delta T = 0\text{ }^{\circ}\text{C}$) did higher salinities occur, and these exceeded the low flow case by no more than 1 ppt and accounted for only 1% to 4% of all possible outcomes (Figures 5.7 & 5.8).

Dilution and Dispersion After Completion of HBGS Re-Powering:

After completion of the re-powering and shake-down of the AES Huntington Beach Generating Station in late 2001, higher generation levels and plant flow rates have been maintained than those observed for the late 1980's and throughout the 90's. To determine the implications of this shift in operational patterns on the probable dispersion and dilution of sea salts from the desalination plant, the long-term analysis methodology was repeated for the post re-powering period, 2 January 2002 - 30 July 2003. The dilution results for the post re-powering period are summarized in Table 8 with salinity probability density functions shown in Figures 5.25 and 5.26 at 150 meters away from the outfall. Comparing Figures 5.25 and

5.26 with Figure 5.7 with 5.8 we find that the low flow rate peak at is greatly reduced and represents only about 6% of the 578 daily outcomes during the post re-powering period. After re-powering, the histogram distribution at 150 meters from the outfall is predominantly unimodal and centered on 35 ppt with 92% of the outcomes giving salinities elevated less than the 10% above ambient. Beyond 150 meters away from the outfall, no outcomes from the 7 controlling variables during the post re-powering period give rise to salinities exceeding 40 ppt. Furthermore, no outcomes at any distance from the outfall during post re-powering conditions reach salinities as high as the low flow event cases. Thus, the operation of a 50 mgd desalination plant at AES Huntington Beach is unlikely to ever match or exceed the low flow case outcomes during the foreseeable future.

Source Water Quality at HBGS Intakes

In the remaining sections of this report (Sections 6-9) a hydrodynamic modeling study was conducted to determine if storm water and waste water are possible constituents of the source water at the intake to desalination plant. The storm water analysis considered flood discharges of the Santa Ana River and Talbert Channel watersheds and was also extended to include computations of recirculation of generating plant effluent between the offshore outfall and in-fall. Analysis of source water make-up further considered the dispersion of the wastefield from the 120" diameter deep ocean outfall located offshore of the Santa Ana River and operated by Orange County Sanitation District (OCSD).

The source water quality modeling was performed for a nearshore domain surrounding the AES Huntington Beach plant which extends alongshore from Seal Beach to Crystal Cove State Beach. The model was initialized for three sets of

extreme environmental conditions to evaluate low flow case effects: 1) a wet weather El Niño winter condition to determine the quantity of ocean water and storm water from the Santa Ana River and the Talbert Channel reaching the AES intakes; and, 2) a summer El Niño condition when net transport by waves and currents flows northward to determine if the OCSD wastefield and Talbert Marsh tidal discharges can reach the AES intakes. The El Niño modeling scenarios provide a reasonable prediction of the maximum quantity of storm water runoff and OCSD wastefield reaching the AES intakes. The conclusions of the source water quality analysis are as follows:

Based on representative and historical data, the investigation provided a reasonable estimate of the likely mix of seawater and storm water at the AES Huntington Beach Generating Plant intakes during a period with extremely high storm runoff from both the Santa Ana River and Talbert Channel:

Over the 24-hour extreme runoff period, source water drawn at the infall is comprised of 0.0003% storm water from the Santa Ana River and Talbert Channel (Figure 7.5). Dilution of Santa Ana River and Talbert Channel storm water is 316 thousand to 1 at the depth of the infall velocity cap.

Over the seven-day extreme runoff period spanning the peak flood runoff event, source water drawn at the infall is comprised of only 0.0001% storm water from the Santa Ana River and Talbert Channel. Santa Ana River and Talbert Channel storm water is diluted to 1 million to 1 at the depth of the infall velocity cap.

For the duration of the 30-day extreme runoff period, the average make-up of the source water reaching the intakes would contain no detectable amount of storm water (Figure 7.11). Dilution of Santa Ana River and Talbert Channel storm

water at the infall velocity cap is 10 million to 1.

For sustained high runoff and low flow operational conditions over a 7-day period of extreme wet weather, only a negligible amount of generating station storm water is re-circulated from the outfall to the infall. At most, 0.3% of the combined plant discharge is recirculated of which no more than 2.1% can be plant storm water based on NPDES permit restrictions. Hence plant storm water is at most 0.007% of the source water in a low flow case scenario (Figure 6.1). For maximum power plant generating levels, only 0.0004% of the source water can be expected to be recirculated plant storm water and about 0.003% for normal power generating levels. At all generation levels, the addition of the concentrated seawater by-product to the discharge of the AES power generating plant eliminates the positive buoyancy of the thermal plume and thereby reduces the size and temperature anomaly of the thermal footprint in the offshore waters. On average, the addition of concentrated sea water by-product to the thermal effluent of the generating station will reduce the size of the thermal plume by about 46%.

For low flow case summer El Niño conditions during flood tide (when typical coastal transport is most likely to reverse and flow northward), the wastefield of the OCSD deep outfall was found to disperse no closer than the 15 meter depth contour off Huntington Beach, about 2 km offshore (Figure 9.4). Dilution of the wastefield at the intake to AES Huntington Beach was calculated at 1 part per thirty million, indicating that even without the OCSD Disinfection Resolution of 2002, no total coliforms from the wastefield would be detectable in the source water. Similar calculations on the dispersion of tidal flux from the Talbert Marsh during spring tides found dilution of marsh waters to be 1 part per one hundred thousand at the intake, indicating that marsh coliforms would be non-

detectable in source water (Figure 8.3).

SECTION 11: BIBLIOGRAPHY

11) Bibliography

- Archibald, E. M., 2002, "Watershed sanitary survey and source water assessment for Huntington Beach desalination facility", submitted to Poseidon Resources, August 2002 , 68 pp.
- Archibald, E. M., 2004, "Watershed sanitary survey and source water for Huntington Beach desalination project", submitted to Poseidon Resources, 20 October 2004 , 2 pp.
- Armi, L. A., 1979, "Effects of variations in eddy diffusivity on property distributions in the oceans," *Jour. of Mar. Res.*, v. 37, n. 3, p. 515-530.
- Bograd, S. , Chereskin, T., and D. Roemmich, 2001, "Transport of mass, heat, salt and nutrients in the southern California current system", *Journal of Geophysical Research*, vol 106, no C5, pp 9255-9275
- Berkoff, J. C. W., 1972, "Computation of combined refraction-diffraction," *Proc. 13th Coastal Eng. Conf.*, p. 471-490.
- Boas, M. L., 1966, *Mathematical Methods in the Physical Sciences*, John Wiley & Sons, Inc., New York, 778 pp., 1966.
- CRWQCB, 1993, Waste discharge requirements for Southern California Edison Company Huntington Beach Generating Station Orange County, CA-0001163.
- CDIP, 2004, "Coastal Data Information Program", <http://cdip.ucsd.edu/>
- Dalrymple, R. A., J. T. Kirby and P. A. Hwang, 1984, "Wave diffraction due to areas of energy dissipation," *Jour. Waterway Port, Coast, and Ocean Engineering*, v. 110, p. 67-79.
- Durst, C. S., 1924, "The relationship between current and wind," *Quart. J. R. Met. Soc.*, v. 50, p. 113 (London).
- Gallagher, R. H., 1981, *Finite Elements in Fluids*, John Wiley & Sons, New York,

290 pp.

Grant, S., C. Webb, B. Sanders, A. Boehm, J. Kim, J. Redman, A. Chu, R. Mrse, S. Jiang, N. Gardaner, and A. Brown, 2000, Huntington beach Water Quality Investigation, Phase II, prepared for National Water Research Institute, County of Orange, 156 pp.

Grant, S.B., Kim, J.H. , Jones, B.H., Jenkins, S.A. and J. Wasyl, (in press), "Surf zone entrainment, long-shore transport, and human health implications of fecal pollution from tidal outlets," *Jour Geophys. Res.*, 49 pp.

Hammond, R. R., S. A. Jenkins, J. S. Cleveland, J. C. Talcott, A. L. Heath, J. Wasyl, S. G. Goosby, K. F. Schmitt and L. A. Leven, 1995, "Coastal water clarity modeling," *SAIC*, Tech. Rpt. 01-1349-03-4841-000, 491 pp.

Inman, D. L. and S. A. Jenkins, 1996, "A chronology of ground mine studies and scour modeling in the vicinity of La Jolla," *University of California, San Diego*, Scripps Institution of Oceanography, SIO Reference Series 96-13, 26 pp.

____ S. A. Jenkins and M. H. S. Elwany, 1996, "Wave climate cycles and coastal engineering practice," *Coastal Engineering, 1996, Proc. 25th Int. Conf.*, (Orlando), ASCE, New York, v. 1, Ch 25, p. 314-27.

____ and S. A. Jenkins, 1997, "Changing wave climate and littoral drift along the California coast," p. 538-49 in O. T. Magoon et al., eds., *California and the World Ocean '97*, ASCE, Reston, VA, 1756 pp.

Jenkins, S. A. and D. L. Inman, 1985, "On a submerged sphere in a viscous fluid excited by small amplitude periodic motion," *Jour. Fluid Mech.*, v. 157, p. 199-124.

____ and J. Wasyl, 1990, "Resuspension of estuarial sediments by tethered wings,"

Jour. of Coastal Res., v. 6, n. 4, p. 961-980.

Jenkins, S. A. and J. Wasyl, 2001, "Hydrodynamic modeling of source water make up and concentrated seawater dilution for the ocean desalination project at the AES Huntington Beach Power Station, Part 1: analysis of issues to receiving water, " submitted to Poseidon Resources, revised 20 December 2001 , 111 pp.

Jenkins, S. A. and J. Wasyl, 2002, "Hydrodynamic modeling of source water make up and concentrated seawater dilution for the ocean desalination project at the AES Huntington Beach Power Station, Part 3: analysis of salinity profiles and exposure time, " submitted to Poseidon Resources, 1 August 2002 , 26 pp.

Jones, A.D.G., and W Major, 2003, "The role of the AES Powerplant in surf zone water quality of Huntington Beach, California", *Proc World Oceans Conf.*, 2003, IEEE, New Jersey, p 1487-1496.

Kirby, J. T., 1986a, "Higher-order approximations in the parabolic equation method for water waves," *Jour. Geophys. Res.*, v. 91, C1, p. 933-952.

_____, 1986b, "Rational approximations in the parabolic equation method for water waves," *Coastal Engineering*, 10, p. 355-378.

_____, 1986c, "Open boundary condition in the parabolic equation method," *Jour. Waterway, Port, Coastal, and Ocean Eng.*, 112(3), p. 460-465.

Komar, P. D. and D. L. Inman, 1970, "Longshore sand transport of beaches," *Jour. Geophys. Res.*, v. 75, n. 30, p. 5914-5927.

KOMEX, 2003, "AES Huntington Beach Generating Station surf zone water quality study", draft report submitted to California Energy Commission, August 4, 2003, 268 pp + app.

- Lazara, B. J. and J. C. Lasheras, 1992a, "Particle dispersion in a developing free shear layer, Part 1, Unforced flow," *Jour. Fluid Mech.* 235, p. 143-178.
- Lazara, B. J. and J. C. Lasheras, 1992b, "Particle dispersion in a developing free shear layer, Part 2, Forced Flow," *Jour. Fluid Mech.*, 235, p. 179-221.
- LePage, S., 2004, "Salinity tolerance investigation: supplemental report for the Huntington Beach Desalination Project", submitted to Poseidon Resources, 22 May August 2004 , 29 pp.
- Liedersdorf, C. B., K. E. Smith and L. Ruh-Ming, 1992, "The Talbert Channel ocean outfall project," *Coastal Engineering Practice '92*, ASCE, New York, p. 745-54.
- List, E. J., G. Gartrell and C. D. Winant, 1990, "Diffusion and dispersion in coastal waters," *Jour. Hydraulic Eng.*, v. 116, n. 10, p. 1158-79.
- Longuet-Higgins, M. S., 1970, "Longshore currents generated by obliquely incident waves," *Jour. Geophys. Res.*, v. 75, n. 33, p. 6778-6789.
- Martin, J. E. and E. Meiberg, 1994, "The accumulation and dispersion of heavy particles in forced two-dimensional mixing layers, 1: The fundamental and subharmonic cases," *Phys. Fluids*, A-6, p. 1116-1132.
- Marine Biological Consultants, Inc. 1980. National Pollutant Discharge Elimination System receiving water monitoring report, Huntington Beach Generating Station. August 1980 survey. Prepared for Southern California Edison Company, Rosemead, CA. 80-RD-109. 43 p. plus appendices.
- Marine Biological Consultants, Inc. 1981. National Pollutant Discharge Elimination System receiving water monitoring report, Huntington Beach Generating Station. August 1981 survey. Prepared for Southern California Edison Company, Rosemead, CA. 81-RD-117. 39 p. plus appendices.

- MBC Applied Environmental Sciences. 1982. National Pollutant Discharge Elimination System receiving water monitoring program, Huntington Beach Generating Station. Prepared for Southern California Edison Company, Rosemead, CA. 82-RD-130. 34 p. plus appendices.
- MBC Applied Environmental Sciences. 1983. National Pollutant Discharge Elimination System receiving water monitoring program, Huntington Beach Generating Station. Prepared for Southern California Edison Company, Rosemead, CA. 83-RD-145. 37 p. plus appendices.
- MBC Applied Environmental Sciences. 1984. National Pollutant Discharge Elimination System receiving water monitoring program, Huntington Beach Generating Station. Summer 1984 survey. Prepared for Southern California Edison Company, Rosemead, CA. 84-RD-135. 50 p. plus appendices.
- MBC Applied Environmental Sciences. 1985. National Pollutant Discharge Elimination System receiving water monitoring program, Huntington Beach Generating Station. Summer 1985 survey. Prepared for Southern California Edison Company, Rosemead, CA. 85-RD-99. 33 p. plus appendices.
- MBC Applied Environmental Sciences. 1986. National Pollutant Discharge Elimination System, 1986 receiving water monitoring report, Huntington Beach Generating Station, Orange County, California. Prepared for Southern California Edison Company, Rosemead, CA. 86-RD-54. 35 p. plus appendices.
- MBC Applied Environmental Sciences. 1987. National Pollutant Discharge Elimination System, 1986 receiving water monitoring report, Huntington Beach Generating Station, Orange County, California. Prepared for Southern California Edison Company, Rosemead, CA. 87-RD-83. 48 p. plus

appendices.

MBC Applied Environmental Sciences. 1988. National Pollutant Discharge Elimination System, 1988 receiving water monitoring report, Huntington Beach Generating Station, Orange County, California. Prepared for Southern California Edison Company, Rosemead, CA. 88-RD-57. 46 p. plus appendices.

MBC Applied Environmental Sciences. 1989. National Pollutant Discharge Elimination System, 1989 receiving water monitoring report, Huntington Beach Generating Station, Orange County, California. Prepared for Southern California Edison Company, Rosemead, CA. 90-RD-01. 45 p. plus appendices.

MBC Applied Environmental Sciences. 1990. National Pollutant Discharge Elimination System, 1990 receiving water monitoring report, Huntington Beach Generating Station, Orange County, California. 1990 survey. Prepared for Southern California Edison Company, Rosemead, CA. 90-RD-85. 46 p. plus appendices.

MBC Applied Environmental Sciences. 1991. National Pollutant Discharge Elimination System, 1991 receiving water monitoring report, Huntington Beach Generating Station, Orange County, California. 1991 survey. Prepared for Southern California Edison Company, Rosemead, CA. 91-RD-25. 48 p. plus appendices.

MBC Applied Environmental Sciences. 1992. National Pollutant Discharge Elimination System, 1992 receiving water monitoring report, Huntington Beach Generating Station, Orange County, California. 1992 survey. Prepared for Southern California Edison Company, Rosemead, CA. 92-RD-009. 50 p.

plus appendices.

MBC Applied Environmental Sciences. 1993. National Pollutant Discharge Elimination System, 1993 receiving water monitoring report, Huntington Beach Generating Station, Orange County, California. 1993 survey. Prepared for Southern California Edison Company, Rosemead, CA. 93-RD-009. 49 p. plus appendices.

MBC Applied Environmental Sciences. 1994. National Pollutant Discharge Elimination System, 1994 receiving water monitoring report, Huntington Beach Generating Station, Orange County, California. 1994 survey. Prepared for Southern California Edison Company, Rosemead, CA. 94-RD-008. 53 p. plus appendices.

MBC Applied Environmental Sciences. 1995. National Pollutant Discharge Elimination System, 1995 receiving water monitoring report, Huntington Beach Generating Station, Orange County, California. 1995 survey. Prepared for Southern California Edison Company, Rosemead, CA. 96-RD-002. 59 p. plus appendices.

MBC Applied Environmental Sciences. 1996. National Pollutant Discharge Elimination System, 1996 receiving water monitoring report, Huntington Beach Generating Station, Orange County, California. 1996 survey. Prepared for Southern California Edison Company, Rosemead, CA. 97-RD-001. 56 p. plus appendices.

MBC Applied Environmental Sciences. 1997. National Pollutant Discharge Elimination System, 1997 receiving water monitoring report, Huntington Beach Generating Station, Orange County, California. 1997 survey. Prepared for Southern California Edison Company, Rosemead, CA. 97-EA-07. 58 p.

plus appendices.

MBC Applied Environmental Sciences. 1998. National Pollutant Discharge Elimination System, 1998 receiving water monitoring report, AES Huntington Beach L.L.C. Generating Station, Orange County, California. 1998 survey. Prepared for Southern California Edison Company, Rosemead, CA. and AES Huntington Beach L.L.C. 98-EA-04. 59 p. plus appendices.

MBC Applied Environmental Sciences. 1999. National Pollutant Discharge Elimination System, 1999 receiving water monitoring report, AES Huntington Beach L.L.C. Generating Station, Orange County, California. 1999 survey. Prepared for Southern California Edison Company, Rosemead, CA. and AES Huntington Beach L.L.C. 99-EA-03. 47 p. plus appendices.

MBC Applied Environmental Sciences. 2000. National Pollutant Discharge Elimination System, 2000 receiving water monitoring report, AES Huntington Beach L.L.C. Generating Station, Orange County, California. Prepared for AES Huntington Beach L.L.C. 52 p. plus appendices.

MBC Applied Environmental Sciences. 2001. National Pollutant Discharge Elimination System, 2001 receiving water monitoring report, AES Huntington Beach L.L.C. Generating Station, Orange County, California. Prepared for AES Huntington Beach L.L.C. 54 p. plus appendices.

MBC Applied Environmental Sciences. 2002. National Pollutant Discharge Elimination System, 2002 fish impingement monitoring report, AES Huntington Beach L.L.C. Generating Station, Orange County, California. Prepared for AES Huntington Beach L.L.C. 15 p. plus appendices.

NCDC, 2004, National Climate Data Center Document Library:

<http://www4.ncdc.noaa.gov/ol/documentlibrary/datasets.html>

- Neumann, G., 1952, "Ober die komplexe Natur des Seeganges, Teil 1 and 2," *Deut. Hydrogr. Zeit.*, v. 5, n. 2/3, p. 95-110, n. 5/6, p. 252-277.
- _____and W. J. Pierson, Jr., 1966, *Principles of Physical Oceanography*, Prentice-Hall, Inc., Englewood Cliffs, NJ, 545 pp.
- Nielsen, P., 1979, "Some basic concepts of wave sediment transport," Series Paper No. 20, *Institute of Hydrodyn. and Hydro. Eng., Tech. Univ. of Denmark*.
- OCSD, 1993, Orange County Sanitation District, Marine Monitoring Annual Report
- OCSD, 1999, Orange County Sanitation District 1999 Strategic Plan, Program Environmental Impact Report, prepared by EA Engineering Science Associates, MEC Analytical Systems Inc., and KP Lindstrom, Inc., 461 pp + Appendices.
- OCSD, 2000, Orange County Sanitation District, Marine Monitoring Annual Report.
- OCSD, 2001, Orange County Sanitation District Surfzone Bacteriology Monitoring at URL address: <http://www.ocsd.com/Environment/BeachMon>.
- Oden, J. T. and E. R. A. Oliveira, 1973, *Lectures on Finite Element Methods in Continuum Mechanics*, The University of Alabama Press.
- Pineda, J., 1991, "Predictable upwelling and shoreward transport of planktonic larvae by internal tidal bores," *Science*, vol. 253, p. 548-51.
- Pineda, J., 1999, "Circulation and larval distribution in internal tidal bore warm fronts," *Limnology and Oceanography*, vol. 44, p. 1400-14.
- Radder, A. C., 1979, "On the parabolic equation method for water-wave propagation," *J. Fluid Mech.*, 95, part 1, p. 159-176.
- Roemmich, D. 1989, "Mean transport of mass, heat, salt and nutrients in southern California coastal waters", *Deep-Sea Research*, vol 36, no 9, pp 1359-1378.

- Schmidt, W., 1917, "Wirkungen der ungeordneten Bewegungen im Wasser der Meere und Seen," *Ann. D. Hydr. u. Marit. Meteorol.*, vol. 45, p. 367-381.
- Schoonmaker, J. S., R. R. Hammond, A. L. Heath and J. S. Cleveland, 1994, "A numerical model for prediction of sub-littoral optical visibility," *SPIE Ocean Optics XII*, 18 pp.
- SIO, 2001, "SIO shore station, Scripps Pier",
<http://www-mlrg.ucsd.edu/shoresta/mnSIOMain/siomain.htm>
- Stommel, H., 1949, "Horizontal diffusion due to oceanic turbulence," *Journal of Marine Research*, v. VIII, n. 3, p. 199-225.
- Tenera Environmental, 2004, "Location of the AES Huntington Beach Generation Station Intake", submitted to Poseidon Resources, 27 February 2004 , 3 pp.
- Thorade, H., 1914, "Die Geschwindigkeit von Triftströmungen und die Ekman'sche Theorie," *Ann. D Hydr. u. Marit. Meteorol.*, v. 42, p. 379.
- Schmidt, W., 1917, "Wirkungen der ungeordneten Bewegungen im Wasser der Meere und Seen," *Ann. D. Hydr. u. Marit. Meteorol.*, vol. 45, p. 367-381.
- Schoonmaker, J. S., R. R. Hammond, A. L. Heath and J. S. Cleveland, 1994, "A numerical model for prediction of sub-littoral optical visibility," *SPIE Ocean Optics XII*, 18 pp.
- Wang, H. P., 1975, "Modeling an ocean pond: a two-dimensional, finite element hydrodynamic model of Ninigret Pond, Charleston, Rhode Island," *Univ. of Rhode Island, Marine Tech. Rpt.*, #40, p. 1-58.
- Weiyan, T., 1992, *Shallow Water Hydrodynamics*, Water & Power Press, Hong Kong, 434 pp.

Note on concentrated seawater dilution on the seafloor for the ocean desalination project at the AES Huntington Beach Generating Station

Submitted by:

Scott A. Jenkins, Ph. D. and Joseph Wasyl
Dr. Scott A. Jenkins Consulting
14765 Kalapana Street, Poway, CA 92064

Submitted to:

Poseidon Resources
17011 Beach Boulevard, Suite 900
Huntington Beach, CA 92647

16 October 2006; Revised 25 February 2010

1) Introduction:

This is a supplement to Appendix- C (from Jenkins and Wasyl, 2004) of the now-approved City of Huntington Beach Re-circulated Environmental Impact Report on the Ocean Desalination Project at the AES Huntington Beach Generating Station, referred to herein as the REIR (2005). Extreme event model scenarios of brine discharge in Appendix C have not been exceeded by ocean and atmospheric conditions occurring since certification of the REIR, and consequently it is still a valid and up-to-date report in that respect. This supplemental hydrodynamic report evaluates areas of seabed affected by elevated salinity under “stand alone” operational circumstances. If in the future, the Huntington Beach Power Station were to cease the use of once-through cooling; or if the power plant were to permanently alter their cooling system's historical operations and reduce its long-term seawater intake; the proposed desalination facility would intake water directly from the Pacific Ocean via the existing power plant intake pipe in order to bring in source water. Specifically, we evaluate long term operation of the

proposed desalination plant using the minimum once-through flow rate available with the existing hydraulic infrastructure that will allow the production of 50 mgd of potable water by reverse osmosis (R.O.). This production rate requires approximately 100 mgd of once-through flow rate.

Using various minimum flow rates, we consider the operational regime when the source water is unheated and has the same temperature as ambient ocean temperature ($\Delta T = 0^{\circ} C$). The objective of this supplemental hydrodynamic analysis is to determine the area of seabed around the outfall that is subjected to salinity of 40 ppt or higher. The 40 ppt threshold is based on the biological analysis of salinity tolerance found in Appendix-S of the REIR (from Graham, 2004) as well as additional studies by LePage (2004).

Altogether there are seven primary variables that enter into a solution for the simultaneous dispersion and dilution of the waste heat from the generating station and concentrated seawater from the desalination plant. These seven variables may be organized into ***boundary conditions*** and ***forcing functions***. The boundary condition variables control the source strength (concentrated sea salts) and background conditions and include: generating station flow rates and ΔT (which we fix at the outset), ocean salinity ocean temperature, and ocean water levels. The forcing function variables affect the strength of ocean mixing and ventilation and include: waves, currents, and winds. As detailed in Appendix-C of the REIR, overlapping 20.5 year long records for each of the seven controlling variables are reconstructed. These long-term records contain 7,523 consecutive days of daily mean values between 1980 and 2000.

The hydrodynamic analysis of salinity for these unheated stand-alone operational conditions considers two sets of outcomes; 1) an extreme event analysis that extracts the worst case from long term data sets of controlling

variables; and, 2) a probability analysis of the full set of all possible outcomes given by the period of record of the controlling variables. The extreme events are rare with a recurrence probability of less than 1 %.

2) Extreme Event Analysis:

Minimal ocean mixing conditions become the dominant set of environmental processes in defining worst case for the stand-alone conditions of this supplemental study. Following the statistical search criteria in Appendix-C of the REIR for extracting worst case mixing conditions, the following set of parameters are used to initialize the hydrodynamic model for the extreme event analysis:

1. AES intake flow rate = 152 mgd
2. Desalination production rate = 50 mgd
3. Combined discharge = 102 mgd
4. Ocean salinity = 33.52 ppt
5. End-of pipe combined discharge salinity = 49.9 ppt
6. Discharge temperature anomaly, $\Delta T = 0^{\circ} \text{C}$ (unheated)
7. Discharge density anomaly, $\Delta \rho / \rho = 0.88 \%$ (unheated)
8. Wave height = 0.16 m
9. Wave period = 8 sec
- 10) Wave direction = 255°
- 11) Wind = 0 knots
- 12) Tidal range = Syzygian spring/neap cycle
- 13) Daily maximum tidal current = 8.7 cm/sec

Using these parameters, the hydrodynamic model simulates the maximum salinity levels during tranquil ocean conditions wherein ambient mixing is minimal. The low mixing conditions as listed above are a one time occurrence in the period of record, but are run in the model as a 30-day long simulation to insure a steady state worst case. By perpetuating these low mixing conditions for 30 continuous days, the recurrence interval is one month every 13 to 31 years (page C-133 of Appendix-C, REIR). While interacting with these unusually quiet receiving waters, the RO units would withdraw approximately 100 mgd from the 152 mgd source water flow and return 50 mgd of concentrated seawater to the discharge stream. The resulting combined discharge from the plant outfall would be 102 mgd at salinity of 49.9 ppt. The unheated discharge is heavier than the ambient seawater, with a change in specific volume of - 0.88%. The choice of 152 mgd for the intake flow rate was the result of numerical experiments with the hydrodynamic model aimed at achieving certain water quality objectives discussed in Section 5.

The 30 day average of the model simulation of bottom salinity is plotted in Figure 1 for the unheated 152 mgd scenario with worst case mixing boundary conditions as listed above. Bottom salinity decreases with increasing distance from the outfall according to the color bar scale in the upper right hand corner of the figure, where the ambient background ocean salinity is 33.52 ppt. The 40 ppt salinity contour is too small to illustrate, but encloses 0.7 acres. All the contours are asymmetric about the outfall with the 40 ppt contour having an average radius of 100 ft.

All the bottom salinity contours display this same general down-drift (southeastward spreading) distribution for the 30 day averages due to ebb-dominance of the tidal currents (see Figure 4.3 on page C-137 of Appendix-

C, REIR). An ellipse (type-b ellipse with major axis shore-parallel and discharge source alternating between the two foci) is a reasonable geometric approximation of the plume. Throughout the 30-day time step progression of model solutions, the ellipse changes its eccentricity and swaps foci with the discharge source between ebb and flood tide. The eccentricity is larger during ebb tide (more alongshore spreading, southeastward), and smaller during flood tide (less alongshore spreading, northwestward) because the tidal currents are ebb-dominated toward the south. During slack water, the eccentricity of the ellipse goes to zero as the plume becomes a circle. The best approximation for the area that is perpetually exposed to 40 ppt or greater during the 30 day progression is a circle whose radius sweeps out an area equivalent to that inside the 30-day average of the 40 ppt contour. The average radius of the 40 ppt contour is given in the tenth row of Table 1 at the end of the conclusions (Section 6) of this technical note.

Figure 1 represents a worst case assessment of the amount and distribution of bottom habitat area exposed to salinity of 40 ppt or higher during stand-alone operations (unheated $\Delta T = 0^{\circ} \text{C}$). The maximum seabed salinity found anywhere inside the 40 ppt contour in Figure 1 is 44.2 ppt on the rock footing of the outfall tower. Because the worst-case mixing conditions and unheated stand-alone operations are both historically rare, the joint probability of the Figure 1 scenario has a recurrence probability of about 0.04% to 0.1%.

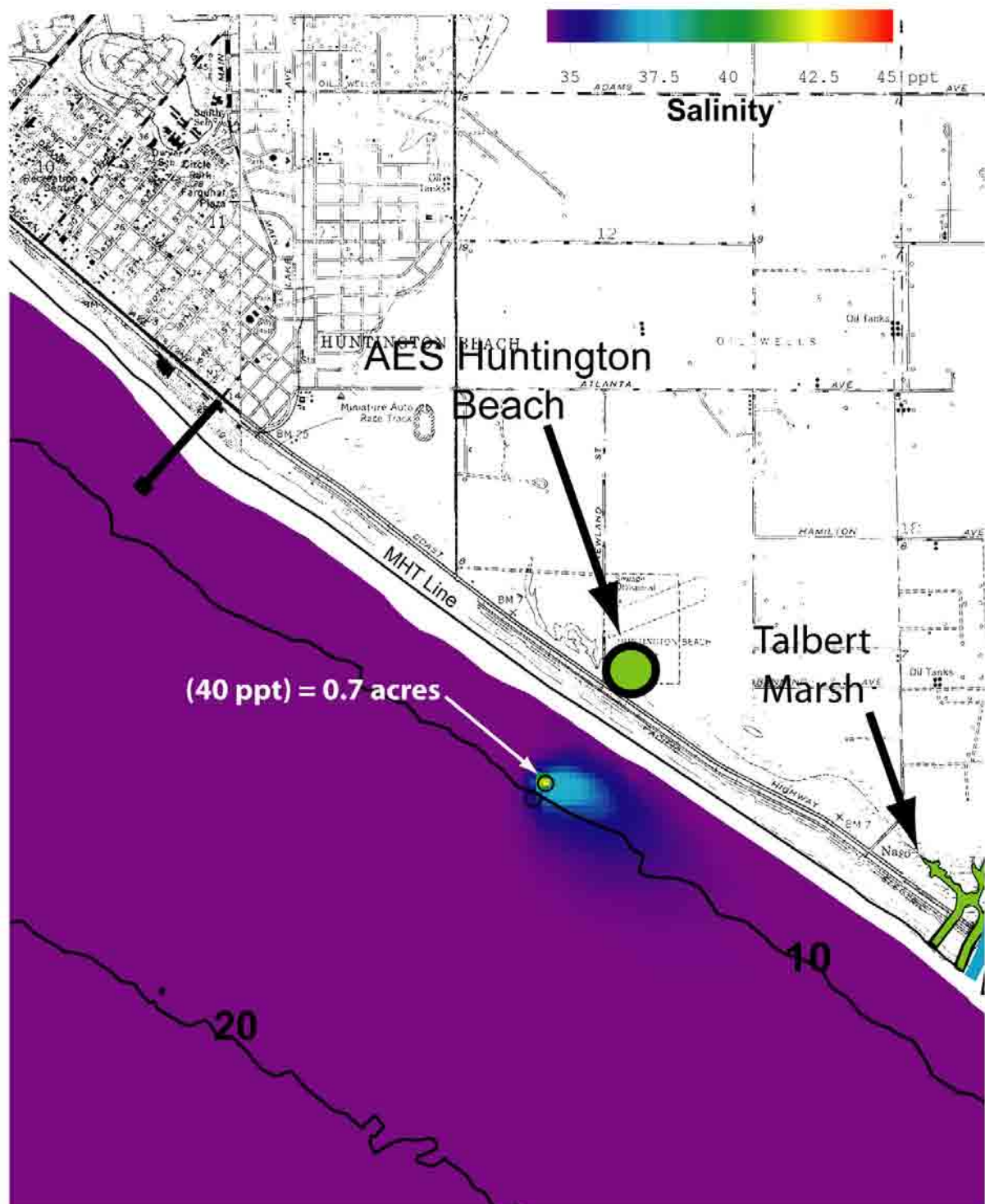


Figure 1. Bottom salinity for standby conditions: $\Delta T = 0^\circ \text{C}$; R.O. production = 50 mgd, plant flow rate = 152 mgd (worst case ocean mixing). Depth contours in m MSL, salinity indicated by color bar scale in upper right corner.

3) Long-Term Probability Analysis:

The marine environment around the AES Huntington Beach Generating station has both short-term and long-term variability due to the interplay between climatic variability and certain local features associated with the physical setting, in particular the irregular shelf bathymetry. El Niño events cause significant warming and stratification of the coastal ocean around AES Huntington Beach over recurrence periods of 3 to 7 years. These warm El Niño events are superimposed on seasonal warming cycles (Figure 2c). The salinity field shows similar variability due to the same sets of climatic and seasonal mechanisms (Figure 2b). El Niño events bring floods causing river discharges of fresh water which depress the salinities of the coastal oceans in the vicinities of river mouths. Similar variations occur inter-annually as seasonal changes in wind patterns move different water masses with different salinities into and out of the Southern California Bight. Therefore, the local environment already has a natural degree of variability in temperature and salinity (Figures 2b & c) on which the activities of the generating station and desalination plants are superimposed. In the following analysis the once-through flow rates through remain constant, fixed at the minimum flow rate of 152 mgd (Figure 2a) while the remaining variables (*boundary conditions* and *forcing functions*) are allowed to change day by day according to the 20.5 year period of record (Figures 2 and 3).

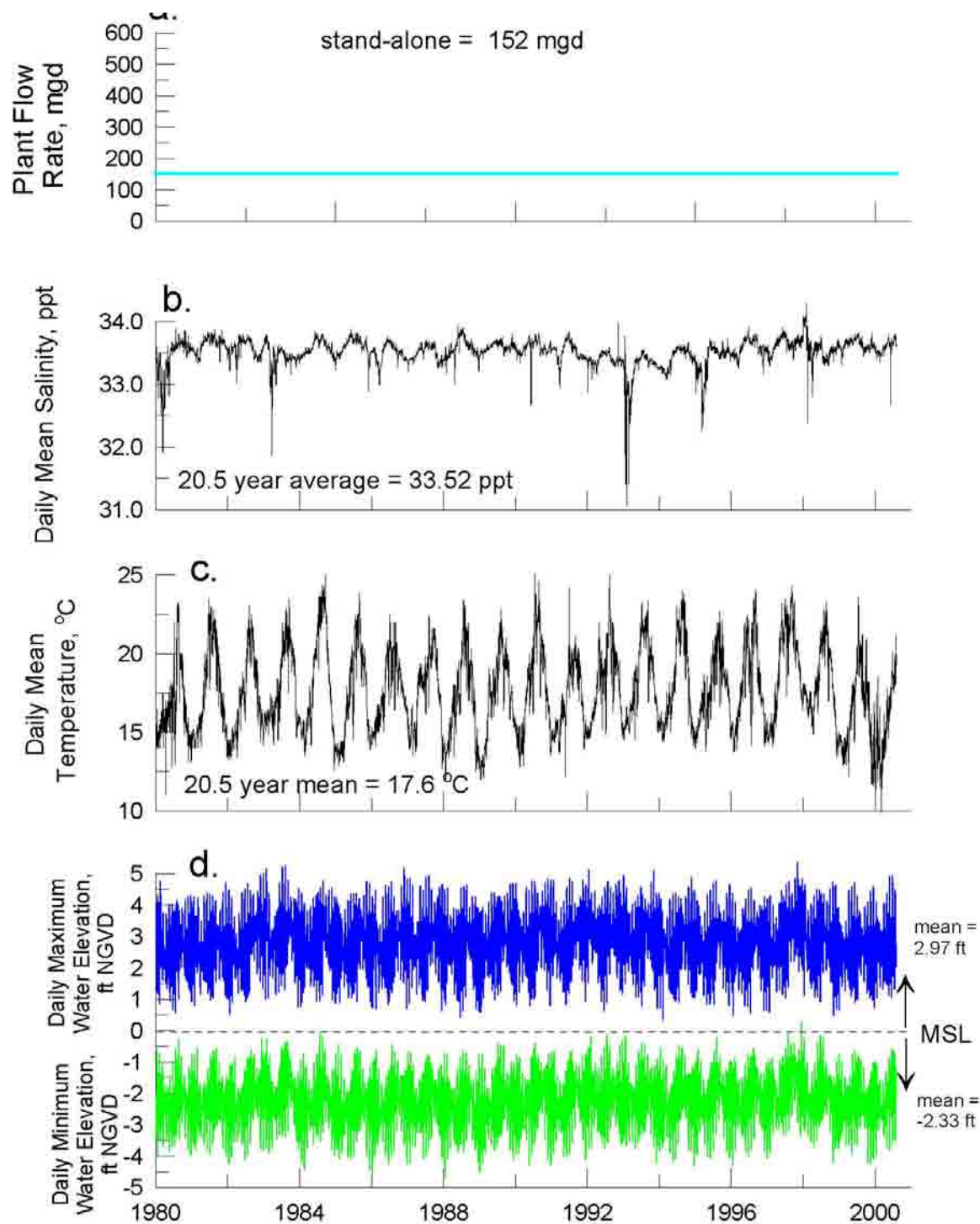


Figure 2. Controlling environmental variables for brine dilution, boundary conditions: a) plant flow rate b) daily mean salinity, c) daily mean temperature, and d) daily high and low water elevations. [data from MBC, 1980-2001; OCSD, 1993, 2000; SIO, 2001]

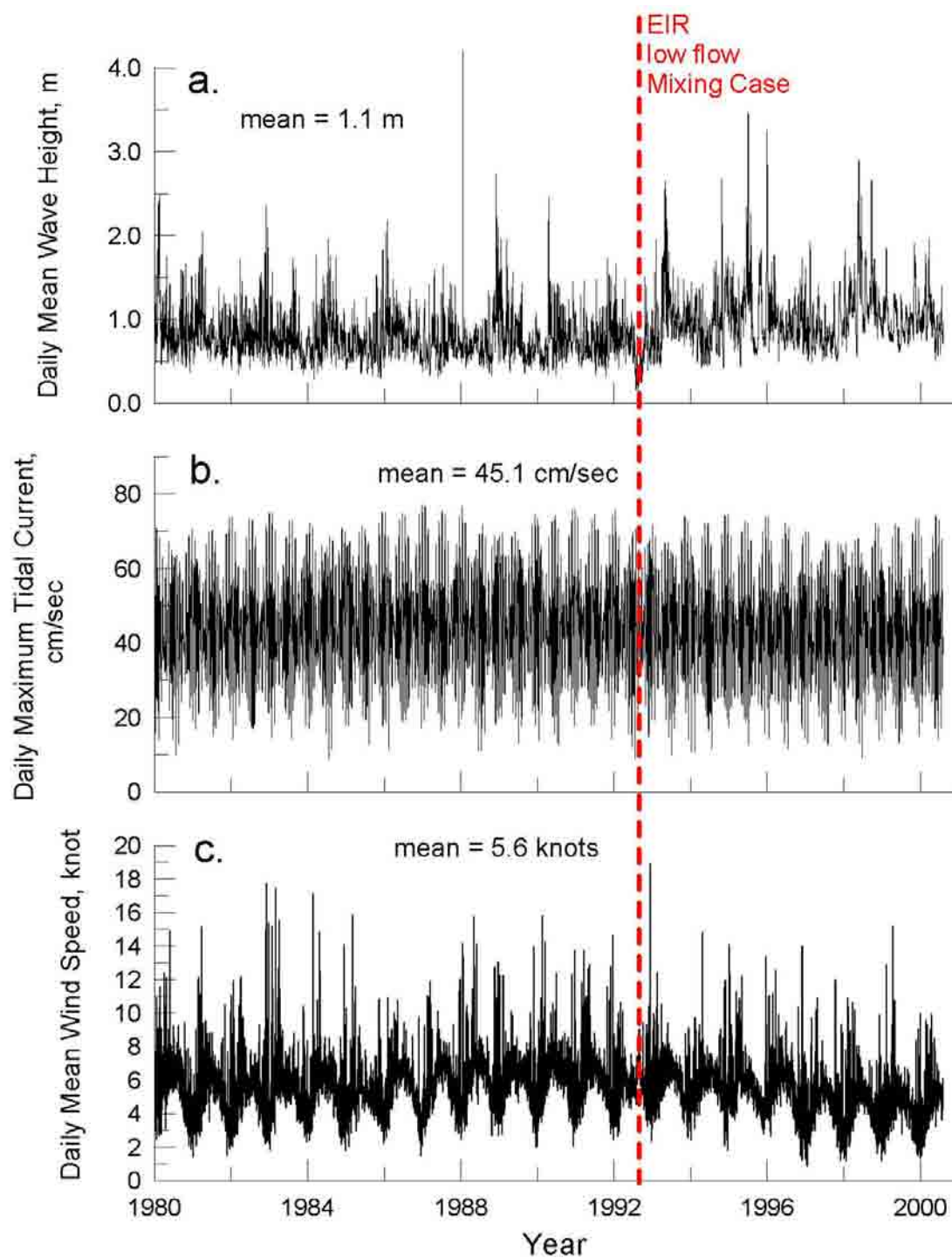


Figure 3 20.5 year record of forcing for the Newport Littoral Cell [centered at Huntington Beach, CA]. a) daily mean wave height (CDIP), b) daily maximum tidal current velocity (Station 8d), and c) daily mean wind (Station 8d). [data from CDIP, 2001; SIO, 2001; NWS, 2001; App.C, REIR, 2005]

The ocean forcing functions (Figure 3) that will mix and carry away the heat and concentrated seawater are likewise modulated by El Niño events, seasonal changes in weather patterns and by diurnal and semi-diurnal changes in tidal stage. The waves, currents and winds used to specify the worst-case mixing conditions in Section 2 is shown by the red dashed line in Figure 3. The historic boundary conditions from Figure 2 and the forcing functions from Figure 3 were sequentially input into the model, producing daily solutions for the salinity field discharged from the stand-alone operations of the desalination plant (circulating sea water at 152 mgd and producing product water at 50 mgd). The input stream of seven controlling variables from Figures 2 & 3 produced 7,523 daily solutions for the salinity field around the outfall. A numerical scan of each of these daily solutions searched for the locus of points on the sea floor having salinity of 40 ppt, and then calculated the area inside the closed contour formed by those points. The acreages inside the daily 40 ppt solution contours were then entered into histogram bins at 0.25 acre increments for ultimately assembling a probability density function and cumulative probability from the 7,523 outcomes.

Figure 4 gives the histogram of acreage inside the 40 ppt bottom salinity contour for the 152 mgd stand-alone operating scenario. The median of the 7,523 daily solutions is 0.21 acres, and there were no outcomes greater than 0.72 acres, consistent with the extreme event analysis in Section 2 (Figure 1). In fact the worst case outcome from Figure 1 is so rare its histogram bar in Figure 4 is less than a line width, consistent with the estimated recurrence probability of about 0.04% to 0.1%. The locus of red bars in Figure 4 represents the probability density function according

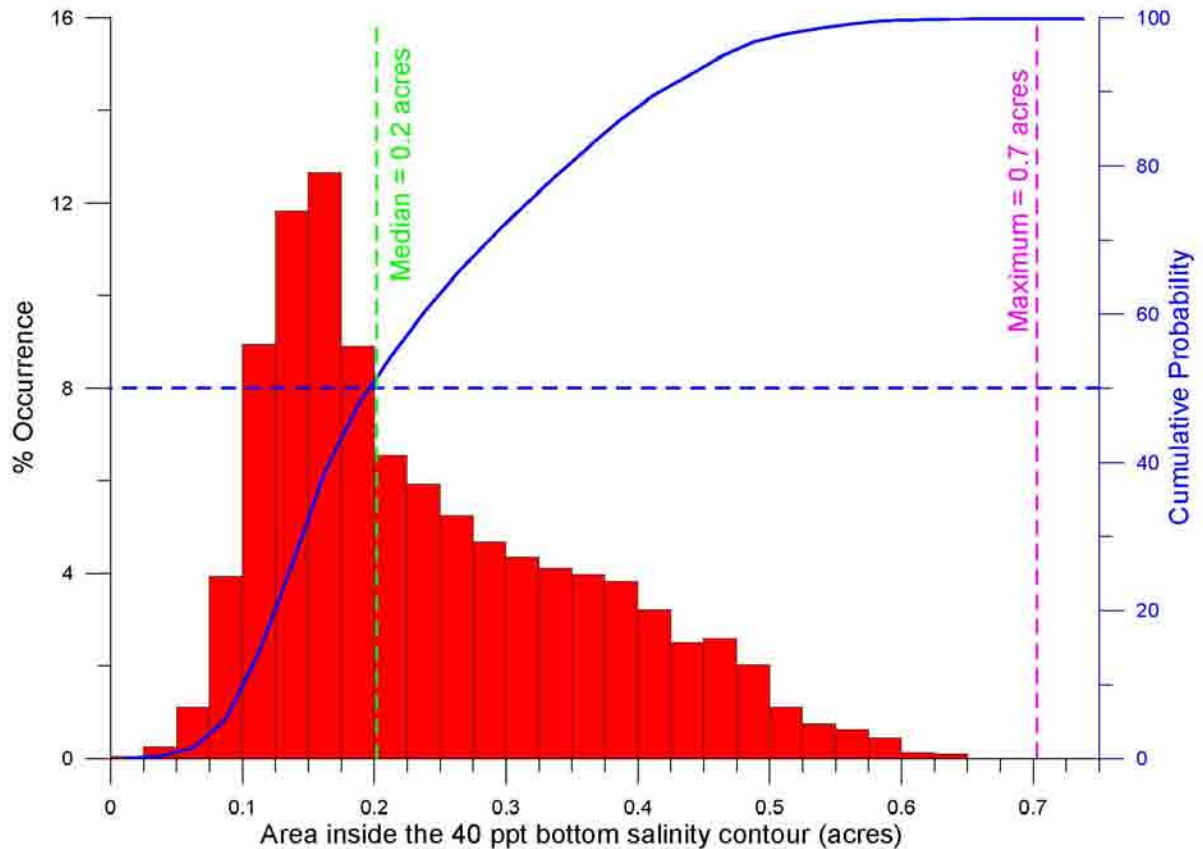


Figure 4. Histogram of acreage enclosed by the 40 ppt bottom salinity contour for desalination production rate of 50 mgd and intake flow rate = 152 mgd with $\Delta T = 0^\circ \text{C}$. Percent occurrence based on historic observations of ocean forcing and water mass properties 1980-2000 (7,523 daily outcomes).

to the scale of % occurrence on the left hand side of Figure 1, while the blue curve is the cumulative probability according to the scale on the left hand side. Inspection of the cumulative probability function in Figure 4 reveals that 90% of the outcomes resulted in less than 0.4 acres inside the 40 ppt bottom contour.

4) Plume Exposure Time for Drifting Organisms:

Pelagic organisms drifting in the nearshore currents can be carried through the discharge plume along trajectories governed by the *Lagrangian drift*. The Lagrangian drift is the mean motion of a particle that would be observed by following that particle along its drift trajectory. The drift rates of an organism passing through the plume are calculated as described on pages C-157-162 of Appendix C of the REIR. Here we supplement that analysis to consider the stand-alone worst case whereby the power plant is not generating and the desalination plant is utilizing 152 mgd of unheated source water flow with $\Delta T = 0^{\circ} \text{ C}$.

The maximum exposure time of a drifting pelagic organism passing through the discharge plume for the unheated 152 mgd stand-alone operational case with worst case mixing is plotted as a black line in Figure 5. Salinity in the inner core of the discharge plume does not exceed 49.9 ppt, for which exposure time of a drifting organism is 9 minutes. Exposure to the outer core where salinities are nominally 45 ppt, is 39 minutes, and about 1.9 hours along the outer fringes of the outer core where salinities decline to 38 ppt. The exposure time is 1.4 hrs at 40 ppt. In the salt wedge where salinities range from 33.58 ppt to 34 ppt, exposure times never exceed 9.3 hours.

5) Discussion of Water Quality Objective:

The stand-alone operational simulations at 152 mgd intake flow rate are based on achieving sufficient in-the-pipe dilution so that salinity does not exceed 40 ppt, beyond 100 ft from the discharge tower. This result is aimed at meeting the 0.3 TUa objective of Requirement III.C.4(b) of the *California Ocean Plan* (even though concentrated seawater is not a toxin), as it would

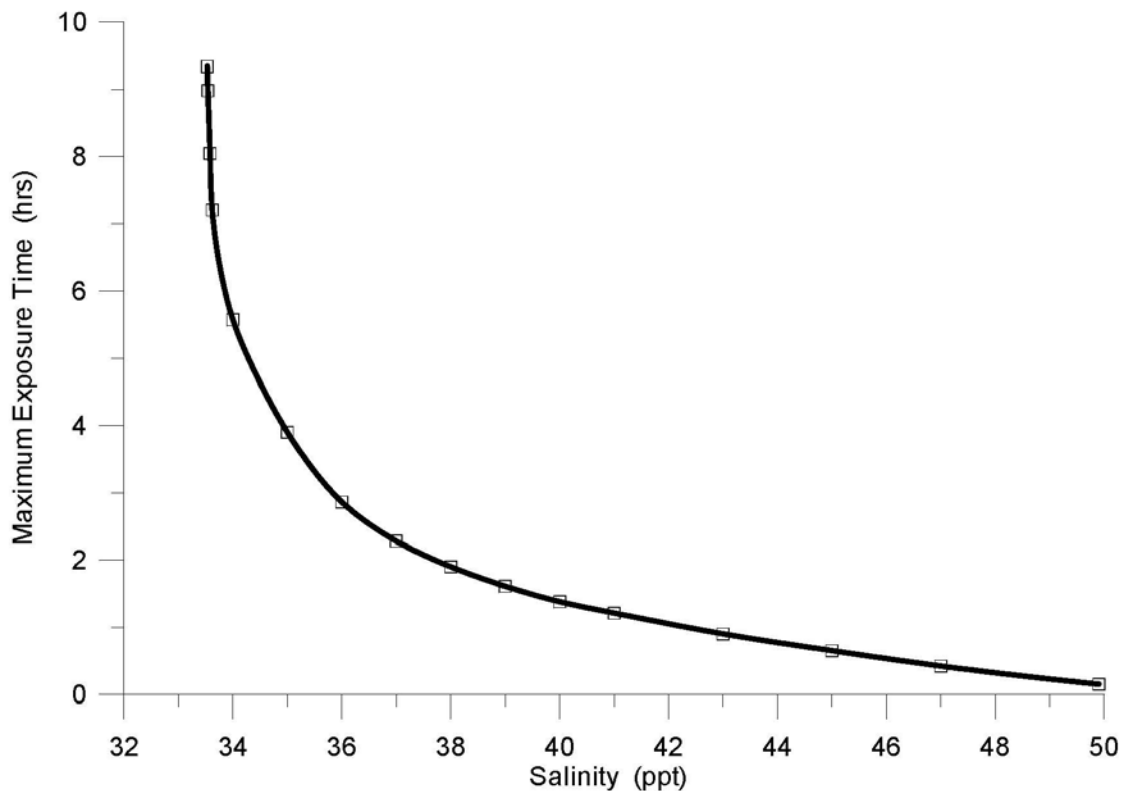


Figure 5. Maximum exposure time of a drifting organism passing through the discharge plume of concentrated seawater from the AES Huntington Beach outfall for augmented stand-alone worst-case at $\Delta T = 0^{\circ}\text{C}$ and 152 mgd intake flow rate (black)

apply to a *Zone of Initial Dilution (ZID)* measuring 1000 ft in radius as stipulated in RWQCB (2007) for the Huntington Beach Generating Station and the co-located Huntington Beach Desalination Project. For worst case mixing conditions as defined in Section 2, intake flows would have to reach 152 mgd to meet this version of the 0.3 TUa objective. If the 152 mgd stand-alone operating point is subjected to long-term mixing conditions, then seafloor salinity remains under 40 ppt beyond 54 ft from the discharge tower. Therefore, the intake flow rate could be reduced to 144 mgd to satisfy the 0.3 TUa objective with a 1000 ft ZID under long-term mixing conditions.

6) Conclusions:

Taking various unheated minimum intake flow rates, we use a hydrodynamic model to calculate the area of seabed subjected to salinities of 40 ppt or greater. The unheated regime represents a hypothetical circumstance in which: the generating station has been permanently shut down or has altered their cooling system's historical operations and reduce its long-term seawater intake; and the desalination facility operates circulation and supplemental pumps to supply source water to the reverse osmosis (RO) units. From these hydrodynamic simulations we conclude:

- a)** The unheated discharge produced by desalination using 152 mgd of intake flow results in a median outcome of 0.2 acres of sea bed being exposed to salinities of 40 ppt or greater, while 90 % of the time less than 0.4 acres of sea bed are so affected. The worst-case outcome for the 40 ppt seabed footprint was found to be 0.7 acres. The recurrence probability of this worst case outcome is estimated at 0.04% and 0.1% from historic environmental and operating conditions.
- b)** Heated source water produces a smaller footprint of elevated salinity over the seafloor with lower peak salinity than that obtained with unheated source water.
- c)** Unheated source water causes an insignificant increase in the time that drifting organisms are exposed to salinity exceeding 40 ppt in the water column.

The stand-alone, hydrodynamic simulations at 152 mgd intake flow rate are based on achieving enough in-the-pipe dilution so that salinity does not exceed 40 ppt beyond 100 ft from the discharge tower. This objective is aimed at meeting the 0.3 TUa objective of Requirement III.C.4(b) of the

California Ocean Plan (even though concentrated seawater is not a toxin), as it would apply to a *Zone of Initial Dilution (ZID)* measuring 1000 ft in radius as stipulated in RWQCB (2007) for the Huntington Beach Generating Station and the co-located Huntington Beach Desalination Project. From these simulations we conclude:

d) For worst case mixing conditions, intake flows must reach at least 152 mgd to meet this version of the 0.3 TUa objective; but could be reduced to 144 mgd under long-term mixing conditions in order to satisfy this objective. The 152 mgd stand-alone scenario results in a 1.4 hour exposure period for drifting organisms encountering salinity exceeding 40 ppt in the water column under worst case mixing conditions. Maximum salinity in the inner core of the discharge plume does not exceed 49.9 ppt, for which exposure time of a drifting organism is 9 minutes.

7) References:

- Graham, J. B., 2004, "Marine biological considerations related to the reverse osmosis desalination project at the Applied Energy Sources, Huntington Beach Generating Station," Appendix-S in REIR, 2005, 100 pp.
- Jenkins, S. A. and J. Wasyl, 2004, "Hydrodynamic modeling of source water make-up and concentrated seawater dilution for the ocean desalination project at the AES Huntington Beach Generating Station," Appendix-C in REIR, 2005, 298 pp.
- LePage, S., 2004, "Salinity tolerance investigation: supplemental report for the Huntington Beach Desalination Project", submitted to Poseidon Resources, 29 pp.

REIR, 2005, "Re-circulated Environmental Impact Report Sea Water Desalination Project at Huntington Beach," City of Huntington Beach, prepared by RBF Consulting, April 5, 2005, 10 sections + append.

RWQCB, 2007, California Regional Water Quality Control Board, Santa Ana Region, staff response to SWRCB/OCC File A-1776, page 10, 23 February 2007, 15 pp.